# THE GROWTH, STRUCTURE AND PROPERTIES OF SPUTTERED BARIUM TITANATE THIN FILMS

A THESIS SUBMITTED FOR THE DEGREE OF

DOCTOR OF PHILOSOPHY

IN THE UNIVERSITY OF ASTON IN BIRMINGHAM

ROBERT MALCOLM NEWMAN B.Sc.



PHYSICS DEPARTMENT

SEPTEMBER 1972.

## ABSTRACT

The design and construction of a sputtering system for the deposition of barium titanate thin films is described.

The growth and structure of barium titanate films deposited on a variety of substrates, including amorphous carbon films, potassium bromide single crystals, and polycrystalline gold films has been studied. Films deposited on all substrates at room temperature were amorphous. Polycrystalline titanate films were formed on polycrystalline and amorphous substrates at temperatures above 450°C while films with a pronounced texture could be epitaxially deposited on single crystal potassium bromide above a temperature of only 200°C.

Results of dielectric measurements made on the films are reported. Amorphous films were highly insulating (resistivities ~$10^{14}$ ohm.cm with dielectric constants of between 10 and 20. Polycrystalline films had a lower resistivity (~$10^{8}$) but yielded dielectric constants of over 500. Films deposited on polycrystalline gold in the temperature range 220-450°C gave dielectric constants between 110-150 suggesting the existence of a metastable short range order in the films. These films had losses typically of 0.04 and temperature coefficients of capacity of about 0.1%°$C^{-1}$ and suggest the possibility of an application in high value thin film capacitors.

A peak in the temperature variation of the permitivity of polycrystalline barium titanate films was observed at a temperature of about 90°C but no evidence of ferroelectric behaviour could be found.

The conductivity and optical constants of films deposited on polycrystalline gold substrates were also studied. Films deposited at room temperature gave a time dependent leakage current while the conductivity and characteristics of films deposited above 200°C varied considerably. All leakage characteristics were explained in terms of space charge limited

found to be between 2.1 and 2.2.

INDEX.

CHAPTER 6. THE GROWTH AND PROPERTIES OF BARIUM TITANATE SPUTTERED FILMS

# CHAPTER ONE

## BARIUM TITANATE: PROPERTIES AND APPLICATIONS IN MICROELECTRONICS.

### 1.1 Thin Film Microelectronics.

The use of thin films in microelectonics is now well known and extensive. Work is well established on thin film active devices (1-7) and switching elements and memory cells for computer applications (8-10). Piezoelectric thin films are used as transducers and digital delay lines (11-13). Passive circuit elements are so advanced that thin film R-C networks with attached semiconductor active devices are produced commercially by a number of manufacturers. Thin film capacitors generally utilise silicon oxide, tantalum oxide or alumina but for a high value capacitor a large surface area is required. In order to reduce this a thinner layer of dielectric can be used but this decreases the breakdown strength of the device so that a limit is imposed on the improvement. The only other possibility of increasing the capacity per unit area is to use a high permitivity material (14). Barium titanate falls into this categary having a permitivity ranging from two hundred to many thousand. This material also has other properties which offer device possibilities worth pursuing. These properties, some of which are mentioned below, are discussed in more detail in the next section. In certain crystalline forms it exhibits a permanent electric polorisation which is reversible and shows a hysterisis, a property which because of the similarity to the magnetic hysterisis in ferromagnetic materials is known as ferroelectricity. It follows from this behaviour that barium titanate will also be piezoelectric and pyroelectric. The polorisation switching capability provides a possible computer application as a matrix store. This was suggested by Anderson (15) in 1952 and considerable work has been carried out on bulk crystals with that object (16-18). Barium titanate is used in ceramic form as a good piezoelectric material for transducers. This is because the high

dielectric constant of the ferroelectric means the electro-mechanical coupling coefficient can be as high as 0.5 (19). Much work has been aimed at controlling the anomalies in the permitivity and piezoelectric properties of ceramic barium titanate (McQuarrie 20 ) both for transducers of all kinds and for bulk capacitors. The pyroelectricity and variation of permitivity with temperature suggest a possible application as a bolometer for infra red detectors (21). Other device applications arise from the non-linear, anomalous properties of the material. The variation of permitivity with bias voltage means that the value of a barium titanate capacitor can be changed electrically. This and other non-linearities lead to applications in varactor diodes (22) harmonic generators (23) and dielectric power amplifiers (24). Optical non-linearities lead to possible applications in the use of lasers as light beam switches and beam demodulators (25,26). Although most of the references to applications mentioned above concern bulk barium titanate many of the devices would be of even more interest if they could be produced in thin film form. This is because at reduced thickness polorizing voltages would be smaller and heat dissipation improved thus reducing unwanted thermal hysterisis. Few attempts at producing barium titanate films have been reported in the literature. But they do suggest that it might be possible to improve the quality and properties of the films with a view to using them in device applications. This project was therefore aimed at producing such films.

## 1.2. The Properties of Barium Titanate.

### 1.2.1 Crystal Structure.

Barium Titanate is a member of a group of compounds called perovskites which all have the same or almost the same structure. Many but not all of the members of this group are ferroelectric or anti-ferroelectric. The perovskite structure illustrated in diagram 1.1. is cubic with the space group Pm3m. In barium titanate each titanium atom

is surrounded by six oxygen atoms arranged at the corners of a regular octahedron. The Ti O octahedrons are arranged in a cubic structure with the barium atom at the body centering position. Above 120°C barium titanate has this perfect perovskite structure with a unit cell of 4Å. Below 120°C the structure undergoes a transition to a tetagonal unit cell which can be derived from the cubic form by being stretched parallel to one of the cube edges. The tetragonal axial ratio is only 1.01 so the discrepancy between the two structures is only slight. The space group is P4mm and the tetrad axis is unique. This is the structure barium titanate normally has at room temperature. Further transitions occur at about 0°C to orthorhombic Bmm2 with a unique diad axis and at -90°C to rhombohedral R3m with a unique triad axis. Barium titanate can also take a hexagonal form produced by quenching the pure material from high temperatures (1500°C). It is ferroelectric below 120°C in all forms except the hexagonal structure. Since the discovery of ferroelectric behaviour in barium titanate some thirty years ago extensive studies of the various properties of the material have been made and form the subject of many papers and reviews, see in particular the recent review by Smolenskii and Krainik (27). Most of the other properties are also a function or consequence of the various crystal structures of barium titanate in that in all three forms below 120°C it has a unique axis and is non centrosymmetrical. It follows from Newman's principle (28) which states that any property of a crystal must have a minimum symmetry which includes the symmetry of the point group of the crystal, that for a material to be pyroelectric or piezoelectric it cannot be centrosymmetrical and must include a polar axis. A polar axis is one of which the two ends are not related by any symmetry element of the point group; a unique axis is a polar axis. It also follows that a material which is ferroelectric will automatically be pyro and piezoelectric while all pyro and piezoelectrics will not be ferroelectric.

A list of the more interesting properties of barium titanate is given below and each is discussed in more detail in the following sections:-

(1) Ferroelectric at R.T. with a Curie Point of 120°C

(2) Pyroelectric.

(3) Piezoelectric.

(4) Temperature and Field sensitive dielectric constant of up to 10,000 near 120°C.

(5) High refractive index 2.46 at 120°C.

(6)Birefringent.

(7) Large electro-optical effect.

1.2.2 Ferroelectric.

Ferroelectrics are materials which possess a spontaneous electric polarisation Ps which can be reversed by applying a suitable electric field. This process is accompanied by a hysterisis similar to the hysterisis between the magnetic induction B and magnetic field H in ferromagnetics and the name is taken from analogy with these materials. Diagram 1.2.a shows a typical hysterisis loop of polarisation against applied field, showing the coercive field $E_c$ necessary to switch the polarisation. The polarisation is a function of crystal orientation and the change in polarisation on switching is greatest parallel to the unique axis of the crystal. The hysterisis loop can be observed using a Sawyer Tower circuit (29) as shown in diagram 1.2.c. The capacitor C has a small impedance compared to the specimen so that the x signal on the oscilloscope is proportional to the applied field E. The y signal will indicate any change in polarisation of the specimen due to the displacement current flowing through the capacitor C and for a sinusoidal input a loop is produced. If in the same circuit the capacitor is replaced by a small resistor R, the voltage across R will be proportional to the switching current transient $i_s$ and this can also be displayed on the oscilloscope. $i_s$ is a function of applied field E so a square wave input is used giving repetetive switching and a transient as shown in

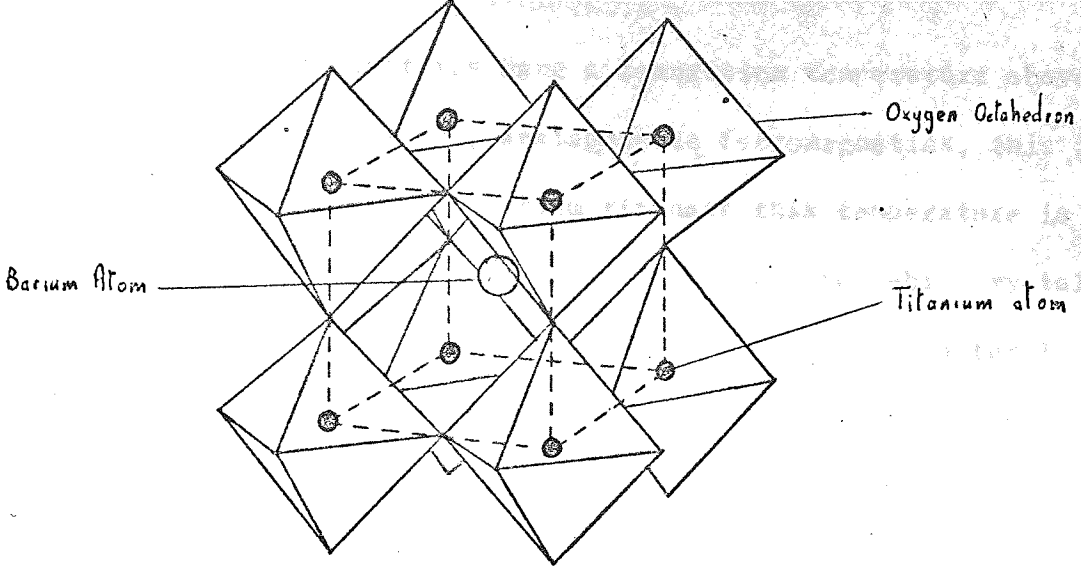


Figure 1.1.

Barium Titanate Crystal Structure

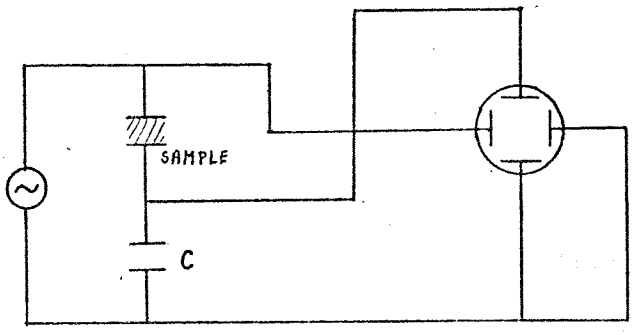


Figure 1.2.(c)

Sawyer Tower Circuit.

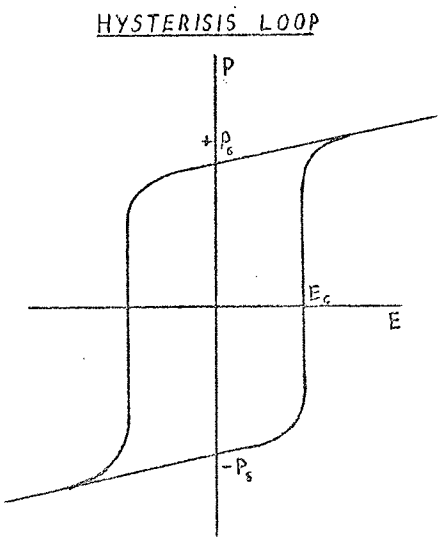


Figure 1.2.(a)

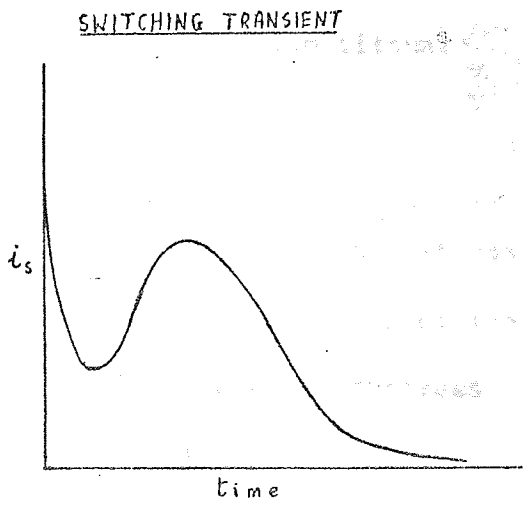


Figure 1.2.(b)

diagram 1.2.b. All ferroelectrics have a transition temperature above which the property disappears and, analagous to ferromagnetics, this is called the Curie Temperature. In barium titanate this temperature is 120°C corresponding to the transition from tetragonal to cubic crystal structure. Anomolous effects also occur at the other two structural transitions mentioned in section 1.2.1 but the ferroelectricity is maintained. Diagram 1.3 shows the variation of the spontaneous polarisation over the whole temperature range.

1.2.3. Pyroelectric

Pyroelectricity is the name given to the effect of a material developing an electric polarisation when its temperature is uniformly changed. If there is a uniform small change in temperature $\Delta T$ the change in polarisation $\Delta P$ is given by the tensor equation 1.1 where $p_i$ are pyroelectric coefficients. Barium titanate is pyroelectric

$$\Delta P_i = p_i \Delta T \qquad 1.1$$

below the Curie temperature due to the variation of spontaneous polarisation with temperature as already shown in diag. 1.3. Chynoweth (30) and Burfoot and Latham (31) have measured transient currents in barium titanate due to this effect produced in the former by illuminating the crystal with pulses of heat energy in the form of a flashing light. This property gives rise to the possibility of using barium titanate as an infra red detector.

1.2.4. Piezoelectric.

A material which developes an electric polarisation when a stress is applied to it is said to be piezo electric. The polarisation Pi is again given by a tensor equation (1.2) where $\sigma_{ij}$ is the applied stress

$$P_i = d_{ijk} \sigma_{jk} \qquad 1.2$$

and dijk are piezoelectric moduli. The converse effect also exists, that is the development of a strain in the material due to an applied field. Barium titanate is piezoelectric below 120°C and has moduli under certain conditions some hundred times greater than quartz (32). This

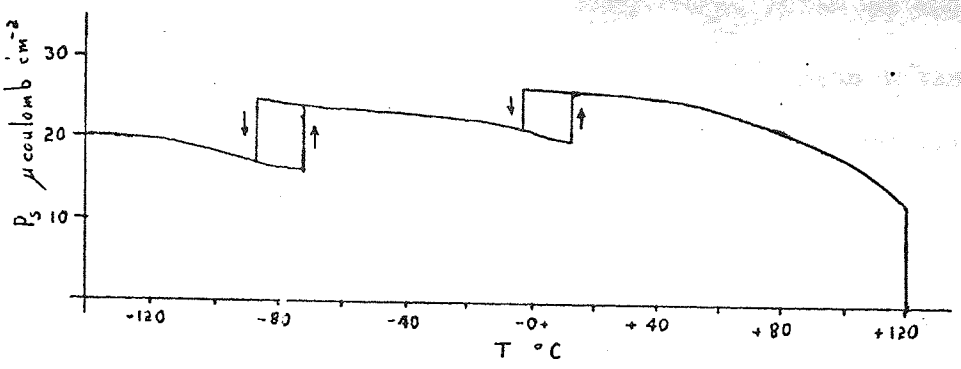


Figure 1.3

Spontaneous Polarisation.

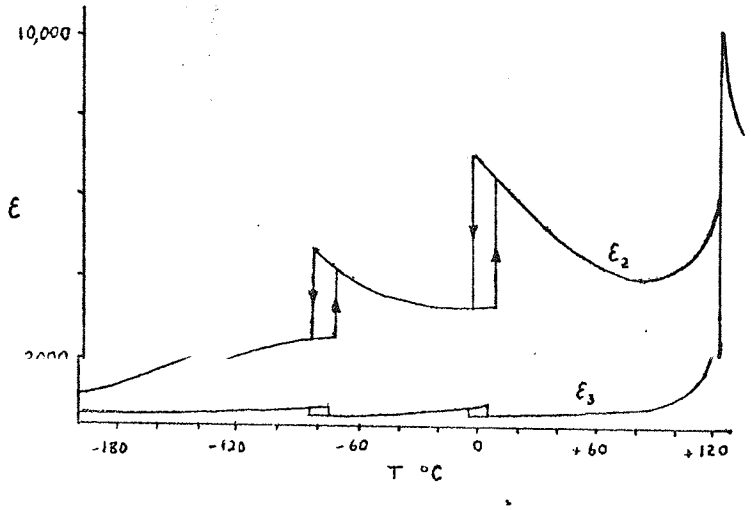


Figure 1.4.

Permitivity

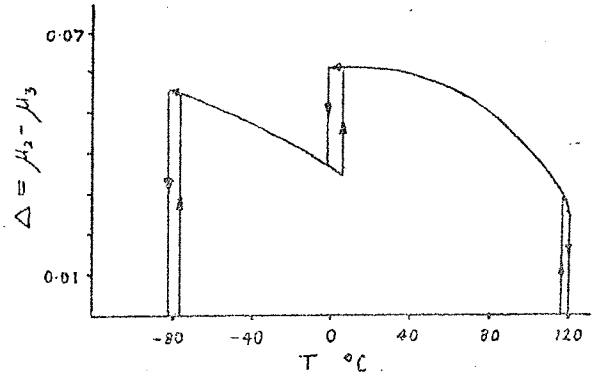


Figure 1.5.

Birefringeance

and the good electro mechanical coupling due to the high dielectric constant makes the material ideal for transducers which do not require exact frequency stabilisation. A ceramic form of barium titanate is usually used and can be fixed in a variety of shapes to be used in ultrasonic generators, loud speakers, delay lines, strains gauges etc.

1.2.5 Permitivity.

Permitivity is also a tensor property given by equation 1.3 where

$$D_i = \varepsilon_{ij} E_j \qquad 1.3$$

D is the electric displacement and E the electric field and the permitivity $\varepsilon_{ij}$ and dielectric constant tensor Kij are connected by equation 1.4 where $\varepsilon_o$ is the permitivity of free space. The values

$$\varepsilon_{ij} = \varepsilon_o K_{ij} \qquad 1.4$$

of the $\varepsilon_{ij}$ components are such that only those with i = j are non zero and $\varepsilon_1 = \varepsilon_2 \neq \varepsilon_3$ where $\varepsilon_3$ is the permitivity parallel to the unique tetrad axis in the tetragonal structure and $\varepsilon_1$ and $\varepsilon_2$ are parallel to the other main axis. The variation of $\varepsilon$, measured at a low voltage, with temperature is shown in diagram 1.4 after Merz (33). Above 120°C the permitivity falls rapidly but not discontinuously following the Curie Wiess law given by equation 1.5., where C is a constant of the order of $10^5$ deg, and $T_o$ the Curie Temperature. The permitivity is also a function of the applied field both below and above Curie temperature (34).

$$\varepsilon = \frac{T - T_o}{C} \qquad 1.5$$

1.2.6 Refractive Index and Birefringence.

At visible and ultra-violet frequencies it is normal to consider the optical constants instead of the dielectric constants but from Maxwells equations the two are related at any given frequency by equations 1.6 and 1.7. $\mu$ is the refractive index, k the extinction coefficient

$$\mu^2 - k^2 = K' \qquad 1.6$$

$$2\mu k = K'' \qquad 1.7$$

and $K'$ and $K''$ the real and imaginary parts of the dielectric constant respectively. $K''$ is proportional to the losses in the material and if these are small compared to $\varepsilon$ the approximation given in equation 1.8

$$\mu = \sqrt{K} \qquad 1.8$$

holds. Barium Titanate has a high refractive index with a peak value of 2.46 at the Curie temperature (Busch et al 1948) (35). In the non cubic forms below this temperature barium titanate exhibits double refraction. From equation 1.4 the permitivity tensor components are not all equal and the indicatrix, that is the geometric shape whose radius in a given direction is proportional to the refractive index in that direction, becomes an ellipsoid. In the orthorhombic form all three semi-axes of the ellipsoid are unequal and there are two special sections which are circular. Perpendicular to these sections the birefringence is zero and the two directions are called the primary optic axes of the crystal. In this form barium titanate is then biaxial. In the trigonal and tetragonal forms the indicatrix ellipsoid is formed by rotation of an ellipse, having only one circular section, so barium titanate is uniaxial. Birefringence measurements determine the differences between the principle refractive indices and are very sensitive. In barium titanate the birefringence is a function of temperature (36) and shows discontinuous changes coinciding with the structural transitions as shown in diagram 1.5 after Kay and Vousden (37). Above the Curie temperature barium titanate is cubic and optically isotropic.

1.2.7 Electro Optical Effect.

The indicatrix described in the last section is represented by equation 1.9 where Bij is the relative dielectric impermeability

$$B_{ij} x_i x_j = 1 \qquad 1.9$$

tensor the principle components of which are reciprical of the principle dielectric constant components and are related to the refractive index by equation 1.10. In general it is found that the

$$B_\ell = \frac{1}{K_\ell} = \frac{1}{\mu_\ell^2} \qquad 1.10$$

indicatrix is a function of the applied field (electro-optical effect) and the applied stress (photoelastic effect) and the changes are described by equation 1.11, where Zijk and $\pi_{ijkl}$ are the electro optical

$$\Delta B_{ij} = z_{ijk} E_k + \pi_{ijkl} \sigma_{kl} \qquad 1.11$$

third ranking tensor components and the photoelastic fourth ranking tensor components, $E_k$ is the applied field and $\sigma_{kl}$ the applied stress. The two properties are difficult to distinguish being inter-related and the size of the effect depends on the mechanical condition of the crystal. In practice the effects are usually measured using birefringence techniques when changes in $\Delta = \mu_2 - \mu_3$ with applied field are determined. The high electro-optical effect in barium titanate makes it attractive for an interesting application suggested by Wohlers and Leib (1964) (25) concerning the control of laser beams and called a "beam switch". The device uses the Fabrey-Perot principle to cut off light of a wavelength which is determined by the voltage controlled refractive index of the crystal. The same device could lead to a method of extracting information from a modulated laser beam.

## 1.3 Preperation of Thin Film Barium Titanate.

Considering the vast amount of literature written on bulk barium titanate surprisingly little work has been done on producing it in thin film form and most papers on the subject are very recent. A table comparing most of the previous preperations and the important properties of the films produced is given by Slack (38). The methods of preparation used can be divided into vacuum deposition and other methods. Most of these other methods are of little interest in this project, but for completeness they are briefly discussed below.

### 1.3.1 Non Vacuum Preparations.

Thin sections of barium titanate have been produced by Bursian et al (39), by grinding and etching single crystals down to thicknesses of a few microns. (~6). They found the hysterisis loop and permitivity

to be a function of thickness, the latter varying between 500 and 1500 over the thickness range. Barium titanate has been chemically precipitated (Section 2.1) from solution onto platinum by Luré (40) and crystallised on sheet platinum by the evaporation of potussium fluoride from a solution of $KF/BaTiO_3$ by Devries (41). Luré post baked his films of thickness 2-3.5 microns and observed a hysterisis loop and measured permitivity of 10,000. Titanate films have been produced by Hultquist and Sibert (42) using anodisation (Section 2.1) and films have been prepared on platinum by a slip casting technique at a temperature of 1600-1700°C in an oxygen atmosphere by Bursian and Smirnova (43). They produced films with thickness ranging from 5-50 microns and found permitivities between 4000 and 6000 and a hysterisis loop the shape of which depended on the slip thickness.

1.3.2. The Vacuum Deposition of Barium Titanate.

Of the papers previously published on the vacuum formation of barium titanate films, all but one author used an evaporation technique as the deposition process. The use of two main types of substrate is reported:- (1) metal surfaces. (2) non metal single crystals. The metal substrates were used in order to make electrical measurements on the films and the single crystals in attempts to epitaxially deposit the material. Consequently the growth and properties of the films are best considered in terms of this substrate classification.

1, 3.2.1. Metal Substrates.

All authors used either platinum or a platinum series metal, either in sheet form or deposited as a thin film on quartz or some other glassy material. The first vacuum deposition of barium titanate by Feldman (44) used unheated platinum sheet as the substrate and evaporated from a resistively heated hungsten filament source (Section 2 2.1). A variation of composition occured through the thickness of these films due to dissociation of the titanate and considerable tungsten contamination was present in them. The films of 1-2 microns thickness were reacted by post

baking in air to 1200°C before any electrical measurements were made. A dielectric constant of 230 is reported which seems very low considering the ferroelectric nature of the films, indicated by the observation of a hysterisis loop and a peak in permitivity at around 120°C. Sekine and Toyoda (45) have also evaporated barium titanate from a tungsten source while Masson and Minn (46) and Muller et al (47) used flash evaporation from iridium sources. (Section 2 2.4). Sekine and Toyoda reported the appearance of crystalline growth in films deposited on platinum when either the substrate temperature or post baking temperature exceeded 500°C. Electrical measurements were made on films 2-3$\mu$ thick which had been post baked above 1000°C. Films baked at 1000°C had a dielectric constant (K) of only 20 while those baked at 1200° had K's up to 1500. One film baked at 1200°C containing 5% strontium showed a hysterisis loop and permitivity anomalies at the bulk transition temperatures of 120°C, 0°C and -80°C. Mason and Minn found crystal growth present in films deposited at ambient temperatures and then post baked in air at a temperature of 500-600°C or in situa at a substrate temperature of 600-700°C and in a partial pressure of oxygen. These films were again not ferroelectric unless baked to 1200°C after which a peak in permitivity at 120°C also occured. The dielectric constant of the films, which were 1.5$\mu$ thick, was only 100-300. Müller et al reported dielectric constants K of 400-700 depending on thickness for films deposited above 350°C while films deposited below 350°C had K's of 20 but lower dc leakage currents. Feuersanger et al (48) deposited barium titanate onto platinum held at a temperature in excess of 800°C and in an oxygen partial ptessure by simultaneously electron beam evaporation from two sources, one charged with barium oxide and the other with titanium dioxide. After subsequent heat treatment to above 1000°C dielectric constants of about 1000 were measured but no ferroelectric behaviour was observed. The first reference to the deposition of barium titanate by sputtering is found in a short note by Vu Huy Pat and Baumberger (49). They R.F. sputtered barium

titanate onto room temperature platinum substrates and reported both a dielectric constant of 1600 and the observation of a hysterisis loop only after post baking to an unstipulated temperature. Two other papers reporting the sputtering of barium titanate have been published during the later stages of the present work by Shintani and Tada (50) and Pratt and Firestone (51) while Toombs (52) reported on sputtering barium lanthanum titanate. Shintani et al and Toombs both used diode DC sputtering (Section 2 3.4) from reduced targets while Pratt et al used RF triode sputtering (Section 2 3.5) all depositing on heated platinum substrates. Shintani reported dielectric constants as high as 1700 for films deposited at 1000°C while Pratt found a variation of K from 16-300 for films deposited from room temperature to 900°C and K up to 1900 if the films deposited at 500°C were post baked to 1400°C. Toombs reported K below 100 up to a deposition temperature of 500°C and up to 200-250 at temperatures of 700°C for $Ba(La)TiO_3$. No definite ferroelectric behaviour was observed in any of these experiments and both Pratt and Toombs also reported severe cracking of the films at high deposition temperatures.

1 3.2.2 Single Crystal Substrates.

The crystalline growth of barium titanate thin films has been observed at lower temperatures on some single crystal substrates. Epitaxial growth of single crystal or textured polycrystal films has been reported by Brown (53) Müller et al (54) and Slack (38) all using a flash evaporation deposition technique. Brown deposited on alumina and silicon and observed distorted hysterisis loops and epitaxial growth only for films deposited on silicon at 900°C and post baked to 1000°C. Müller and Slack both deposited on sodium and lithium fluorides single crystals and reported epitaxial temperatures of 550-600°C on both crystals. Müller et al deposited on a number of other crystals Ge, Si, NaCl, $CaF_2$, PbS, MgO and mica but found the films to be only polycrystalline. They also reported epitaxy at 630°C

on gold films epitaxed in the (100) plane on lithium fluoride, but found the structure mechanically unstable if the Au or $BaTiO_3$ were thicker than about 200 Å. No electrical measurements could be made on these films because of the substrate material. Slack overcame this difficulty and made measurements on films deposited on sodium fluoride, NaF, by separating the films from the crystal. This was achieved by floating the films off NaF in water, picking them up and silver pasting them down onto a metal sheet. Metal was then evaporated through a mask onto the films to form top electrode areas. The dielectric constant, K, was found to be a function of film thickness varying from 65-400 in the thickness range 0.1 - 0.8 microns using pure $BaTiO_3$ and between 40 and 150 using 98% pure $BaTiO_3$ as the starting material. The films were ferroelectric, hysterisis loops and switching transients being observed, but showed no peak in permitivity at 120°C.

1.3.3 Summary of the Properties of Thin Film Barium Titanate.

Measurements made on thinned down bulk crystals and cast barium titanate slips indicate that the ferroelectricity permitivity and other properties of the material become a function of thickness as it is reduced to 1-10 microns (43, 55). It has even been suggested by Ivanchik (56) that there should be a thickness limit below which the small crystallites in the film would cease to be switchable. Films of thickness less than a few microns can only be produced by vacuum deposition. There is some general agreement but much detailed inconsistency in the properties reported for such films of barium titanate. In all cases deposition at ambient or below a given temperature is reported to lead to an amorphous film structure. Above this temperature, which is a function of substrate material, the film growth can be polycrystalline, textured polycrystalline or even single crystal in nature, again depending on the substrate. There is general agreement that crystal growth on platinum is polycrystalline but the

film crystallization temperature reported varies from 400°C (47) to 700°C (46). The dielectric constant of amorphous barium titanate is ≤ 20 but the value reported for polycrystalline films on platinum show very large variations. Sekine and Toyoda (45) reported the value of 20 unaltered even after baking to 1000°C. Only after baking to 1200°C is the dielectric constant increased to 1500, while other authors report much higher values without baking 400-700 (47), 300 (51), 1000 (48), 1700 (50). Ferroelectric behaviour was not observed in any films deposited on platinum that were not baked to 1200°C. Vu Huy Pat et al reported ferroelectric behaviour in sputtered barium titanate but other authors failed to verify this even after baking to 1400°C. Most films showed some permitivity anomaly around the Curie temperature of barium titanate whether or not they showed ferroelectric behaviour. Barium titanate can be epitaxially deposited on silicon and on sodium or lithium fluoride, with crystallization temperatures of 900°C and 500-600°C respectively. Films deposited on silicon are ferroelectric only after baking and had a dielectric constant of 100. The titanate films deposited on sodium fluoride were the only films reported to be ferroelectric without post baking and had dielectric constants a function of film thickness. Little work has been done on the conductivity of any titanate films but generally amorphous films are reported to have a much higher resistivity than crystalline films.

# CHAPTER TWO

# THIN FILM TECHNOLOGY

## 2.1 Thin Film Processes.

The term thin film is usually taken to mean layers with thickness ranging from less than a monolayer to several microns ($10^{-6}$m), which are deposited on a substrate some $10^{3}$ times or more thicker, and there are numerous processes available for producing such films. The very first films in this range of thickness were produced by chemical or electrochemical methods and these and processes of a similar type are still commonly used. Such processes are (1) Electroplating (2) Chemical reduction, (3) Electroless Plating, (4) Vapour Plating. All of these methods are not compatible with other microelectronic and integrated circuit processes due to the high temperatures involved or the necessary emmersion in solution and have been rejected as deposition methods in this investigation. Another method of doubtful compatibility because of the solutions used but of interest as an oxide forming process is anodization. This process is similar to electroplating and the apparatus used is generally the same. It is found for some metals, used as anodes, instead of their ions dissolving they react with oxygen ions from the solution forming an adherent oxide coating on the anode. The layer thickness is limited and is dependant upon the applied voltage. Anodization is used for forming protective coatings and for producing dielectric layers for some thin film capacitors.

## 2.2 Vacuum Evaporation.

Vacuum evaporation requires much more sophisticated equipment than most of the methods mentioned before, but it is equipment that is becoming increasingly commonplace in research and development laboratories. The first requirement is to reduce the pressure in a deposition chamber some $10^{6}$ times or more using vacuum pumps and traps, and vacuum evaporation did not become popular until advances in vacuum technology in the early twentieth century made this possible. The necessary vacuum techniques

will be discussed later. The charge of material to be deposited is held in a suitable container and heated by some means until the charge melts, and then evaporates. A substrate is placed in the chamber such that a film condenses on it. Any deposit pattern can be prepared by the use of a mask placed close to the substrate surface. There are various means of heating the charge and these and their suitability to the preperation of barium titanate thin films is discussed in the following sections.

2.2.1. Resistive Heating.

In this case a high current is passed through a filament or boat made of a refractory metal in which the evaporant charge is situated and the Joule heating effect is used to evaporate it. Numerous types of boats and filament are commercially available for this purpose. Alternatively the charge sits in a ceramic crucible and is heated by radiation or conduction from a filament. Barium titanate and many of the materials used in microelectronics are such that they cannot be evaporated from these normal sources because of their high melting point, approaching that of the refractory metals, or because they alloy or chemically react with both metal and ceramic sources causing source destruction. One method of heating the charge designed to overcome this difficulty is the electron beam evaporation source.

2.2.2. Electron Beam Evaporation.

Electron Beam Evaporation is a deposition technique in which the charge is directly heated by a high energy beam of electrons. Various experimental arrangements have been described.[57,58,59] This method has the advantage for high melting point materials that the charge is not heated via a boat or filament and is hotest at the point evaporating. Indeed in some arrangements the hearth holding the charge is water cooled. The electron beam can be bent by a permanent magnet and focused on the charge so that the hot filament is out of direct line with the source or substrate thereby removing the possibility of tungsten contamination.[58,60]

2.2.3. Evaporation of Dielectrics.

Most dielectrics have high melting points approaching those of the refractory metals and this limits the source materials that are useable. Dielectrics are also compounds and it is found when a compound is evaporated it fractionally distills depending on the individual vapour pressures of its components. The vapourisation rate Ra of an individual component "a" is given by equation 2.1 (61) where C is a constant, $p_a$ is the partial pressure of the component, $M_a$ its molecular weight and T the temperature. In the case of metal oxides loss of

$$R_a = C p_a \sqrt{\frac{M_a}{T}} \qquad 2.1.$$

oxygen may occur either due to dissociation or to reduction by the source material and the film will be deposited as a mixture of the oxide, a lower oxide, the parent metal and oxides of the source material. The rate of reaction with the source depends upon the free energy of oxidation of the metal used and decreases for the refractory metals in the order tantalum, niobium, molybdenum, tungsten, rhenium, and iridium. Electron beam evaporation removes any problem of high source temperatures due to the melting point of the dielectric. However, under electron bombardment, because there is no path for the electron current to drain away a dielectric would charge up preventing any further bombardment. This problem has in fact been overcome by a number of means but compounds still suffer dissociation, in fact the situation is worse because of the presence of a beam of ionizing electrons. An evaporation process developed specifically to overcome fractional distillation is flash evaporation.

2.2.4. Flash Evaporation.

Flash evaporation is the term used to describe a method of thin film formation which is actually a series of discrete evaporations each of a small mass of a compound. A metal boat is held at a temperature in excess of that required to evaporate the compound, and small grains or pellets of the compound are dropped at a given rate on to the boat.

The evaporation of each pellet is instantaneous, or at least all of one pellet has evaporated before the arrival of the next. This means despite any dissociation of a given pellet the correct proportion of the compound constituents will be arriving at the substrate over any normal time period. Alternatively the grain delivery rate and boat temperature can be controlled so that a liquid pool of the compound is allowed to form but is maintained at a constant size. In time the composition of the pool reaches an equilibrium such that the vapour leaving it has an overall composition, the same as the arriving grains (47). Either system requires a mechanical method of delivering the grains or pellets at a constant and controlled rate opperating within the vacuum chamber. The evaporation rate will generally be lower than for any ordinary process.

2.2.5. The Evaporation of Barium Titanate.

Barium titanate has a melting point of 1620°C and under vacuum requires a vapourising temperature of approximately 2200°C which is approaching the melting point of most of the refractory source materials in common use. They will consequently have a high vapour pressure at the vapourising temperature, for example molybdenum $5.10^{-3}$ torr, tantalum $1.10^{-6}$ torr and iridium $3.10^{-4}$ torr, and this will lead to metallic film contamination. As described in section 2.2.3 at this temperature barium titanate will also be chemically reduced by all these materials. It is found for instance that molybdenum, tantalum and niobium are quite quickly completely destroyed by the reaction. The Titanate is a mixed oxide comprising of the two simple oxides titanium dioxide, $Ti\ O_2$ and barium oxide, Ba O. Barium oxide melts at 1923°C but sublimes at 1539°C with a vapour pressure of $10^{-2}$ torr, while titanium dioxide does not reach a comparable vapour pressure below 1729°C. Consequently dissociation is inevitable using conventional thermal evaporation and, as reported by Feldman (44) films are

graded in composition. The only method that would seem feasible is flash evaporation with careful choice of materials because even higher metal temperatures are required than the conventional source, in order to ensure instantaneous evaporation of each pellet. Molybdenum, tantalum and niobium are unsuitable as described and tungsten results in highly contaminated films, 10-20% tungsten oxide impurity (47). Iridium and rhenium have been used in flash evaporation sources but contamination is still reported. The former leads to iridium levels approaching 2% while rhenium sources give films with up to 1% contamination.

## 2.3. Sputtering

Sputtering is the ejection of atoms or molecules from a target when bombarded by energetic particles. The phenominum wasdiscovered many years ago by Grove (62) and was first used for depositing thin films as early as 1877 (63) when the degree of vacuum attainable was such that thermal evaporation was not possible. However, when improved pumping systems produced lower pressures, thermal evaporation became the major technique for thin film production. Indeed, sputtering fell out of use for this application and was considered "dirty", due to the higher pressure necessary and high sensitivity to contamination in the usually used glow discharge sputtering arrangement. But since about 1950 improved technology and the increased interest in refractory metals for electronic application, which are impossible to evaporate by the normal method, have led to a revival of low and high pressure sputtering as techniques for thin film deposition.

### 2.31. Theories of Sputtering.

Originally, it was thought that the bombarding ions caused local hot spots called thermal spikes on the target surface and sputtering was due to the thermal evaporation of target material from these areas (64, 65). This would mean the ejected atoms should show a cosine angular distribution and have a Maxwellian velocity distribution. Also

there would be a variation of sputtering rate with the heat of sublimation of the target material. Study of the velocity distribution of sputtered atoms was not possible at the time because the ejected atoms are electrically neutral, but before such experiments were performed sputtering phenomenae were observed which were inconsistant with thermal evaporation. Webner (1955) (66) and others studied the sputtering of single crystal targets and found that the atoms were ejected preferentially in certain crystalographic directions, usually associated with the planes of closest packing in the crystal. Indeed even for a polycrystalline target Webner (67) found the ejected atoms had a non cosine distribution. A theory was first proposed by Stark (68) in 1909 involving the direct transfer of momentum from the bombarding ion to the atoms of the target. Silsbee (69) in 1957 had pointed out that the transference of momentum in a crystalline solid might be strongly influenced by the well ordered lattice of the crystal and had introduced the idea of the momentum being focussed into certain crystalographic directions, consisting of close packed rows of atoms. This theory was further supported by other experimental facts; namely that the energies of sputtered atoms, typically 10eV are much greater than from corresponding thermal evaporation 0.2eV; that there is a threshold energy of bombarding ions below which sputtering does not occur; that there is then a region where sputtering rate is proportional to ion energy and that at higher ion energies the rate saturates and then decreases presumeably due to deep ion penetration and consequentlymore energy loss within the target. While the details of the theory of sputtering is still a matter for debate it is now more or less accepted that the ejection of the sputtered atoms or molecules is due to a momentum transfer process consisting of a number of collisions in the target which can be to some extent focussed by the regular atomic arrangement of the target.

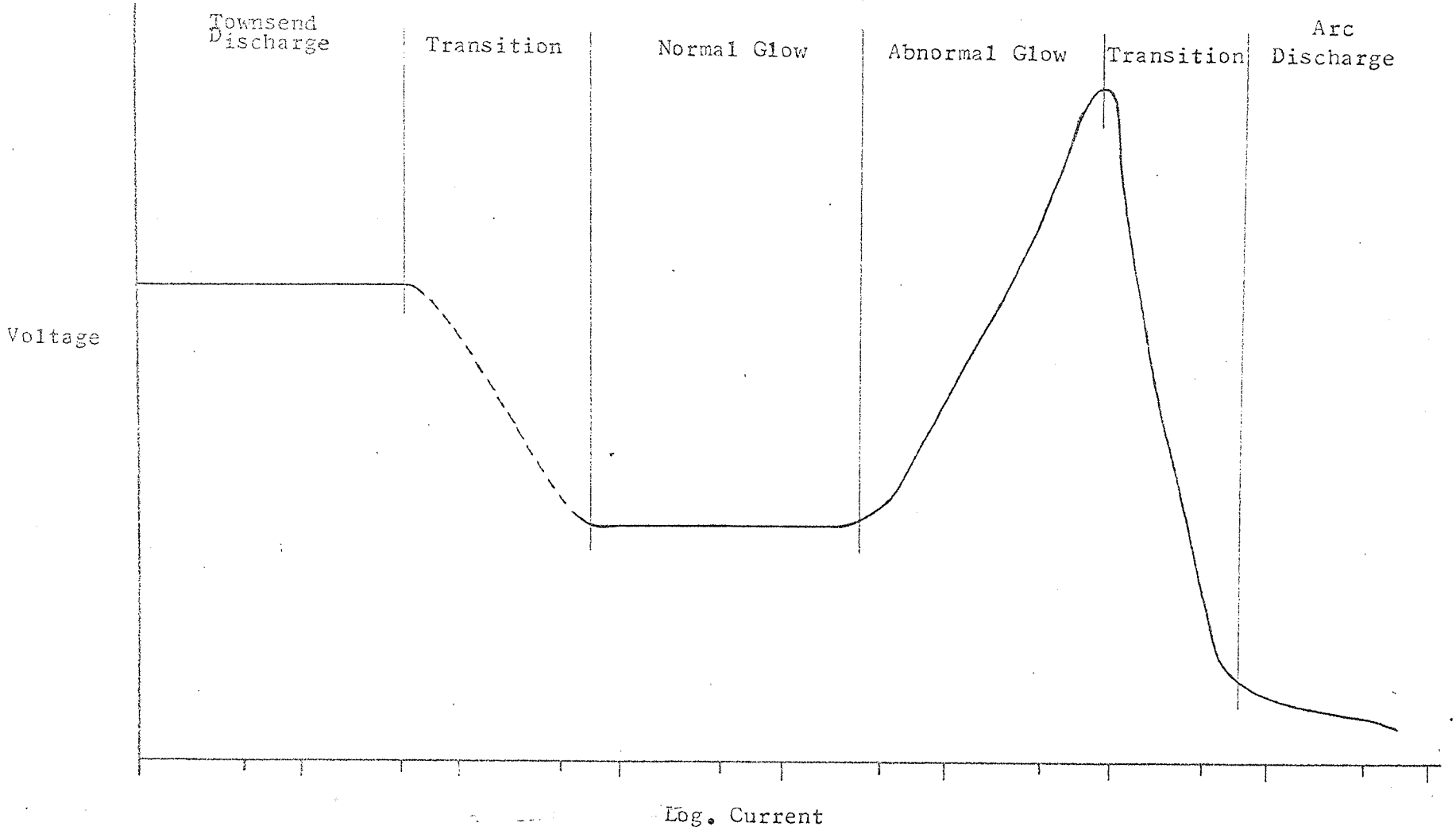


Figure 2.1.

Characteristics of a Glow Discharge.

2.3.2. The Glow Discharge.

A simply produced source of ions for sputtering purposes is a glow discharge. There are many phenonenae which can occur in gas discharges depending on the pressure, the applied voltage and electrode configuration and numerous review papers (70) have been written on the subject. Only those phenomenae relevant to the use of glow discharges for sputtering will be mentioned here. When a potential is applied between two parallel plates in a gas at a low pressure the resulting voltage-current pressure characteristics can be split into a number of regions as shown in figure 2.1. The discharge consists of several light and dark areas called glows and dark spaces, as can be seen in figure 2.2(a). Figures 2.2(b) and (c) show the variation of potential and light intensity along the length of a discharge. Most of the potential is dropped across the Crookes dark space and it is here ions are accelerated towards the cathode. Sputtering is performed in the abnormal glow region of the characteristics when all the cathode is covered by the cathode glow. Increase in current can only be obtained by an increase in voltage given by equation 2.2. where V is the voltage,

$$V = A + \frac{B\sqrt{j}}{p} \qquad 2.2$$

j the current density, p the pressure and A and B constants. The length of the Crookes dark space (d) is determined by the mean free path of electrons leaving the cathode. The mean free path is inversley proportional to pressure, so as the pressure in a discharge is decreased this dark space grows until the plane of the anode enters it, when the discharge is extinguished. In the normal glow the product pd is a constant, for argon~0.3 torr. cms. However in the abnormal glow region the product pd is also a function of voltage and is given by equation 2.3.

$$pd = C + \frac{DB}{V-A} \qquad 2.3.$$

where C and D are also constants. For sputtering it is usually arranged that the anode is positioned in the cathode glow at a distance approximately 2d from the cathode as this position tends to give the best

Figure 2.2.(a)

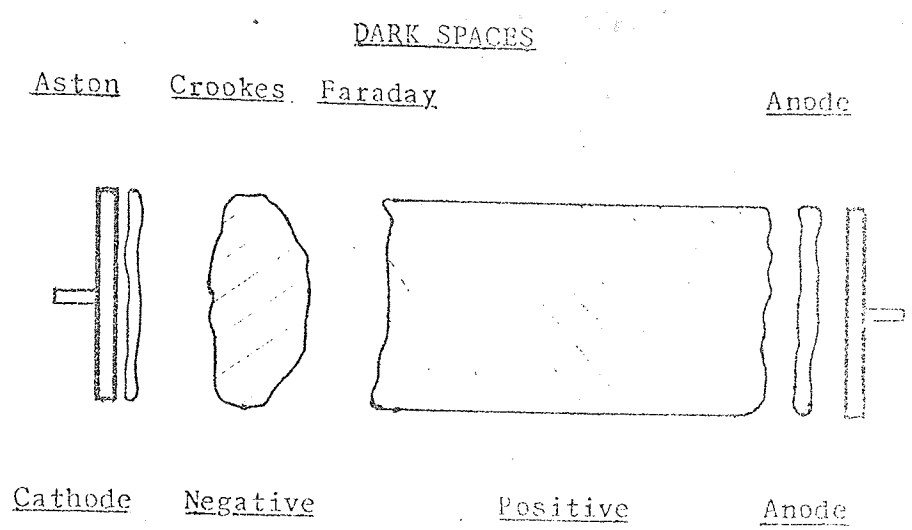


Figure 2.2.(b)

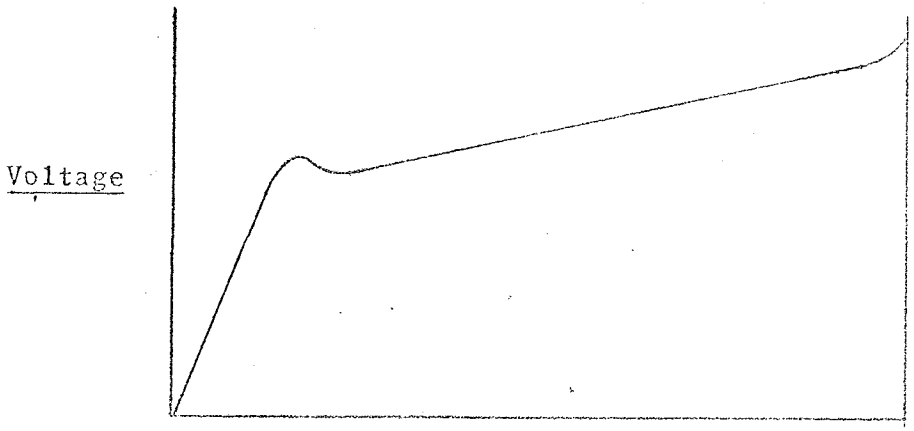


Figure 2.2.(c)

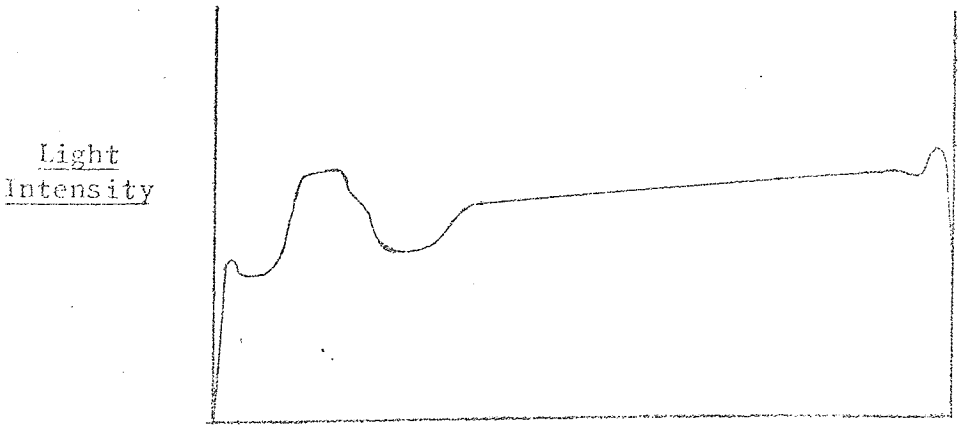


Figure 2.2.

Properties of a Glow Discharge.

uniformity of deposition. The fact that at distances less than d the discharge is extinguished is used to effect by placing any earth shielding at the back of the target and around the high tension lead through conductors at a distance less than d so that no discharge will occur. It should be noted that the bombarding ions will suffer collisions with the gas atoms of the discharge gas and the number of collisions will increase with pressure. This is also true of the sputtered atoms and puts an upper limit on the pressure because eventually they will begin to be prevented from reaching the anode. Since ions and electrons have vastly different masses recombination in the discharge is uncommon and the discharge will spread to the sides of the chamber or other obstructions where recombination is easier. This is undesirable as it reduces the number of ions and hence the sputtering rate, so objects intruding into the discharge should be avoided.

To maintain a discharge at pressures below the normal range 10-100 millitorr a number of methods can be used. The number of electrons can be increased by use of a thermal source of electrons, the ionisation probability can be increased by the use of a magnetic field or the discharge can be run at R.F. frequencies. All three techniques allow the discharge to be run at lower pressures 0.5-10 millitorr and will be more fullydiscussed later.

2.3.3. Diode Sputtering.

This is the simplest form of sputtering apparatus and consists of the two plane parallel plates of a glow discharge with a seperation of approximately 2d. The cathode acts as the target and is made of the material to be sputtered. The cathode receives a high negative potential while the substrates are placed on an earthed anode plate. The operation of such a system is to pump the chamber down to as low a pressure as possible and then bleed gas, usually argon, into the chamber to the required pressure normally 20-100 millitorr. Apart from the problem

of collisions due to the high pressure, it also gives a high probability of gas inclusion in the resulting film. As a result, more sophisticated systems such as triode sputtering were developed to reduce the pressure needed.

2.3.4. Triode Sputtering.

In order to increase the mean free path of the ions and sputtered atoms and decrease the probability of gas atom inclusion, the pressure needs to be down to a few $10^{-3}$torr. To produce a discharge at this pressure the number of electrons or their ionising efficiency has to be increased. In triode sputtering this is done by striking the discharge between a thermionically emitting hot cathode at earth potential and an anode at a positive potential, introducing the target as a third electrode which can draw ions out of the existing discharge. The discharge can be confined by a longitudinal magnetic field ( 0-200 gauss) which will also increase the path length of randomly moving electrons and hence improve their ionising efficiency. With this arrangement first used by Ivanov et al (71) the anode potential need only be 0-100 V and the sputtering rate can be changed by altering the target voltage with no direct effect on the discharge. The substrate is placed opposite and parallel to the target and the sputtering pressure is such that it can be placed at a distance within the mean free path of the ejected atoms (~5 cms at $10^{-3}$torr). However the increased complexity is a disadvantage as the electron source, usually a tungsten filament has to be water cooled, and so does the anode and possibly the target.

A number of geometrical electrode arrangements have been suggested (72) and many papers have been published on the use and properties of triode sputtering systems (73,74,75).

2.3.5. Tetrode Sputtering.

It has been reported by Muly and Aronson (76) and others that the introduction of a fourth electrode as a grid or auxillary anode situated

just above the anode in the triode arrangement further improves system properties. Operation is then possible down to $2.10^{-4}$ torr with improved stability and with target voltage having even less effect on discharge characteristics.

2.3.6. Bias Sputtering.

If, in any of the systems mentioned, the substrate is biassed negatively with respect to the anode the film being produced will be continually ion bombarded during deposition. The effect of the bombardment will not only be, to some extent sputter the growing film but also to remove contaminants from the film surface, in a similar way to discharge cleaning ref (77). This idea was first suggested by Freichs (78) and has been shown to improve film properties (79) and, in the case of gold deposition on sodium chloride, to improve epitaxy (80).

2.3.7. Getter Sputtering.

The efficient gettering action of freshly prepared films for reactive gases was used to advantage by Theurer and Houser (81) to reduce the partial pressure of exygen and other gases to as low as $10^{-10}$ torr near the substrate compared to the chamber pressure of $10^{-6}$ torr. The technique employs a metal enclosure within the vacuum chamber and an auxillary target which, when sputtering, getters the reactive gases entering the inner enclosure, in which the main target is situated and film deposition takes place.

2.3.8. Reactive Sputtering.

All metals and most semiconductors can be deposited as thin films by the methods so far mentioned, but dielectric films present a new problem. A dielectric target could not conduct away current, and positive ions bombarding it would build up a surface charge neutralising the accelerating potential until after a very short time the ion bombardment would cease. Some dielectric films, however, can be produced by sputtering using a technique fairly recently reviewed by Kay (82) and Schwartz (83) called reactive sputtering. The target is still metallic

but a reactive gas is mixed with the inert gas of the discharge and reacts with the metal atoms being sputtered. The reaction can occur at the target, at the substrate, or in flight. The technique has been used sucessfully to deposit oxides, (84,85,86) sulphides, (87) nitrides (88) and other compounds. For more complicated compounds such as perovskites however, the production of films with the correct stochiometric ratio becomes very difficult. But the sputtering of almost any material became feasable with the development of Radio Frequency Sputtering.

2.3.9. Radio Frequency Sputtering.

The build up of positive charge on a dielectric target can be overcome by the use of a high frequency accelerating potential. This was first suggested by Webner (89) and then demonstrated by Anderson et al (90). However Davidse and Maissel (91) were the first to describe the application of the technique to the deposition of dielectric thin films. Radio Frequency fields can be applied to any of the sputtering systems discussed.

2.3.9.1. Theory of R.F.Sputtering.

Any insulator or insulated conductor placed in a gas discharge must, in equilibrium, float at a potential, with respect to the plasma, which ensures it receives equal numbers of positive and negative charges. The insulator thus becomes slightly negative, because otherwise the electrons, with a higher mobility than the ions would have a higher probability of striking the insulator surface. As a result insulated components in a glow discharge are under slight ion bombardment, a fact made use of in ion bombardment cleaning (77). The bombardment energy is enough to remove weakly bound contaminants but is insufficient to produce any sputtering. R.F. Sputtering relies on increasing this self biassing to values sufficient to cause sputtering of a dielectric target. The method used is to place the target over a conducting plate to which the high frequency potential is applied.

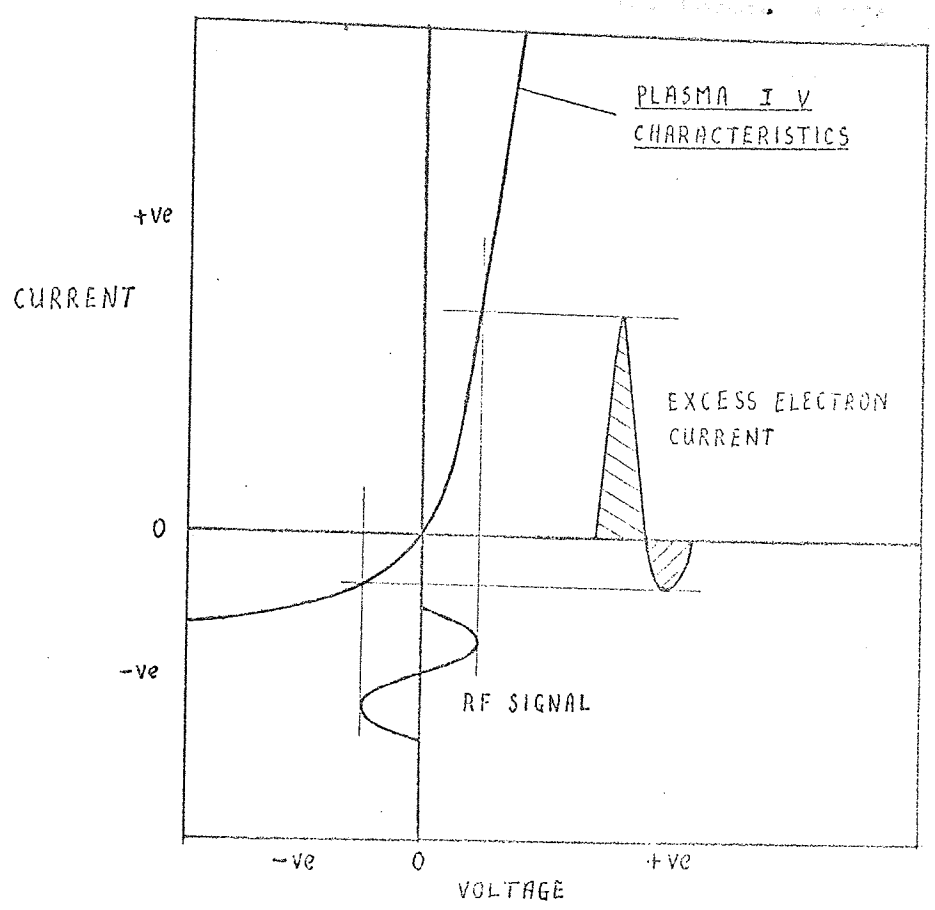


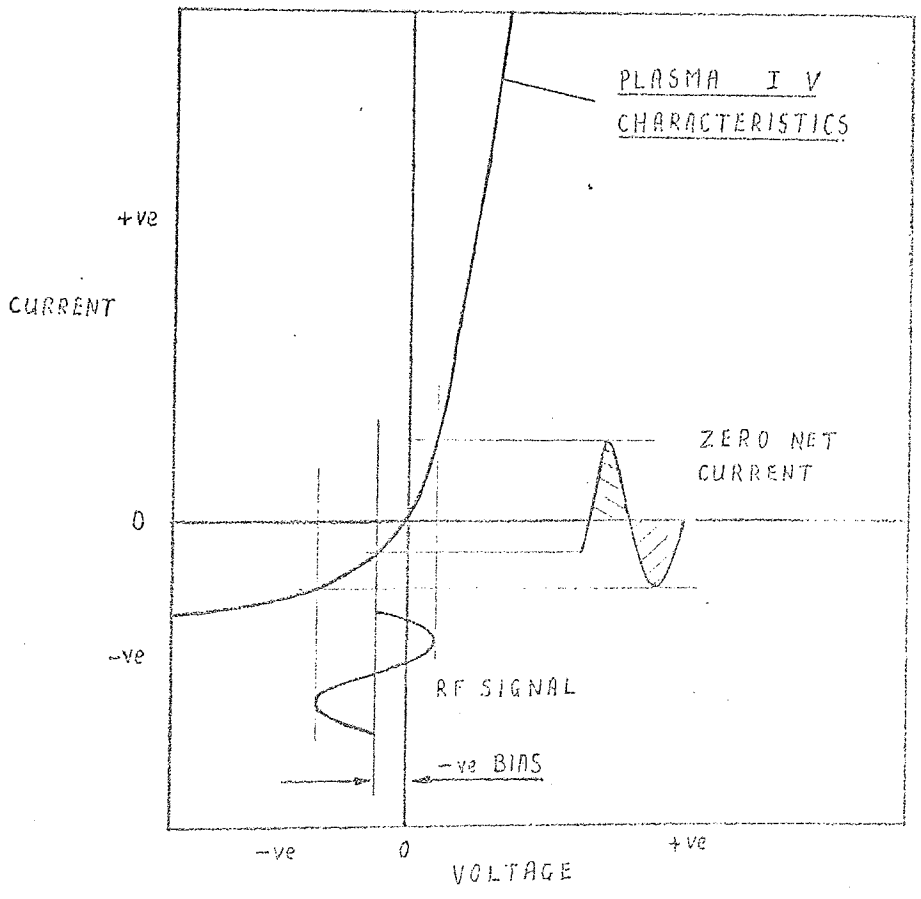


Figure 2.3.

Self Biassing of a R.F.Electrode in a Discharge

To reach equilibrium, the target surface will bias negatively until it receives no net charge from the plasma, forming a positive ion sheath around the dielectric. The process was explained by Butler and Kino (92) with the aid ofadiagram, (figure 2.3.) which shows the biasing necessary for equilibrium. They also developed a theory to quantitatively explain the effect. Anderson et al (90) indicated the frequency required for effective sputtering by considering the ion transit time, and the variation of sheath thickness with time, and argued as follows: The ion sheath will extend into the plasma a distance d varying with time roughly as indicated in figure 2.4. A positive ion will be accelerated towards the target only when the sheath extends beyond its position and will in general take several cycles before it reaches the target. Consequently the ion energy on reaching the target will be less than that equivalent to d max and there will be a large spread in ion bombarding energies. If we assume that the ion current is constant with time the target potential in the negative half cycle region will decrease due to positive charge build up at a rate given by equation 2.4. where I is positive ion current

$$\frac{dV}{dt} = -\frac{I}{C} \qquad 2.4.$$

and C target capacity. Using typical values for I and C of 20mA $cm^{-2}$ and 20pF $cm^{-2}$ we find the rate of fall of potential is $10^{9}$ $V.sec^{-1}$ . Taking the condition that we do not wish the fall to be more than 100 V, before the polarity reverses, then the frequency required is of the order of 10 M.Hz.

2.3.9.2. Electrode Arrangements for R.F.Sputtering.

The method used by Anderson (90) in the original suggestion of R.F.Sputtering was to introduce a dielectric target into a supported low pressure discharge as in triode sputtering. But Davidse and Maissel (93) noted that at sufficiently high pressures (~$110^{-2}$ torr) a self sustained glow discharge could be initiated and maintained using an R.F. target as the cathode of a diode sputtering arrangement. Further-

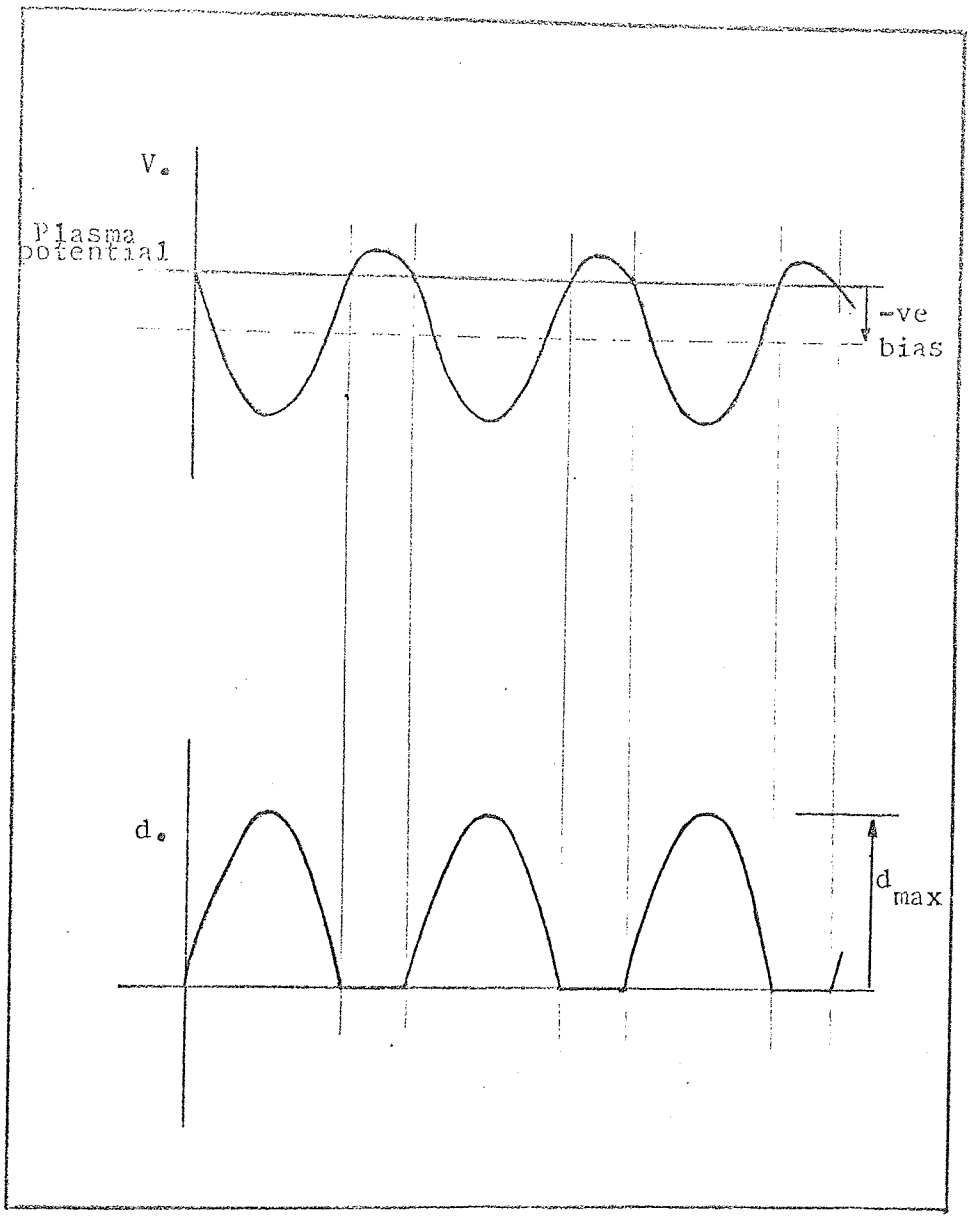


Variation of target potential (V) and positive ion sheath thickness (d) with time.

Figure 2.4.

more the operating pressure could be reduced, to the order of $1.10^{-3}$ torr, by the application of a magnetic field (up to 200 gauss) normal to the target. The magnetic field also had the effect of confining the glow, increasing its stability and allowing easier tuning of the R.F. They also found that unlike D.C. sputtering, where for a given deposition rate, the power required is a function of area only, the shape of the target had a considerable effect on rate, circular targets being much preferred. The R.F. electrode needs to be water cooled because of the high dissipation of energy occuring at its surface during ion bombardment and this means some complication in electrode and feed through design. To prevent sputtering from or breakdown to the back of the metal R.F. electrode it has to be shielded and to prevent excessive temperature rises during deposition the shielding usually also has to be water cooled.

2.3.9.3. Grounded or Non Grounded Electrodes.

The R.F. potential, in both triode and diode systems so far mentioned, is connected between the target electrode and earth. The self capacity of the dielectric target causes the negative D.C. bias which leads to plasma ion sheath formation and hence sputtering. However in this symetrical arrangement all earthed parts of the vacuum system could also feed R.F. power into the plasma forming sheaths which could result in undesirable sputtering. In view of this Holland, Putner and Jackson (94) suggested an arrangement in which the R.F. potential is fed to two non grounded electrodes forming two halves of the target electrode. The electrodes can be two semicircular "D"s or an inner disc and outer anulus, both of which arrangements can have a circular target placed in front of them. They found the disc and anulus preferrable because the high fields at the corners of the "D"s made that arrangement susceptible to electrical breakdown. Another arrangement of non grounded electrodes is as the two halves of a roof, but in this case two targets are required one for each electrode. The advantage of non grounded

electrodes is dubious as the arrangement will probably behave as two seperate R.F. sputtering systems coupled to earth, as though the centre of the feeding R.F. tank coil was connected to earth. This has been pointed out by Toombs (95) who also showed that sputtering of earthed parts of a grounded system is unlikely as even with equal areas of target and earthed components, the highest bias expected under typical conditions is 20 eV, which is below the threshold sputtering energy for anything other than atomically clean surfaces. However his argument based on maintaining charge neutrality in the plasma at all times and neglecting transit times is oversimplified and itself somewhat doubtful. But in any practical situation the area of the earthed components is much larger than the area of the target and both must receive the same total current. Consequently the sheath voltage around the earthed parts will be much smaller than on the target. Indeed no contaminants from earthed components have been found in films deposited with a diode grounded system (95) and a film builds up on substrate supports and other earthed parts of the system during deposition.

The various arrangements for sputtering are shown in figure 2.5. A number of systems are commercially available, a triode system is marketed by C.V.C. called "Plasmavac", a normal diode system by M.R.C. Polaron while balanced non grounded systems are produced in disc and anulus form by Edwards High Vacuum and in roof top form by Varian, called "Plasma Peak".

2.3.10. The Advantages of Sputtering.

Sputtering has numerous advantages over evaporation as a thin film deposition technique for use in device or thin film circuit production both as a process and because of the improved properties of the films produced. A major production advantage is the absence of very hot sources and associated assemblies and the corresponding lack of wear and distortion caused by them. Other advantages are listed over.

(1) Versatillity.

Sputtering can be performed in many modes chosen to suit particular applications and practically any material can be deposited by one or more of the various arrangements already described. It can be used to deposit refractory materials that could not be simply evaporated. Furthermore this deposition can be accomplished with the material at room temperature or less. This includes high melting point dielectrics which can be deposited by reactive or R.F. sputtering.

(2) Controlability.

Sputtering is a comparatively slow process and the deposition rate is a strict function of target voltage at a given pressure. Consequently rates and film thicknesses can be much more easily controlled than for evaporation. Rates as low as less than 10 Å per second can be accurately controlled and reproduced.

(3) Alloy or Compound Deposition.

In the evaporation of alloys or compounds it is extremely difficult to maintain the correct composition or stoichiometry, (section 2.3.4) but sputtering does not suffer from this disadvantage. This is because sputtering is a "cold" process and dissociation temperatures are not reached and the sputtering of components is a function of their individual sputtering yields which are similar (96), certainly of the same order of magnitude. It follows that alloys and compounds can be much more easily deposited in controlled and known compositions using sputtering and many examples are available (97,98,99).

(4) Adhesion.

One of the basic requirements in thin film work is a good adhesion between film and substrate. Adhesion is difficult to measure quantitatively but it is generally acknowledged that sputtered films adhere better than do evaporated films. This is probably a function of much higher depositing atom energies (up to 10eV cf 0.05 eV) but could also be associated with charge effects. Chapman (100) has also shown that

sputtered films have a higher resistance to scratching.

(5) Epitaxy.

Epitaxial films are those whose crystal structure is influenced by the structure of the substrate. Due to the island nature of film growth (101) films are normally polycrystalline because the islands are randomly orientated. However under the influence of certain substrate structures the islands form in an aligned or orientated manner producing textured or single crystal films. The uses of such films are numerous (102) and their production has received much attention (103). Factors influencing epitaxy are the nature of the substrate, substrate temperatures and deposition rate (104). It has been found that for a given deposition rate sputtered films epitaxiat much lower substrate temperatures (105, 106, 107). The effect is thought to be again due to the higher atomic energies involved and due to the substrate cleaning action of the discharge. As an example silver deposited at 0.2 Å per second on sodium chloride epitaxes at 150°C when evaporated but is epitaxial at room temperature when sputtered.

2.4. Summary of Processes Suitable for the Deposition of Barium Titanate.

Due to the high melting point and compound nature of barium titanate normal evaporation processes cannot hope to deposit pure or stoichiometric films of the material. The only really feasible evaporation process for compound materials is flash evaporation but this process still produces contaminated films. Using evaporation processes, crystalline films of barium titanate have been deposited on single crystal alkali halides at temperatures in excess of 550°C and on platinum or platinum films only with post deposition baking to above 900°C. Sputtering is a deposition process better suited to producing stoichiometric films of compound materials and should also produce epitaxy at lower substrate temperatures. Sputtering is also a more controlable process particularly if low deposition rates are required in order to improve film crystallinity. Of the sputtering processes

only reactive or R.F. sputtering can deposit insulators. Barium titanate is a complicated double oxide which would probably prove difficult to deposit using reactive sputtering but should be easily deposited using R.F. sputtering. R.F. sputtered insulators are reported by Pliskin et al (107) and others (108,109) to have better physical and electrical properties than evaporated films of the same materials and the process is thought to automatically have the advantage of better film properties caused by bias sputtering as the ions weakly bombard the substrate each half cycle of the R.F. Consequently it was decided to use R.F. sputtering as the deposition process and at the onset of the project no previous report of the R.F. sputtering of barium titanate could be found.

2.5. Choice of R.F.Sputtering System.

The laboratory in which this work was to be done was part of the Solid State Group concerned with various properties of thin films produced by a number of methods. However no sputtering facilities were available and this was an ommission which needed rectifying, in view of the increasing application of the technique in thin film work. Financial considerations prohibited the purchase of any commercial apparatus so it was decided to design and develop a sputtering system with various uses. The object was to design on one pumping station a system capable of sputtering with triode, grounded diode and balanced diode arrangements, by an inter change of top plate and components in the chamber. Of the balanced arrangements, the disc and annulus system was preferred due to the use of only one dielectric target compared to the "Peak" system. To make electrical measurements on dielectric layers a metal - insulator - metal (M.I.M.) structure is required. It would be desirable, in order to reduce contamination and prevent the formation of metal oxide layers, to produce some of these M.I.M. devices in one pump down. Accordingly the apparatus was designed to incorporate this facility.

Electrode arrangements for R.F. sputtering.

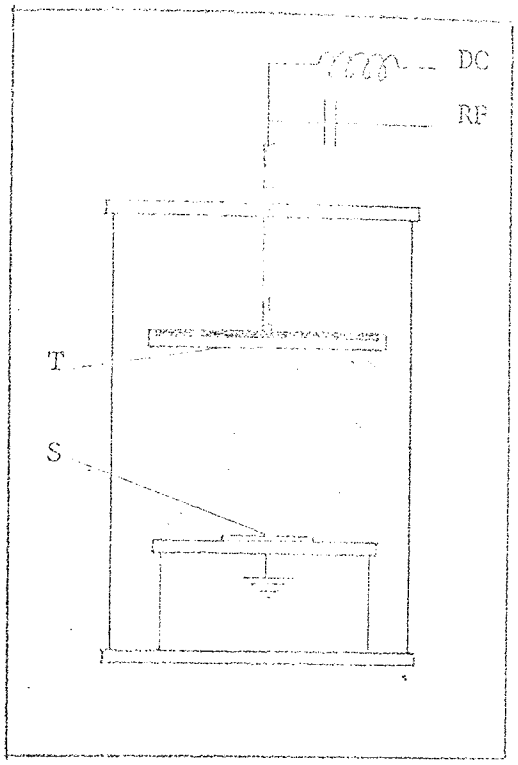


Diode

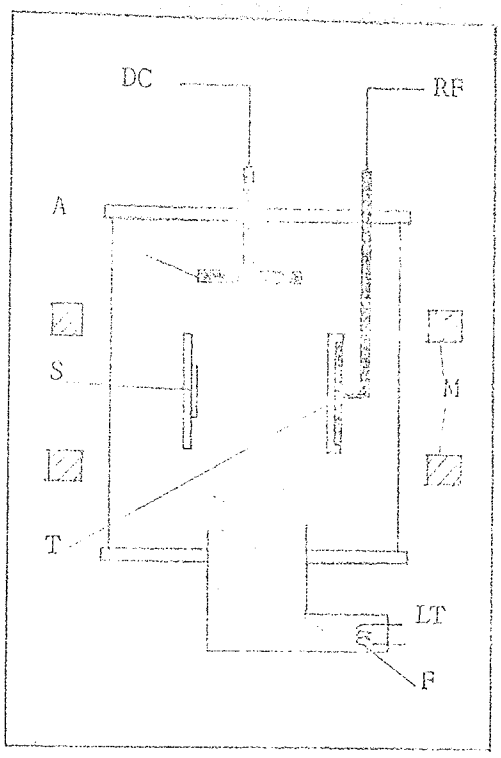


Triode

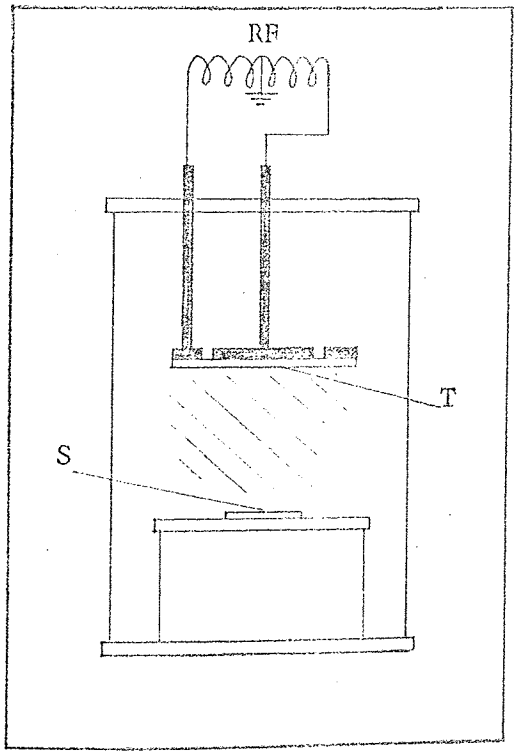


Disc and Annulus

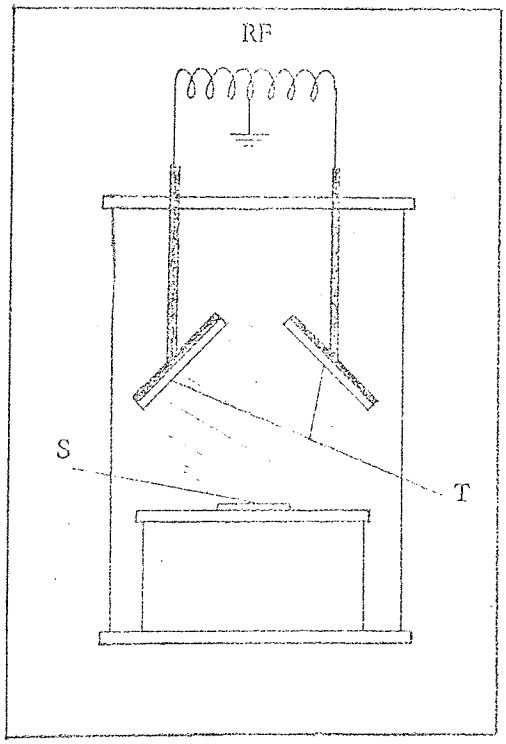


"Plasma Peak"

T. target S. substrate M. magnetic coils

F. filament A. anode

## 2.6. The Vacuum Requirements.

To obtain any reliability and consistency in the production and properties of thin films the first requirement is a vacuum chamber having a very low leakage and outgassing rate with a pumping system capable of reducing the pressure in it to a very low level. The traditional pumping system for vacuum work is the mercury or oil vapour diffusion pump with a mechanical backing pump. Lately in research applications using ultra high vacuum ($P<10^{-8}$ torr), the ion pump or titanium sublimation pump backed with sorption pumps have become popular while in production applications the thermo molecular and Rootes blower pumps are common and have appealing characteristics (110) In the present project the ultimate pressure required ($\leqslant 10^{-6}$ torr) falls only into the high vacuum range and the pumps used were chosen due to their availability and adequacy. The laboratory had in stock a selection of oil diffusion pumps with the corresponding traps and oil scaled rotary pumps. No objection could be seen to their use in this application and the pumping system was designed around them. Although sputtering is performed at a relatively high pressure, the ultimate pressure of the system should be just as good as for evaporation because of the ionising capability of discharges. In a pumping system using oil the backstreaming rate must be very low because any long chain carbon compounds will be cracked by the discharge producing carbon and light hydrocarbon products. Similarly water vapour present in the discharge will be ionised producing active oxygen and hydrogen near to the film substrate.

CHAPTER THREE

# THE DESIGN AND CONSTRUCTION OF THE DEPOSITION APPARATUS.

## 3.A. The Vacuum System

### 3.A.1 Vacuum Requirements.

With the object of designing a deposition station, capable of sputtering in one of either triode, grounded diode or non grounded diode configurations by making a simple internal chamber conversion, and noting the points made in sections 2.6 and 2.7, the following system requirements were recognised.

1. A minimum chamber size of 12" high by 12" diameter (the height is necessary for triode configuration and M.I.M. structure deposition).

2. An ultimate pressure of $\leqslant 10^{-6}$ torr.

3. Negligible backstreaming rates from both vapour and mechanical pumps.

4. A relatively quick (2-3 hours) pump down and change round time.

5. Good pressure monitoring gauges particularly over the pressure range $5\ 10^{-3}$ - $5\ 10^{-4}$ used for sputtering.

6. Argon and oxygen gas bleeds with close control of their partial pressures.

The conductances of all the components used and calculations of anticipated pumping speeds etc. used during the design of the vacuum system are given in Appendix 1.

### 3.A.2 The Vacuum Chamber and Vacuum materials.

The vacuum system including the chamber is shown in figure 3.1. The chamber comprised of a 12" diameter $\frac{1}{4}$" thick borosilicate glass cylinder 18" long with flat ground ends. These were sealed by L gaskets to the top and base plates which both had leadthough ports let in them to allow the introduction of electrical and other supplies into the chamber. The base plate was supported on a $\frac{1}{4}$" thick duralumin plate bolted to the cast iron square section frame work of the welded trolly which was also designed to house all the electrical supplies. All rubber seals on the

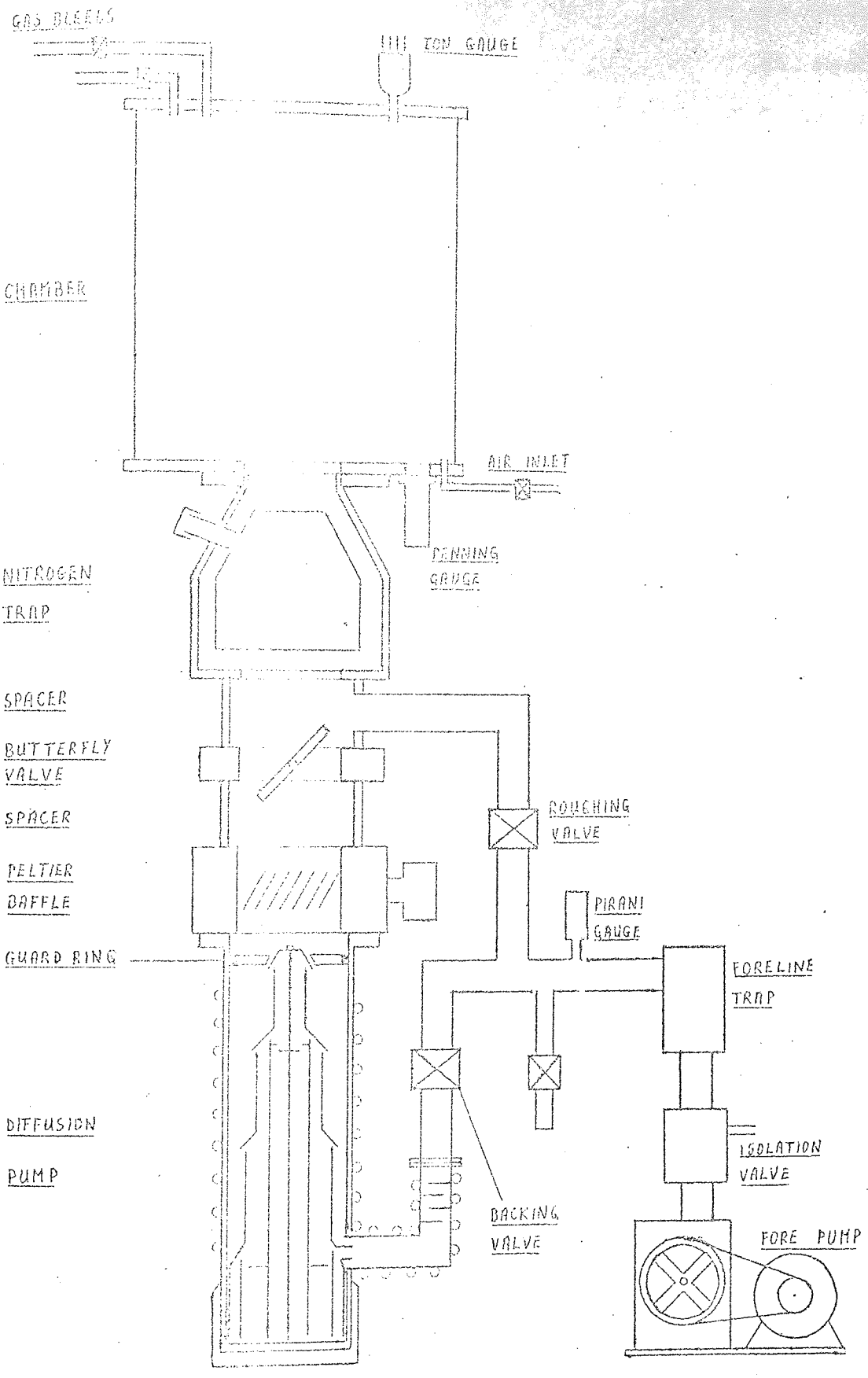


Figure 3.1.

The Complete Pumping System

high vacuum side were made with "Viton" rubber because of its vastly superior properties compared to neoprene and other elastometer materials (110). The chamber furniture and sputtering components were constructed either from stainless steel or a hard aluminium alloy. EN 58B (type 321 Am'), a non magnetic stainless steel, was used and is one of the steels usually recommended for vacuum applications (111). Duralumin was also used particularly for sputtering system components because aluminium has a much lower sputtering rate than most metals, having a sputtering yield of 0.11 compared to copper 0.48 for 100eV argon ions (112) and it has been recommended lately to be nearly as good as stainless steel for vacuum system construction (113). Grease was not generally used on vacuum joints but where its use was unavoidable, as in rotory seals, Apiezon N grease was used which has a vapour pressure as low as $10^{-8}$ - $10^{-9}$ (114). Special precautions were taken with the machining of chamber furniture to avoid the introduction of virtual leaks, for example a groove was milled in the ends of the main support studding where it screwed into the base plate so that the blind tapped holes could pump out more easily. Ceramic parts in the chamber were made out of "Ceramtek", a commercially available machinable ceramic. The material can be easily turned and hand worked before being fired with a claimed maximum dimensional change of only 0.5% (115). Polytetra fluoroethylene (P.T.F.E.) was used for making insulating spacers in parts of the target assemblies. P.T.F.E. has a maximum working temperature of 300°C and an outgassing rate after 1 hours pumping of $3.10^{-7}$ torr.lt. $sec^{-1}.cm^{-2}$ (116) and is the only plastic that is advised as useable in high vacuum applications (117).

3.A.3 The High Vacuum System.

3.A.3.1. The Pumping Column.

Noting the required ultimate pressure, the proposed chamber volume, and conductance of the trapping system, and estimating very roughly likely outgassing and leakage rates it was considered that a 6" diffusion pump

would be large enough to give a reasonable pump down time. Of the pumps available in the laboratory an Edwards F 603 three stage fractionating pump appeared to be exactly what was required and was used. The pump had an unbaffled speed of 600-650 lt.sec$^{-1}$ and required a fluid charge of 200ccs. Silicone DC 705 oil was used because of its lower back-streaming rate 10 ($\mu$gm.min$^{-1}$.cm$^{-2}$) for DC 704 oil under the same conditions (118) and lower vapour pressure compared to other easily available oils (119). The diffusion pump heater loading was 1300 watts and the power for it and the thermo-electric baffle was fed through a four pole 10 amp "Donovan"contactor. The pump and baffle cooling water was taken from mains to drain and the flow was continually monitored by an "Edwards" FSMI flowtrol unit. The minimum recommended flow at 15°C water temperature was 1.9 lt min and the flowtrol contained a pressure differential switch which operated below this rate to disconnect the power to the coil of the contactor. Any damage due to overheating of the pump or baffle was thereby avoided. A guard ring, a copper cap in thermal contact with the cooled walls of the pump, was positioned at the mouth of the diffusion pump to shroud the top jet deflector and provide a cooled barrier. The guard ring reduces oil backstreaming ten times from 0.2 mgm.cm$^{-2}$ min$^{-1}$ to 0.02 under the same conditions (120) but also decreases the conductance to the chamber. The NTM6A liquid nitrogen trap was positioned above the QSB6 quarter swing butterfly valve as a better ultimate pressure is attainable with that arrangement (121). The trap had a liquid coolant capacity of 5 lt and was capable of remaining cold for 24 hours on one filling. As the cold trap was above the butterfly valve, initial high vacuum pumping had to be done with the trap empty so another trap was required directly above the diffusion pump. A DCB6 thermoelectric baffle available in the laboratory was installed using the same water flow as the pump. The baffle works on the large Peltier effect of bismuth telluride. The semiconductor is made into elements connected in series so that at a

PLATE 1

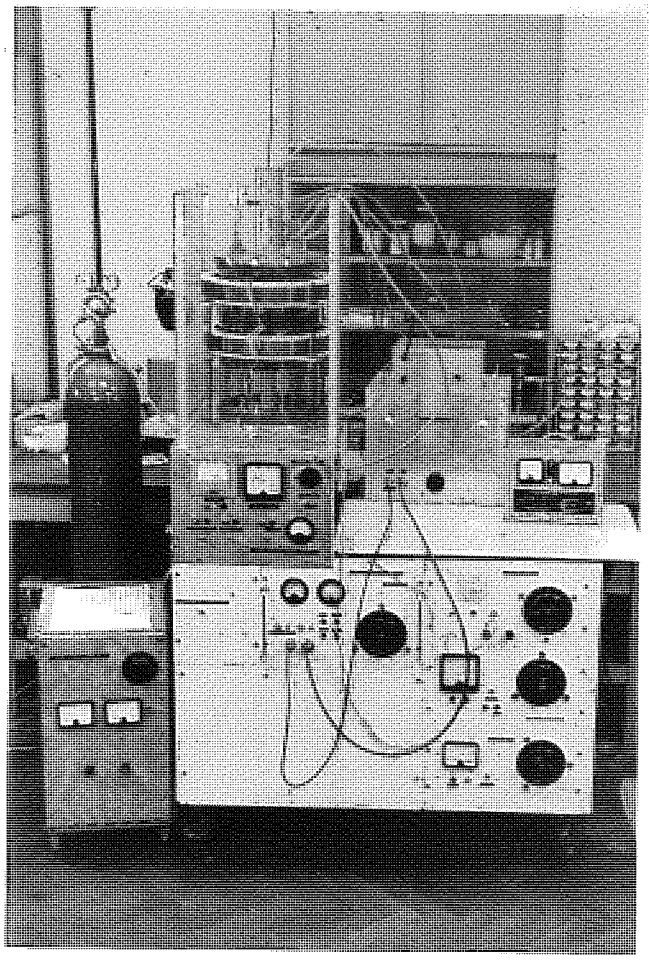

PLATE 11

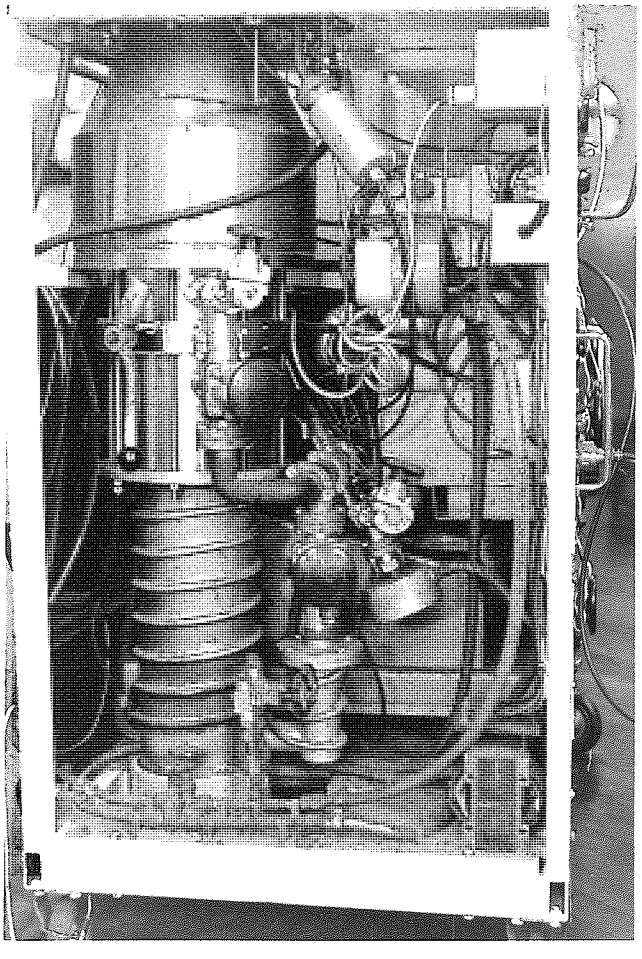

D.C. current of 20 amps a negative temperature differential of 28°C can be maintained between the vanes of a Chevron type baffle and the water cooled block. Two "Edwards" 6" spacers were required on each side of the butterfly valve to allow for the full swing of the sealing plate. All the components of the high vacuum pumping column were sealed with viton "O" rings and held together and supported from the base plate of the chamber by stainless steel studding.

3.A.3.2. The top cold trap.

During film deposition another liquid gas cooled trap could be used. This was supported from the chamber top plate by its own liquid leadthroughs. The leadthroughs were specially designed with a long vacuum insulated conduction path between the liquid coolant and the viton sealing gasket and one is shown in figure 3.2. The trap consisted of a circular stainless steel plate with the central section milled out to allow the target leadthroughs to pass through it. The coolant pipes led from the leadthroughs and were brazed directly to the plate. When operated liquid nitrogen was continuously pumped through the pipes by a "Speedivac" liquid gas circulating pump. The position of the trap between the argon inlet and the discharge region meant that any traces of water vapour or other potentially ionisable vapours could be removed from the vicinity of the target.

3.A.4. The Fore Pumping System.

3.A.4.1. The Rotary Pump.

A Speedivac E.S 250 rotary pump was available in the laboratory and was considered adequate to produce a backing pressure lower than that required (0.35 torr) having a pumping speed of 290 lt.sec$^{-1}$, approximately the rate recommended by the diffusion pump manufacturers. Speedivac Nos 18 oil was used and the pump had a manually operated ballasting valve which was used to assist in the pumping of condensable vapours. The fore pumping lines illustrated schematically in figure 3.1. consisted of " Edwards" 1" coupling components using nitrile "O" ring demountable

joints and brazed permanent joints. A stainless steel flexible coupling was incorporated in the fore line near the rotary pump to reduce the transmission of vibration to the chamber and for the same reason the pump was only indirectly fixed to the trolley via anti vibration mountings. A magnetic isolation valve was situated directly above the rotary pump and a vacuum switch (Edwards VSK 1B) was coupled into the fore line. The vacuum switch was connected in series with the coil of the contactor (Section 3.A.3.1) so that in the case of a major leak or failure of the vacuum system the pumping system and sputtering HT supplies would be switched off. A side arm was available in the fore line to which could be coupled a leak detector head if necessary and an oil mist filter (Vokes OMF 200) was included in the exhust of the rotary pump.

3.A.4.2. Fore Line Trap.

While backstreaming from diffusion pumps has received considerable attention and great care is taken to reduce it with vapour traps, until recently no such attention had been given to rotary pump backstreaming. The rotary pump can cause backstreaming contamination during the roughing cycle and along the backing line causing contamination of the vapour pump oil resulting in an increase of the ultimate pressure of the system. Since 1967 work has been done on this problem, by determining the rate of backstreaming (123,124), the backstreaming oil composition (125,126) and the best method of trapping these oil products. It is reported that the rotary pump oil decomposes into light fractions (127) and that this degradation occurs on exposing oil to rubbing metal surfaces (128). Baker and Stanisforth (129) have described a foreline trap suitable for quick cycling systems by using a quartz microbalance to measure the backstreaming rate. Of many inorganic sorbants they tested both at room temperature and at liquid nitrogen temperature they concluded that activated dust free alumina pellets were the most suitable. The effectiveness of alumina for this purpose was confirmed by Fulker (130)

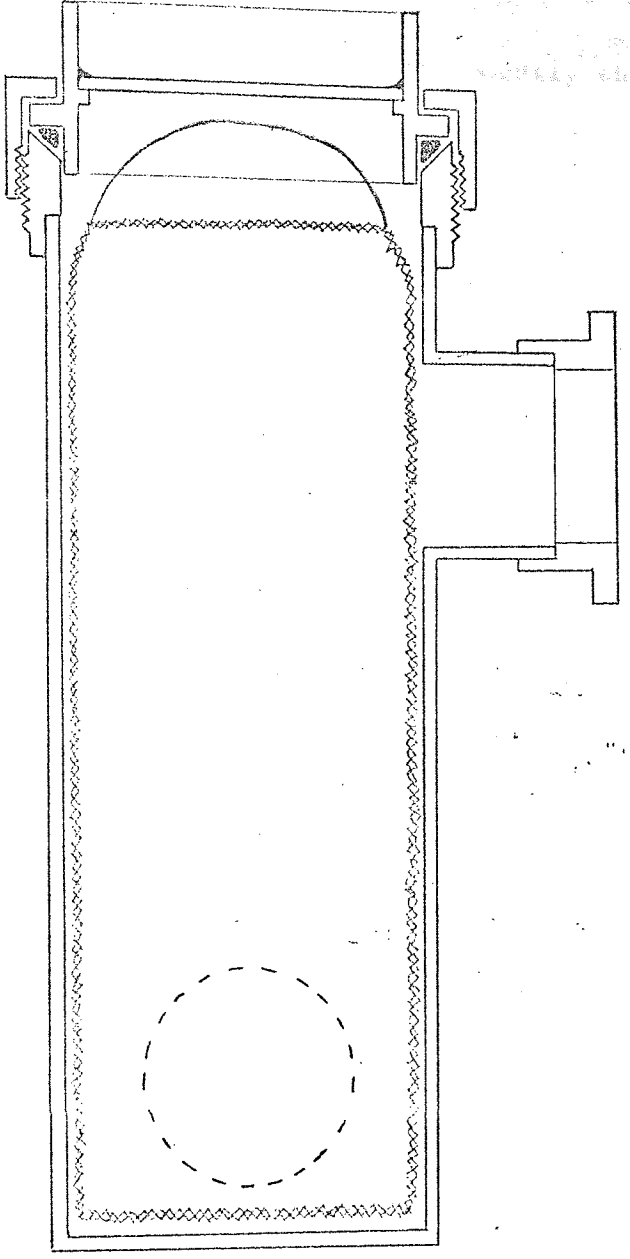

Figure 3.3.

Fore Trap Design.

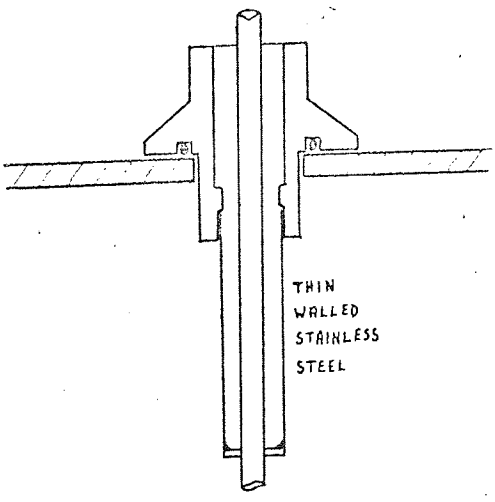


Figure 3.2.

Liquid Nitrogen leadthrough

using mass spectrometry measurements. Consequently an activated alumina trap capable of being easily recharged was designed into the fore line. The design is shown in figure 3.3., the copper mesh cage sitting snugly into the outer case so that the gas has to pass through the alumina. The alumina used was 5/16" activated non dusting pellets supplied by B.D.H. and was easily changed by removing the 2" top "O" ring coupling and withdrawing the cage. The alumina could be regenerated by baking in a vacuum oven to a temperature of 350-400°C.

3.A.5. Pressure Measurement.

The fore pressure and the chamber vacuum during the roughing cycle were measured with Pirani gauges which covered the pressure range 760-0.001 torr. The ultimate vacuum was measured using an IOG12 hot filament ionisation gauge, pressure range $10^{-3}$ to $10^{-10}$ torr. The ion gauge meter reading became unstable when the discharge was operated and the gauge therefore could not be used for measuring the pressure when sputtering. Consequently a cold cathode magnetically assisted Penning discharge gauge was used to monitor the pressure during film deposition. The Penning gauge operated between pressures of $10^{-2}$ and $10^{-5}$ torr and had a sensitive range around the region of gas pressure used for sputtering ($5\ 10^{-3} - 5\ 10^{-4}$ torr).

3.A.6. Gas Bleeds.

Both Argon and Oxygen gas bleeds were required in the chamber. These were let in through bored 7B blank leadthroughs sealed into the top plate. The gases used were commercially pure supplied from gas cylinders at a pressure of about 2500 lbs per square inch via a reducing valve. These valves were permanently set at a pressure of 5 lb per square inch and the admission and partial pressure of the gases was controlled by fine control needle valves (Speedivac LB2). $\frac{1}{4}$" bore flexible stainless tubing was used to connect the gas cylinders to the needle valves and the needle valves to the leadthroughs. The demoutable joints were sealed with viton gaskets and the permanent seals were

brazed with easy flow number 2 hard solder. The argon needle valve was mounted on the main front panel while the oxygen valve was "in line", located near the oxygen cylinder.

3.A.7. Operation of the Vacuum System.

Before assembling the vacuum system and chamber funiture all components were thoroughly cleaned and degreased, particularly those that had been in contact with soldering fluxes and machining oils, using acids and ultrasonic agitation in organic solvents where possible. All handling in the chamber was done wearing nylon gloves to reduce the contamination due to finger grease. Deposition times employed during the investigation varied from less than one hour to as long as ten hours, but were generally no longer than four hours. Normally, starting in the morning a substrate could be loaded, the chamber pumped down, the substrate heated to the desired temperature and the deposition completed in the same day. The substrate could then be unloaded the following morning and another one loaded. When not in use, the chamber was kept under vacuum with the pumps on but not pumping the chamber; the rotary pump being left backing the diffusion pump. To guard against the danger of impolsion of the glass cylinder the chamber was surrounded by a safety box. This was made out of $\frac{1}{4}$" perspex sheet bolted onto aluminium angle and was supported on the duralumin plate. To remove it, the front perspex panel could be quickly unscrewed and the rest slid off backwards. The chamber could be let up to atmospheric pressure by opening the air admittance valve on the main front panel. The procedure employed for a film deposition was as follows; The substrate was loaded so as to have the top plate off the chamber for as short a time as possible and just before replacing the plate the substrate was blown with a rubber squeeze to remove any dust from its surface. The thermocouples and heater were then checked for electrical continuity and the safety box put in position before shutting the backing valve and opening the roughing valve. Noting the pressure with the Pirani gauge, the chamber was then roughed out to less than $1.10^{-1}$ torr,

when the roughing valve was closed and the backing valve and main butterfly swing valve opened. The Penning gauge was then used and when the pressure read $1.10^{-4}$ the heater was switched on, the liquid nitrogen trap filled and the ion gauge operated. If the top trap was used nitrogen was not circulated until the substrate had reached temperature and the chamber had reached a pressure of $1\text{-}2.10^{-6}$ torr. Every pump down was timed and recorded so that any slight deteriation in pumping efficiency could be quickly noticed and rectified. When a percentage of oxygen was required in the sputtering gas this was bled in through the needle valve and its pressure monitored for five minutes with both the Penning and Ion gauges to allow it to stabilise before admitting the main sputtering gas, argon. The system was then ready for the discharge to be struck and the deposition to proceed. After completing the deposition the top trap was warmed by blowing compressed air through it and the liquid nitrogen trap emptied using a pressure discharge tube. This was sealed into the nitrogen filler tube with a rubber bung and reached down to the bottom of the trap. Vapourizing nitrogen in the trap then built up a pressure and in quite a short time the trap was emptied through the discharge tube.

## 3.B. The Deposition System.

### 3.B.1 Requirements.

From the conclusions of Sections 2.4.10, 2.5 and 2.6 it was evident that the apparatus had to satisfy the following requirements:

1. The target system wanted to be easily convertable between a triode sputtering arrangement, a grounded diode arrangement and a balanced non-grounded system.

2. A substrate heater was needed capable of raising the substrate to a temperature of 500°C.

3. Resistive heated evaporation sources needed to be included with a mechanically operated mask changing and substrate positioning system for the production of M.I.M. sandwich structures in one pump down.

4. A shutter would be required to allow a pre sputter period before

deposition of the film proper.

5. All necessary electrical, water and mechanical leadthroughs would have to be positioned in the base plate or top plate.

It was decided to use two top plates one for the triode arrangement and the other to be convertable between the two diode systems. The triode and the balanced (non grounded) diode system will be only briefly described as they were not used to deposit barium titanate.

3.B.2. The Triode Sputtering System.

The arrangement is shown in the schematic diagram (figure 3.4.) and pictured in plate III and is basically that described in Section 2. 4.5. The filament was a three strand tungsten wire spiral supported from two 150 A water cooled type 9A "Edwards" leadthroughs and could be changed by removing the top side plate. The discharge could be assisted by the plentiful supply of electrons provided by passing 60-90 A through the filament. The plasma channel was rectangularly shaped to spread the discharge evenly over the face of the target. The anode was a water cooled stainless steel plate and for the same reason was also rectangular in shape. The false base plate stopped the spread of any plasma to the electrical leadthroughs below it. The two magnetic coils were supported outside the chamber wall in a Helmholtz arrangement to create up to $1{\cdot}0.10^{-2}$ Wb.m$^{-2}$ parallel to the discharge. This and the thermionic electrons enabled a 10A discharge to be maintained between the earthed filament and the anode by a potential of about 70V at a pressure as low as a few $10^{-3}$torr. The R.F. or H.T. supply was fed through the baseplate and connected to the target by a coaxial line consisting of 4BA studding surrounded by a 1" stainless steel tube. This coaxial line turned through a rightangle behind the target, which was supported from the tube. The target consisted of a thin sheet of molybdenum connected to the studding with the target material in front of it and a plate of ceramic behind it to prevent any back sputtering of molybdenum. The substrates were supported opposite the target at a distance of about 5 cm.

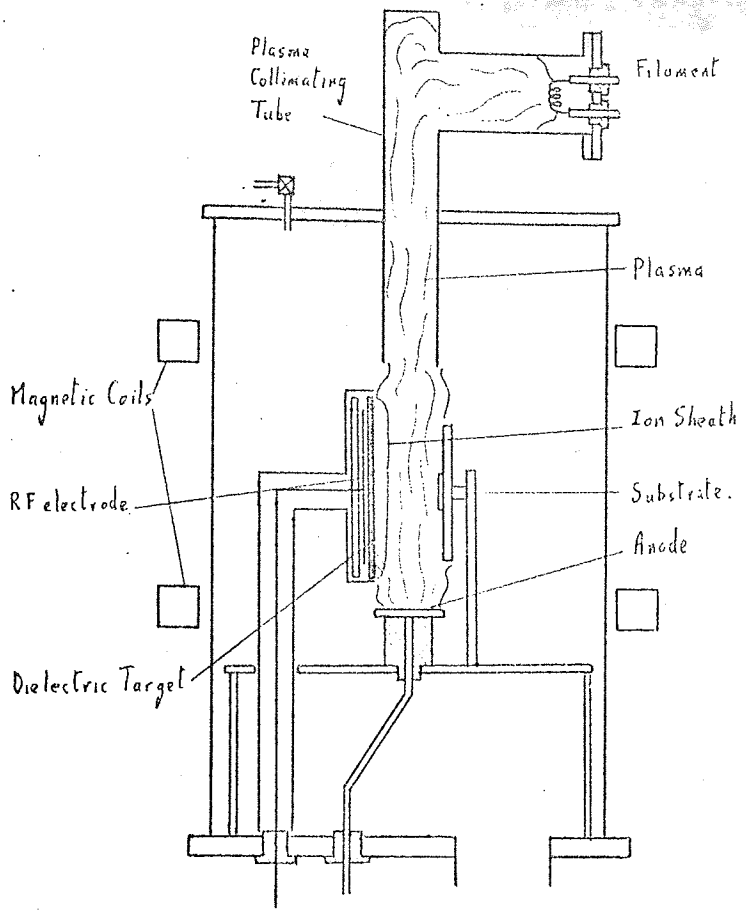


Figure 3.4.

Triode Sputtering System

Figure 3.5.

Non Grounded Diode System.

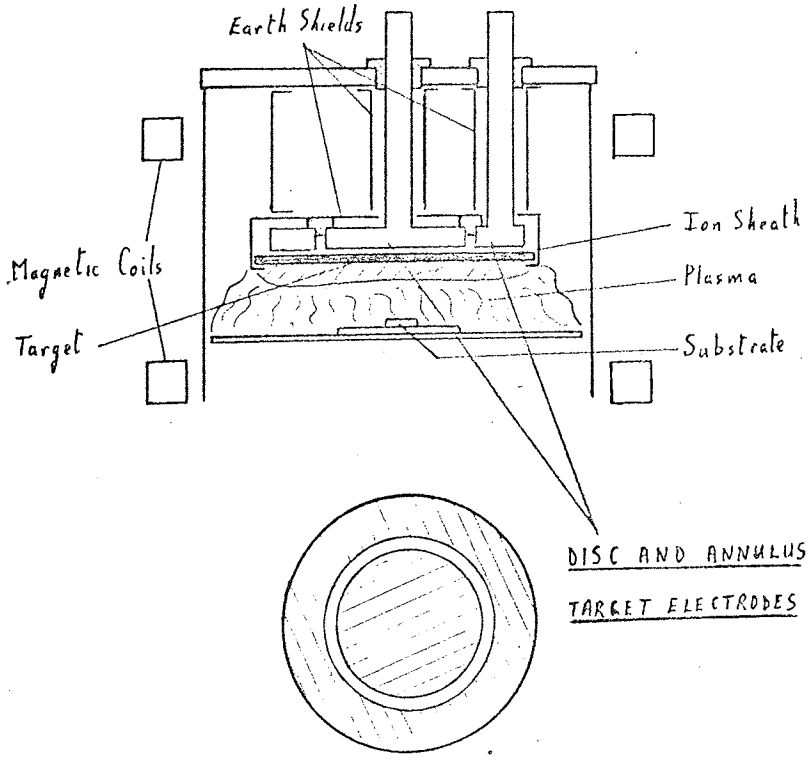

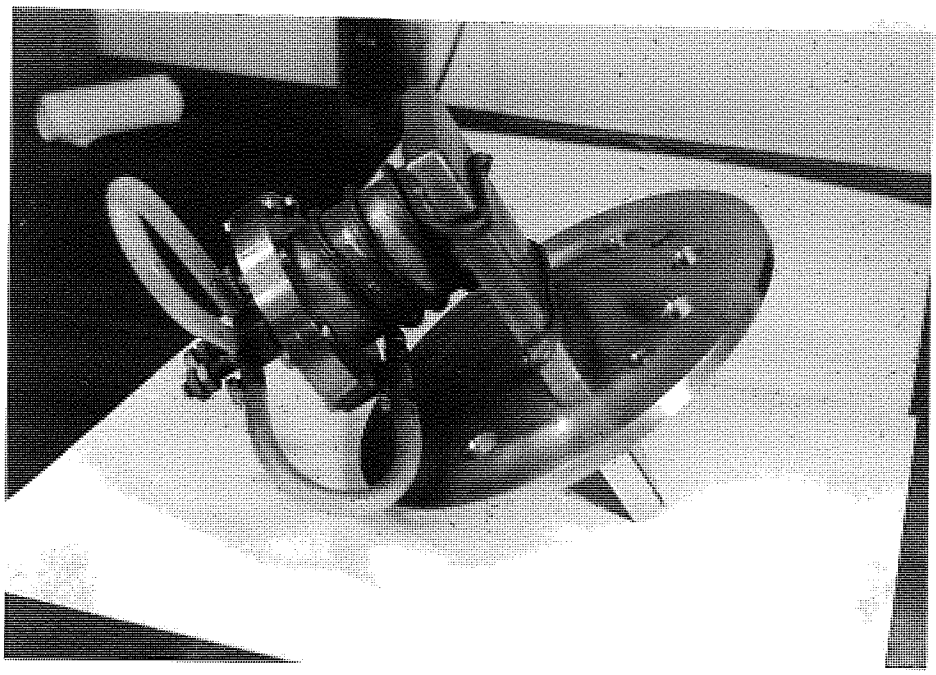

PLATE III

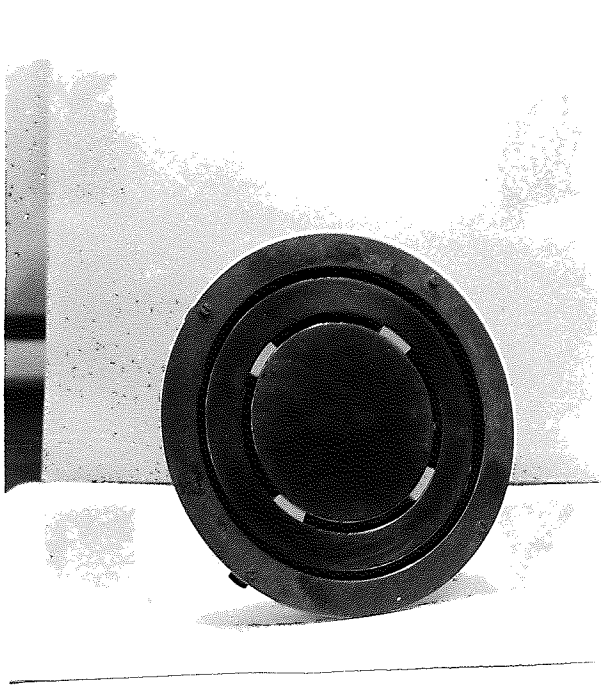

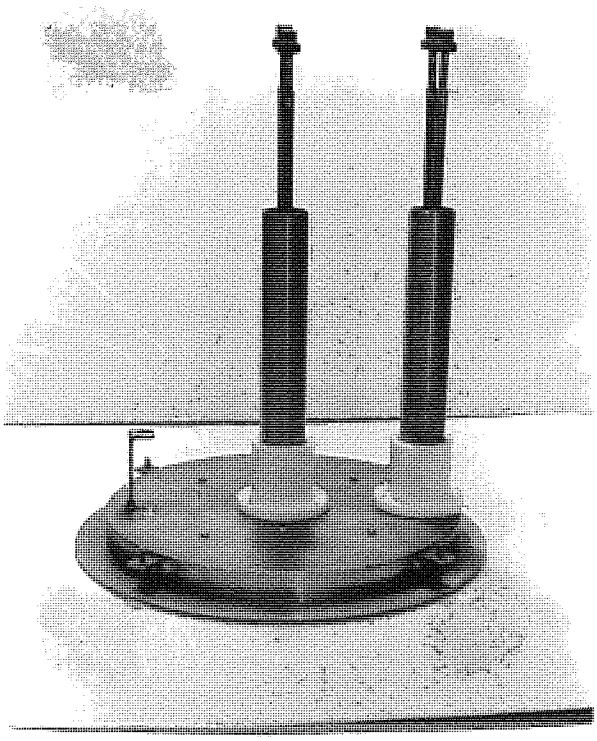

PLATE IV

3.B.3 The non grounded diode system.

This system used the same top plate and chamber furniture as the grounded system and these will be described in detail later (Sections 3.B.4, 3.B.5.) The electrode arrangement is shown in figure 3.5. and plate IV. It consisted of a hollow disc and annulus, both machined in two parts out of stainless steel and welded together. The water cooling and electrical connections were made by 1" stainless steel tubes welded into the back of the electrodes and passed through the top plate using specially designed leadthroughs. The electrodes were held at the correct spacing by P.T.F.E. spacers which were bolted to the earth shield. The leadthrough tubes were also earth shielded to prevent them being sputtered by $1\frac{1}{2}$" diameter tubing bolted to the top plate and reaching down to the target shield. The target itself over lapped the target electrodes and was supported round its perimeter by a flat ring hung from the earth shield by adjustable bolts. The magnetic coils were again used and the system operated up to 3 KV RF at a pressure of 1-2 $10^{-3}$torr. The system has been used for depositing quartz films used in two undergraduate final year projects at this university.

3.B.4 The Grounded Diode System.

3.B.4.1. The Top Plate.

The top plate served both to form a seal at the top of the chamber and acted as the support for the target electrodes and the top cold trap. A workshop drawing of the design is given in figure 3.6. It was machined out of a 14" diameter EN58B stainless steel flame cut blank and given good machining finishes on both sides to accept elastometer seals. The two 1" diameter holes with 45° chamfers, and surrounding equi spaced tapped holes were for the target leadthroughs, which will be described later. Other than these holes, four holes of a size recommended for "Leybold Herreaus" 1" leadthroughs and two holes recommended for "Edwards" type 7 leadthroughs were bored in the plate as shown. Of the 1" holes two were used to support the top cold trap, one had the ion gauge sealed

into it, and the remaining spare was sealed with a blank plug. The IOG 12 glass ion gauge was connected to the leadthrough via a kovar glass to metal seal and the two "Edwards" type 7 ports were used for the argon and oxygen gas inlets.

B.4.2. The Target Electrodes.

The target electrode and earth shield were both made in two demountable parts and a drawing of them assembled is given in figure 3.7. The section of the earth shield facing the discharge and the target backing plate electrode were turned out of duralumin while the rear half of both were machined from stainless steel blanks with the steel water tubes welded to them. The water cooling compartments were sealed from the vacuum by aluminium wire seals which were tightened by the bolts spaced around the two components. When assembled the target electrode and the earth shield were spaced at a distance just less than the first dark space of an argon discharge at $10^{-3}$ torr, by a P.T.F.E. collar situated around the target electrode water tube and extending 1" up its length. This centre tube also acted as the R.F. lead and was shielded by a $1\frac{1}{2}$" stainless tube bolted to the top plate and reaching down to overlap the P.T.F.E. collar. The barium titanate target was glued to the target backing plate with "Araldite", a resin suitable for use at high vacuum (131) having a vapour pressure quoted by the manufacturers of $10^{-7}$ torr and an out gassing rate after 24 hours baking at 85-100°C as low as a few $10^{-10}$ torr.lt.sec$^{-1}$cm$^{-2}$ (132). The target was supported from the top plate by the water/R.F. lead 1" tube, while the earth shield was supported on the one side by the 1" tube and on the other by a stainless steel bracket bolted to both the top plate and the rear of the shield. A number of target backing plates were made so that the target could be changed by substituting that one component.

B.4.3. R.F. water cooled leadthrough.

The same leadthroughs and top plate were used for the two diode systems consequently in the grounded system the water cooling tube to the earth shield passes through an insulated leadthrough when it is not necessary because in

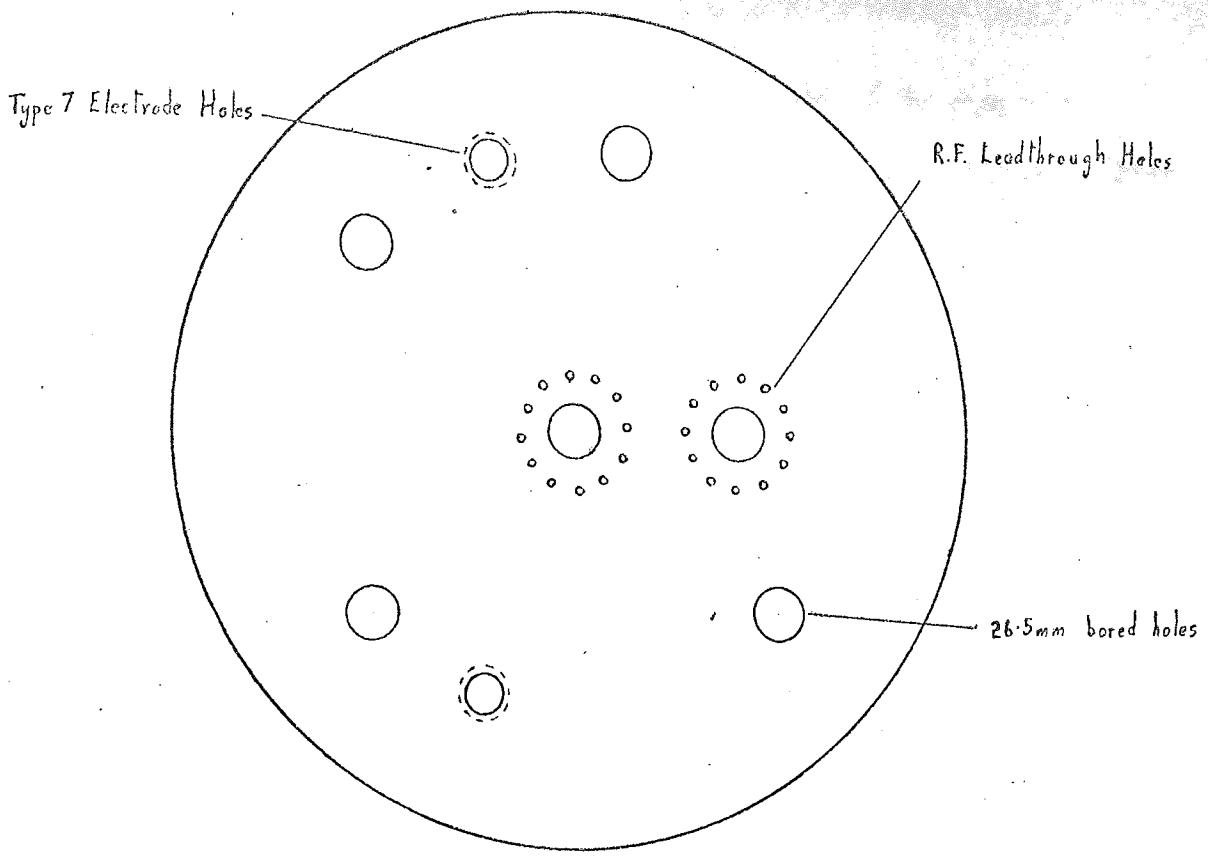


Figure 3.6.

Top Plate 13" dia. $\frac{1}{2}$" thick. stainless steel.

Figure3.7

Diode electrical assembly

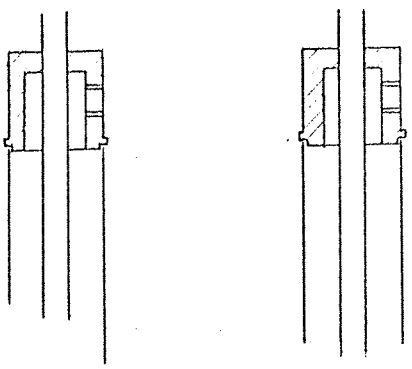

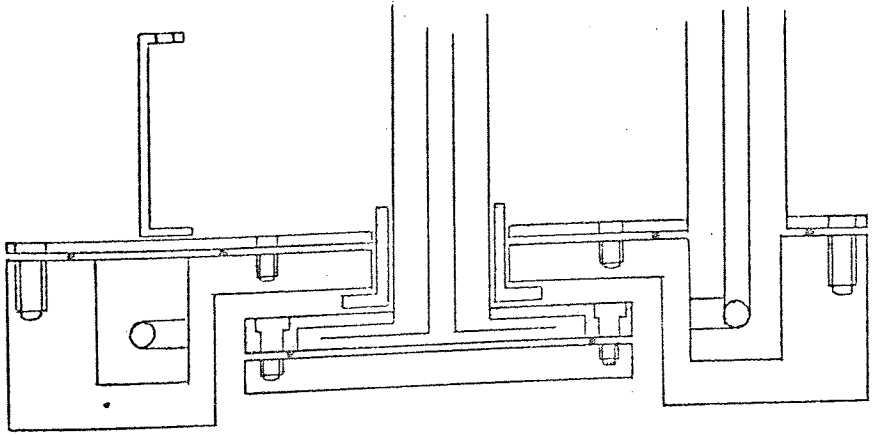

is drawn in figure 3.8 and the whole grounded diode top plate complete assembly is pictured in plate V. It can be seen that the P.T.F.E. collar is sealed into the top plate by gasket A and tightened by 6 equispaced 2BA bolts. The seal between this collar and the water/electrical lead tube is then made by gasket B which is tightened by bolting down the P.T.F.E. washer with the other 6 equispaced 2BA bolts. The joints were designed so that in the seal tight position the seal area is 5% greater than the elastometer area as recommended by Roth (132). The tube is prevented from being sucked into the vacuum by the brass collar. Water connections are made to the target and earth shield by $\frac{3}{8}$ B.S.T unions, one screwed into the side of the 1" tube and the other brazed onto the $\frac{1}{4}$ tube protruding from its end.

3.B.5. Target Manufacture.

The high price of commercially available hot pressed targets (Polaron M.P.C.) made it desireable to attempt the production of a suitable target in the laboratory. With a target diameter of 4" most presses available were too small and those large enough would have required complicated moulding apparatus and could have delivered only a small force per unit area. Consequently it was decided to try to make the target without pressing the titanate powder. The first attempts were made using commercial grade barium titanate which was ground with a motor and pestle and shaken through a 100 mesh sieve before being used. The method was then to mix the powder with distilled water to form a slurry which was poured into a mould, made out of perspex and ebonite. A glass cover was then put over the mould and the slurry allowed to slowly dry in air or under the gentle radiant heat of an electric light. When completely dried out the powder was found to form a cake which had shrunk away from the walls of the mould and while delicate if handled carefully could be slid off the perspex onto a piece of platinum foil. The platinum with the powder cake on it was then placed in an oven and fired. Platinum was used rather than any form of firebrick because barium titanate at its melting point will disolve or react with practically all fireclays or

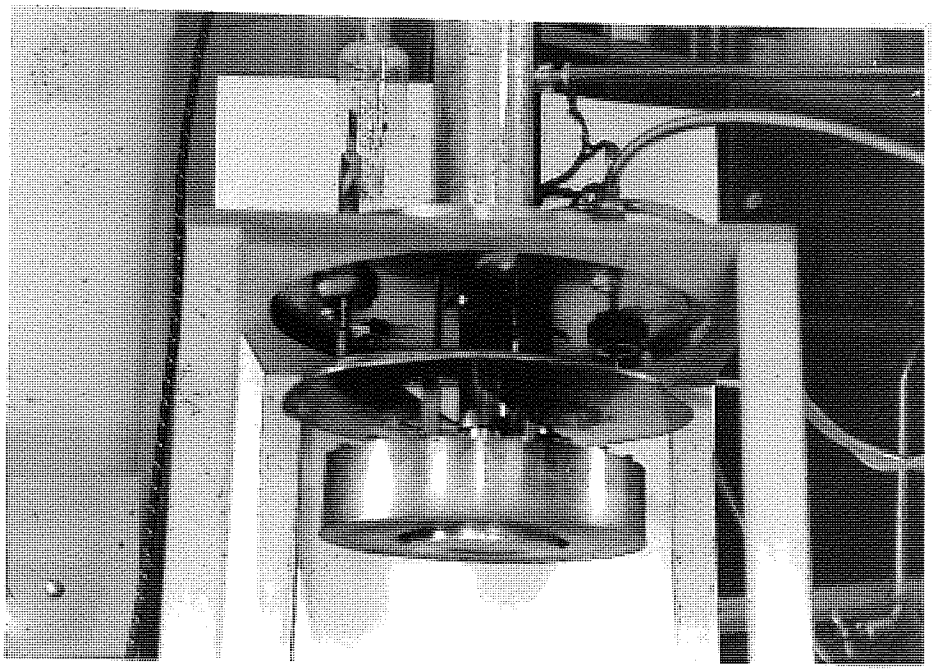

PLATE V

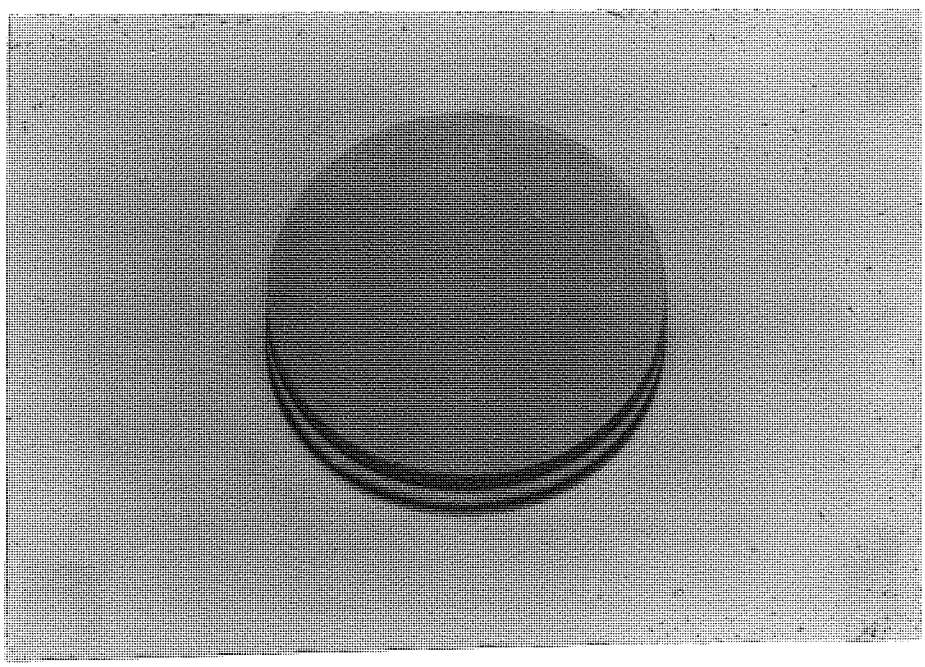

PLATE V1

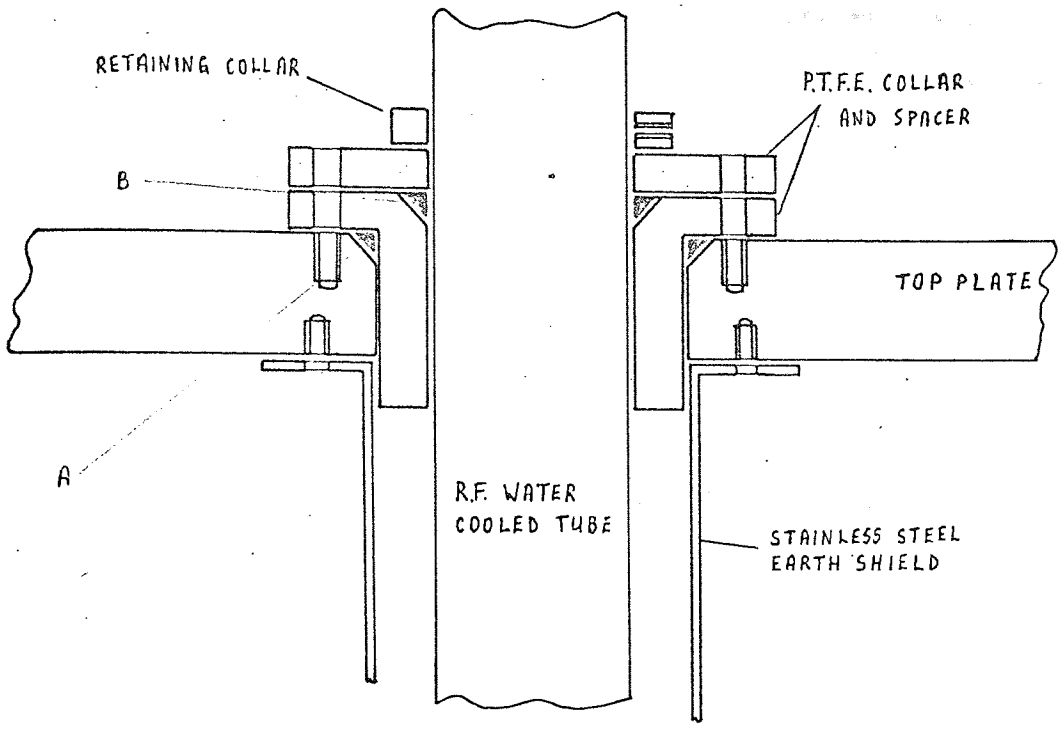


Figure 3.8.

R.F. Leadthrough

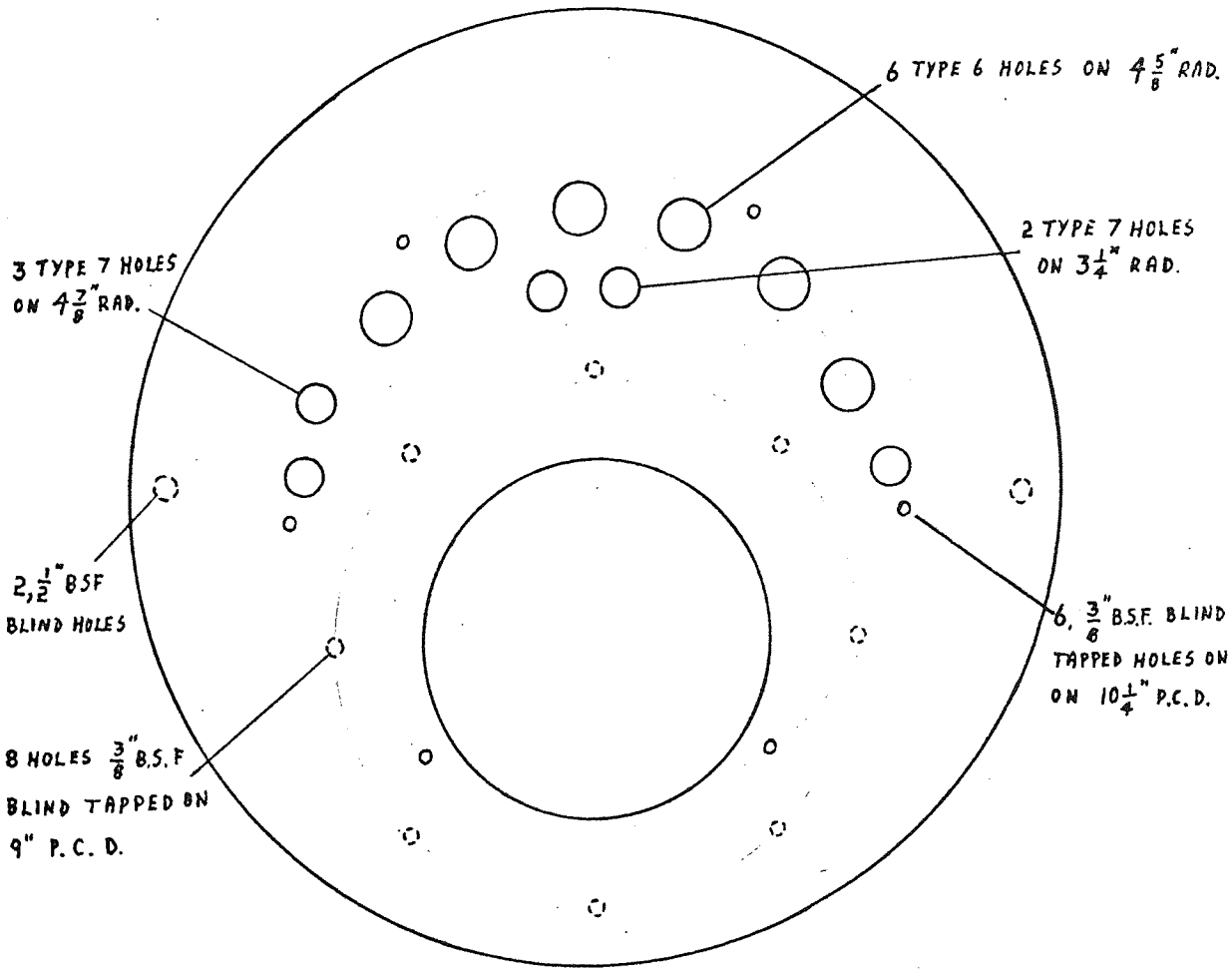


Figure 3.9.

Baseplate 16" Dia. 3/4" Thick. Stainless Steel

scale model of the final target size. In this way the best water powder mixture, method of cooling and firing cycle were decided upon and the shrinkage on firing and fired density determined. This enabled the mass of powder and the mould dimensions for the final target to be calculated. As a result a mould $4\frac{7}{8}$" in diameter $\frac{3}{8}$" deep with a perspex base and a 5°chamfer on the ebonite walls was used. The first target was made using 260 gms of the commercial grade barium titanate mixed with 100 cc's of distilled water. It was air dried for two days and fired on a 0.005" thick platinum sheet. The temperature was raised very slowly up to 150°C and then raised at full oven wattage to 1250°C and after two days cooled down over a period of 24 hours. The target produced is shown glued to it duralumin target backing plate in plate VI and was used in the first depositions and for some of the films used for determining film structure. A second target was made by the same method using 99% pure "Optron" barium titanate (B.D.H.). Unlike the first, however, this did not fire completely remaining slightly powdery but was still acceptable and was the target used in the preperation of the majority of the films including those on which electrical measurements were made.

3.B.6. Chamber Furniture.

3.B.6.1. Baseplate.

The baseplate served as a support both for the pumping stack and for the chamber furniture. It also carried the majority of electrical and mechanical leadthroughs. The final baseplate design is shown in figure 3.9. and it was made out of an E.N.58B flame cut stainless steel blank 16" in diameter and 1" thick. The upper surface was given a good machine finish to allow the L gasket to seal satisfactorily. The six $\frac{3}{8}$" B.S.F. blind tapped holes let into the upper face were to hold the studding from which all the chamber interior structure was supported. Four leadthrough ports were bored into the baseplate for Edwards type 6 leadthroughs, five for type 7 leadthroughs and two for 1" Leybold leadthroughs. The two blind tapped holes in the underside were used to bolt the baseplate firmly to the duralumin support plate, and the

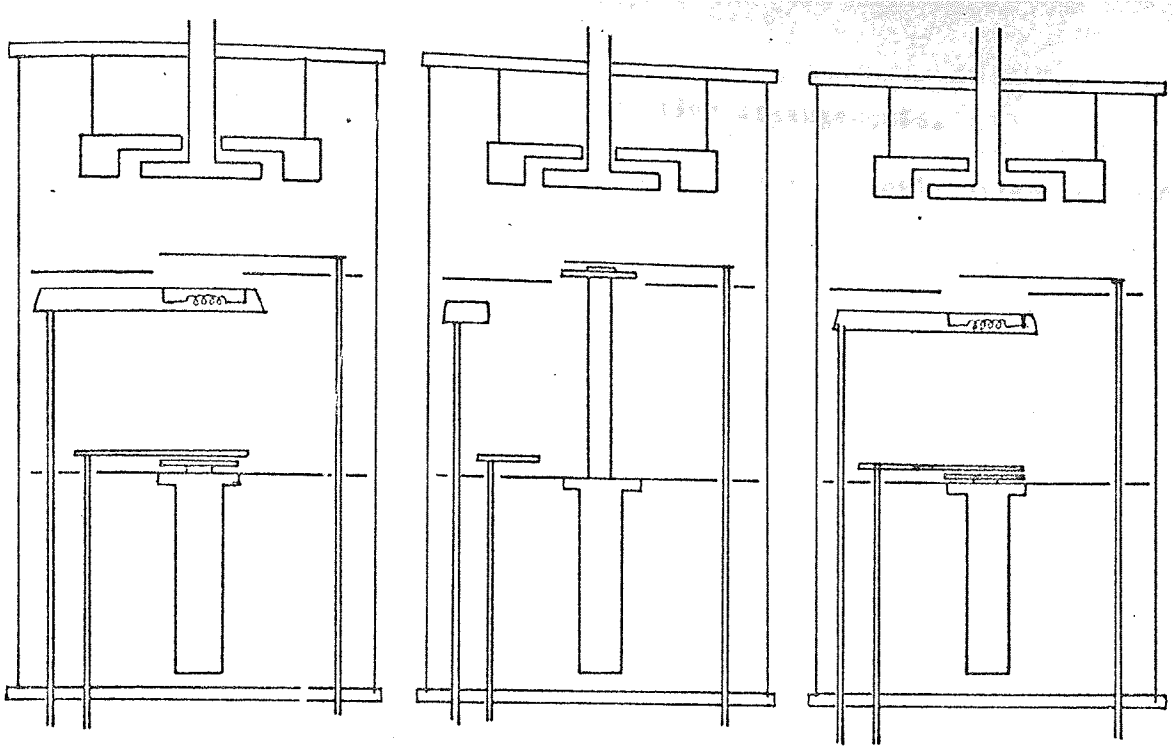

a.Metal 1 b.Insulator c Metal 2

Figure 3.10

Operation of the M.I.M.deposition system

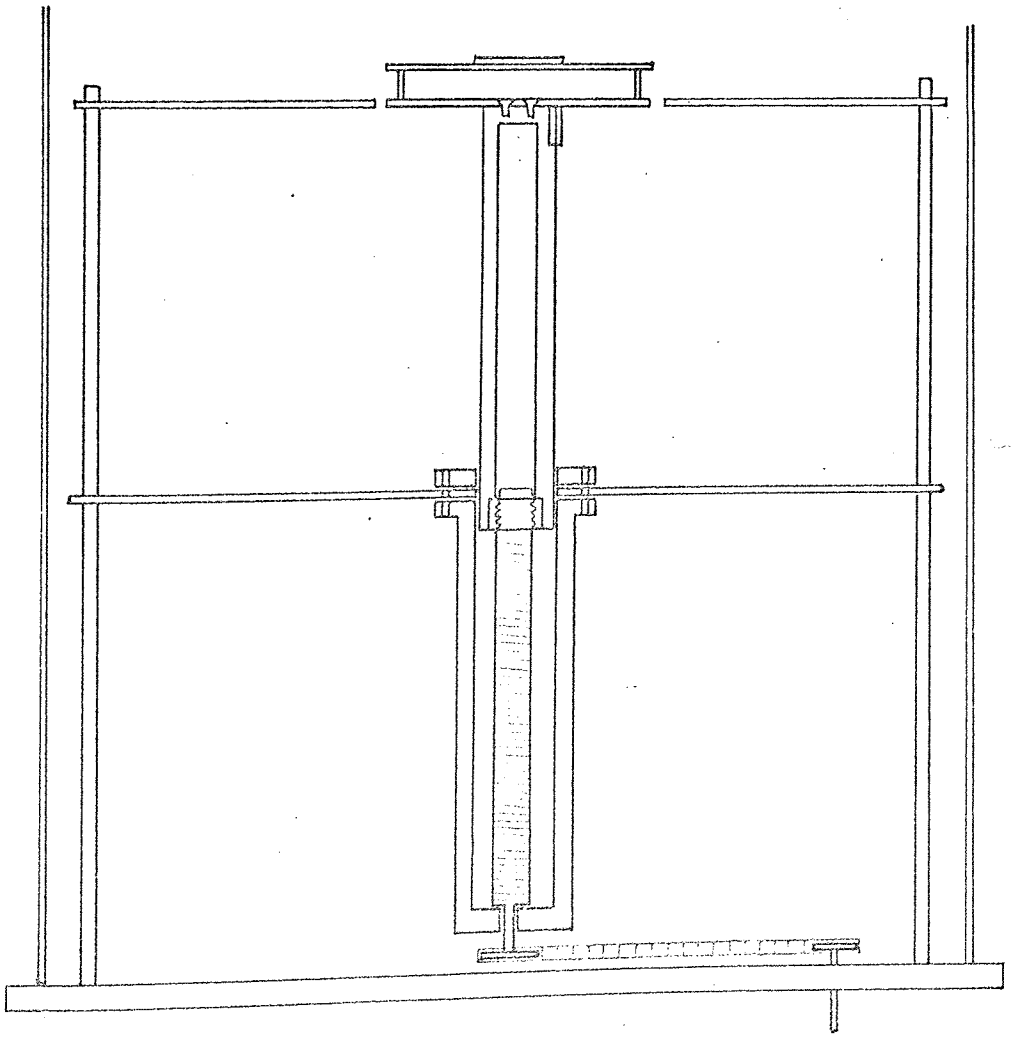

Figure 3.11

Lifting Mechanism

3.B.6.2. M.I.M. deposition system.

3.B.6.2.1. Substrate changeover and deposition arrangements.

The diode sputtering electrodes already described only extended some 6-7" into the 18" high chamber leaving considerable volume available for the metal evaporation apparatus. The operation of the whole mechanism designed to produce M.I.M. sandwiches in one pump down is illustrated in figure 3.10. The substrate has two positions, one shown in figures 3.10a and 3.10c for metal evaporation and the other shown in figure 3.10b for the deposition of the sputtered insulator. The substrate is moved between the two positions by the lifting mechanism drawn in detail in figure 3.11. The duralumin rising section was keyed into the outer case so that when the cog was rotated it did not turn with the nut fixed to the bottom of it but was forced to move up the stainless steel studding. The cog was chain driven from a $\frac{1}{8}$" rotating leadthrough which translated the motion from outside the vacuum chamber. Two stainless steel alignment pins were hard brazed into the substrate holder and located into the mask holder fitted on the sputtering false baseplate, limiting the upward travel of the substrate. The case or body of the lifting mechanism was bolted to a second false baseplate for the evaporation region which prevented metal being evaporated over the electrical leadthroughs. The shutter could be operated in the sputtering region to allow pre sputtering by rotating the extended $\frac{1}{8}$" stainless steel rod of a rotatable leadthrough. The metal evaporations were done from two tungsten wire resistively heated sources. These were clamped at both ends between small stinless steel plates and insulated from each other and earth at the live end by "Ceramtek" spacers. The evaporation assembly, as shown in plate VII, was housed in a stainless steel sheet cover to prevent evaporation upwards and supported from a $\frac{3}{8}$" rotatable leadthrough sealed in the baseplate. This enabled the assembly to be swung clear when the substrate was being raised or lowered but allowed the filaments to sit directly over the substrate when being used. Electrical connections to the evaporation sources was made using $\frac{1}{4}$" diameter flexible copper plated wire covered with "Douroglas" sleeving

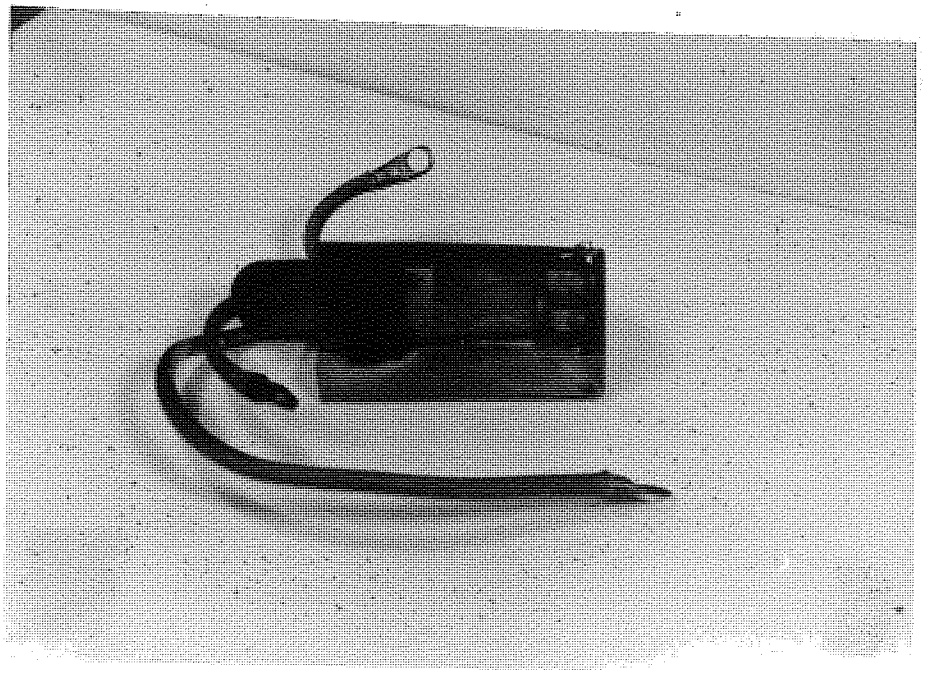

PLATE V11

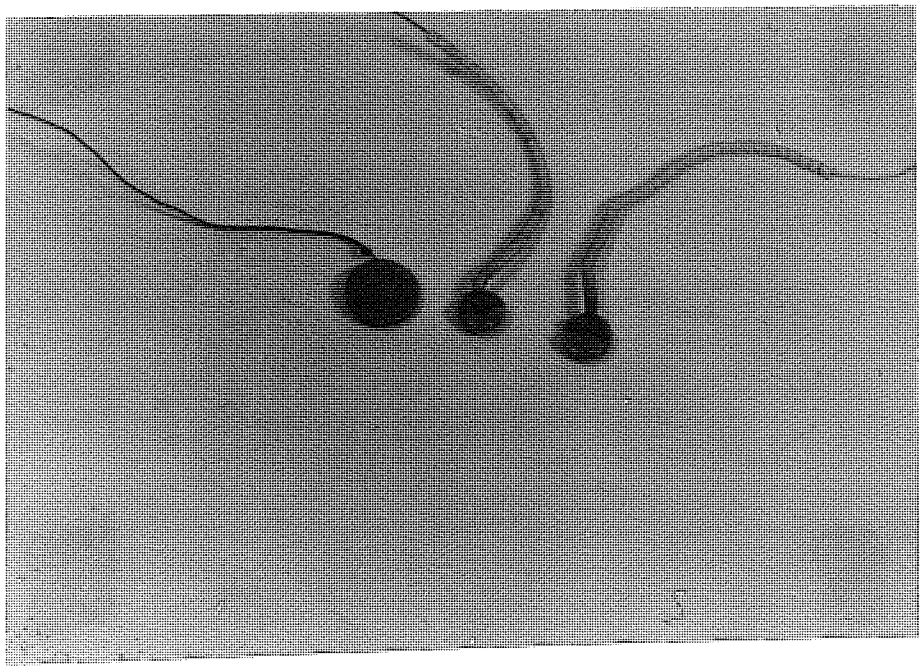

PLATE V111

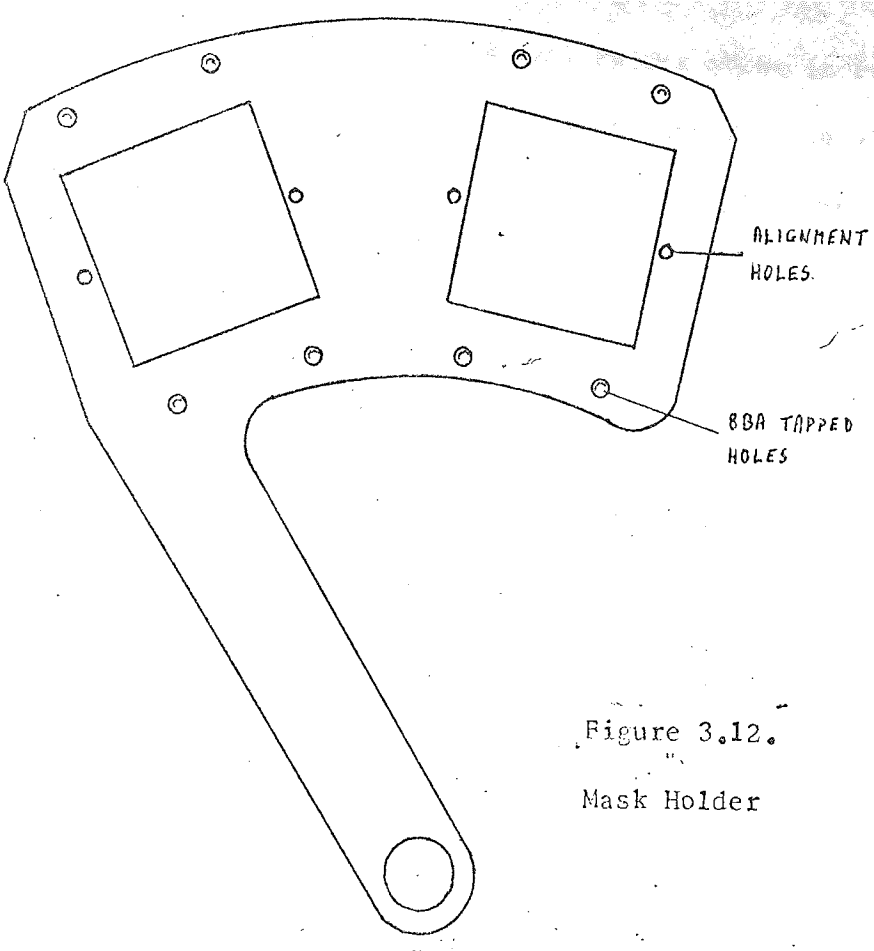


Figure 3.12.

Mask Holder

Figure 3.13

Masks.

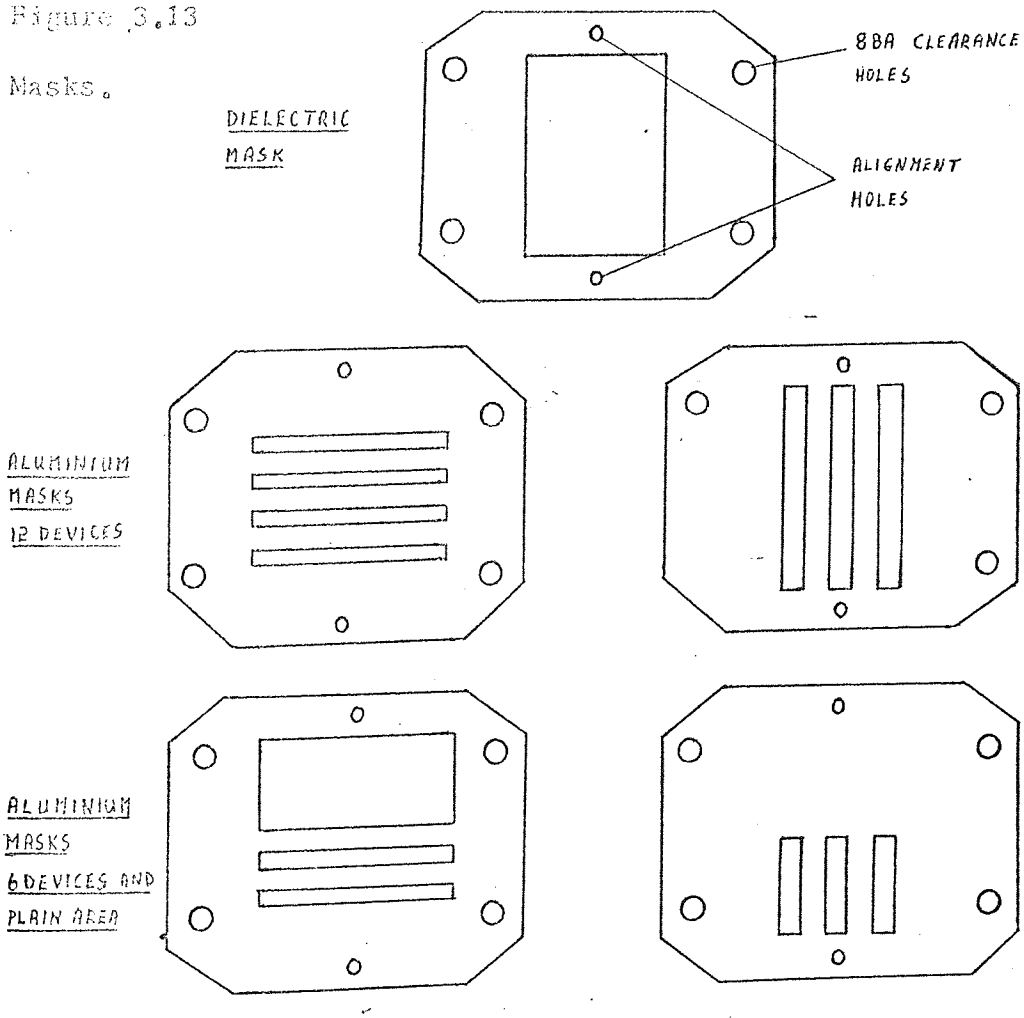

and connected to baseplate leadthroughs. A mask holder shown in figure 3.12 was attached to another $\frac{1}{8}$" rotatable leadthrough and designed to allow the first or second metal deposition mask to be rotated into place and located on the substrate holder alignment pins. This could also be rotated clear of the lifting section when necessary. The masks could be easily changed in the mask holder and their production and design is described in the next section.

3.B.6.2.2. Deposition Masks.

The masks used for the M.I.M. depositions are shown in figure 3.13. The first series produced twelve 3mm x 2mm c pacitor areas and the second 6 similar areas with a region for Elipsometric or other non destructive analytical measurements. Connection to the 6 or 12 capacitors was made from the ends of the two appropriate capacitor crossover strips and required only 5 or 7 leads respectively. The masks were made from 2-3 x $10^{-3}$" stainless steel sheet using a photolithographic etching process (Microponent Development Ltd.) to master drawings provided. The masks were etched from one side only so that the undercut produced an angle on the deposit shaping mask edges.

3.B.6.3. Substrate Heater.

The substrate heater was wound on a cut out mica former out of 1/16" wide 36 gauge nichrome strip with a resistance of 3.27$\Omega$.yd$^{-1}$. Copper and stainless steel plates were bolted either side of the heater element and insulated from the nichrome strips by thin sheets of mica. The heater assembly was supported by four 6BA stainless steel bolts $\frac{1}{4}$" above a thin stainless steel heat shield as shown in figure 3.14. A substrate holder made of copper was fitted or bolted on to the copper side of the heater and could be interchanged depending on the substrate used. The holder shown in the figure 3.14. is for 1" square glass substrates while the holders for thin flat substrates carbon grids and the KBr single crystals used are shown in plate VIII.The substrate temperature was measured using either a copper-constatan or chromel-alumel thermocouple which were held by a stainless steel spring onto the actual

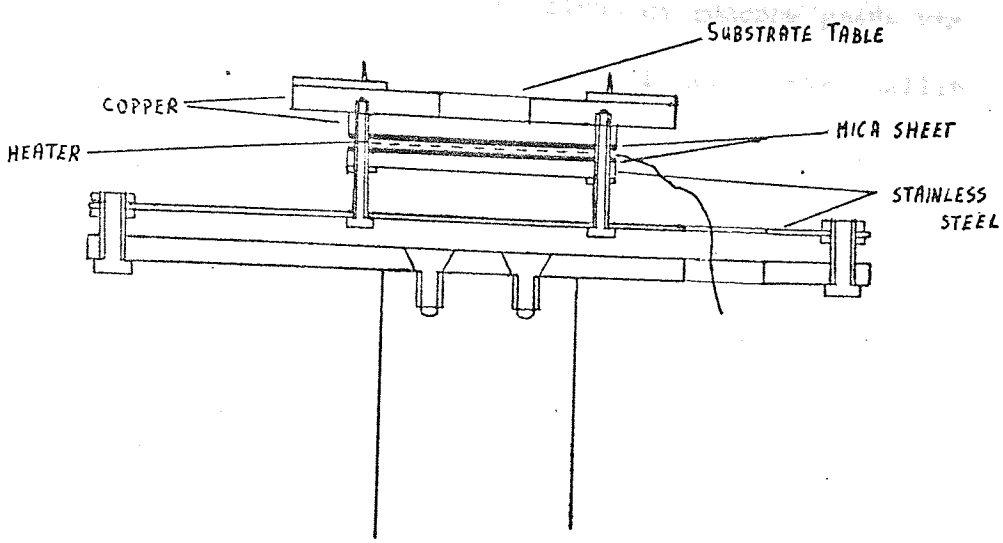


Figure 3.14

Substrate Heater

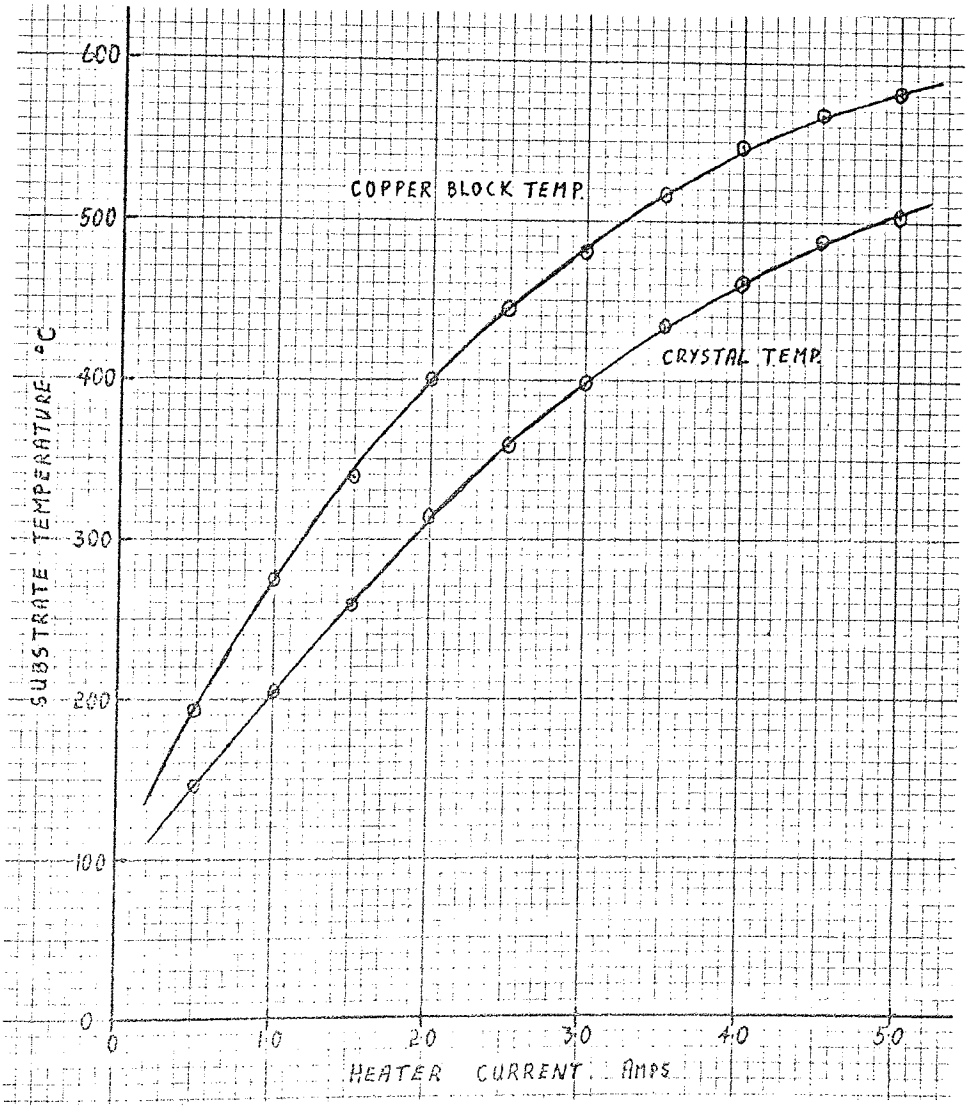


Figure 3.15

Substrate Heater Characteristics

substrate surface, except in the case of electron microscope grids when a thermocouple was hard brazed to the grid holder. In some cases callibration curves were made of the copper holder temperature against the substrate surface temperature so that the latter could be estimated from the copper temperature in cases where it was undesirable to monitor the substrate surface. The heater had a cold resistance of 4 ohms and at a maximum rating of 5 amperes produced a substrate temperature of 500°C. Figure 3.15 shows a curve of substrate temperature and copper holder temperature against heater current for a 1" square glass substrate.

3.B.7 The Magnetic Coils.

All three of the sputtering arrangements under construction were reported to be more stable or efficient if a magnetic field is maintained parallel to the discharge. (Sections 4.4. and 4.5). A field of 100-200 gauss is recommended (91) and this, because of the vacuum, has to be produced by coils placed outside the chamber. Two coils were used in a Helmholtz arrangement(134) spaced a distance $\frac{d}{2}$ apart, where d is the coil diameter, because as illustrated in figure 3.16 the net magnetic field is higher and roughly constant over the distance between the coils. The coils were designed with the aid of equations 3.1. and 3.2. Equation 3.1 gives the flux density due to the two coils, both of ni ampere turns and radius R m. The $(\frac{5}{4})^{\frac{3}{2}}$ factor is a result of the coil configuration. Equation 3.2. gives the temperature rise of a coil in degrees centigrade where c is a constant of about 150, W is the total wattage in the coil in watts, and A is the surface area of the coil exposed to free air, plus half the area enclosed by metal plates, expressed in square inches. The coil formers were made using sheet duralumin and perspex at an inside diameter of 13" to allow for passage over the chamber. The coils were wound from 17 S.W.G. enamelled copper wire on a low bed lathe. 620 turns were wound on each coil giving a resistance of approximately 8Ω per coil and at a current of 3.5A should produce an axial field

$$B = \frac{4\pi 10^{-7} ni}{(\frac{5}{4})^{\frac{3}{2}} R} \quad Wb.m^{-2} \qquad 3.1$$

$$t = c\frac{W}{A} \quad °C \qquad 3.2$$

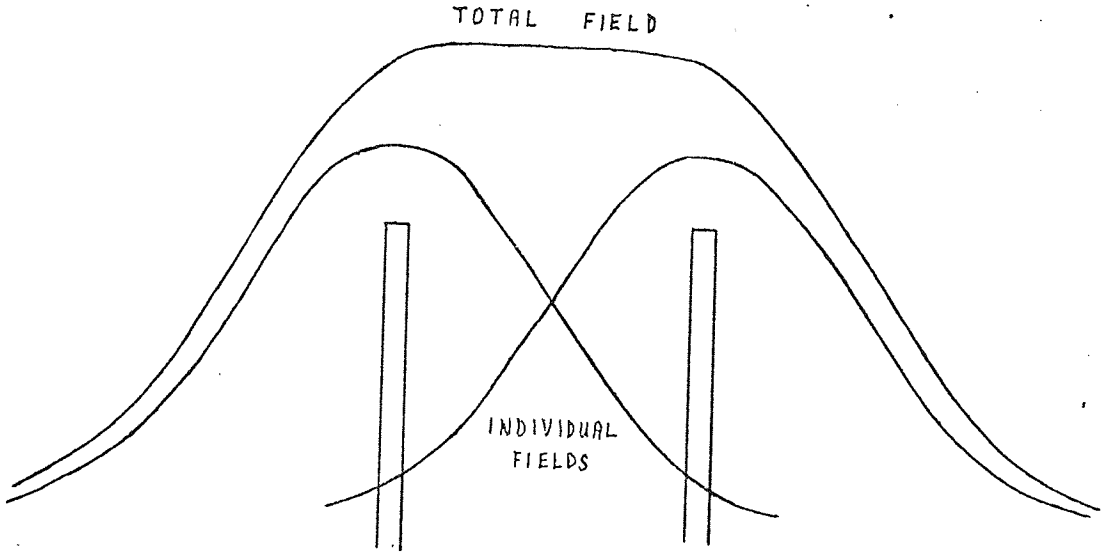


Figure 3.16

Helm holtz Coils

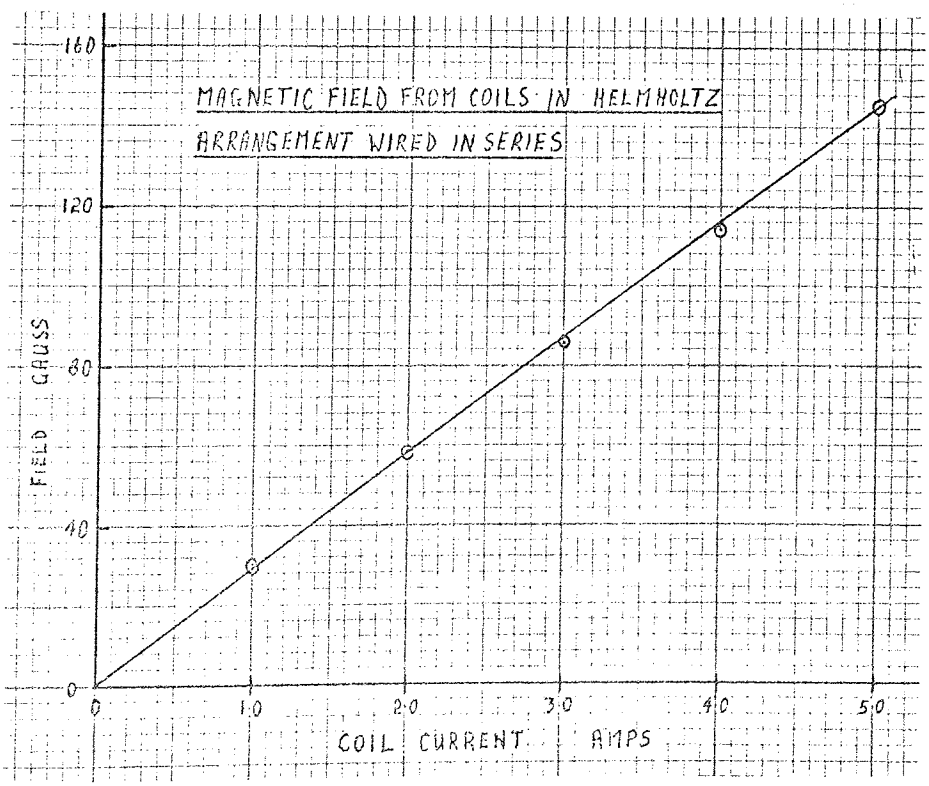


Figure 3.17

of 1.1.10 Wb.m$^{-2}$ with a predicted temperature rise of 70°C. The actual performance of the coils is shown in figure 3.17 where the centre point axial field, measured using a Hall effect magnetometer, is plotted against coil current.

## 3.C. Electrical Circuits and Supplies.

### 3.C.1. Thermoelectric Baffle Supply.

A power supply was required for the thermoelectric baffle to provide a maximum of 30A at a DC voltage of 4.8 V with a maximum ripple of 10%. The circuit designed and used is shown in figure 3.18 and consisted of a full wave bridge with a choke input filter designed to criterian given by Dayal in a "Mullard" publication (135). The silicon power diodes were mounted on heatsinks to the manufacturers specification and the whole circuit was cooled by a fan (Airflow Developments type 26 BT). The circuit was assembled and mounted directly behind the main front panel using "Lektrokit" packaging components. This meant that the on/off switch was alongside the other vacuum swithces and the adjacent ammeter provided a convenient check on the operation of the baffle.

### 3.C.2. Triode Main Discharge Supply.

The triode discharge required a power supply rated at 15A and 300V DC with a ripple of less than 5% and incorporating a variable current limiting resistor. Due to the high power rating and low ripple required of this supply it was decided to use a three phase circuit. Again using Dayal criteria, the full wave bridge rectified circuit shown in figure 3.19 was developed. The silicon power rectifiers were mounted on heat sinks insulated from each other and mounted in the case by a "Tufnal" rod. The voltage was regulated by the three ganged variacs and one of the transformer windings was connected in delta to suppress harmonics. A choke input filter was used and a 5 ohm 500 watt rheostat mounted on the side of the case was used as the current limiting resistor. The circuit was built into a seperate "dexion" trolley which could be wheeled about when required and is shown in plate I.

### 3.C.3. The filament Supply

A low voltage high current supply was required for both the thermionic

Figure 3.18

Thermoelectric Baffle Supply

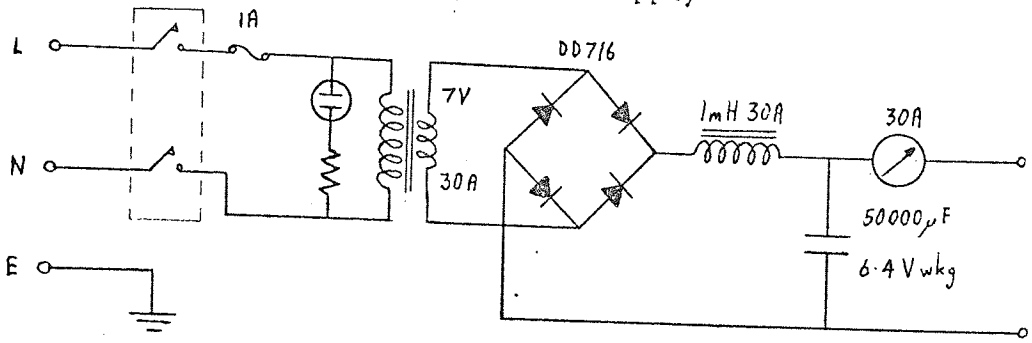


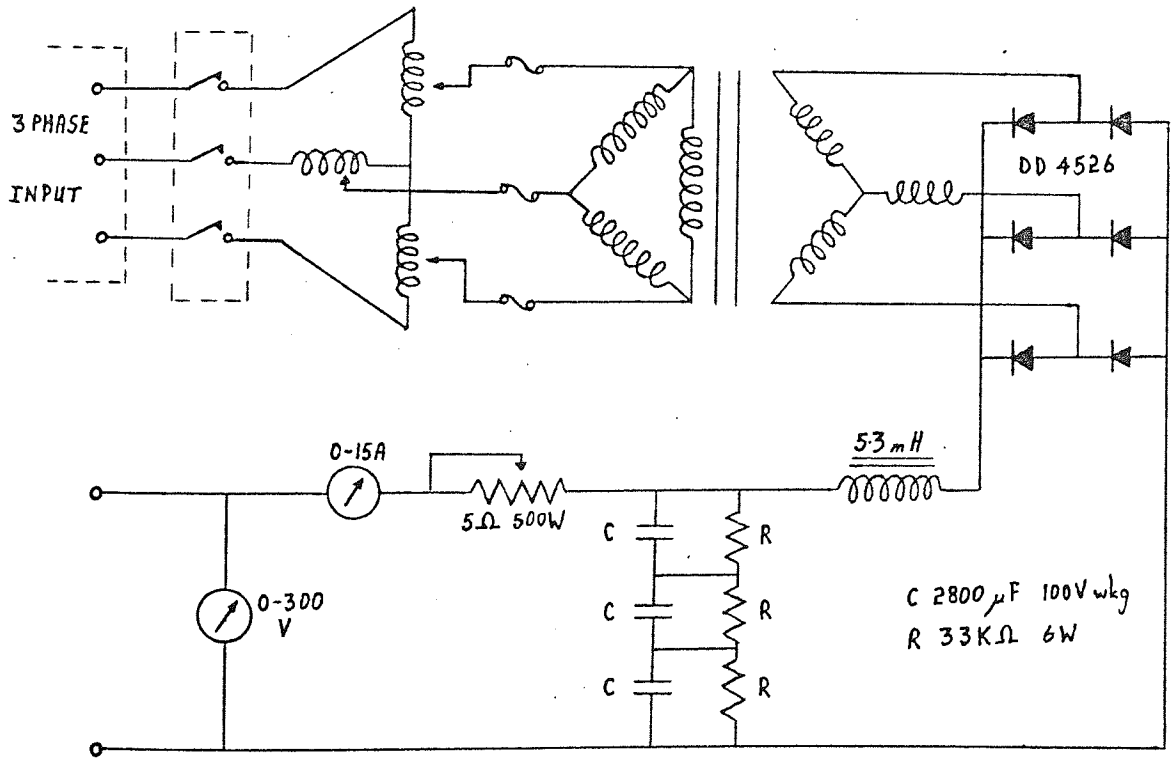


Figure 3.19

Triode Discharge Supply

filament of the triode system and the tungsten metal evaporation filaments. The power supply required, 100A, 12V, was provided by the simple circuit shown in figure 3.20. It consisted of a high current transformer supplied from an 8A variable transformer and the current was measured on a one amp F.S.D meter using a 100 to 1 pick up coil. $\frac{3}{4}$" diameter, rubber covered, flexible, copper welding cable was used for the high current leads with connectors brazed on the ends. The supply controls were mounted on the front of the deposition trolley.

3.C.4 Magnetic Coil Supply.

The magnetic coils had a resistance of 8-9 ohms each and a current up to 4A was necessary, so series operation resulted in a power requirement of 5A 100V DCwith a ripple of less the 5%. Using the same criteria as already discussed to determine the values of the capacitor and resistor in the filter, the final circuit used was as in figure 3.21. The output from the 100V 5A transformer is fed to a full wave bridge of silicon diodes and thence to the resistive filter. The resistors in series with the smoothing capacitor ensured equal sharing of the voltage. The circuit was mounted with "Lektrokit" components onto a front plate which was house on the main deposition trolley.

3.C.5. R.F. Generator Supply.

The R.F. generator was built in two parts, the R.F. oscillator, and the DC high voltage supply. The DC supply was built using "Lektrokit" components controls on a front plate bolted with the other electrical supplies on the deposition trolley, but with the HT transformer and choke mounted on the base of the trolley. The oscillator was built into an aluminium sheet and expanded aluminium case situated on top of the deposition trolley, so that only short R.F. leads were required to reach the target electrode connections on the chamber.

C.5.1. R.F. Oscillator.

The oscillator circuit is shown in figure 3.22 with the alternative final stages for grounded and balanced outputs. The circuit was similar to

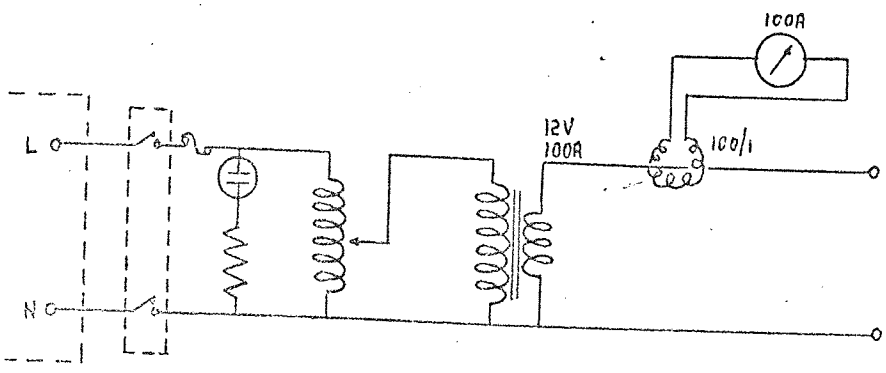


Figure 3.20

Filament Supply

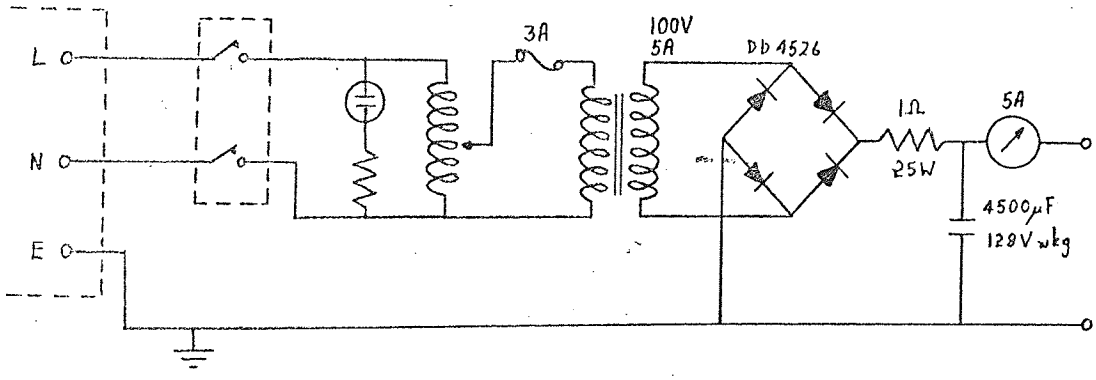


Figure 3.21

Magnetic Coil Supply

one known to be already in use for R.F. sputtering (136) and was operated with Class C push pull output. The plate coils for both the balanced and grounded output were wound out of $\frac{1}{4}$" copper tubing while the pick up coil for the grounded system was wound out of 3/16" tubing. The dimensions of the coils were calculated using equation 3.3 (137) where n is the number of

$$L = \frac{a^2 n^2}{9a + 10b} \mu H \quad 3.3$$

turns, a the radius of the former and b the length of the coil, which gives an estimation of the inductance of air cored coils. The value of the tuning capacitor was determined by the LC resonant frequency required and had a $\frac{1}{4}$" air gap between plates to prevent voltage breakdown. The circuit was designed to oscillate at about 10 MHz. In the grounded output the pick up coil was mounted from a rotatable ebonite rod and could be moved in and out of mesh with the plate coil. In this way it was adjusted to give maximum coupling. An RF discharge represents a complicated complex impedance load (138) and a number of papers have been written on the best method of achieving an impedance match to the oscillator output (139, 140). In the present case the highest possible deposition rate was not required indeed for epitaxial work it is general for the rate to be very low, so the only matching control used was the out put capacitor which was adjusted to transfer the maximum power to the discharge. The 1mH chokes used in the R.F. filters on the DC high voltage lines were made from 22 S.W.G. enamelled copper wire wound on a $1\frac{1}{2}$" diameter glass tube in only one layer. In this way the possibility of breakdown which may occur in multilayer chokes was avoided. The TY4 400 triode valves were air cooled by two fans (Airflow Developments 26BT) fitted one on each side of the case. The 3KV DC from the HT supply was connected to the oscillator using Uniradio nos 21 coaxial cables with Plessey brass Mark 4 coaxial male and female connectors. The same cable was used for connecting the RF to the target electrodes. The oscillator box, with grounded output connections, can be seen in plate I.

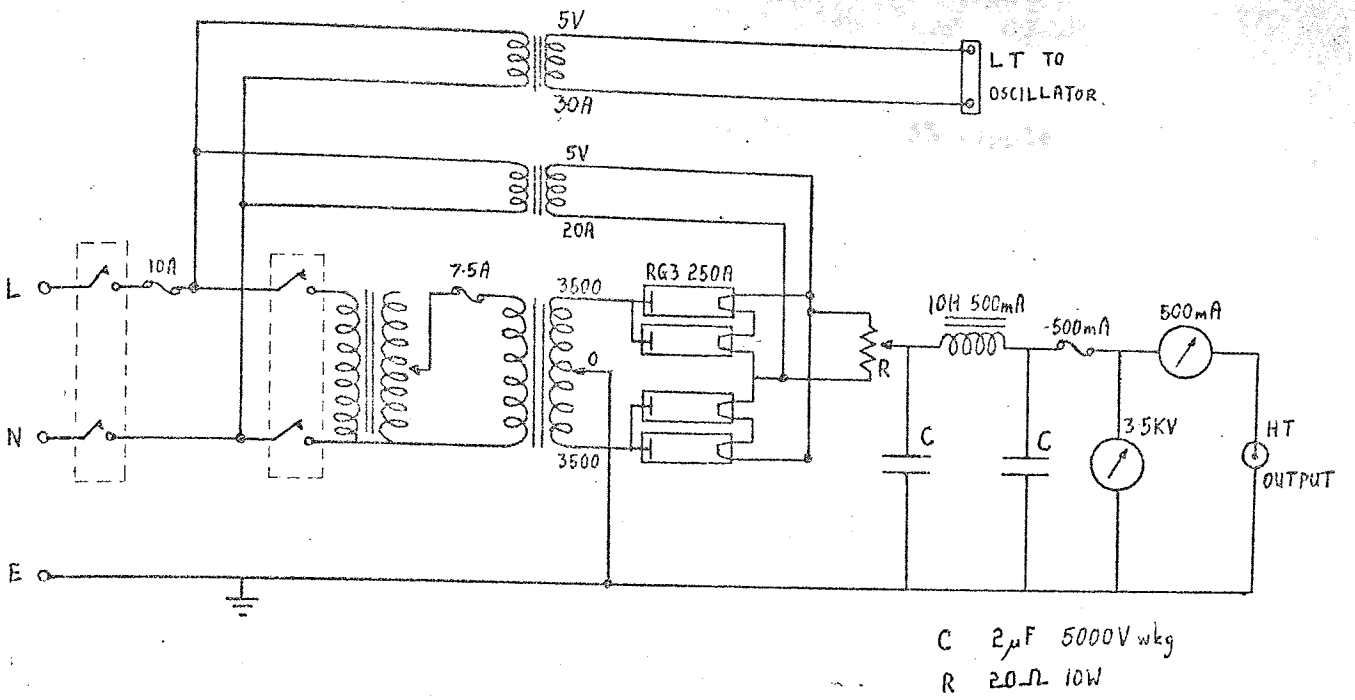


Figure 3.23.

Oscillator HT Supply

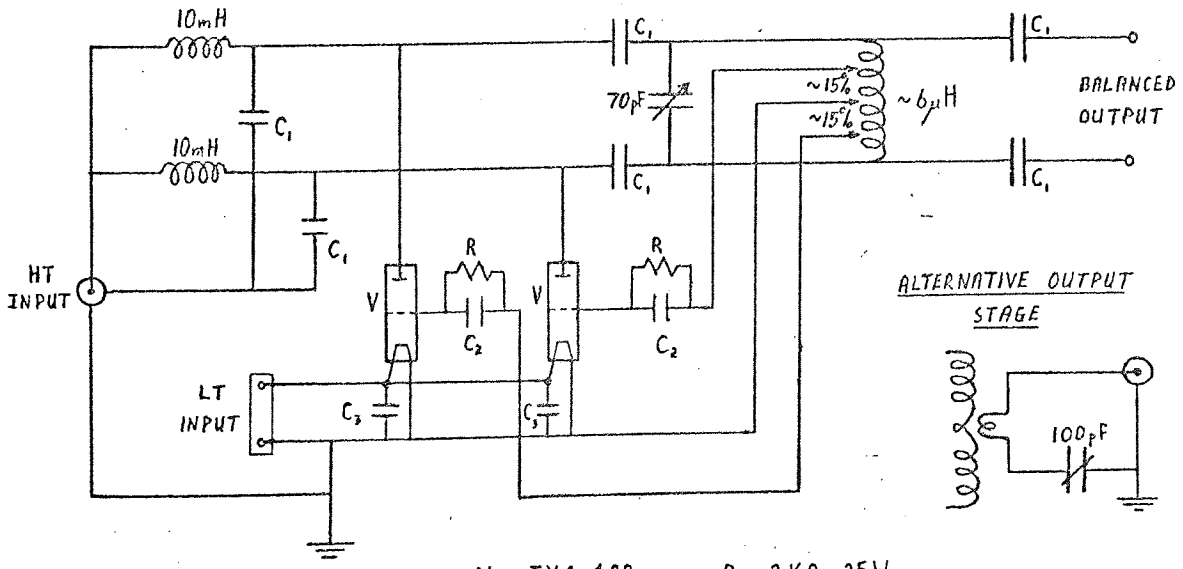


V TY4 400 R 2KΩ 25W

$C_1$ 1000pF 10KV wkg $C_2$ 125pF

$C_3$ 0·01μF (micc)

Figure 3.22

Oscillator Circuit

3.C.5.2. HT DC Supply.

| | | | |
|---|---|---|---|
| Oscillator HT Requirement | 3000 V | 500mA DC | 5% ripple |
| Valve Heaters | 5V | 28 amps AC | |

The oscillator valve heater transformer was also situated in the HT supply so that the HT could not be applied to the oscillator valves without the heaters being on. The HT circuit used is shown in figure 3.23. The output from a centre tapped full wave rectified bridge with mercury filled valves was smoothed by a choke input filter with component values again calculated using the Dayal criteria. An electrostatic 3.5 KV voltmeter was used for measuring the high voltage and the 500mA ammeter was well insulated from the case using perspex. Two on/off control switches were used, one operating the power to the heaters of the valves of both the HT supply and RF oscillator and the other, which was wired through the heater switch controlled the power to the HV transformer. This was necessary because the mercury diodes always required a warm up period of two minutes, which had to be extended to thirty minutes if the heaters had not been operated for more than a few days. The HT supply was initially tested using a dummy load consisting of three 2100 Ω resistance nets wired in series and hung from a "dexion" frame. The circuit was found to be adequate for the supply of 500 mA at 3KV. The whole RF generator circuit was tested using six 100 watt light bulbs as a dummy load and was found to oscillate at a frequency of 8 MHz.

3.C.6. Substrate Heater Supply.

The Nichrome strip heater had a cold resistane of 4 ohms and a current rating of 5amps so the heater power supply was required to provide a maximum AC output of 20V, 5A. The circuit used is shown in figure 3.24. A 20V, 300 VA transformer was fed by a 3A variable transformer and the current was measured directly, on a 10A rectified moving iron meter. The supply was constructed using "Lektrokit" and also mounted on a front panel bolted to the deposition trolley.

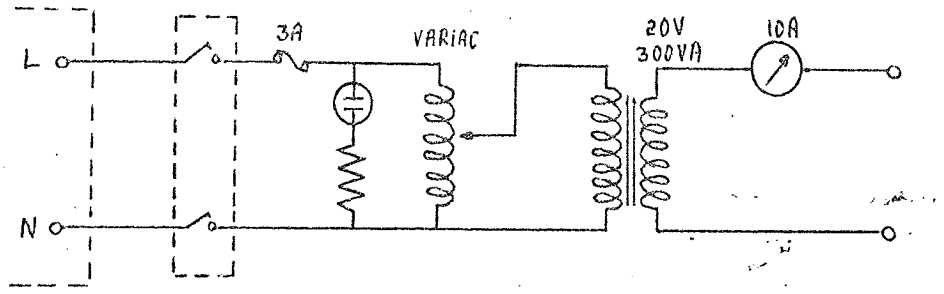


Figure 3.24

Substrate Heater Supply

## 3.D. Operation and performance of the Deposition System.

### 3.D.1. Substrate Preperation.

A number of different substrates were used each with a unique preperation so they will be dealt with in turn.

#### 3.D.1.1. Carbon film on Electron microscope copper grids.

Carbon films were produced in the usual way be creating an arc between two carbon rods in a vacuum and depositing on pieces of freshly cleaned mica. The film thickness was judged by the discolouation caused to a piece of white procelaine, on which was dropped a spot of apiezon oil. The carbon did not stick to the oil giving an uncoated region for comparison. Polaron 3.05 mm types C 200 and C 400 copper grids were used and were coated with carbon as follows. The grids were placed on a gauze immersed under water in a petri dish. The dish had a glass top sealed into its base so that it could be drained, and was supported on a tripod. The carbon film was floated off the mica onto the surface of the water and by draining out the water was allowed to settle over the gauze. When dried the copper grids with their carbon coating could be picked off the gauze with tweezers. The quality of the film on the grid could be checked using the Reichert MF optical microscope discussed in Section 4.2. Care was taken at all stages, particularly while drying, to minimise the dust falling on the grids and they were kept in an LKB Specimen grid box, which is a special container having one space for each grid. The grids were then transfered straight from the grid box to the substrate heater grid holder in the chamber, read for deposition.

#### 3.D.12. Potassium Bromide Single Crystals.

The potassium bromide single crystals available were in the form of slabs 4 mm thick, 1" wide and $1\frac{1}{2}$" long. It is a material with a very wide range of useful infra red transmission 1 to 25 $10^{-6}$m. and like most alkali halides has been often used in the formation of various epitaxial films. The pieces used as substrates were 4mm wide $\frac{3}{4}$" long and about 2mm thick and were cleaved just prior to loading in the chamber. A one sided razor blade, stored under vacuum when not in use, was used for this purpose. The blade was

held parallel to the cleavage face and tapped with an ebonite rod and usually, a good single piece seperation resulted.

3.D.1.3. Epitaxial Gold Films.

It was decided during the project to try to epitaxially deposit barium titante onto gold. For this either single crystals of gold had to be purchased or gold had to be itself first epitaxially deposited onto some other substance. Clearly the second alternative was much cheaper and was adopted. Potassium chloride single crystals were available in the department and gold was known to epitax with the required (100) oxientation parallel to (100) cleaved faces of the crystal (141). The crystals were available in the same form as the potassium bromide and were cleaved in the same manner. A standard vacuum coating unit was used and a series of depositions were performed in order to roughly determine the best conditions to produce 100//100 epitaxy. The gold was premelted onto a tungsten spiral source and the crystals cleaved just before loading into the chamber. The cystals were heated using a simple molybdenum wire mica insulated heaterwhich was run directly off an 8 A "Variac" and drew up to 5A current. The position of the cystals with respect to the source, the substrate temperature and the deposition rate were varied for each deposition. An epitaxial temperature of 380°C is quoted by Chopra (141) but this is likely to be affected by deposition rate, film thickness, whether the crystal was cleaved in air or vacuum, and other parameters. Depositing gold on air and vacuum cleaved sodium chloride, for example, Matthews (142) reported (100) nuclei predominated initially but with increased thickness (111) nuclei occured which grew faster in the latter case but slower in the former case. In our system gold deposition rate was not actually measured so the variation made to the parameter was very approximate. In the short time devoted to this question no definite conditions which produced (100) parallel epitaxy every time were found. In fact in some cases when gold was deposited onto several pieces of potassium chloride at one time, some gold films were 100% (100) orientated, others mixed (100) (111) and yet others mainly (111) orientated. However each gold film was checked on

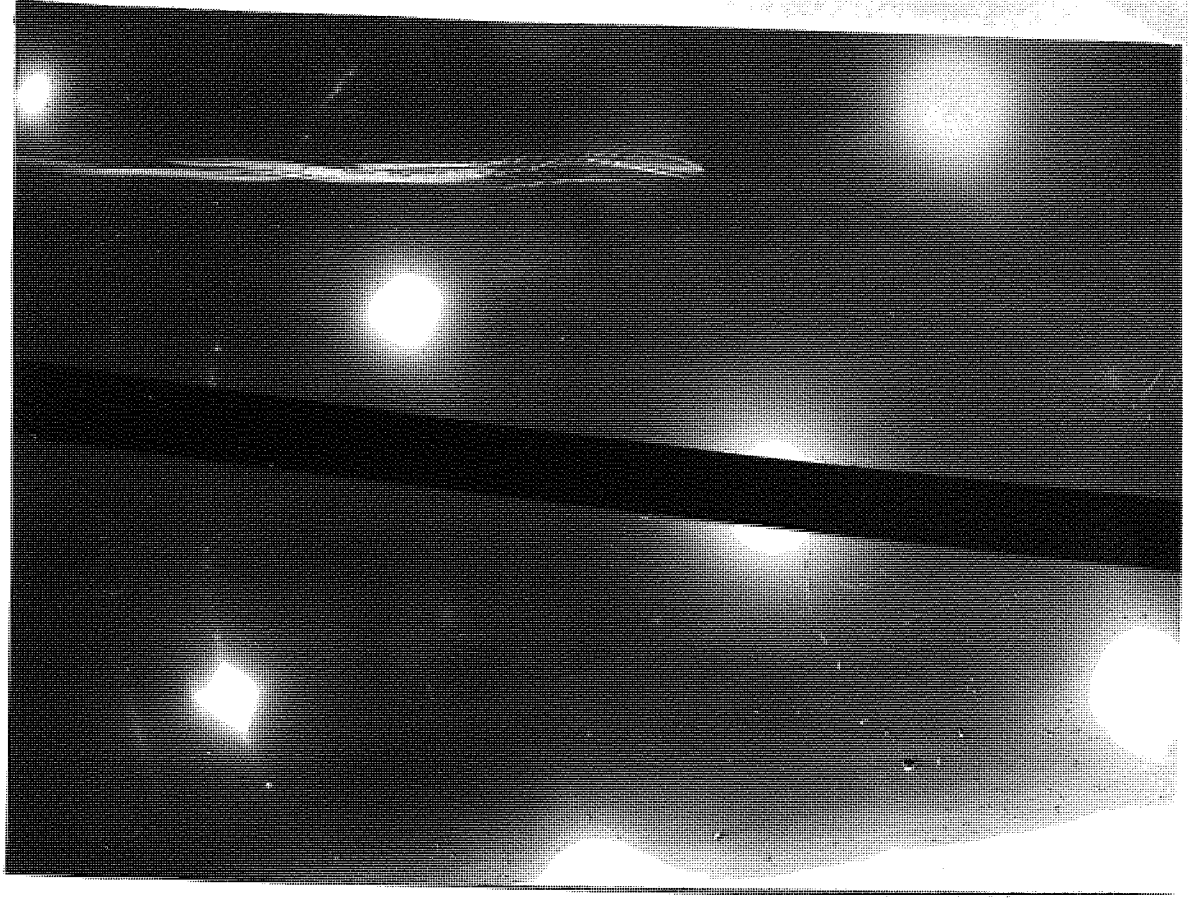

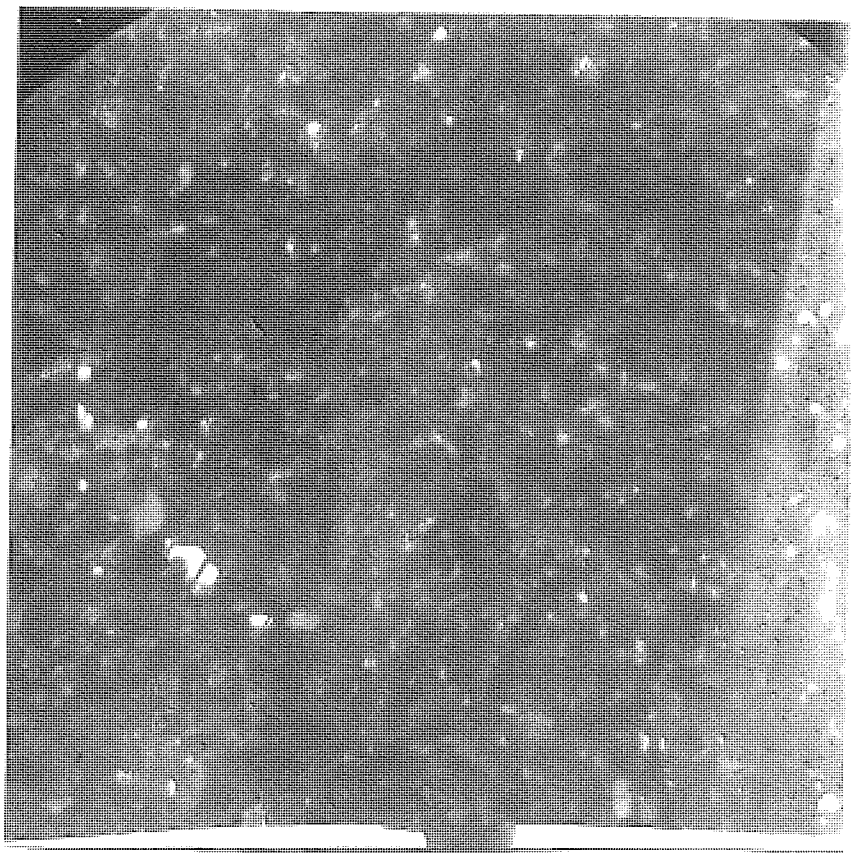

GOLD FILM

X 27K

PLATE IX

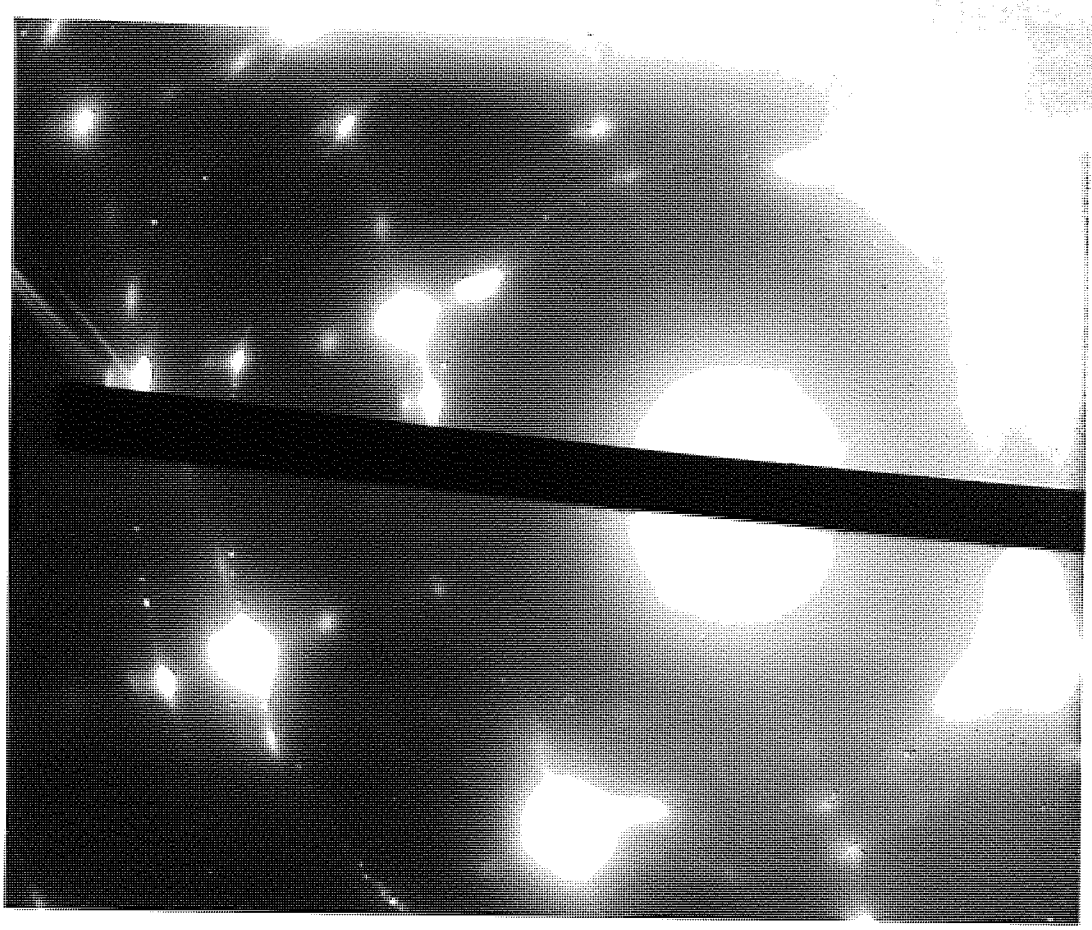

PLATE X

its substrate using the goniometer Xray diffraction set discussed in Section 4.6 and only films with 100% or almost 100% (100) orientation were used as substrates for the titanate. Figure 3.25 shows the chart output from the Xray goniometer of several films with different deposition conditions as stated. To confirm the epitaxy of the gold on the crystals some gold films which gave 100% (100) orientation using the Xray diffractometer were inspected in the electron microscope. To do this the films were floated off in water picked up on copper grids and examined by selected area diffraction (Section 4.3.2). Plate IX shows an electron micrograph and diffraction pattern of the (100) film and plate X shows an intersting case of twinning of the crystal structure of another part of the same film.

3.D.1.4. "Chance" microscope glass slides.

The M.I.M. sandwhich structure films were deposited onto ordinary 1" square 1/16" thick "Chance Bros" microscope slides. These were cleaned by a process including a final vapour degreasing stage first suggested by Lowe (143). The slides were either cleaned seperately or in a wire cage that prevented them touching one another. The cage loaded with substrates was emmersed in a beaker of a dilute solution of "teepol" and heated to boiling on a hot plate. The beaker was then agitated in an ultrasonic tank for ten minutes. The detergent solution was then thoroughly rinsed away with distilled water and the glass slides ultrasonically agitated for five minutes in the water. The water was then rinsed away with isopropyl alcohol and the beaker filled so as to just cover the substrates. The alcohol was heated to boiling on the hot plate and the substrates were slowly withdrawn one at a time through the vapour and put in individual plastic substrate boxes. Despite this glass cleaning process the adhesion of aluminium films deposited on the glass was occasionally not good enough to support a gold wire hot compression bonded electrical contact (Section 3.D.4). Consequently, as other workers in the field have done (143,144) a thin, 300 Å, layer of nichrome was deposited before the aluminium to form pads for the electrical connections. The chrome content in nichrome reacts with most glasses causing much improved adhesion

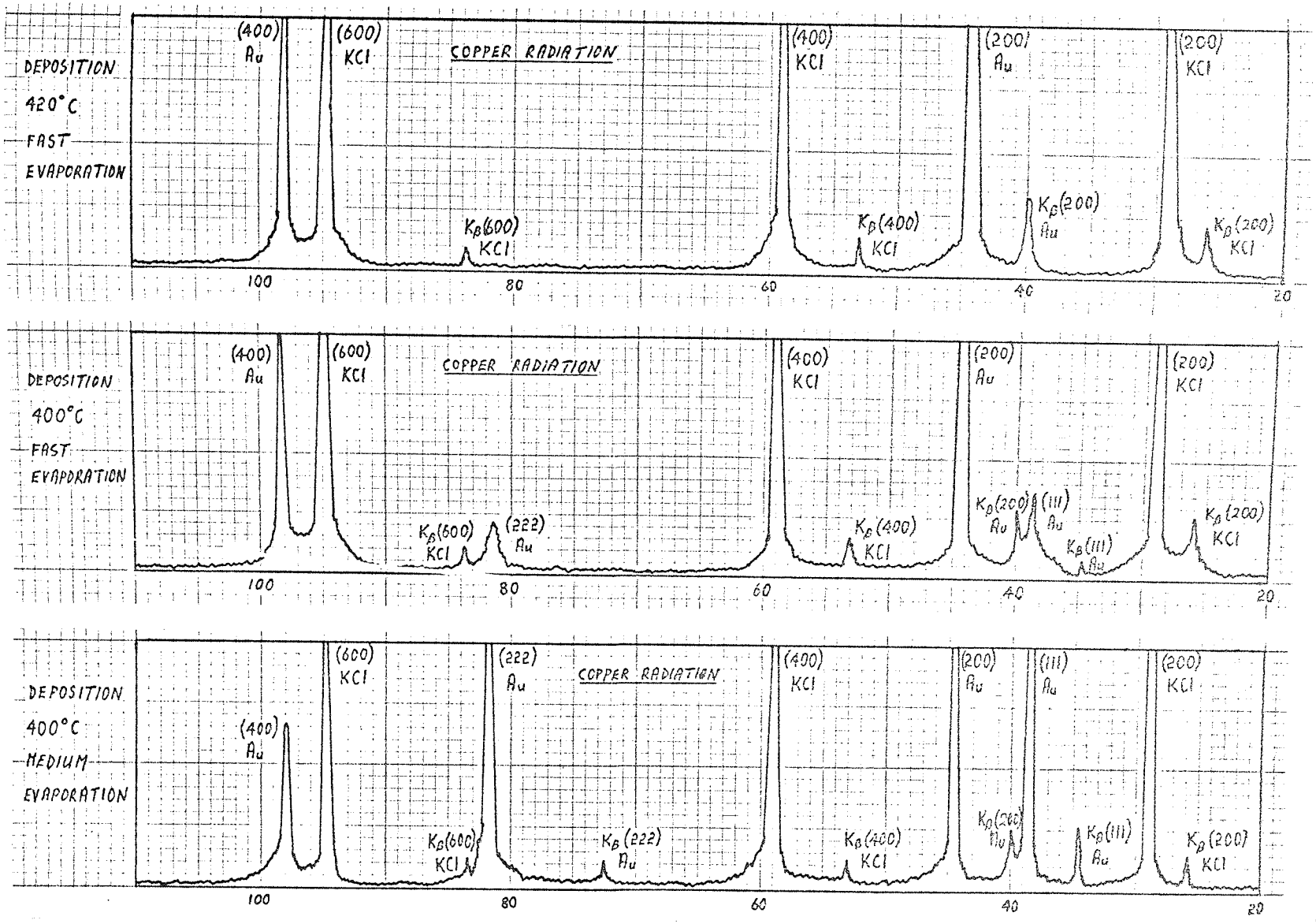
DEPOSITION
420°C
FAST
EVAPORATION
(400) Au
(600) KCl
COPPER RADIATION
(400) KCl
(200) Au
(200) KCl
Kβ(600) KCl
Kβ(400) KCl
Kβ(200) Au
Kβ(200) KCl
100
80
60
40
20
DEPOSITION
400°C
FAST
EVAPORATION
(400) Au
(600) KCl
COPPER RADIATION
(400) KCl
(200) Au
(200) KCl
Kβ(600) KCl
(222) Au
Kβ(400) KCl
Kβ(200) Au
(111) Au
Kβ(111) Au
Kβ(200) KCl
100
80
60
40
20
DEPOSITION
400°C
MEDIUM
EVAPORATION
(400) Au
(600) KCl
(222) Au
COPPER RADIATION
(400) KCl
(200) Au
(111) Au
(200) KCl
Kβ(600) KCl
Kβ(222) Au
Kβ(400) KCl
Kβ(200) Au
Kβ(111) Au
Kβ(200) KCl
100
80
60
40
20

Figure 3.25

between the glass, itself, and aluminium deposited over the nichrome. The bonding pads were deposited through modified deposition masks in another vacuum kit in the laboratory, described elsewhere (145). The glass slides were put through the cleaning process described and loaded with tweezers into the vacuum kit. Apporximately 200 Å of nichrome and 500 Å of aluminium deposited, in one pump down, from single wire tungsten sources were used to form the pads. After deposition of the bonding pads, substrates were taken through the final stage of the cleaning process, that is the boiling alcohol, again, before being loaded in the chamber for titanate deposition.

3.D.1.5. Gold/Nichrome film deposited on Glass.

Thin microelectronic circuit arrays are often based on a nichrome/gold-resistor/conductor system deposited on glass and the use of sputtered barium titanate films in this system was investigated. The substrates, 7059 Corning glass with coatings of 250 Å of nichrome and 2000 Å of gold were kindly provided by J.Lucas Gas Turbine Equipment Ltd. The substrates had been etched, leaving clear glass down two sides so that overlap capacitors could be made, as shown in figure 3.26. The 3 x 2 cm slides were cut in half, so as to fit in the substrate heater, before being cleaned for deposition. The same cleaning process was used as for the "Chance" glass slides and bonding pads were again deposited when necessary.

3.D.2. The Deposition Procedure.

The operation of the vacuum system had already been described in Section 3.A.7. The deposition procedure was the same for all substrates except when an M.I.M. titanate sandwhich structure was deposited. In this case the bottom electrodes were evaporated using 4N aluminium with the substrate in the lower position and the first mask in place. The mask holder was then lifted and it and the evaporation sources were rotated clear to allow the substrate table to be wound up and located in the dielectric mask holder on the upper false baseplate. All other substrates were loaded with the substrate table in the upper position. The titanate deposition proceded when the substrate temperature and base pressure were reached. The gas bleeds were flushed and the

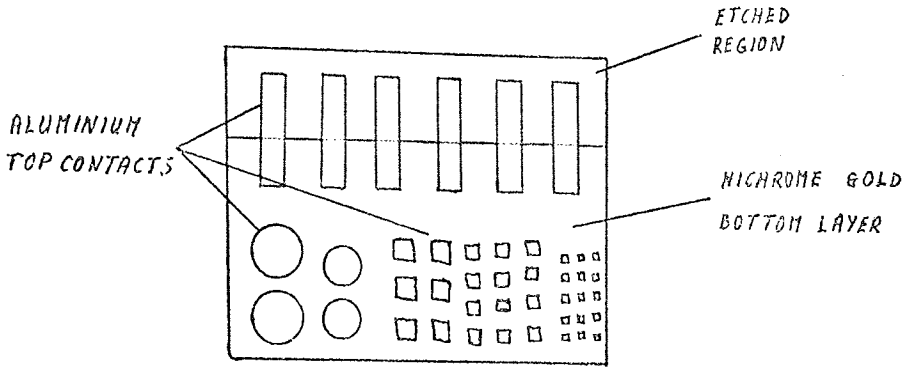


Figure 3.26

Overlap and Top Contact Capacitors

on Gold Films on Glass

pressure allowed to settle down, as described in Section 3.A.7, before the discharge was ignited, as follows. After checking that the shutter was closed, the R.F. voltage was wound up so that the DC supply meter read about 1000V and the magnetic coil current was set to about 3.5A. The argon pressure was then increased by opening the needle valve until the discharge struck. The pressure could then be slowly lowered to as low as $1.10^{-3}$ torr and the HT increased to the required valve without extinguishing the discharge. For a given HT voltage the pressure and coil current were adjusted in the ranges $1.10^{-3}$ - $3.10^{-3}$ and 3-4A to give a stable discharge. The Oscillator plate tuning capacitor was adjusted to give minimum plate current at resonance and the matching capacitor was adjusted to give maximum plate voltage compatible with discharge stability. Once established the discharge stayed stable for long periods, (several hours), requiring only occasional adjustments to the settings, usually the pressure. The shutter was kept closed for 10-15 minutes after igniting the discharge to allow contaminants and absorbed gases to be removed from the surface of the target before deposition commenced. It was important that the target water cooling, which was taken from mains to drain, should be flowing when the discharge was ignited so the tap was always turned on before the R.F. supply was switched on. When a deposition was complete the HT to the oscillator was wound down and after two minutes the heater and gas bleeds were switched off. The pumping system was allowed to continue pumping the chamber until the substrate temperature fell below 100°C and the pressure fell to $\leqslant 1.10^{-6}$ torr before the target cooling water was turned off and except when depositing M.I.M. structures the main butterfly valve was shut. In the case of M.I.M. sandwiches, the substrate was lowered to the bottom position and the mask holder swung into place and lowered down to locate the 2nd top electrode mask on the substrate table. The aluminium sources were rotated to sit directly over the substrate and the high current filament lead transfered to the leadthrough feeding the second tungsten filament. The source was heated and when the aluminium evaporation was completed the butterfly valve was closed. The deposition procedure was then

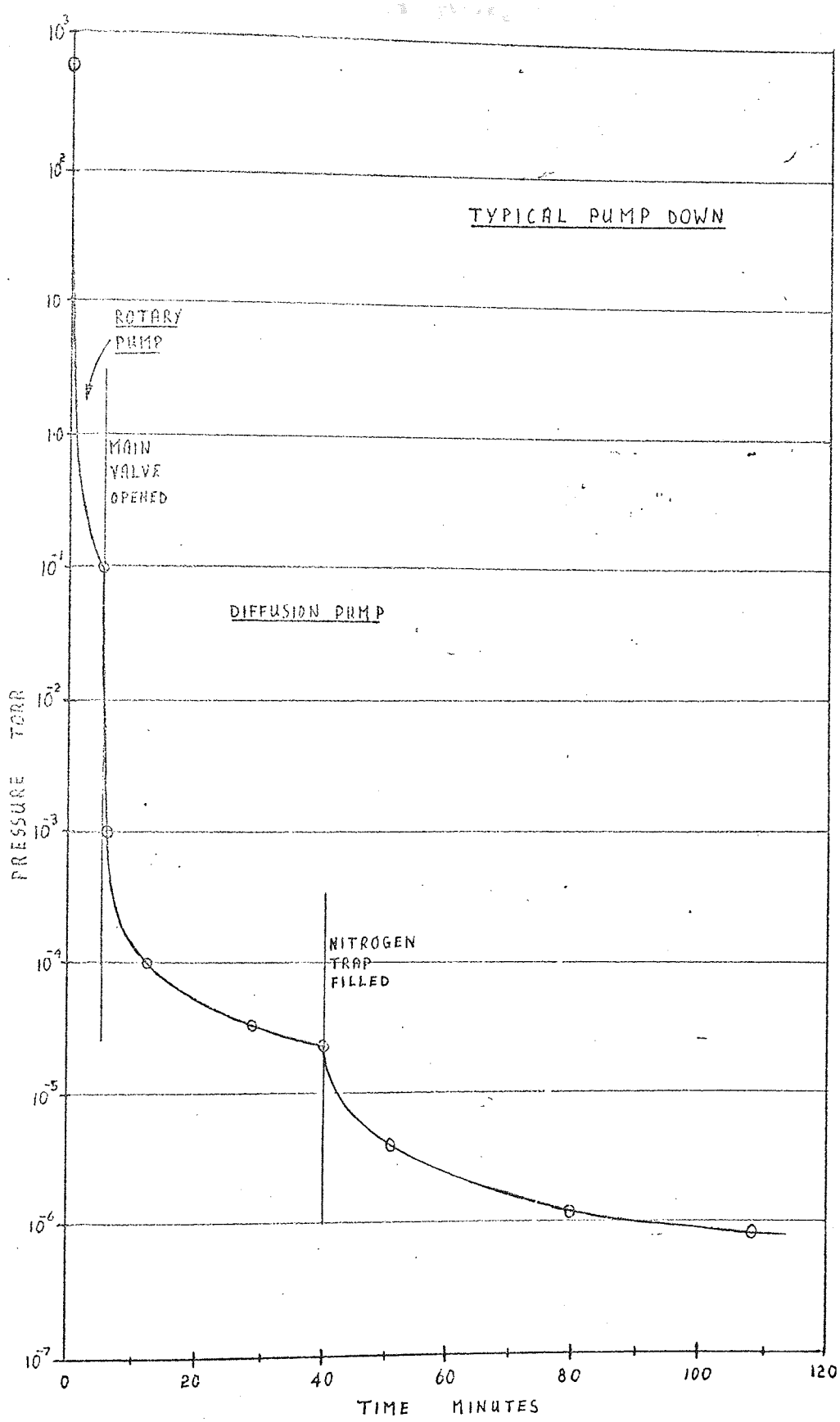


Figure 3.27

Pump Down

completed by shutting down the pumping system as described in Section 3.A.7.

3.D.3. Performance of the deposition system.

3.D.3.1. Vacuum performance.

Figure 3.27 shows the progress of a typical pump down plotting chamber pressure against time. When the heater was used the period of time between $1 10^{-4}$ and $1 10^{-6}$ torr was extended up to $1\frac{1}{2}$ hours depending on the required substrate temperature. The top trap when used was operated after the substrate temperature had been reached and the pressure improved to a 2-3 $10^{-7}$ torr only a few minutes after liquid nitrogen circulated completely round it

3.D.3.2. Sputtering deposition rate.

Barium titanate deposition rate was found to be a function of the plate coil HT voltage as can be seen from figure 3.28. This plots the deposition rate, for a large number of films all deposited at the same pressure and magnetic fields, against plate voltage. Changes in rate for a given voltage can be explained by slight changes in pressure or matching conditions or by variations in substrate temperature or deposition time. It was found that the deposition rate fell off by up to 10% during a deposition of several hours. The deposition rate also fell slightly with increased substrate temperature. This is shown in figure 3.29 where the deposition rate on potassium chloride fell as the crystal temperature was increased from 250° - 350°C. This is no doubt due to a decrease in sticking coefficient with the higher energy of the impinging atoms on the hotter substrate surface. Davidse and Maissel (93) reported a very large reduction in the deposition rate of R.F. sputtered quartz with the introduction of a small percentage of oxygen into the sputtering gas, but this was not observed for barium titanate. The highest percentage of oxygen used was 10% and this caused no significant reduction in deposition rate. In the account of film properties a number of films are reported as having been deposited at ambient temperature, which meant the heater was not used. However as might be expected the substrate did warm up during deposition due to the heating effect of the discharge so the mean

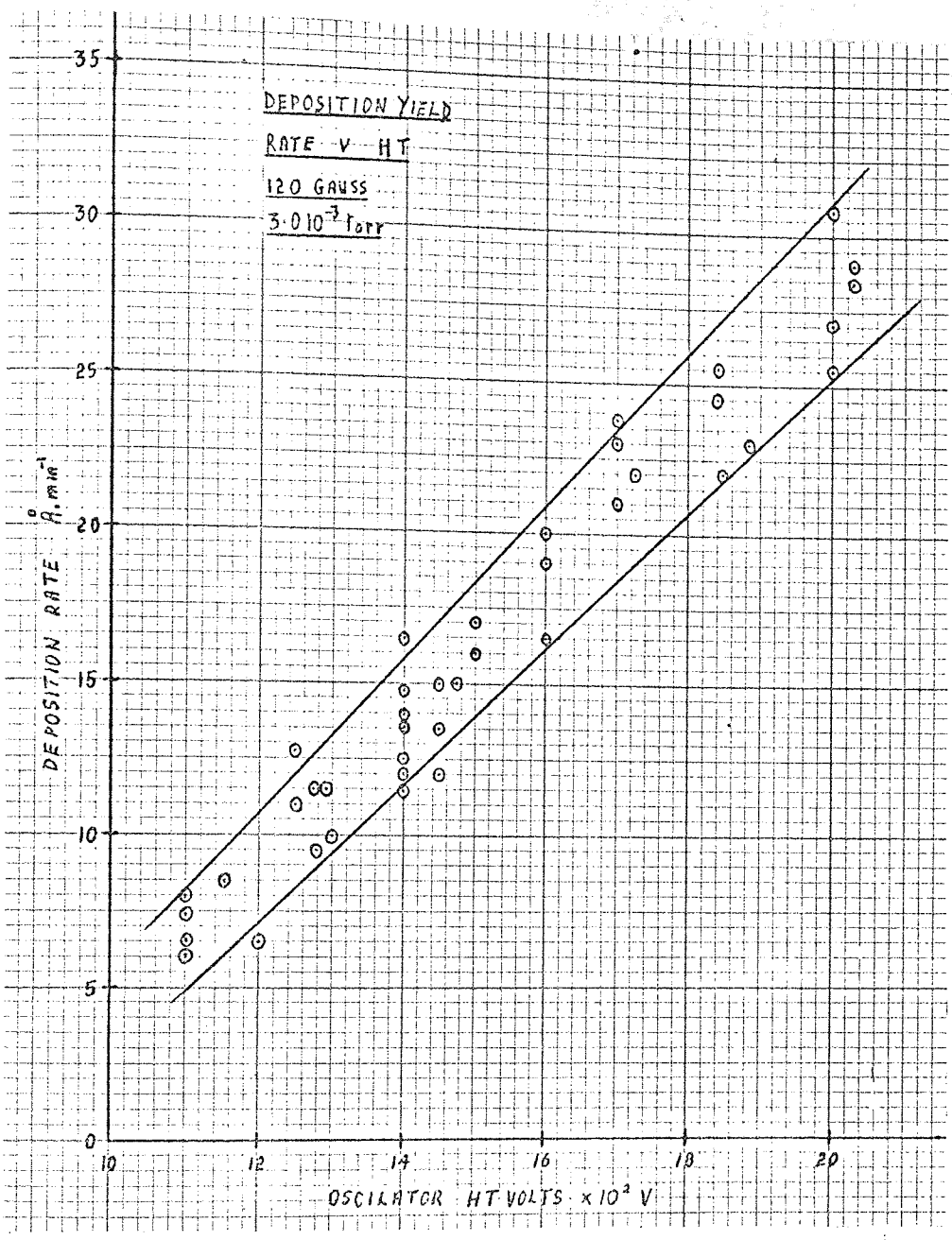


Figure 3.28

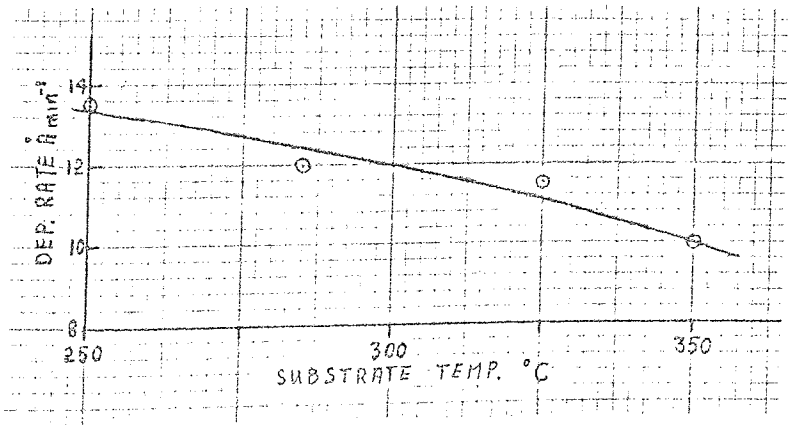


Figure 3.29

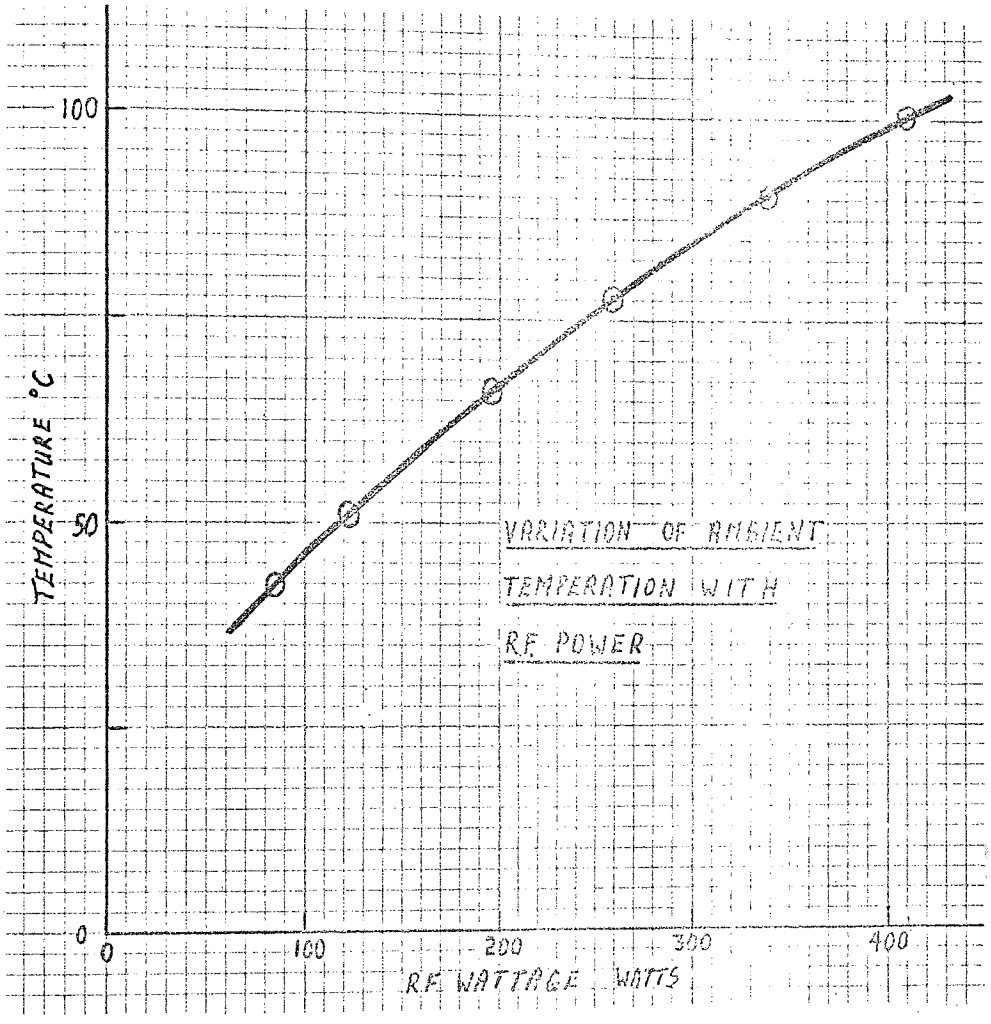
100
50
0
TEMPERATURE °C
0
100
200
300
400
RF WATTAGE WATTS
VARIATION OF AMBIENT
TEMPERATION WITH
RF POWER

Figure 3.30

substrate ambient temperature is some way above room temperature. The magnitude of this effect can be seen in figure 3.30 which shows the temperature as a function of the power applied to the oscillator. To obtain this plot the discharge was allowed to run for at least 30 minutes at each setting before the temperature was measured to ensure thermal equilibrium had been reached.

3.D.4. Gold wire hot compression bonding.

Electrical contact was made to isolated top electrodes on the titanate films using a gold wire light pressure contact (Section 4.8). Contact to base electrodes or overlap top electrodes was made using a hot wire compression bonding technique. The bonder used which is shown in plate X1 was made in the laboratory but incorporated a Tempress Research Company capillary wire heater. This was run at a maximum of one ampere using a rheostat to limit the current from a 12V car battery. The 0.003" gold wire was fed from the spool through the heater capillary and the end was melted into a ball with a small gas flame. The gold wire was withdrawn until the ball was tight against the bottom of the capillary heater and allowed to heat up. The position where the bond was to be made could be accurately adjusted using the two mutually perpendicular vernier translators. The heater assembly was then wound down with the third vernier translator until the spring at the top of the heater column caused pressure and heat to be applied to the gold ball - substrate interface. After a few seconds the heater was wound away and a firm bond was found to have been made to the metal film on the substrate. The gold wire could then be cut at a suitable length using a fine metal clipper and the free end prepared to make the next bond. A block heater was available for heating the substrate to improve the bond but in most cases this was found to be unecessary.

PLATE X1

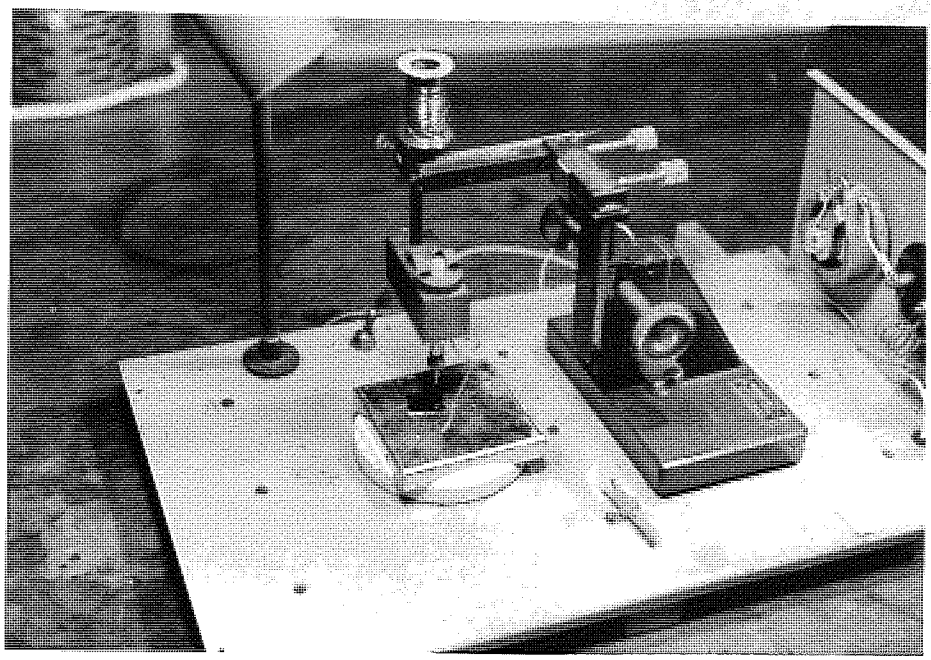

PLATE X11

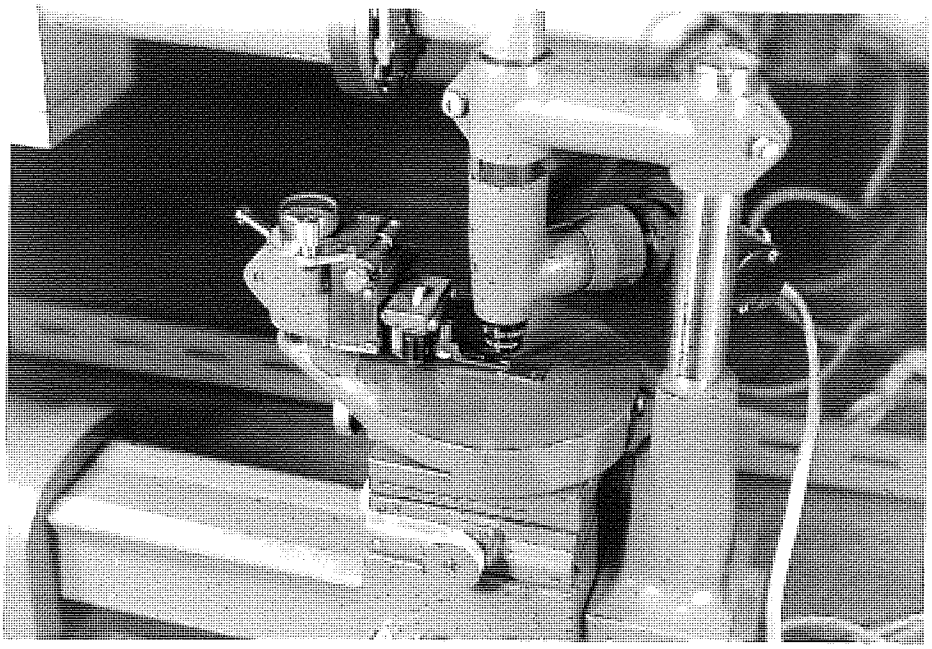

PLATE X111

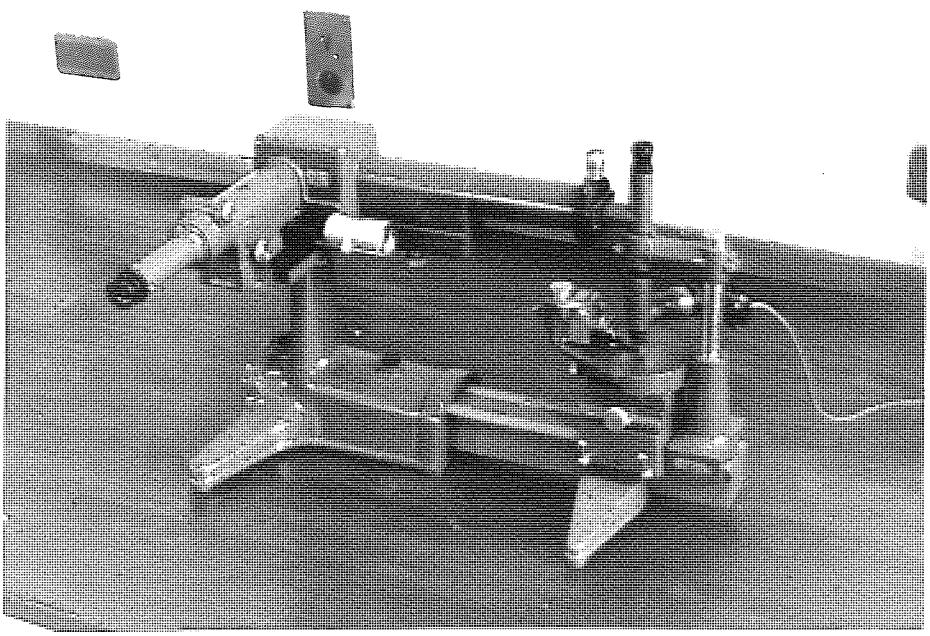

# CHAPTER FOUR

## MEASURING TECHNIQUES

### 4.1. Film Thickness.

Film thickness was measured using the technique of Multiple Beam Interferometry, developed by Tolansky and his co-workers.[144] There are two basic methods; one produces Fizeau fringes of equal spacing using monochromatic light, while the other produces fringes of equal chromatic order using white light. The second method was employed because it has a higher resolving power for thinner films. To measure film thickness using this technique, a sharp step has to be produced by masking off part of the substrate during deposition. A highly reflective opaque film is then deposited which accurately contours the step. A multiple beam interferrometer is then formed by placing a small half silvered optical flat over the coated step. This is illuminated normally with white light and the fringe system is viewed through a spectrometer. The apparatus used was a commercially produced accessory allowing film thicknesses to be measured using a Hilger and Watts N 130 interference microscope, and is shown in plates X11 and X111 Plate X11 shows the screws which can be adjusted to position the optical flat exactly parallel to the substrate. Multiple reflections occur in the air gap between the half silvered flat and the opaque reflecting coating on the substrate. For a series of wavelengths through the spectrum the path difference on reflection is such that interference occurs and dark fringes appear. At the film step, there is a step in the wavelength at which the interference fringes occur. The resulting view as seen in the spectrometer is shown in figure 4.1 and by measuring the wavelengths of the fringe positions the film thickness can be determined using equation 4.1. where $n_1$ is a whole number

$$t = \frac{n_1}{2} \Delta \lambda_1 \qquad 4.1$$

called the fringe order and is given by equation 4.2. The targets of

$$n_1 = \frac{\lambda_2}{\lambda_1 - \lambda_2} \qquad 4.2$$

sputtering systems represent effectively continuous sources so perfectly sharp steps are impossible to produce due to shaddowing. As a result the

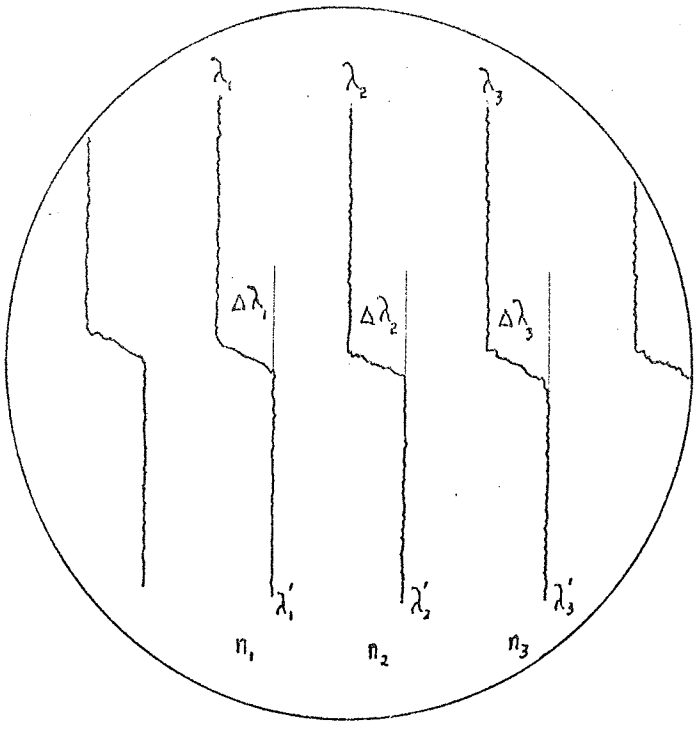


Figure 4.1.

Appearance of Film Thickness Fringes

masking plate needed to be as thin as possible. In general film thicknesses were not measured on the substrate itself but on a specially included thickness substrate. This was found necessary when depositing on single crystal substrates and was employed for nearly all other substrates. The thickness substrate used was a $\frac{1}{8}$ oz. Chance microscope glass slip cut to approximately 4 mm square. A similar piece half that size was laid on top of it to produce the film step. This thickness substrate was positioned on the substrate heater to maintain it at the same height and at roughly the same temperature as the substrate. In spite of these precautions the appearance of the step in the specrometer was not sharp and in some cases made the exact step width difficult to measure. As a result film thickness measurements have an accuracy at the best of about $\pm$100 Å. In the case of deposition substrates other than glass the use of glass slip thickness substrate makes the assumption that the sticking coefficients of the sputtering atoms is not much different on the two substrate materials. This condition was roughly fulfilled as the interference colour of thicker films was noted to be the same on both substrates.

4.2. Optical microscopy

Films deposited on all substrates except carbon coated electron microscope grids were viewed and photographed using a "Reichert" MeF Universal Camera optical microscope. The films could be viewed in dark or light fields using transmitted and reflected light with magnifications using low power attachments ranging from as low as x 11 up to x 3000.

4.3. Electron Microscopy

The electron microscope is an ideal tool for studying the texture, crystal structure and structural defects of thin films. It can be used in two ways, one giving a highly magnified electron image of the specimen with a resolution down to 10 Å, and the other giving a diffraction pattern of the specimen. The instrument available was an A.E.I EM6 microscope to which a high resolution electron diffraction heating stage could be attached.

4.3.1. Electron Diffraction.

Diffraction patterns of a specimen can be obtained by two methods, transmission, when the film must be thin enough for the electrons to penetrate through it, and reflection when grazing electron incidence is required. In reflection information is obtained about the surface layers of the film while in transmission information is obtained from the whole volume of the film. Of course for very thin films the methods are equivalent. The diffraction stage was fitted just below the projector lens of the microscope and had controls for two translatory and two rotational movements. The specimen holder accommodated either normal microscope grids or small planar specimens glued to a specimen support post. The stage could be operated in either the reflection or transmission mode by rotation of the specimen. The stage contained a heating attachment which used a secondary beam of electrons to heat the molybdenum microscope grid specimen holder up to temperatures of 1200°C. The temperature was measured with a chromel alumel thermocouple pressed onto the edge of the grid itself. Alternatively at low power the electron beam could be used to neutralise electron charge build up on an insulating specimen during reflection diffraction. Titanate films deposited onto or picked up on microscope grids were easily loaded but films still on other substrates were cut to fit and then attached to the specimen posts using "aquadag", in order to maintain a conduction path for the impinging electrons. The stage was operated using only the first condensor and objective lenses of the microscope to focus the electron beam on the specimen and the diffraction pattern was displayed on the screen. Diffraction patterns were also obtained from films on microscope grids loaded into the normal specimen stage by inserting a diffraction appeture, removing the objective appeture and switching the projector lens to diffraction. The pattern was then focussed on the screen using the projector difraction control potentiometer.

4.3.2. Electron Micrography.

Due to the low penetrating power of electrons transmission microscopy was limited to films of thickness ~1000 Å. The technique was used to examine films of thickness 300-1100 Å deposited onto single crystals of potassium bromide. These films were floated off the crystals in a petri dish of distilled water and picked up on carbon coated grids (this technique is described in more detail in Section 6B 1.1) and allowed to dry. The microscope was used for examining the films at magnifications up to x 120,000. This technique can be used with transmission diffraction in an analytical technique called selected area diffraction when a particular area of the field of view of the transmission picture can be selected using the diffraction aperture. The geometry was such that a 0.25 mm aperture selected an area only 6.25μ in diameter. This aperture cuts off the diffraction electrons from all other parts of the specimen so, if the microscope is switched to diffraction, a pattern resulting from the selected area only, is seen on the screen. In this way variation in structure and texture across a particular film was examined.

4.4. Scanning Electron Microscopy.

A scanning electron microscope builds up a picture of a specimen by examining the intensity of electrons emitted from the object as a function of position, as an electron beam is scanned across it. This is done by tilting the specimen at an angle to the beam and using a scintillating photomultiplier detector system. The equipment used in this investigation was a "Cambridge Instruments" S.E.M. The instrument has a magnification up to 30,000 x and gives a resolution of 200Å. This comares with 1000 Å for the optical microscope and 10 Å for the electron microscope. The S.E.M. has the advantage over transmission electron microscopy of being able to produce direct images of opaque specimens and has a much greater depth of focus, approximately half the width of field, than the optical microscope. Films could therfore be examined without being removed from their substrates. Specimens were prepared by cuttingto size and attaching to the aluminium

specimen posts with aquadag in order to allow leakage of charge from the specimen surface.

4.5. Infra Red Spectroscopy

Potassium bromide is transparent for much of the infra red region and can be used satisfactorily in the wavelength range 1-25.$10^{-4}$cm. Films deposited on this material could therefore be readily examined by Infra Red Spectroscopy. A "Grubb Parsons" Spectromaster was available for this purpose. The instrument had two ranges 1-5$\mu$ and 5-25$\mu$and used a split beam technique, comparing the relative intensity of two beams after one has passed through the specimen. Powdered, trial specimens of barium titanate were examined by dispersing the powder in dry potassium bromide and pressing in a cylindrical die to form a clear disc, which could fit directly into the specimen holders. A stainless steel jig, opaque to infra red radiation, was made to support the film coated potassium bromide crystals in the specimen holders and, for increased sensitivity, a blank crystal was supported in the comparator beam path.

4.6. Xray Diffraction.

A "Philips" Xray set which could be used for powder and back scattering work and another "Philips" set with a goniometer stage and chart recorder output were both available for limited use in the Physics Department Xray laboratory. All Xray diffraction results quoted were obtained using these instruments. If enough material was available the specimens for the powder camera were prepared by grinding and sieving the powder before tipping it into a thin glass capillary. These capillaries were sealed in very fine points and the powder was worked down to the bottom until a sufficient length of the capillary was full. This was then cut off and stuck into the rotating centre of a Debye Scherrer camera with plastercine. When only a limited amount of powder was available it was glued to a very thin glass rod using a structureless adhesive and the rod was again fixed in the camera with plastercine. This thicker specimen caused broader lines to the powder photograph but was otherwise satisfactory. For checking the structure of films deposited on glass

or crystalline material the goniometer stage was used and the films were supported at the correct height on the usual specimen holders using plastercine or cellotape.

Xray diffraction is much less sensitive than electron diffraction because the diffracted intensities are considerably smaller ($\sim 10^{-3}$ times). Diffraction lines are also broadened as the crystallite size is reduced resulting in the loss of lines for specimens composed of small crystalites. The broadeneing is a function of the Xray wavelength, making the effect negligeable in electron diffraction. Consequently Xray diffraction lines are often not observed unless the films are thick (~microns) or are orientated in a given crystal direction.

4.7. Permitivity (Capacity) Measurements.

The capacitance and dissipation factor ($\tan \delta$) of sandwich metal-titanate-metal structures was measured using either a Marconi TF 2700 or a Wayne Kerr B 221 universal bridge. The metal electrodes formed a parallel plate condenser so that the low frequency dielectric constant could be calculated using equation 4.3. where C is the capacity, A the

$$C = \frac{\varepsilon A}{d} \text{ Farads} \qquad 4.3.$$

plate area in m, t the film thickness, m and $\varepsilon$ the permitivity. The Marconi bridge operated at 1000 Hz to an accuracy of 1% while the Wayne Kerr operated at 1592 Hz with an accuracy of 0.1% over a range from $1.10^{-6}$ F to $0.1.10^{-12}$ F. Permitivities were measured for titanate films deposited onto aluminium films or gold films on glass and gold films on potassium chloride. For the M.I.M. strip capacitor design the measurements were made between gold wires bonded to the respective contact pads. For the gold/nichrome on glass substrates overlap strip electrodes or very small top electrodes were evaporated through a machined mask or a fine gauze respectively. Top electrodes evaporated through gauzes with a choice of mesh size were also used in depositing the second capacitor plate for films deposited on potassium chloride. This reduction in capacitor area reduced the probability of a shorted device due to pinholes or other

large physical faults in the titanate film. The substrate was supported on the table of a micromanipulator with one manipulator arm, as shown in plate XIV. The bottom electrode connection was always made by a bonded gold wire, soldered to the L.T. bridge lead. For devices where the top electrode was not overlapped and a bonded wire could not be used a pressure connection was made with a 0.002" gold wire. One end of the wire was soldered to the bridge detector lead and the other end fed through a short capillary tube supported on the arm of the micromanipulator. The length of wire that protruded from the capillary was bent so that it exerted a weak pressure on the substrate when lowered to make contact with the top electrode of the film capacitor. The wire was accurately positioned over the small capacitor areas using the micromanipulator viewing through the long range x 10 binocular microscope To obtain the maximum accuracy from the Wayne Kerr bridge an open circuit null point had to be set, to allow for the impedance of the leads. This was done by adjusting the capacitor and resistor trim controls, with the gold wire lifted just clear of the top electrode. The Wayne Kerr bridge was the more accurate and also gave the more reliable results for capacity, when the dissipation factor was high (>1). The Marconi bridge was however much quicker to operate so initial measurements for each film were made with it, and the accurate measurements with the Wayne Kerr. To measure capacity and dissipation factor over a range of temperatures (20-180°C) a small block heater was placed on the manipulator table as shown in plate XIV. The heater was wound out of 30 gauge 2mm michrome strip on a "cindanio" former and was run directly from a mains driven 3A Variac. The substrates were placed on top of the heater block and the temperature was measured with a copper constantan termocouple clamped onto the substrates.

4.8 Current-Voltage Characteristics over a range of temperature.

Electrical characteristics were measured for sandwich titanate capacitor films deposited on glass. The measurements were performed in a cryostat over a range of temperatures extending from liquid helium

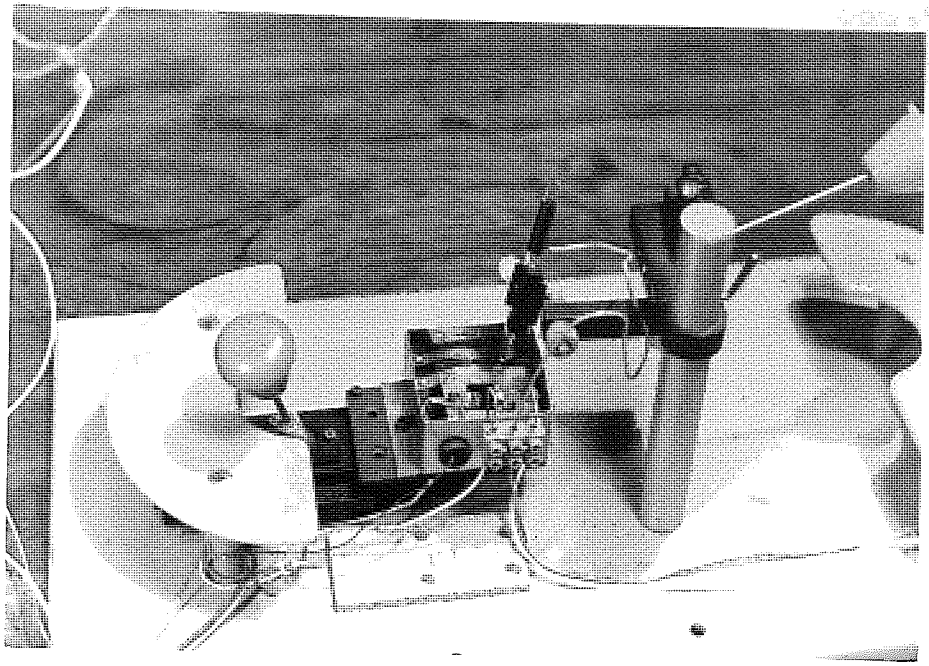

PLATE XIV

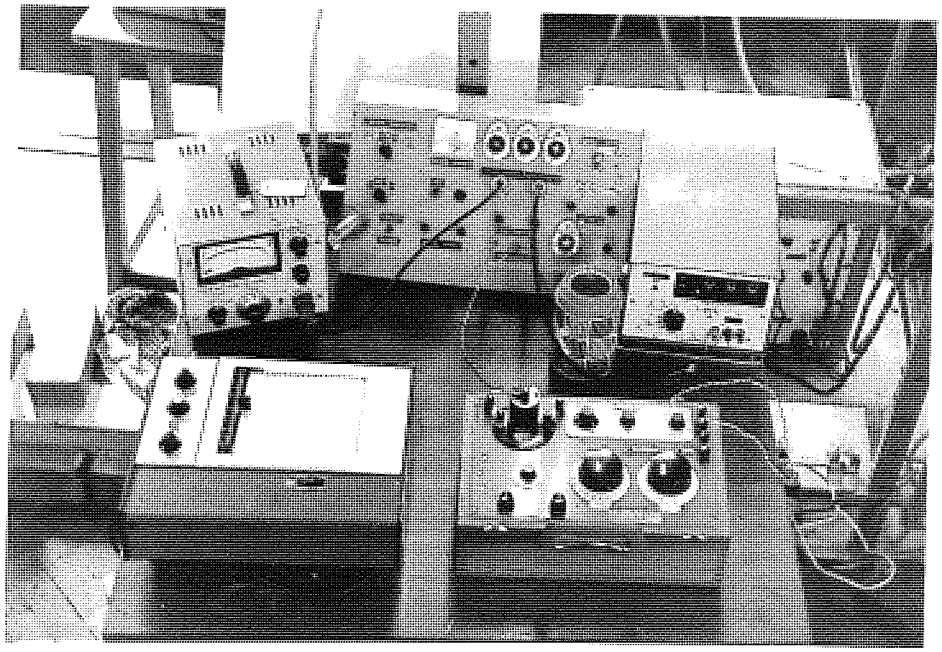

PLATE XV

temperature to 360°K.

4.8.1 V.I measuring circuit.

The circuit used for the measurements is shown in figure 4.2. The voltage was measured with a moving coil (Unipot Microameter, 120mV F.S.D.) or digital voltmeter and the current was measured with a Keithley 150 B microvolt ammeter. Any desired voltage could be produced between the detector leads by adjusting the helical potentiometers, and it was applied to a given capacitor using the two rotary wafer switches. The current measured was often very small ( $10^{-12}$A) so it was essential to ensure very high leakage resistancies and very low A.C. pick up. The latter was achieved by enclosing the whole circuit in an earthed case and using screened cable for all external interconnections. The case and other equipment can be seen in plate XV. The batteries were also included in the case and stood on a $\frac{3}{8}$" block of P.T.F.E. to reduce stray capacitive effects. Leakages of various sections and components in the circuit were checked with a "norma" 266T Terrohmeter. In this way it was found that in order to maintain the leakage resistances above $10^{12}\Omega$ the rubber washers in the Plessey plugs had to be removed and the positive and negative detector leads had to be connected through seperate rotary switches. The current for a given voltage generally took a little time to fall to a steady value and in some cases changed continuously so the 100mV. F.S.D. output from the microammeter was fed to a Bausch and Lomb VOM5 chart recorder so that the current could be continuously monitored. According to the specification of the ammeter a current in excess of 100mA would damage the current sensing resistor so a current limiting 1 K$\Omega$ resistor was included to protect the meter in the event of a breakdown of the device under test.

4.8.2. The Cryostat.

A large helium recovery plant was already installed in the laboratory and an Oxfrod Cryogenics cryostat was available for use both of which can be seen in plate XVI. In order to make current measurements over the temperature range from liquid helium temperature to above room temperature it was

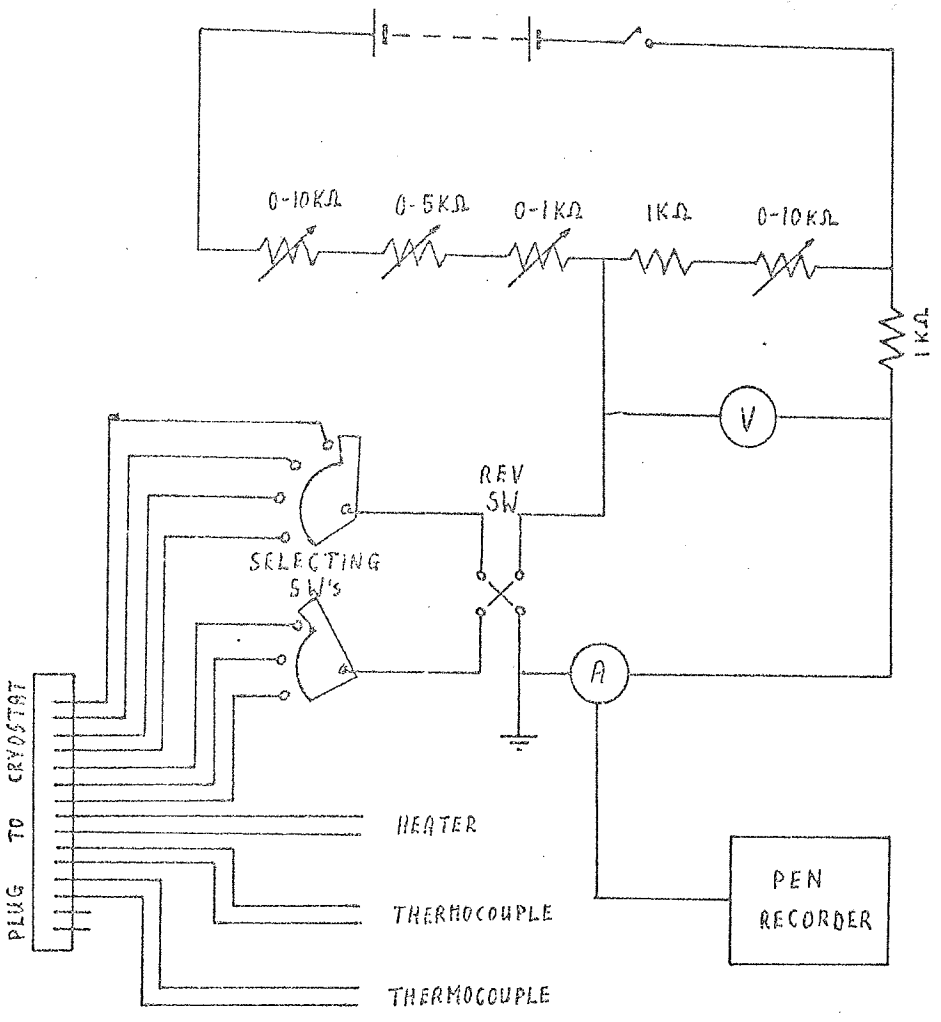


Figure 4.2.

Electrical Measuring Circuit

PLATE XV1

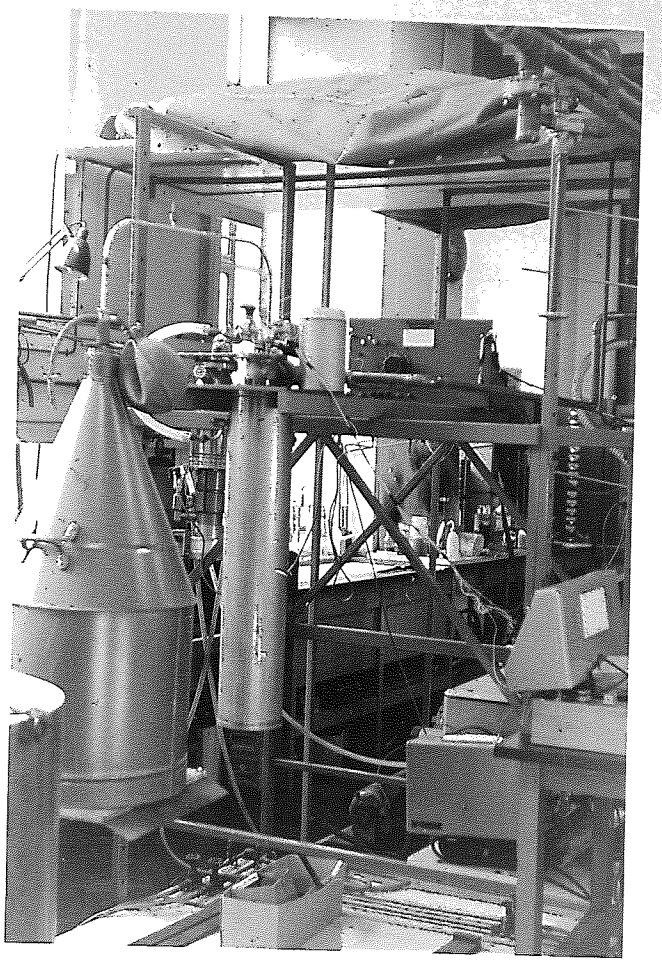

PLATE XV11

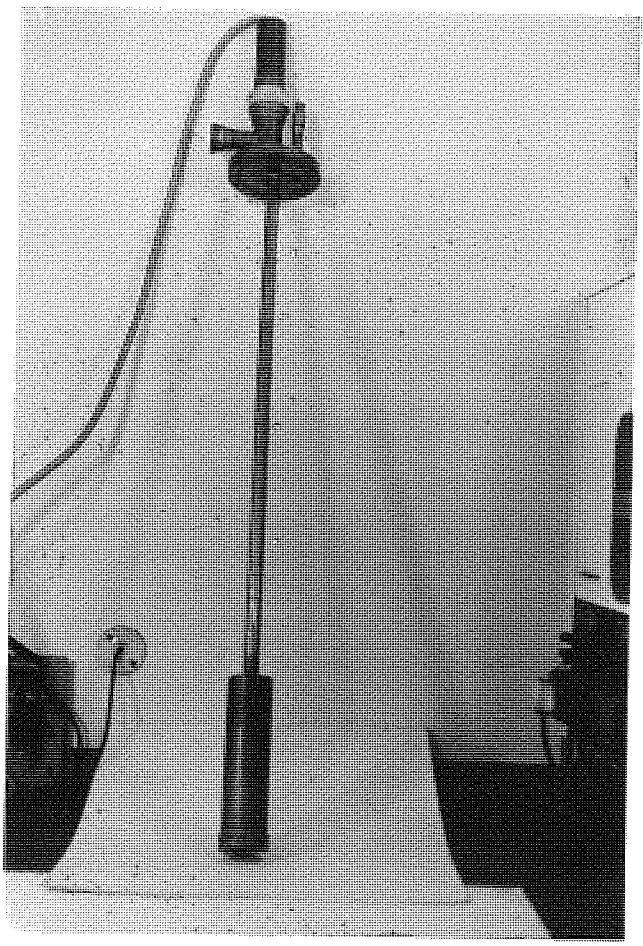

necessary for the substrates to be fixed on a block supported in a vacuum compartment all of which could be lowered into the cryostat. A vacuum was necessary to prevent the build up of frost on the substrate at low temperatures which would have occured under normal atmospheric conditions and would have made current measurements meaning less. The substrate block also needed a heater to maintain other than fixed point temperatures and all electrical leads needed to be introduced into the vacuum through leak tight seals and connected to the substrate in a demountable manner. The apparatus designed to achieve this is shown in figure 4.3. and plate XV11 The vacuum compartment was supported from the brass cryostat top plate by $\frac{5}{8}$" diameter 18 S.W.G. stainless steel tube 28" long. This tube served as the pumping line and the low thermal conductivity of stainless steel prevented any serious heat loss between the liquid coolant and the brass plate at room temperature. All the electrical leads were fed down this tube to the vacuum compartment and were sealed into the top of the vacuum column by glass to metal seals soldered into a drilled blanked off "Edwards" 1" vacuum screwed coupling. The vacuum was maintained through the side arm, which was coupled with Edwards couplings and valves to a Pirani gauge, a gas needle inlet valve, and the main pumping line. This was connected to a 1" diffusion pump by 1" diameter stainless steel flexible tubing. The pump was trapped by a 1" NTMI liquid nitrogen trap and backed by an ES 250 Rotary pump. The substrate holder and block heater could be removed from the vacuum compartment by unscrewing the bottom brass plate, releasing the indium wire seal and withdrawing the assembly. The substrate holder and heater former were machined in one piece out of a copper rod so that they could be maintained at the same temperature and are shown in plate XV111 A temperature differential between them and the brass plate at liquid coolant temperature could be maintained by the poor thermal conductivity of the part brass part stainless steel support rod. The electrical connections to the substrate were made via solder pins supported in a perspex frame bolted to the substrate block. The enamelled copper leads

from the measuring circuit were permanently connected to the pins while the gold bonded wires were individually soldered to the pins for each substrate. The substrate was held in place by strong stainless steel clamps in order to ensure good thermal contact and the copper constanton thermocouple was held under one of them, insulated from the film and the clamp by very thin mica sheet. To reduce the heat flow from the substrate along the leads, all the wires were sellotaped to the side of the vacuum compartment before continuing up the tube. When operated, an equilibrium is set up between the heat input per second to the heater and the heat flow down the support rod, above liquid nitrogen temperature radiation losses being negligeable. The system was designed to maintain a substrate temperature of $0^{\circ}C$ at about 25 watts input. The heater was wound out of 36 gauge manganin wire to a resistance of 250 ohms. It had to be operated at D.C. because A.C. caused a high level of pick up on the current measurements. To reach liquid helium temperature it was found necessary to bypass the thermally insulated support rod by inserting a $\frac{5}{8}$" diameter 12 S.W.G. copper tube as shown in plate XVIII. This was because the radiation and other exroneous heat inputs to the substrate were approaching the same order as the heat flow in the support rod. Consequently for both liquid nitrogen and liquid helium fixed point temperatures the copper tube was inserted.

4.8.3. Operation.

Firstly gold wires were bonded on to the device electrode contact pads and the substrate was then clamped in the copper block. The thermocouple was put in place, the gold wires soldered to the connecting pins and a quick check made for short circuits. A manually extruded piece of indium wire approximately $2\frac{1}{2}$" long was used to seal the bottom plate into the base of the vacuum compartment. The whole assembly was lowered into the empty cryostat and the coupling to the pumping line connected. The vacuum compartment was then pumped down until the pirani gauge read less than $10^{-2}$ torr, when the compartment was flushed several times with helium using the needle valve and main pumping valve. The pump was then valved off and the

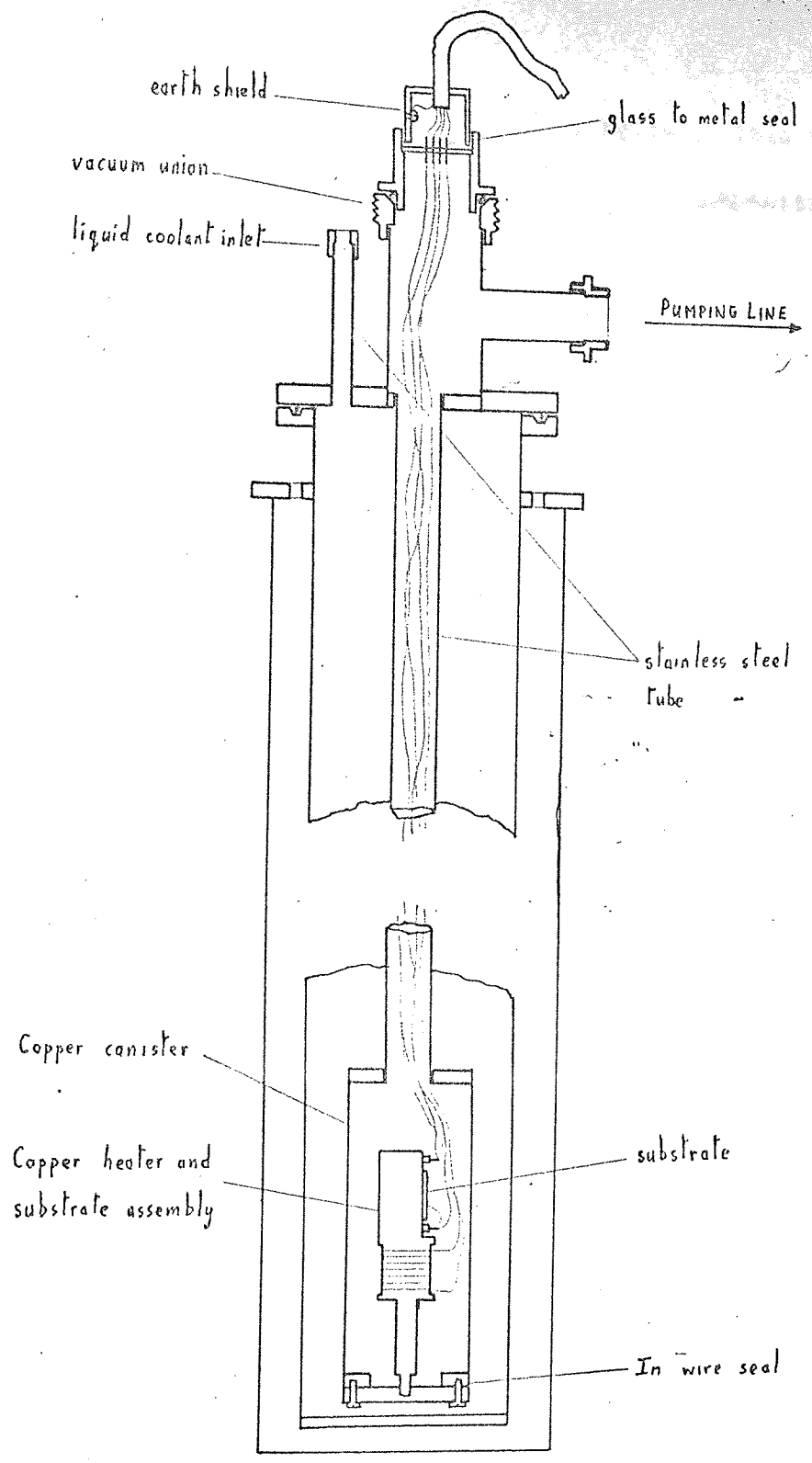


Figure 4.3.

Cryostat.

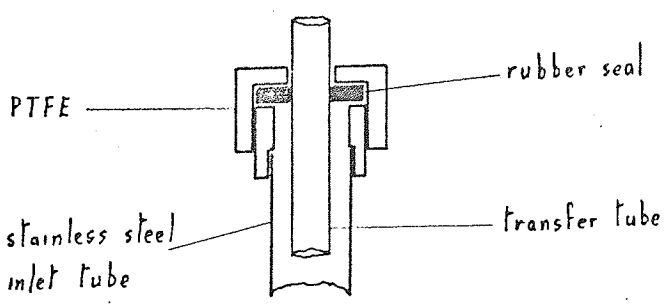


Figure 4.4.

Filler Tube sealing

compartment raised to a small positive pressure of helium. This was done to increase the cooling rate because of the large thermal capacity of the copper block assembly. The liquid coolant was then introduced into the cryostat through the filler tube. For temperatures down to 77°K both compartments of the cryostat were filled with liquid nitrogen which was forced out of a 25 lt. dewar by a pressure of a few pounds per square inch of compressed air. For liquid helium temperatures the outer compartment was filled with liquid nitrogen and one litre was put in the inner compartment to pre-cool the vacuum substrate compartment. When the substrate had cooled to nearly 80°K the liquid nitrogen was removed by pushing a long copper tube through a rubber bung in the filler tube until it reached the base of the cryostat. Pressure then built up in the cryostat due to boiling nitrogen and ejected all the remaining liquid through the tube. Helium was then introduced from a helium dewar with a vacuum insulated transfer tube passed through the filler pipe and sealed as shown in figure 4.4. The P.T.F.E. cap was a tight push fit on the filler tube and allowed the transfer tube to be lowered without breaking the seal. The cryostat is shown being filled with helium in plate XVI. Care had to be taken when lowering the tube into the helium to avoid excessive increase in pressure due to helium boil off. When the tube had been lowered to within 1-2" of the bottom of the dewar the liquid was forced through it by squeezing the football bladder. When the cryostat was filled to above the level of the top of the vacuum compartment the transfer tube was removed and the filler tube sealed with a rubber bung so that no helium escaped but was collected by the recovery plant. The thermocouple output was monitored using the chart recorder and if the heater was to be used it was switched on when the temperature had reached a value approaching the desired temperature. The heater was run from a 120V battery supply and the current controlled by a 10.5Ω, 6.5A rheostat. It was found necessary to use a battery supply because even stabilised D.C. supplies were found to cause considerable

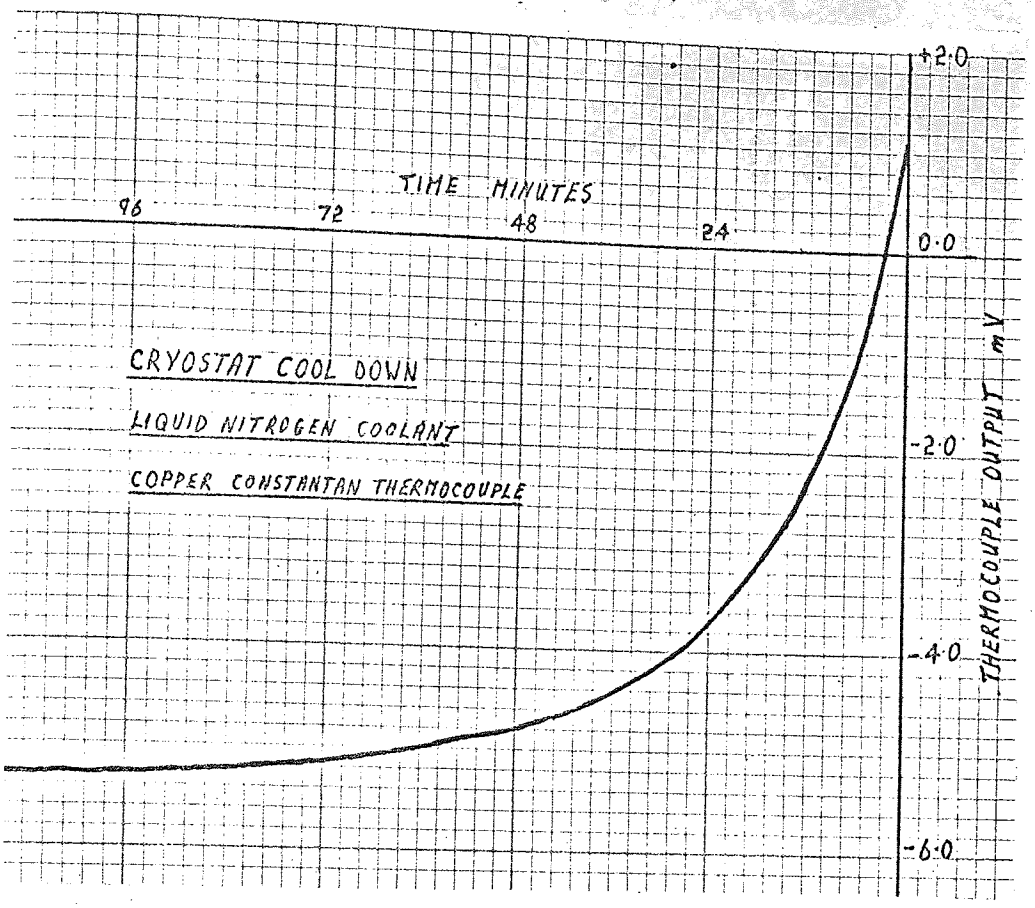


Figure 4.5

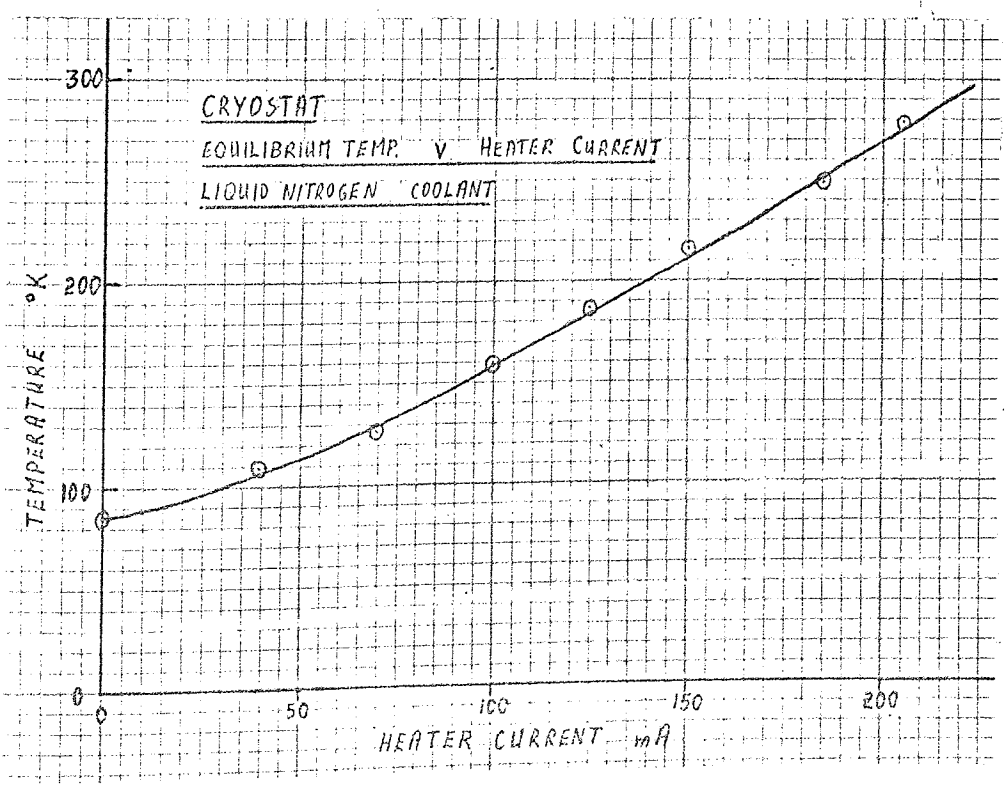


Figure 4.6.

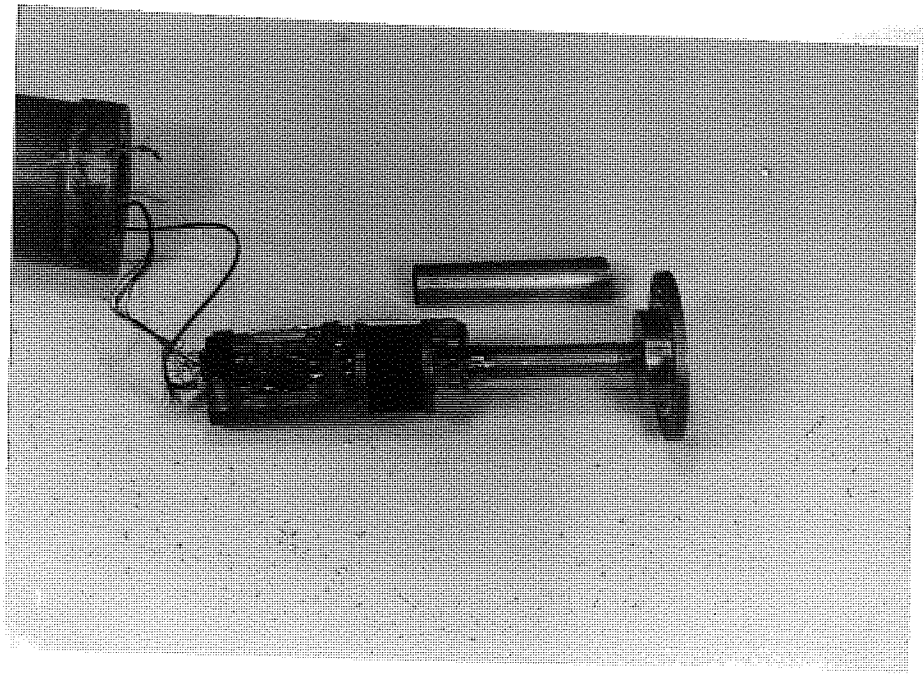

PLATE XVIII

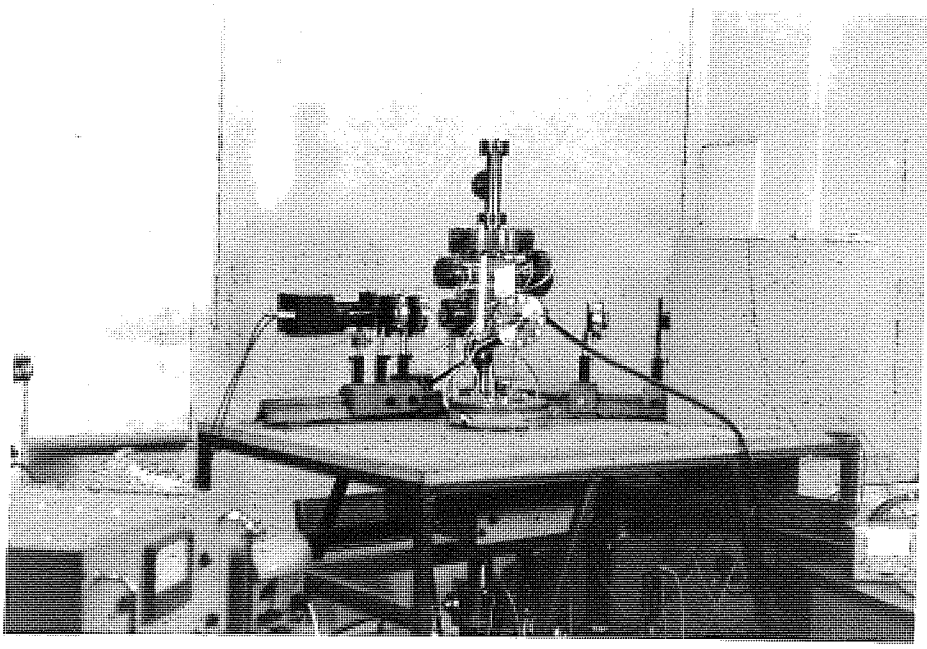

PLATE XIX

erroneous output on the microvoltammeter. An intermediate temperature generally took 2-3 hours to stabilise and figures 4.5 and 4.6 show a typical cool down to liquid nitrogen temperature against time and a graph of heater current versus equilibrium temperature for the system. When the temperature was finally reached the particular capacitor to be tested was selected using the rotary switches. The current was allowed to stabilise, watching the chart recorder output from the ammeter, at each voltage before the current was read and the voltage was then reversed using the reversing switch and a second current reading taken before increasing to the next voltage. In this way characteristics with both polarities could be taken for each capacitive device on a film at a series of temperatures from $\sim 4^{\circ}$K up to $380^{\circ}$K.

## 4.9. Elipsometry

Elipsometry is the measurement of the change in polarisation of light on reflection from a plane surface. The measurement affords a method of determining the optical constants of the reflecting media or in the case of a thin film on a plane substrate, the thickness and optical constants of the film. The technique can be applied to films of thickness, ranging from sub monolayer films to films of a few microns. The index of refraction is determined for all films and if the film is absorbing the absorption coefficient is also obtained. The state of polarisation of light incident on a plane surface is defined by the relationships between the phases and between the amplitudes of the two component plane waves into which the polarised electric field vector can be resolved. These waves are designated p parallel to, and s normal to, the plane of incidence. If p and s are in phase the light is plane polarised and would be represented by a single line on a p s vector diagram. If however p and s have a phase difference between them, of other than $180^{\circ}$ the representation on the vector diagram (figure 4.8) would be an ellipse and the light is said to be elliptically polarised. In general reflection from a surface will change both the phase

Figure 4.8

Polarised Light

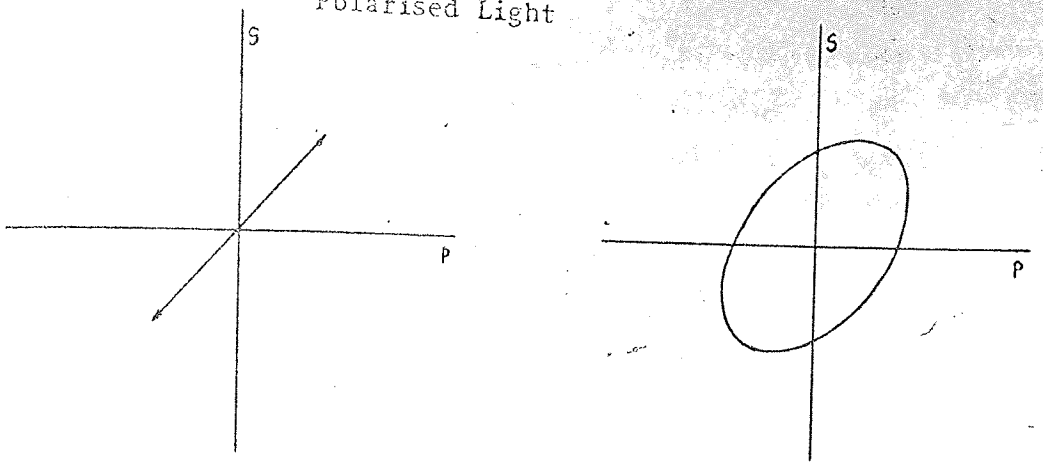


Figure 4.7

Reflection of Light

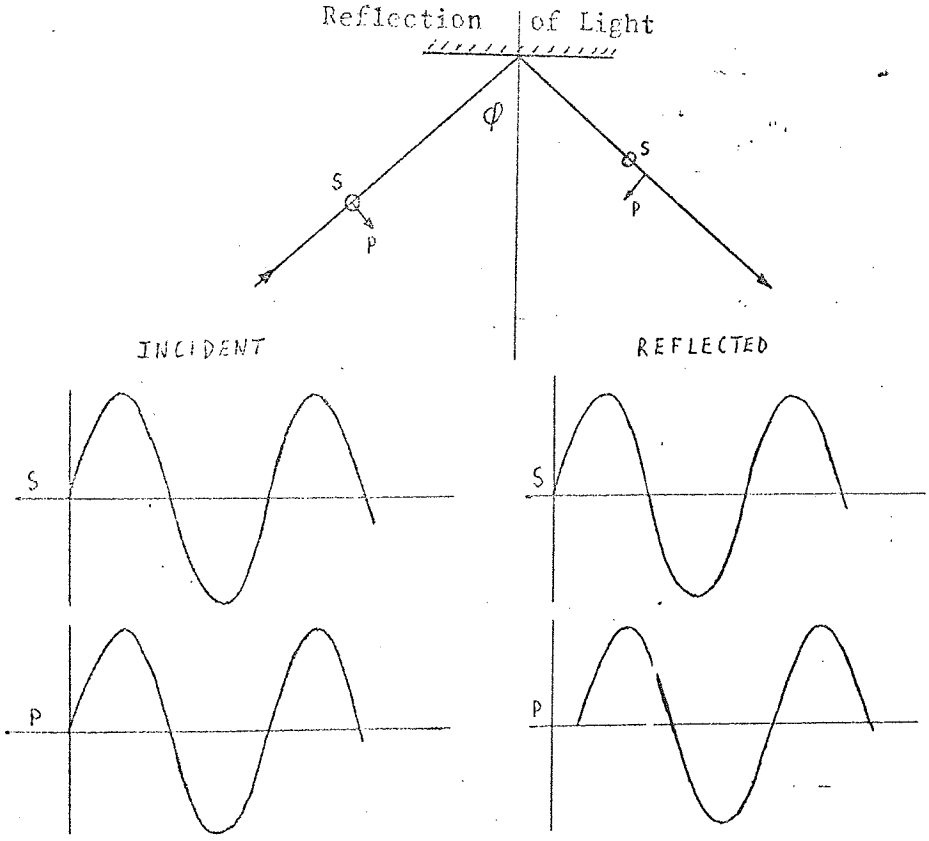


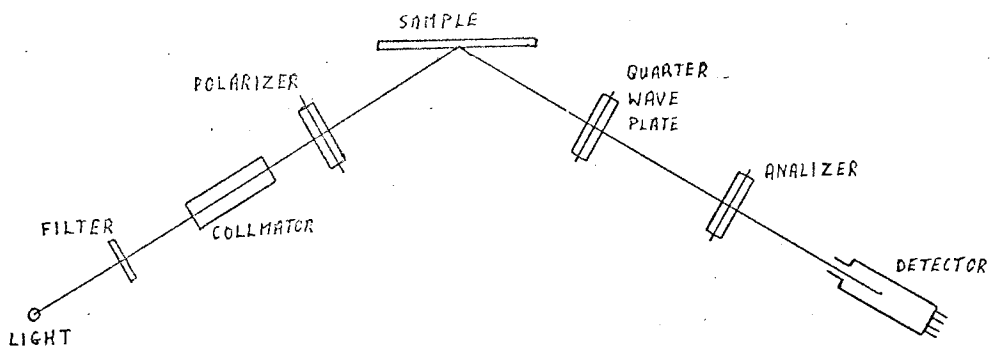


Figure 4.9.

Experimental Arrangement

between the component waves and the ratio of their amplitudes. Designating phase angles $\beta$ and the amplitude of incident and reflected light as I and R respectively we can define two parameters $\psi$ and $\Delta$ which characterise the change in polarisation. It is these parameters which are measured in ellipsometry. It can be seen that $\Delta$ is a measure of the change in phase

$$\Delta = (\beta_p - \beta_s)_R - (\beta_p - \beta_s)_I \qquad 4.4$$

$$\psi = \arctan\left(\frac{R_p}{R_s} \cdot \frac{I_s}{I_p}\right) \qquad 4.5$$

and a measure of the change in relative magnitudes of the amplitudes of the p and s waves. The actual apparatus is shown in plate XIX and while the procedure used is described in detail elsewhere (reference 147) the principle of measurement was as follows: Figure 4.9 shows a schematic representation of the experimental arrangement, light from the 150 watt lamp passed through the 5478 Å filter and into the collimating system. The monochromatic collimated light then passed through the polarizer, was reflected from the sample, passed through the quarter wave plate and the analyzer and finally reached the detector. The quarterwave plate was a mica single crystal, the refractive index of which is a function of crystallographic direction. The behaviour of light passing through it can be understood by re-resolving the polarised light into two perpendicular directions parallel to two of the principle axes of the crystal, known as the fast and slow axes. Light polarised parallel to the fast axis travels faster through the crystal and consequently introduces a phase difference which, depending on the orientation of the light entering the crystal, can change the phase between the p and s waves by any value between $0^\circ$ and $360^\circ$. As a result by correctly setting the polarizer and quarter wave plate the phase change caused by reflection from the sample could be exactly compensated and this will give a measure of $\Delta$. With wave plate and polarizer set in this position the plane polarized light emerging from the plate could then be completely extinguished by a suitable orientation of the analyzer, which was a polarizing plate identical to the polarizer. The analyzer extinction settings for the two alternative compensating positions that

could be found, give a measure of $\psi$. The general interpretation of the measurements is complicated and requires electronic computation. (148) The relationships between $\psi$ and $\Delta$ and the constants of a reflecting system are expressed in terms of Fresnel reflection coefficients. The Fresnel coefficient r for a reflection is the ratio of the incident and reflected field vectors $\underset{\sim}{E}$ and $\underset{\sim}{R}$ given by equation 4.6, where R and E are amplitudes

$$r = \underset{\sim}{R}/\underset{\sim}{E} = R/E\, e^{i\beta} \qquad 4.6$$

and $\beta$ the phase between the two vectors. Considering the reflection of polarised light from a plane substrate the ratio of the Fresnel coefficients of the p and s components of the light is given by equation 4.7 and con-

$$\frac{r_p}{r_s} = \frac{R_p}{R_s}\,\frac{E_s}{E_p}\, e^{i(\beta_p - \beta_s)} \qquad 4.7$$

sidering our definitions of $\psi$ and $\Delta$ equations 4.4, 4.5, substitution yeilds equation 4.8. The Fresnel coefficients for an optically isotropic, clean, plane substrate surface can be expressed in terms of the optical constants

$$\frac{r_p}{r_s} = \tan\psi\, e^{i\Delta} \qquad 4.8$$

of the substrate and the angle of incidence (149). The optical constants of the substrate are then given by equations 4.9 and 4.10 where $\phi$ is the angle

$$n^2 - k^2 = (\sin\phi\tan\phi)^2 \cdot \frac{(\cos^2 2\psi - \sin^2 2\psi \sin^2\Delta)}{(1 + \sin 2\psi\cos\Delta)^2} + \sin^2\phi \qquad 4.9.$$

$$2nk = (\sin\phi\tan\phi)^2 \cdot \frac{\sin 4\psi \sin\Delta}{(1 + \sin 2\psi\cos\Delta)} \qquad 4.10.$$

of incidence, n is the refractive index and k the extinction coefficient, related to the absorption coefficient $\alpha$ by equation 4.11 where $\lambda$ is the

$$k = \frac{\alpha\lambda}{4\pi} \qquad 4.11$$

wavelength of the light.

Now considereing the case of a film covered plane substrate the calculation is much more complicated by the multiplicity of beams produced by internal reflection within the film. The fundamental equation of ellipsometry, by analagy to equation 4.8. is then equation 4.12 where $r_{nm}$ refers to

$$\tan\psi e^{i\Delta} = \frac{r_{01}^p + r_{12}^p e^{-2i\delta}}{1 + r_{01}^p r_{12}^p e^{-2i\delta}} \cdot \frac{1 + r_{01}^s r_{12}^s e^{-2i\delta}}{r_{01}^s + r_{12}^s e^{-2i\delta}} \qquad 4.12$$

the Fresnel reflection coefficient for the interface between medium n and m with the incident beam in medium n. The subscripts refer to media as follows: o ambient, 1 the film and 2 the substrate and $\delta$ is given by

equation 4.13 where d is the film thickness. The Fresnel coefficients can

$$\delta = \frac{360}{\lambda} d \left(n_1^2 - \sin^2\phi\right)^{\frac{1}{2}} \qquad 4.13$$

again be written in terms of the angle of incidence in the ambient medium and the optical constants of the system. The seperation of equation 4.12 into its real and imaginary parts yeilds one equation for $\psi$ and one for $\Delta$. Values of $\psi$ and $\Delta$ can then be predicted for given values of the wavelength of light, angle of incidence optical constants $n_1 k_1$ and $n_2 k_2$ and the thickness of the film d. The wavelength of light and angle of incidence are set by the experimental arrangement and $n_2 k_2$, the optical constants of the film free substrate can be measured, so tables are produced of $\psi$ and $\Delta$ against thickness for given $n_1 k_1$ values. These $\psi$ and $\Delta$ values can by plotted graphically and it is found for non absorbing films, i.e. k = o, the $\psi$ and $\Delta$ values are cyclic functions of thickness, the curves repeating periodically every $180^\circ$ change in $\delta$. The curves for different values of $n_1$ have a common origin at zero thickness and except for extreme values of $n_1$ never intersect. Consequently a given measurement of $\psi$ and $\Delta$ can only fit one value of $n_1$ and provided the thickness is known within the repeating period, the thickness can be exactly determined also. However if the $\psi\Delta$ point falls near the origin of the thickness there is considerable doubt about the assignment of optical constant as the curves closely approach one another. So it is normal to repeat measurements on a number of films of different, approximately known, thicknesses. For absorbing films i.e. $k \neq 0$, the curves for $\psi$ and $\Delta$ are no longer cyclic but with increasing thickness converge on the point equivalent to reflection from the film surface only. Points in the $\psi\Delta$ plane are not unique but correspond to an unlimited number of different sets of film properties. Consequently it is necessary to measure $\psi$ and $\Delta$ for a number of films of accurately known thickness before definate values can be assigned to the optical constants of the film.

# CHAPTER FIVE

# THEREORETICAL CONSIDERATIONS.

## 5.A. Growth and Properties of Thin Films.

### 5.A.1. Parameters Affecting the Properties of Thin Films.

The properties of thin films are a function of three general factors; (1) film thickness. (2) film purity or stoichiometry. (3) film structure. The first is a consequence of the fact that as its thickness is reduced a film stops behaving simply as a thin layer of bulk material. The dimensions are no longer infinite compared to the scale of "electronic" events and the boundaries start to affect the film properties. For dielectric films, measurcable currents can be obtained for small voltages across the film,(note the field may still be high), and the probability of electron tunnelling through the film or into the conduction band of the film is no longer zero. Film purity is limited by the purity of the starting material and the quality of the vacuum. Initially thin film work was plagued by variations in reported film properties which were probably due to deficiencies in these two factors. Improved technology in both the material science and vacuum field means that film purity is no longer a major problem. The purity of sputtered films is therefore expected to be the same as the purity of the target. Due to the high pressure during sputtering there is a possibility of greater gas inclusion than for evaporated films, a factor that has been investigated for a similar system to that employed in this project (150). The impurity is of such a nature (inert argon) that one would expect it to have little influence on film properties. However as discussed in Section 2.2.3 for compound or alloy materials stoichiometry may be affected by the deposition process and changes in film constituent ratios would certainly cause changes in properties. The much smaller change in stoichiometry caused by sputtering was one of the reasons for choosing this method in preference to evaporation, but while Ba/Ti ratios are likely to be unaltered in $BaTiO_3$ sputtered films the loss of oxygen during any separation into molecular or multiple atomic species cannot be discounted.

One way to allow for this is to use a percentage of oxygen in the sputtering gas so that the probability of a dissociated free metal species reacting either in transit or on the substrate surface, as in reactive sputtering (Section 2.3.8), is enhanced and the dissociation is reduced due to the partial pressure of oxygen. Consequently, an indirect parameter, the percentage of oxygen in the sputtering gas, was introduced into the variables noted for each film deposition. Film structure is dependent on a large number of parameters and indeed a variety of abnormal structures can be produced in films of elements, compounds, and alloys which can be formed in no other way (151). The major factors affecting film structure during deposition are listed below, in general order of importance.

1. Deposition Method
2. Substrate material
3. Substrate temperature
4. Deposition rate.
5. Film thickness
6. Deposition angle
7. Electric or Magnetic Field at the substrate.

Post deposition annealing can also have a great affect on the structure of films of crystalline materials. This is because high temperatures promote crystallisation of amorphous structures and crystallite growth of polycrystalline structures as well as causing diffusion effects on loosely bound impurities. The parameters listed here however are all concerned with the growth of the films and are considered in the next section. Since all films prepared in this project were R.F. sputtered the major remaining variable was the substrate material and in the next chapter the structure and properties of the films studied are examined in terms of this parameter.

5.A.2 The Growth of Thin Films.

The growth of thin films is believed to start at nucleation sites. The condensation of a vapour atom is determined by its interaction with the substrate surface atoms. If the incident energy is not too high the atom

will loose its component of velocity perpendicular to the surface and become absorbed, when it is then termed an adatom. The velocity parallel to the surface may not be zero so the atom is not in thermal equilibrium with the surface and can jump from one site to another. The adatom may interact with other atoms and become chemically absorbed or it may re-evaporate into the vapour phase. Condensation is then the net result of an equilibrium between the adsorption and desorption processes. The net probability of an atom being completely adsorbed is called the sticking coefficient. An adatom will reevaporate unless it forms a cluster with other adatoms of greater than a critical size. This means for a given temperature at a given atom arrival rate there will exist a critical size of cluster such that smaller clusters will on average loose an atom by re-evaporation before another is adsorbed and larger clusters will have a probability of growth of more than a half. This is explained thermodynamically by considering the variation of Gibbs free energy with cluster radius. The free energy, which is a summation of the surface energy and volume energy of condensation rises with radius to a maximum at the critical size when it falls with further adatom adsorption. In general this approach yeilds critical nuclei of the size of atomic dimensions which makes the use of bulk thermodynamics very questionable. An alternative approach more suited to small clusters has been made by Walton and Rhodin (152). This considers potential energies of the reacting species and products in an approximate analysis and uses the same hypothesis of critical nuclei. At low temperatures or very high supersaturations the crytical nucleus is a single atom and the random formation of a pair with another atom will produce a stable cluster, so the film will grow spontaneously and randomly. The stability of a pair is derived from there being a minimum of one bond per atom but at higher temperatures or lower saturation a minimum of two bonds per atom may be required for the smallest stable cluster. This requirement could be satisfied by three atoms at the corner of a triangle giving a critical nucleus of two atoms or by four atoms at the corners of a square giving a critical

nucleus of three atoms. Which of the critical nuclei apply under given conditions decide upon which, if any prefered orientation should be present in the film. The general equation for the rate of formation of clusters J of critical size $i^*$ at an atom arrival rate R, density of adsorption sites $n_o$ and substrate temperature T is given by equation 5.1 (153) where

$$J = R\left(\frac{R}{\nu n_o}\right)^{i^*} \exp\left\{E_b^{i^*} + (i^*+1)E_a - E_d\right\} \quad 5.1.$$

$E_b^{i^*}$ is the binding energy of a group of size i, $E_d$ is the diffusion energy, $E_a$ the adsorption energy and $\nu$ the vibrational frequency associated with an adatom. By equating values of J for different sizes of critical nuclei transition temperatures can be determined for changes from one to another which should be of interest in epitaxial growth. Equation 5.2. gives the

$$T_{(i^*=1\text{-}2)} = \frac{-\left(E_a + E_b^3/2\right)}{k \ln\left(R/\nu n_o\right)} \quad 5.2$$

transition temperature between $i^* = 1$ and $i^* = 2$ for example. Epitaxial temperatures will coincide with these sort of transitions and all orientated deposits will have close packed planes parallel to the substrate. The orientation with respect to the substrate is derived by determining how the critical nucleus should be orientated to minimise the displacement of the atoms from potential minima on the substrate. The orientations and structure of films is however not only determined by the nucleation processes but can be greatly affected by coalescence and later growth stages. After the formation of stable nuclei they grow to form observable islands by diffusion controlled processes involving the capture of diffusing adatoms and sub critical clusters. As the islands further increase their size and come closer together the larger ones appear to take in the smaller ones by a process called coalescence. This involves considerable mass transfer and occurs generally very quickly ($< 0.1$ secs). At a certain critical island distribution a rapid large scale coalescence occurs which results in an interconnected network structure. The holes in the network are then slowly filled up in the final stage of film growth. The exact behaviour depends on the material and the deposition conditions but all films follow this general pattern becoming interconnected at somewhere between a 100 Å and a few

100 Å. Film structures can be formed or greatly influenced during the coalescence stage of growth. The influence of the deposition parameters that is those listed in Section 5.A.1. on film structure can be understood then in terms of their effect on the film growth which again depends on their effect on the sticking coefficient, the nucleation density and the surface mobility of adatoms and atomic clusters. Agglomeration, that is the joining together of clusters to form islands increases with higher surface mobility and lower nucleation density. Higher agglomeration means the film will have a larger grain size and have a smaller number of frozen in defects. The major influence is due, as already discussed, to the nature and structure of the substrate. But for a given substrate the substrate temperature can have a large effect on film growth. This is possible because increasing the substrate temperature may aid the desorption of contaminants, lower the saturation, enhance recrystallisation by increasing surface mobilities and provide activation energy for the correct siting of epitaxed atoms in the positions of potential minima. In fact an epitaxial temperature can be defined for most systems which corresponds to the temperature at which a particular structure appears. These factors affected by substrate temperature are also dependent on other deposition parameters so epitaxial temperatures vary with these parameters. Sloope and Tiller (154) and others have established that for certain evaporated films at a given deposition rate R a minimum epitaxial temperature $T_e$ exists given by equation

$$R \leqslant A e^{-Q_d/kT_e} \qquad 5.3$$

5.3. where A is a constant and $Q_d$ the energy of surface diffusion. This is explained in terms of the Walton Rhodin theory of nucleation, or by the assumption that for epitaxy to occur an adatom should on average have time to jump by an activation process to an ordered position before the arrival of the next atom. The amorphous to crystalline and crystalline to monocrystalline transformations can be plotted on a graph of deposition rate versus resiprical temperature showing regions where each phase is produced. Sloope and Tiller (154) found the amorphous to crystalline transition

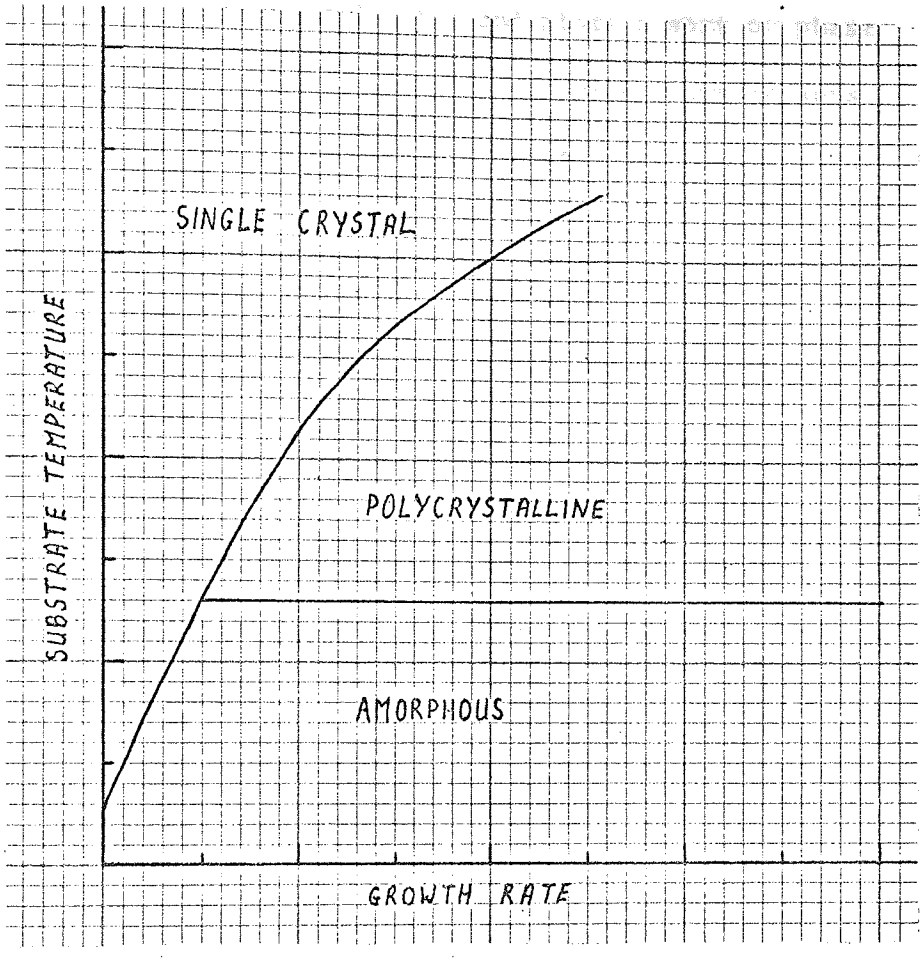
SINGLE CRYSTAL
POLYCRYSTALLINE
AMORPHOUS
SUBSTRATE TEMPERATURE
GROWTH RATE

Figure 5.1

obeyed an exponetial relationship but this transition has been found by other workers to be independent of rate (155). Krikorian (156) has reported similar work on sputtered films and plots a sort of phase diagram of temperature versus deposition rate which shows regions of amorphous, polycrystal and single crystal growth as shown in figure 5.1. Her results show the boundaries of each phase and indicate a sharp triple point where all three phase occur together. While this is in some doubt (155), it is generally agreed that the three phases can coexist in a broad temperature range. Film thickness can affect film structure due to the different coallescence behaviour of the nuclei of two orientations of the same material growing together. In this way while initial nuclei are of one orientation later growth may cause another orientation to predominate. Oblique deposition is known to produce high adatom mobility effects on the substrate (157). But in sputtering due to the continuous source and relatively high pressure the deposition angle of each impinging atom is in general different. However for a given substrate target distance the net average bombarding angle is the same and this was not varied for any of the depositions. It was reported by Moll (158) but completely refuted by Roder (159) and others that an electric field has a major effect on the deposition of barium titanate due to the polarised structure of the ferroelectric,but it is true (160) that a lateral electric field can have small effects on film coalescence processes. In all film depositions a magnetic field due to the magnetic coils and an electric field due to the R.F. negative bias potential were present perpendicular to the substrate but these were only slightly varied between films and no account was taken of them.

5.B. Conduction Mechanisms in Thin Dielectric Films.

The passage of current through sandwich structures of an insulator bounded by two parallel metal electrodes has been extensively studied theoretically and a number of conduction mechanisms have been proposed. There is also a mass of experimental data available giving the J.V.T.

characteristics of a wide range of materials but as yet there is no overall theory which predicts the mechanism for a given material and given ranges of temperature and field. For each material the characteristics have to be measured and tested against the anticipated J=J (VT) relationship for every mechanism, to see which, if any, gives the best approximation.

5.B.1. Band Structure.

Most of the proposed mechanisms make use of electron energy band theory concepts derived for crystalline material. This is not an obvious assumption since films are usually amorphous or polycrystalline. However, lately, the band theory has been attributed more to the close range order of materials, i.e. the actual bonds between atoms, than the periodicity of the lattice (161). This conclusion is supported by the fact that the energy spectrum of semi conductors changes little on transition from the solid to the liquid phase. It is suggested theoretically that the band structures of liquid or amorphous semiconductors consist of the same bands as for the crystal but with broadening of the bands and blurring of the band edges. It is as though the density of states function has tails of localised allowed states which extend into the forbidden gap from both the valence and conduction bands (162). Figure 5.2 and 5.3 show the density of states and the resulting band diagram for such a situation.

5.B.2. Electrical Contacts.

For two films unrelated chemically and deposited seperately one can assume the layers to be reasonably uniform and having a sharp interface. This would not be true for oxidised or anodised films but should hold for seperately deposited gold or aluminium; barium titanate; gold or aluminium layers. There will still however be surface states at the interface due to unsatturated bonds. The presence of these and other ionised impurity sites can affect the type of electrical contact formed between the films. There are three possible sorts of contact, ohmic, which supply and remove the required carriers without space charge, and two types of non ohmic contacts, blocking and injecting. The potential diagrams of the contacts are shown

Figure 5.2.

Density of States

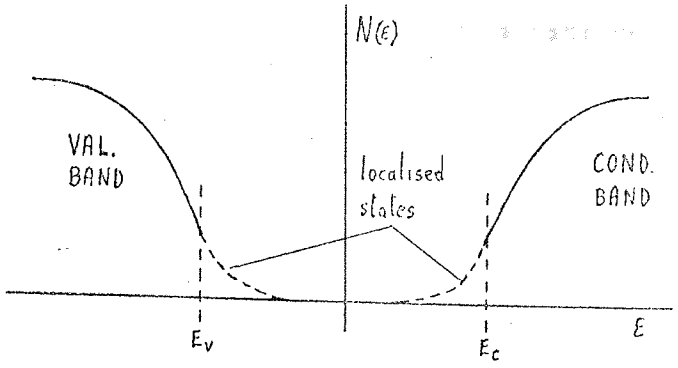


Figure 5.3.

Band Structure

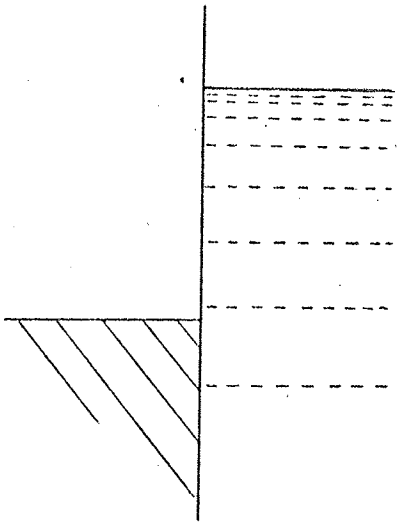

Figure 5.4.

Contacts

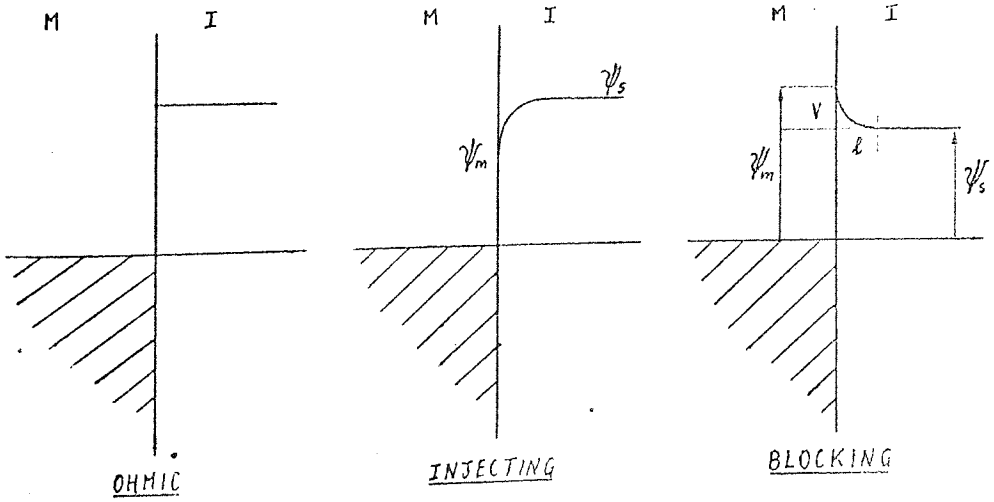

in figure 5.4. It can be seen for injecting contacts $\psi_m < \psi_s$ and for blocking contacts $\psi_m > \psi_s$ The band bending near the interface is due to the presence of space charge and extends over a distance l, related to the barrier height V by equation 5.4., after Jonscher (163), where K is the dielectric constant of the material, V is in volts and N the impurity density in $cm^{-3}$ From this he concluded that for a film of 1000 Å an ionized impurity

$$l = 10^3 \left(\frac{KV}{N}\right)^{\frac{1}{2}} cm \quad 5.4.$$

density of $\sim 4\ 10^{16}\ cm^{-3}$ is necessary to give a barrier of one volt which would seem unlikely as a result of the removal of electrons from the barrier region of an insulator. Consequently band bending will be only slight and an ohmic contact will be one where the contact potential difference between metal and insulator is relatively small and will become injecting at high currents, while a blocking contact is one where the charge in the barrier region produces a relatively high metal insulator contact potential.

5.B.3. Conduction Mechanisms.

Taking into consideration remarks made about the limitations of applying band theory to the behaviour of M.I.M. structures there would appear to be eight possible conduction mechanisms. These are listed below and will be discussed in the following sections in terms of their applicability to the metal - $BaTiO_3$ - metal films studied in this project. It should be noted that there is no reason why two or more of the mechanisms should not be operating simultaneously and independantly of one another while two mechanisms could also operate in conjunction. The conductivity, however, is always a continuous function of field given by an impedance of the system and can be limited either at the metal insulator contact or by the bulk of the dielectric. Contact limited mechanisms are Schottky emission, field emission and thermally assisted tunnelling while, space charge limited, Poole Frenkel,. Ionic and Impurity conduction are all bulk limited.

Contact Limited
- (1) Schottky Emission
- (2) Field Emission
- (3) Thermally assisted tunnelling

Bulk Limited
- (4) Poole-Frenkel Effect
- (5) Tunnelling
- (6) Space Charge Limited Conduction
- (7) Impurity or Hopping Conduction
- (8) Ionic Conduction

5.B.3.1. Contact Limited Conduction.

(1) Schottky Emission (2) Field Emission and (3) Thermally assisted tunnelling have been combined toform a unified theory of conduction in free space by Murphy and Good (164), which can be extended to the solid state. Schottky emission is the thermionic emission of electrons from that part of the tail of the Fermi Dirac distribution which extends above the contact barrier potential, lowered by the applied field. Field emission and thermally assisted tunnelling occur when the field is high enough to assist electrons to tunnel through the barrier or part of the barrier. All three processes are illustrated in figure 5.5. Discrete regions of temperature and field have been defined by Tantraporn (165) where Schottky and Field emission predominate. The general method of calculating the current density is to integrate over all allowed electron energy states in the source, the product of the charge on an electron e, the number of electrons incident on the barrier, $N(T,\mathcal{E})d\mathcal{E}$, and the probability of an electron of that energy

$$J = \int e\, N(T,\mathcal{E}).D(\mathcal{E})\, d\mathcal{E} \qquad 5.5.$$

penetrating the barrier, $D(\mathcal{E})$, as in equation 5.5. In general at low fields and high temperatures the Schottky effect predominates. The lowering of the effective potential barrier by the applied voltage is illustrated in figure 5.6. The barrier lowering is due to image forces and is proportional to $V^{\frac{1}{2}}$ and the normal Richardson Schottky expression for the current density is obtained, viz., equation 5,6, where A is a constant, approximately

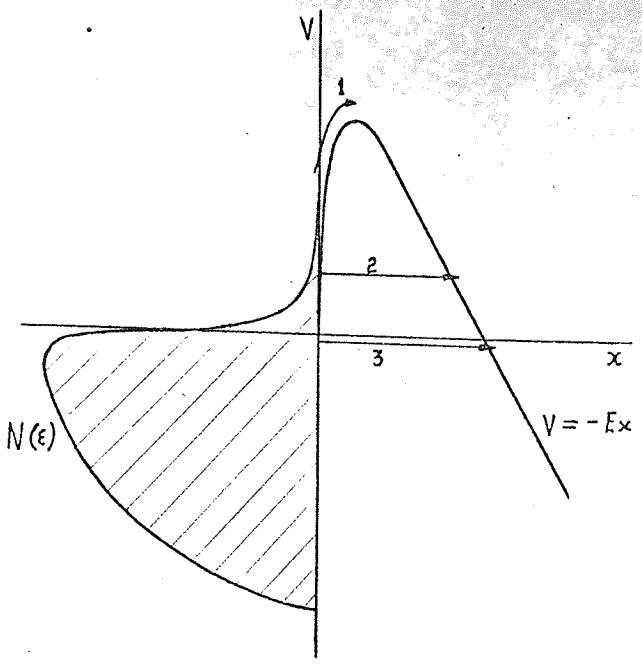


Figure 5.5.

Contact Limited Mechanisms

1. Schottky Emission
2. Thermally assisted Tunnelling.
3. Field Emission

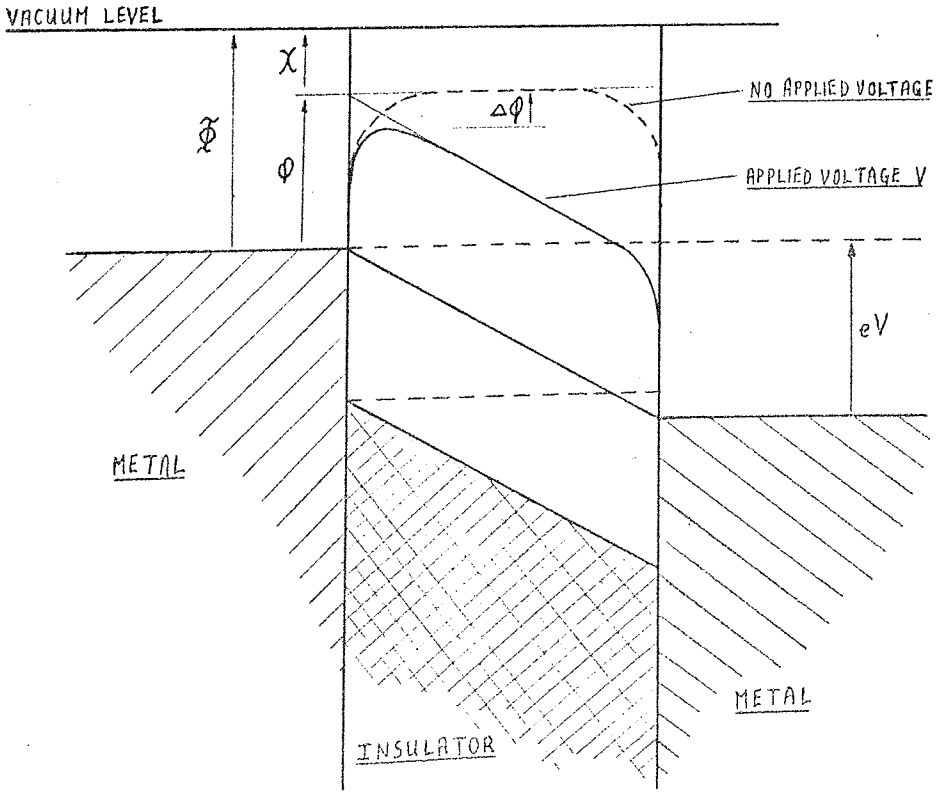


Figure 5.6.

$$J_s = A T^2 e^{-\frac{(\phi - \beta_s V^{\frac{1}{2}})}{kT}} \quad 5.6.$$

120 $A.cm^{-2}.T^{-2}$, $\phi$ is the metal insulator work function and $\beta_s$ is given by;

$$\beta_s = \frac{e^{3/2}}{2(\pi\varepsilon)^{\frac{1}{2}} d} \quad 5.7$$

where e is the electronic charge, $\varepsilon$ the permitivity of the material and d the film thickness. In cases where d is greater than the mean free path of the conduction electrons "$\ell$", Simmonds (166) has shown the normal expression does not conserve energy and the pre-exponential term for thick films becomes a function of $T^{3/2}$. This would be the case for the films studied because while there is conflicting evidence on the value of $\ell$ for insulating films, it is certainly no more than a few hundred angstroms. At low temperatures and high fields the current density equation becomes the normal Fowler-Nordheim expression 5.8. which has very little temperature

$$J_{FE} = B V^2 \exp \frac{\alpha}{V} \quad 5.8$$

dependance. Intermediate between these ideal cases thermionic assisted tunnelling occurs and is governed by equation 5.9. which as the characteristics

$$J_{INT} \simeq C V \exp - \frac{(\phi - \gamma V^{\frac{1}{2}})}{kT} \quad 5.9$$

of Schottky emission and has a temperature dependence given by 5.10 where

$$J_{INT}(T) = \left(1 - \frac{1}{akT - 1}\right) J_s \quad 5.10$$

$a = 2.27.10^6 m^{*\frac{1}{2}} K^{-\frac{1}{4}} E^{-\frac{3}{4}}$, m is the relative effective mass, and E is the applied field. The Fowler-Nordheim relation is applicable when $akT \ll 1$, the Schottky relation when $akT \gg 2$ and when $1 < akT < 2$ equation 5.9. is pertinent. The transition from Schottky emission moves to higher fields, and the length of the intermediate region is reduced, with increasing dielectric constant(167). The dielectric constant to be used is the high frequency figure (168) and taking this as 5 for barium titanate ($k = n^2 = 2.2^2$, n = refractive index) the anticipated transitions for contact limited conduction are given in table 5.1.

TRANSITION FIELDS $V_{cm^{-1}}$ FOR GIVEN TEMPERATURES °K

| TEMPERATURE | 300° K | 80° K | 6° K |
|---|---|---|---|
| SCHOTTKY EFFECT APPLIES AT A FIELD | $< 8\ 10^5$ | $< 1.0\ 10^5$ | $< 3\ 10^3$ |
| FIELD EMISSION APPLIES AT A FIELD | $> 2\ 10^6$ | $> 3\ 10^5$ | $> 10^4$ |

TABLE 5.1.

The breakdown strength of thin dielectric films is typically $10^6$ - $5.10^6$ $V.cm^{-1}$ and instabilities or thermal breakdowns occured in many of the barium titanate films at fields in excess of $5.10^5$ $V.cm^{-1}$. Current measurements were therefore restricted to $<1.10^6$ V.cm and in most cases were made at fields $< 5.10^5$ $V.cm^{-1}$. Consequently field emission is only likely to be observed below liquid nitrogen temperature, when the high energy tail of the Fermi distribution is negligeable. Above room temperature no departure from thermionic emission should be observed and between room temperature and liquid nitrogen temperature the departure should only be at the extreme high field end of the characteristics.

5.B.3.2. Bulk Limited Conduction.

For films thicker than a few hundred angstrom units it is unrealistic to think that the conductivity should not be bulk limited in at least part of the field/temperature range. The limiting factor can be a number of processes other than space charge limited conductivity, applicable to ohmic and injecting contacts, and they are all considered below.

5.B.3.2.1. (4) Poole Frenkel Effect.

The Poole Frenkel Effect concerns the thermal excitation of electrons from donor sites in the dielectric over a field lowered Coulombic barrier in the same manner as Schottky emission and has been reviewed by Jonscher (163). The barrier lowering is illustrated in figure 5.7 and the current density obeys the same relationship as Schottky emission, equation 5.11

$$J = J_o \exp^{-\frac{(\phi - \beta_{PF} V^{\frac{1}{2}})}{kT}} \quad 5.11$$

except $\beta_{PF} = 2\beta_S$ A large number of films undoubtedly exhibit straight line log J v $V^{\frac{1}{2}}$ plots which is usually attributed to the Poole Frenkel effect. However in general they yield values of $\beta_{PF}$ not consistent with that expected using the anticipated values of the fundamental constants, the permitivity and the thickness of the films. Jonscher (163) and Hartke (169) have pointed out that the barrier lowering is not symmetrical

about a given donor site but is a maximum in the direction of the field. Taking this into account the pre-exponential term for the current density includes the applied voltage as shown in equation 5.12. Simmonds (168)

$$J = J_o \cdot \left(\frac{kT}{\beta_{PF} V^{\frac{1}{2}}}\right) \cdot \exp - \frac{(\phi - \beta_{PF} V^{\frac{1}{2}})}{kT} \qquad 5.12.$$

has described a model based on Poole Frenkel emission containing shallow neutral traps and deep donors which results in the barrier lowering term having the form $\beta_{PF} V^{\frac{1}{2}}/2$ . This means the resulting log I v $V^{\frac{1}{2}}$ plot would have a slope which would normally be attributed to the Schottky effect and the analysis therefore can explain otherwise anomolous values of $\beta_{PF}$ . Hill (170) has described another similar mechanism relying on the close proximity of donor centres and the presence of traps, which also explains the anomolous results; while Boon (171) and Hall (172) have appealed to the quantum mechanical nature of the band structure to explain the discrepancies. Hill (167) has also pointed out that at low fields the contribution to the current due to the liberated electrons diffusing against the field cannot be neglected and the exponential factor becomes a sinh term. At higher fields, however, the Poole Frenkel relationship holds. It should be noted that for the Poole Frenkel effect to be the limiting process, the meanfree path of liberated electrons must be such that they have a high probability of being re-trapped otherwise the effect will only be transient. This would be the expected case for the films considered in this project due to the high anticipated densities of traps and donors, and would suggest that the relationship for the current density should include a voltage term in the pre-expontial factor equation 5.13. Simmonds (173), in another

$$J = J_o V \exp - \frac{(\phi - \beta_{PF} V^{\frac{1}{2}})}{kT} \qquad 5.13$$

paper, has described a complete V/I characteristic which is contact (Schottky and assisted tunnelling) limited at lower fields and bulk limited (Poole Frenkel, trap modified) at higher fields in a dielectric containing donors and traps at densities $\sim 10^{18} cm^{-3}$.

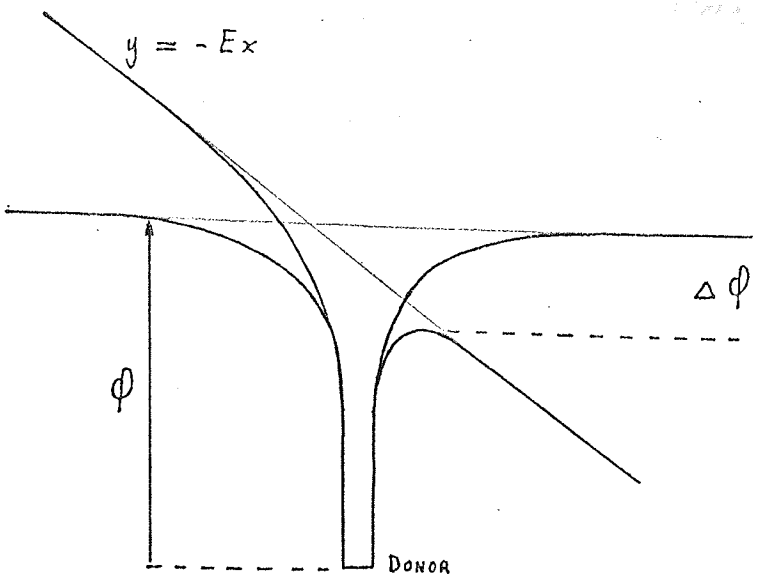


Figure 5.7

Poole Frenkel Field lowering of donor barrier

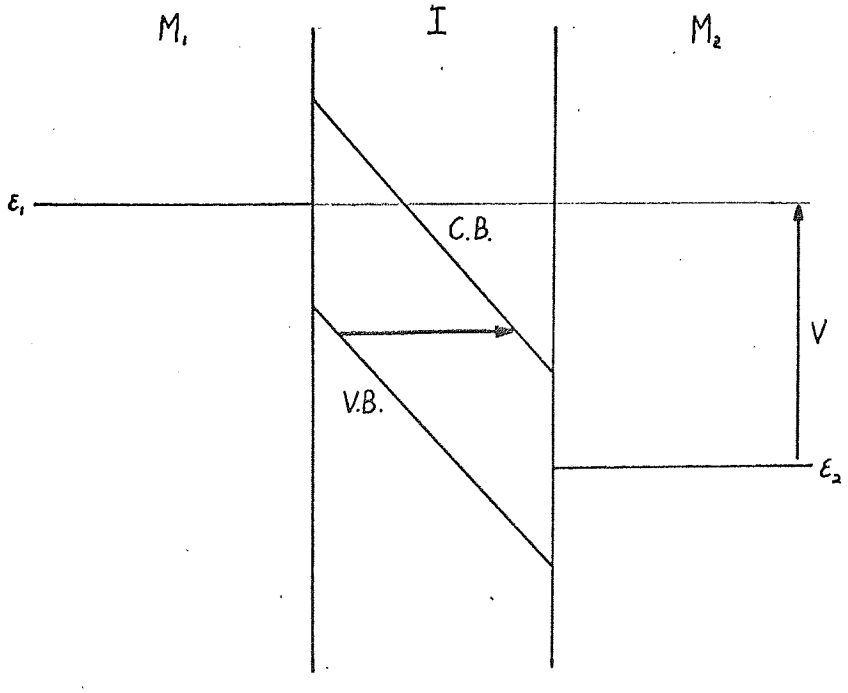


Figure 5.8

Zenor Breakdown.

5.B.3.2.2. Tunnelling.

The wave function of an electron in the source of a sandwich structure can penetrate the insulator, but its amplitude decays exponentially with distance. If the insulator is thin enough for the amplitude to be non zero in the drain electrode then there is a finite probability of the electron passing through the barrier by quantum mechanical tunnelling. This process has been analysed for many field ranges and barrier shapes. Tunnelling can also occur with an applied voltage larger than the insulator band gap, from the valence band to the conduction band of the material (Zener tunnelling), as illustrated in figure 5.8. The resulting conductivities are practically temperature independant, but very thickness dependant such that currents are negligeable at thicknesses greater than 100 Å. Consequently both processes can be discounted for films studied in this project.

5.B.3.2.3. Space Charge Limited Conduction (S.C.L.C.)

3.2.3.1. Trap Free S.C.L.C.

If the metal-insulator contacts are ohmic, that is they can supply an inexhaustible supply of free carriers then space charge limited conduction will occur as in a vacuum diode. At thermal equilibrium the conduction band will contain a number of free carriers due to thermal generation and an equivalent number of holes in the valence band. When, due to an applied field, injection causes an excess of free carriers space charge is created and the current flow, neglecting diffusion is given by equation 5.14, where $n_o$ is the density of thermal free carriers, $\rho$ is the

$$J = (n_o e + \rho)\mu E \qquad 5.14$$

space charge density, $E$ the applied field and $\mu$ the electron mobility. $E$ and $\rho$ are functions of distance along the current flow given by Poissons

$$\frac{\partial E}{\partial x} = \frac{\rho}{\varepsilon} \qquad 5.15$$

equation, 5.15, where $\varepsilon$ is the permitivity of the insulator. The potential in the system is given by equation 5.16 and the equations for the

$$V_x = \int_0^x E\,dx \qquad 5.16$$

conductivity under various conditions are found by the simultaneous particular solutions of these three equations. When the field is low, the density of thermally generated carriers $n_o$ will be much greater than the injected carrier density and $\rho$ can be neglected in equation 5.14. This leads to an initial region when Ohms law will be obeyed; equation 5.17, where

$$J = e n_o \mu \frac{V}{d} \qquad 5.17$$

d is the film thickness. As V is increased the case is soon reached where $\rho \gg n_o$ and $n_o$ can be taken as zero. This leads to the well known Mott Gurney law, equation 5.18. This expression neglects diffusion effects and assumes no variation of mobility with field. The transition from Ohms law to the Mott Gurney relationship occurs at a transition voltage $V_{tr}$ given by;

$$J = \frac{9}{8} \mu \varepsilon \frac{V^2}{d^3} \qquad 5.18$$

$$V_{tr} = \frac{8 e n_o d^2}{9 \varepsilon} \qquad 5.19$$

5.B.3.2.3.2. Electron Trapping.

The presence of traps in the dielectric will reduce the S.C.L. current since a proportion of the injected carriers will be removed. The detailed analysis of the effect of traps is very complicated but simple models have been postulated by Lampert (174), and Rose (175), which can be used to indicate the sort of characteristics one might expect. Traps are described as shallow or deep depending on whether they are at an energy more than one kT above or below the fermi level $E_f$. Deep traps have a low probability of releasing a captured carrier and are in general full while shallow traps have an occupancy which results from a balance between their electron capture and thermal re-emission probabilities. This balance is altered by an applied field because the injected carrier density increases and causes the fermi level to rise through the band gap. This means that with increasing applied field traps can change from shallow to deep and thereby loose their effect of limiting the current. The first model we shall consider concerns a single set of shallow traps all at the same energy $E_t$ with a density of $N_t$. The trap occupancy $n_t$ is given by:

$$n_t = \frac{N_t}{1 + \frac{1}{g} \exp \frac{E_t - E_f}{kT}} = g N_t \exp \frac{E_f - E_t}{kT} \qquad 5.20$$

which for shallow traps reduces as shown, where g is the degeneracy of the trap level. The free carrier density $n_o$ is given by:

$$n_o = N_c \exp \frac{E_t - E_c}{kT} \qquad 5.21$$

where $E_c$ is the energy at the bottom of the conduction band and $N_c$ the density of states at that level. The ratio of free to trapped charge $\theta$ is then given by equation 5.22, which is independant of the injection

$$\theta = \frac{n_e}{n_t} = \frac{N_c}{g N_t} \exp \frac{E_t - E_c}{kT} \qquad 5.22$$

level. The smaller $\theta$ the more effect the traps have. The effect is to delay the onset of the Mott Gurney law because more carriers have to be injected to produce the same space charge due to the proportion lost to traps and to modify the relationship. The transition voltage is now given

$$V_{tr} = \frac{8 e n_o d^2}{9 \theta \varepsilon} \qquad 5.23$$

by equation 5.23 and the Mott Gurney law by equation 5.24. Even in good

$$J = \frac{9}{8} \theta \mu \varepsilon \frac{V^2}{d^3} \qquad 5.24$$

dielectrics $\theta$ is often of the order of $10^{-6}$ so the effect of traps is very pronounced. This theory has been extended to include the reduction in trap depth due to the Poole Frenkel effect (176) and it is found that deviations from the Mott Gurney relationship to higher currents occur above a few $KV.cm^{-1}$. If a field is reached such that sufficient charge is injected into the dielectric to raise the fermi level to the trapping level $E_t$, then all the traps will be filled and the Mott Gurney law will revert to the trap free expression. There will be a very sharp rise in current until the relationship is satisfied and the voltage at which this occurs is called the trap filled limit voltage $V_{tfl}$ and is given by equation 5.25. $\theta$ is also

$$V_{tfl} = \frac{e N_t d^2}{\varepsilon} \qquad 5.25$$

an exponential function of the reciprical of the absolute temperature as can be seen from equation 5.22. Thin films however will not have a single trapping level, as used in this model, or even a number of discrete levels but are most likely to have traps distributed through the energy band gap, as discussed in Section 5.B.1. Considering this fact, Lampert (177) has also discussed a model consisting of a uniform energy distribution of traps

and Rose (175) an exponential distribution. In these models, as the voltage is increased the Fermi level moves through trapping levels and consequently is no longer a constant at a given temperature. For the uniform trap energy distribution $\theta$ is given by equation 5.26, where $n_o$ is

$$\theta = \frac{n_o e d}{VC} e^{tV} \qquad 5.26$$

the initial free carrier density and C the film capacity. The current density is governed by equation 5.27, where t is given by equation 5.28

$$J = \frac{9}{8} \mu \varepsilon \frac{V}{d^2} \left(\frac{n_o e}{C}\right) e^{tV} \qquad 5.27$$

$$t = \frac{C}{N_t e d k T} \qquad 5.28$$

The exact trap distribution in the exponential model is characterised by a temperature $T_t$ such that the number of traps with energy $E_t$ is given by

$$N_t = N_o \exp\left(\frac{E_t - E_c}{k T_t}\right) \qquad 5.29$$

equation 5.29. If $T_t < T$ the trap distribution is localised just below the conduction band and the situation is a special case of shallow traps. In general however the J.V. relationship is given by equation 5.30 where

$$J = e \mu N_c \left(\frac{\varepsilon}{e N_o T_t}\right)^t \frac{V^{t+1}}{d^{2t+1}} \qquad 5.30$$

$T_t/T = t$. This is of higher order in V than simple trapping and the order is also a function of temperature. These two examples show how much the V/I characteritics are determined by the exact distribution and density of traps.

5.B.3.2.3.3. A Criterian for S.C.L.C.

Murgatroyd (178) has derived a relationship for the thickness dependance of the J/V characteristics for space charge limited conduction. It wholds for any trap or donor distribution provided the current is due to only one species of carrier and diffusion is neglected. For S.C.L.C. it is necessary but not sufficient that the relationship holds. The rule, which is that plots of J/L agains $V/L^2$ should superimpose therefore acts as a rejection criterian. For other conduction mechanisms one would expect the plots to be ordered in L.

5.B.3.2.3.4. Double Injection.

The effect of double injection, that is the injection of both elect-

rons from the cathode and holes from the anode, on S.C.L.C. has been considered by Tredgold (178) and Lampert (179) for cases involving no traps and neglecting diffusion. Up to a threshold voltage the current is one carrier space charge limited due to the carrier with the shortest transit time. The J/V characteristics will contain an ohmic region and Mott Gurney relationship up to the commencement of double injection space charge when a negative resistance transition region occurs before J is again proportional to $V^2$ and at even higher fields $J \propto V^3$. No quantitative analytical derivation of the effect of traps on double injection can be obtained but generally one would expect characteristics of the same sort of form. It should be noted that one would normally only expect double injection from M.I.M. structures when the metal electrodes are of different materials, because it is difficult to imagine the same type of contact injecting both holes and electrons. However gold electrodes have been found to act as hole injecting on clean barium titanate surfaces and electron injecting when chemisorbed oxygen present on the surface increased the electron affinity of the material (180).

5.B. 3.2.3.5. Summary.

The observation of S.C.L.C. relies on the insulator metal contacts being ohmic or injecting and the resulting characteristics depend on the presence and distribution of traps in the dielectric. The characteristics are also a function of the nature of the injection, for example a $V^{\frac{3}{2}}$ power law has been derived for spherically symmetrical injection as one would obtain from a point contact (181). In general the characteristics all take the form $J = J_o V^n$ where n is not necessarily a whole number and both it and $J_o$ can vary with temperature. The permitivity $\varepsilon$, present in the numerator of all the current density equations, arises from Poissons equation (5.15) for the variation of field with space charge and is therefore the low frequency premitivity. The high value of this factor in barium titanate, even when reduced due to being in thin film form, (a dielectric constant of 100-200), means the likelihood of observing S.C.L.C. in the material is much greater

than for most materials. For example, using the Mott Gurney trap reduced relationship, equation 5.24, for a film of 5000 Å, assuming ohmic contacts, at a field of $10^5$ V.cm$^{-1}$, putting the ratio of free to trapped carriers $\theta$ as low as $10^{-8}$ and using likely values of the disposable parameters the current density obtained is 0.25 A.cm$^{-2}$. With a capacitor area of $1.10^{-2}$ cm this yeilds a current of $\sim 10^{-7}$ A. Space charge would have an effect on most conduction mechanisms but it is generally neglected. ODwyer (182) however has described a model which contains shallow and deep traps and computed I.V characteristics for a space charge controlled but Schottky and field emission injected current. He found, surprisingly that above fields of $5\ 10^5$ V.cm$^{-1}$ straighter log J against $V^{\frac{1}{2}}$ plots were obtained for field emission than Schottky injected currents.

5.B.3.2.4. Hopping or Impurity Conduction.

In an insulator containing impurity centres, either donor or acceptor, overlap between the wave function of a carrier in one site and a neighbouring empty site means that the carrier can tunnel to that site. This hopping is accompanied by the emission or absorption of a phonon in order to conserve energy, and in the absence of an applied field will be random, so no net current will flow. An applied field produces a gradient of impurity site energy and as the probability of hopping to sites of lower field energy is increased there will be a net flow of current in the field direction. The theory of the electron tunnelling from site to site has been worked out by Miller and Abrahams (183) but is very complex. The final result yields a temperature dependent resistivity given by equation 5.31.

$$\log \rho(T) = f(N) + \frac{E}{kT} \qquad 5.31$$

where $E$ is the activation energy and f(N) a function of the major carrier density. Mycielski (184) proposed a second mode of electron hopping at higher temperatures which entails the electron jumping over the barrier between neighbouring sites. The process is limited by the carrier-phonon interaction and results in a variation of resistivity, equation 5.32, the

$$\log \rho(T) = f'(N) + \frac{E'}{kT} \qquad 5.32.$$

same as for straightforward tunnelling with a modified activation energy $\phi'$. As dielectric thin films are amorphous or polycrystalline, with a high density of impurity sites it seems very likely that impurity conduction should occur particularly at temperatures at which the excitation of free carriers is improbable. The important features of the conductivity are a linear dependance of current on voltage, $J \propto V$, coupled with a weak but finite temperature dependance. The activation energies anticipated would be very small ( 0.001-0.01eV) compared to all other processes.

5.B.3.2.5. Ionic Conduction.

Ionic conduction was observed in ionic crystals many years ago and is often used to explain conduction in anodised films. The conductivity depends on the rate of drift of lattice defects, ions or vacancies, under the influence of an applied field. The method used to calculate the conductivity is to consider the jump frequency of a defect from one site to another over a potential barrier in the same way as one calculates diffusion probabilities. The barrier between sites in the direction of the applied field E is lowered by an amount Eel/2, where e is the electronic charge and l the distance between sites. The jump frequency in the direction of the field $\nu^+$ is increased and the jump frequency in the reverse direction $\nu^-$ decreased

$$\nu^+ = \nu e^{\frac{\phi + Eel}{2kT}} \qquad \nu^- = \nu e^{\frac{\phi - Eel}{2kT}} \qquad 5.33$$

as shown in equation 5.33. The net probability of a defect jumping in the field direction $\nu_p$ is then given by equation 5.34. For low fields where

$$\nu_p = \nu^+ - \nu^- = \nu 2 \sinh \frac{Eel}{2kT} \qquad 5.34$$

$Eel \ll kT$ the equation can be reduced to equation 5.35 and since the charge

$$\nu_p = \nu \frac{Eel}{kT} \qquad 5.35$$

movement associated with each jump is el the current density is given by equation 5.36, where n is the number of defects per unit volume. For higher

$$J = n\nu \frac{Ee^2l^2}{kT} = J_1 T^2 E e^{-\frac{\phi}{kT}} \qquad 5.36$$

fields $E > 10^5$ $V.cm^{-1}$ when $Eel \sim kT$ the assumption can be made that the probability of a backward jump, against the field, is negligeable so the current density is given by equation 5.37. Below fields of $10^4 V.cm^{-1}$ and above

$$J = nel\nu^{+} = J_2 T^3 \exp - \frac{(\phi - Eel/2)}{kT} \qquad 5.37$$

80° K the current density varies linearly with voltage and plots of $J/T^2$ against I/T should be straight lines the slope of which give the activation energy, that is the barrier height. For fields above $10^5$ V.cm$^{-1}$, $J \propto \exp V$ and plots of $\log J/T^3$ against I/T yield the activation energy.

The distinction between ionic and electronic conduction may in some instances be a difficult problem with no definite solution. Ionic conduction is accompanied by material transport and if high currents are passed for long enough periods this should be detectable. Ionic conductivity is also associated with slow polarisation effects, variation of current with time and standing voltages on open circuits. It is usually characterised by lower mobilities and higher activation energies than electronic processes, but these distinctions loose some of their validity when considering amorphous or semi-amorphous thin films.

5.B.4. Summary and Applicability of Conduction Processes.

Hill (185) has examined the nature of bulk limited conduction based on the ionisation of local defects due to an applied field and has found the Poole Frenkel effect to be only a limiting case in a more general analysis. At high temperatures thermal emission dominates while at low temperatures and high fields tunnelling out of the centres dominates. Between these two a thermally assisted tunnelling process occurs with a temperature characteristic of $\log J \propto T^{-3}$. He also shows that if the density of centres is such that the perturbations to the potential overlap then the barrier lowering is proportional to V and Pooles law is obeyed, equation 5.38. For the Poole

$$\log \frac{J}{V} \propto V \qquad 5.38$$

Frenkel effect the exact form of the V/I relationship is a function of whether the emission is spherically symmetrical or along the field direction and whether the mean free path of emitted electrons is independant of field E, proportional to E or proportional to $E^{\frac{1}{2}}$. For all cases of discrete centre emission, however, a normalisation should be possible between field and temperature according to $E^{\frac{1}{2}}T^{-1}$ and plots of $\phi$, given by equation 5.39,

$$\mathcal{J} = J.T^{-n} \exp \frac{\varepsilon_i}{kT} \qquad 5.39$$

against $E^{\frac{1}{2}}T^{-1}$, where n = 3 or 4 and $\varepsilon_i$ is the energy difference between the centre and the conduction band edge. The conductivity relationship can then be reduced to a two variable system given by equation 5.40, where

$$\mathcal{J} = f_n(\alpha \sinh \alpha) \qquad 5.40$$

$\alpha = \beta E^{\frac{1}{2}}/kT$. The distinguishing feature for Pooles law is a normalisation according to $ET^{-1}$ and these characteristic properties give a criterian for the two effects. An equation governing these effects and hopping conduction of the same general form as 5.40 is given by Hill (156) in another paper, where the values of the disposable parameters equivalent to each process are described. The films whose V/I characteristics were examined in this project are unusual because while no crystal structure was determined crystallographically they exhibited values of dielectric constant under certain deposition conditions an order of magnitude above those values associated with amorphous barium titanate. Consequently, while some of the films (deposited at low temperatures) are undoubtedly amorphous other films deposited at higher temperatures are supposed to be in a metastable form of barium titanate showing some degree of ordering at intermediate ranges. Conduction process normally associated with both amorphous and crystalline materials are therefore feasible. The distinguishing characteristics of the various conduction processes and their likely regions of applicability to the films examined are summarised in table 5.2.

| CONDUCTION MECHANISM | | E/T RANGE V.cm⁻¹ °K | J/V RELATIONSHIP | TEMPERATURE DEPENDENCE | ACTIVATION ENERGY eV | OTHER CHARACTERISTICS AND COMMENTS |
|---|---|---|---|---|---|---|
| CONTACT LIMITED | SCHOTTKY EMISSION | $T > 300°C$ all E<br>$80° < T < 300°C$ $E < 10^6$ | $\log J \propto V^{\frac{1}{2}}$ | $\log \frac{J}{T^2}$ or $\frac{J}{T^{\frac{3}{2}}} \propto \frac{1}{T}$ | 0·5 – 1·0 | generally low fields and high temperatures |
| | THERMALLY ASSISTED TUNELLING | INTERMEDIATE | $\log J/V \propto V^2$ | similar to Schottky' | — | shows as deviation from Schottky' at high fields |
| | FIELD EMISSION | $T < 80°$ $E > 10^5$<br>$80° < T < 300°$ $E > 10^6$ | $\log \frac{J}{V^2} \propto \frac{1}{V}$ | negligeable | — | unlikely to be observed due to onset of breakdown |
| BULK LIMITED CONDUCTION | POOLE FRENKEL | $T \gtrsim 150°$ $E > 10^4$<br>same E/T but high donor density<br>$T < 150°$ | $\log J$ or $J/V \propto V^{\frac{1}{2}}$<br>$\log J/V \propto V$ (Poole's Law)<br>Assisted tunelling from centres | $\log J \propto 1/T$<br>$\log J \propto 1/T$<br>$\log J \propto T^{-3}$ | 0·2 – 1·0 | Field lowering coefficient $\beta_{PF}$ a function of trap distribution |
| | HOPPING | LOW T WHEN NOT MASKED BY THERMAL FREE CARRIERS | $J \propto V$ | $\log J \propto \frac{1}{T}$ | 0·001 | |
| | IONIC CONDUCTION | $E < 10^4$<br>$E > 10^5$ | $J \propto V$<br>$\log J \propto V$ | $\log J/T^2 \propto 1/T$<br>$\log J/T^3 \propto 1/T$ | several eV | Slow relaxation times<br>Standing voltages<br>Material transport |
| | SPACE CHARGE LIMITED CONDUCTION | TRAP FREE<br>where $E_{TR} = \frac{8en_0d}{9\varepsilon}$, $E_{TR} \propto \exp 1/T$<br>$E < E_{TR}$<br>$E > E_{TR}$ | $J \propto V$<br>$J \propto V^2$ | $J(T) = \mu(T)\, n_0(T)$<br>$J(T) = \mu(T)$ | — | Thin Films will not be Trap Free |
| | | SHALLOW TRAPS<br>where $E_{TR} = \frac{8en_0d}{9\theta\varepsilon}$, $E_{TR} \propto \exp 1/T$<br>$E < E_{TR}$<br>$E > E_{TR}$ | $J \propto V$<br>$J \propto \theta V^2$ | as TRAP FREE<br>BUT $\theta \propto \exp \frac{1}{T}$ | — | $\theta$ will be at least as low as $10^{-7}$ and probably a lot lower |
| | | DISTRIBUTED TRAPS<br>ALL CASES LOW E HIGH T<br>LINEAR HIGH E LOW T<br>EXPONENTIAL "<br>POINT CONTACT " | $J \propto V$<br>$\log J/V \propto J_0 + tV$<br>$J \propto V^n$<br>$J \propto V^{\frac{3}{2}}$ | as TRAP FREE<br>$J_0(T) \propto \mu(T) n_0(T)$ $t \propto \frac{1}{T}$<br>$J(T) \propto \mu(T)$ $n \propto \frac{1}{T}$ | — | Form of J/V characteristics a function of trap distribution, analysis only possible for these simple cases. |
| | | DOUBLE INJECTION<br>BELOW A THRESHOLD VOLTAGE NEGATIVE RESISTANCE TRANSITION ABOVE THRESHOLD VOLTAGE HIGHER VOLTAGE | SINGLE S.C.L.C.<br>$J \propto V^2$<br>$J \propto V^3$ | | — | No analysis for the effect of traps. Forward and Reverse Characteristics should be different |

TABLE 5.2

# CHAPTER SIX

## THE GROWTH AND PROPERTIES OF BARIUM TITANATE SPUTTERED FILMS.

### 6.A. Film Growth on Amorphous Substrates.

#### 6.A.1. Glass Slides.

Barium Titanate was first sputtered onto glass slides whose temperature was varied in the range from ambient to 500°C. In these early experiments, only the substrate table temperature was measured and substrate temperatures have been assessed by comparison with later results. Consequently the temperatures quoted are not reliable to better than ±50°C. The structure of the films was examined using Xray techniques. The substrate was either mounted in position in the goniometer diffraction stage or the film was scratched off the glass slide using a razor blade and the powder used in a Debye-Scherrer camera. The goniometer recorder traces taken off blank slides and again after deposition were not significantly different, but with the Debye Scherrer camera powder lines were observed for some films. It was found that films deposited at temperatures below 400°C were amorphous, while those deposited at 450°C or above were polycrystalline. Amorphous films gave an Xray powder photograph showing one wide diffuse band at a "d" spacing 4Å while the polycrystalline films exhibited most of the barium titanate lines shown by the original target material, as can be seen in plate XVIII. The diffuse line at 4Å was found to be present in all films and this suggested that either some amorphous phase was always present or that the line was associated with the experimental arrangement or the small grain size. As plain glass substrates did not allow electrical measurements and the method of examining film structure was unsatisfactory other films were deposited onto different materials.

#### 6.A.2. Amorphous carbon.

Barium titanate was next deposited on amorphous carbon films supported on electron microscope grids so that the titanate film structure

TARGET POWDER

AMORPHOUS FILM

POLYCRYSTALLINE FILM

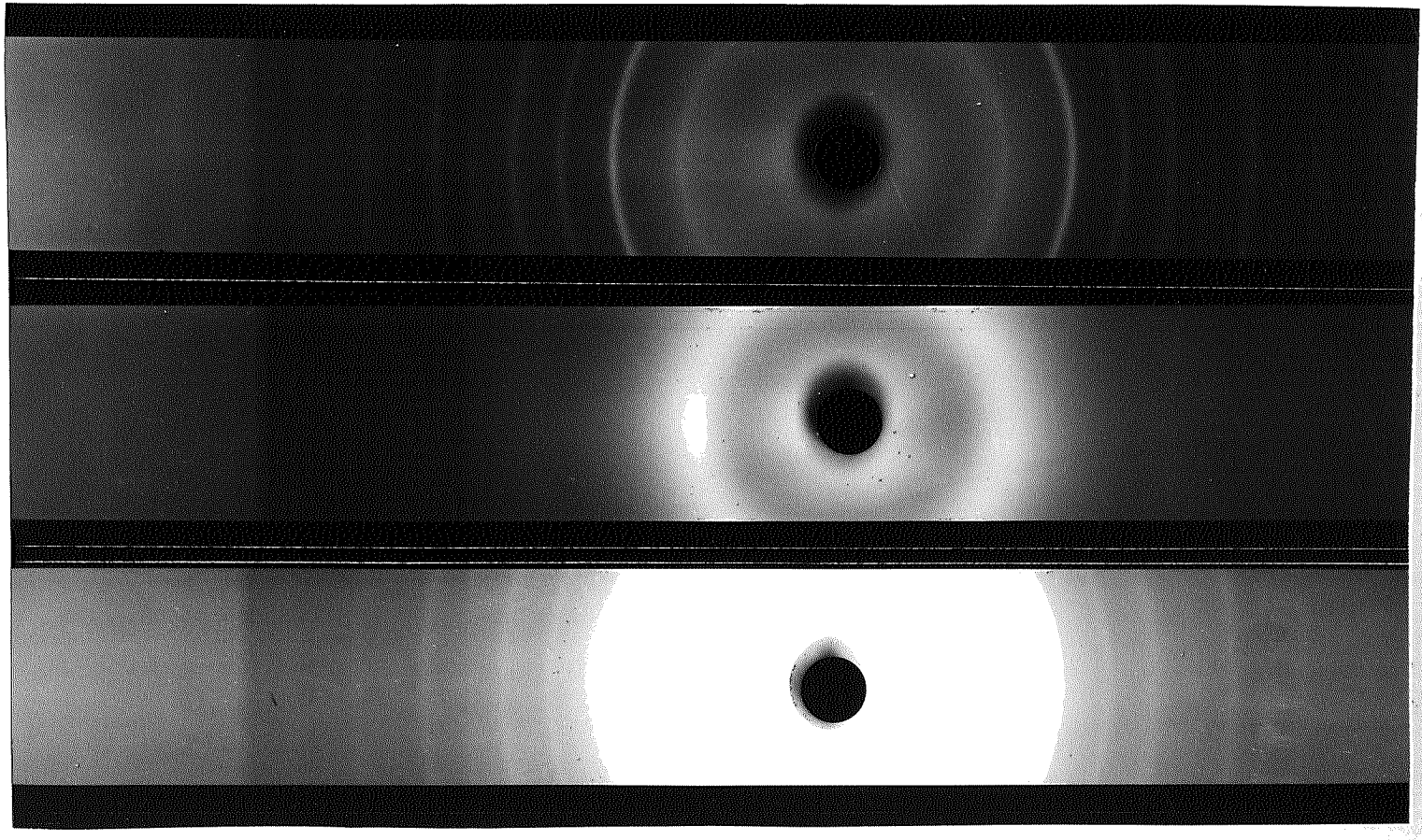

PLATE XV111

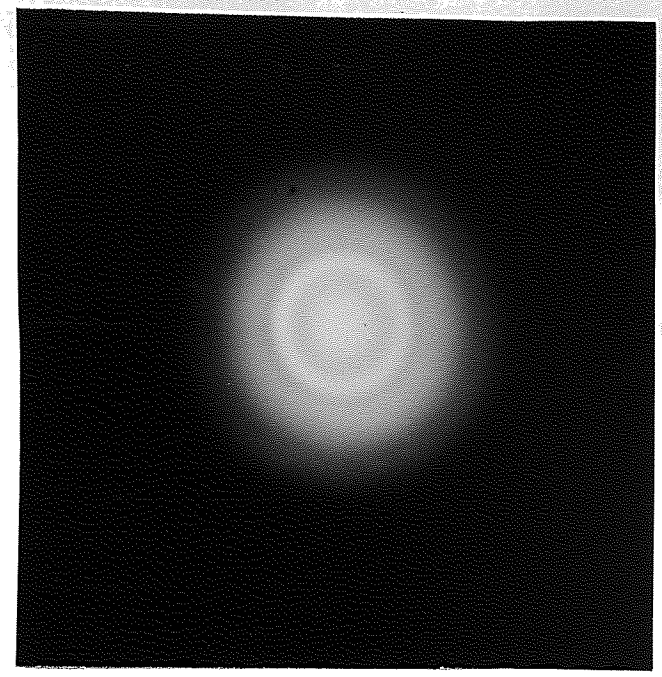

PLATE XIX

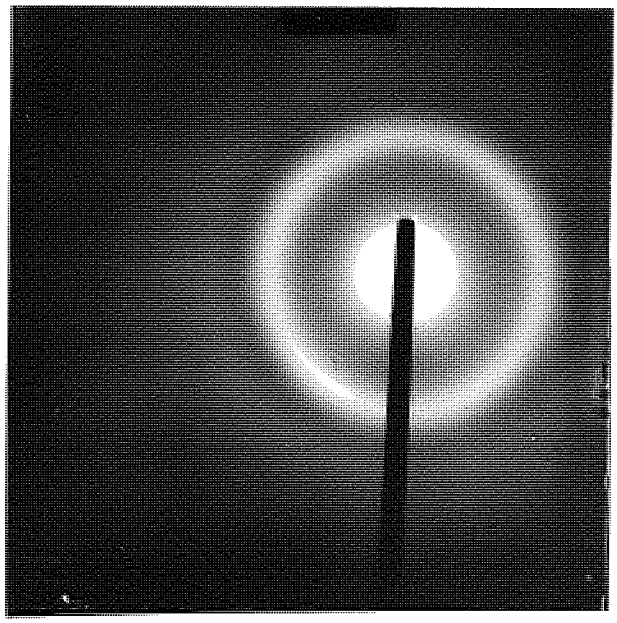

PLATE XX

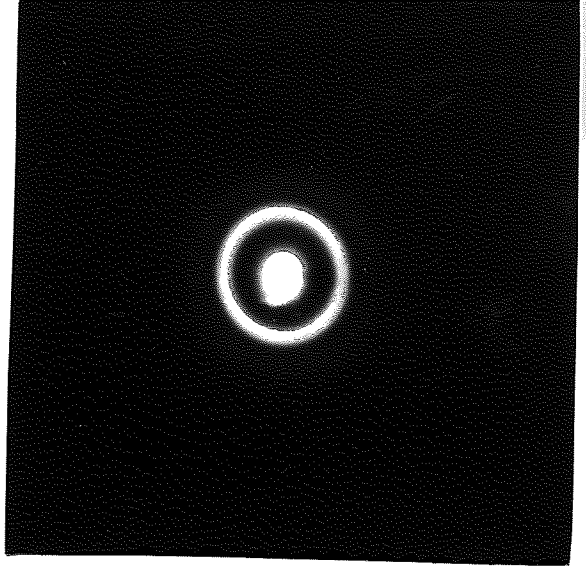

ROOM TEMP.

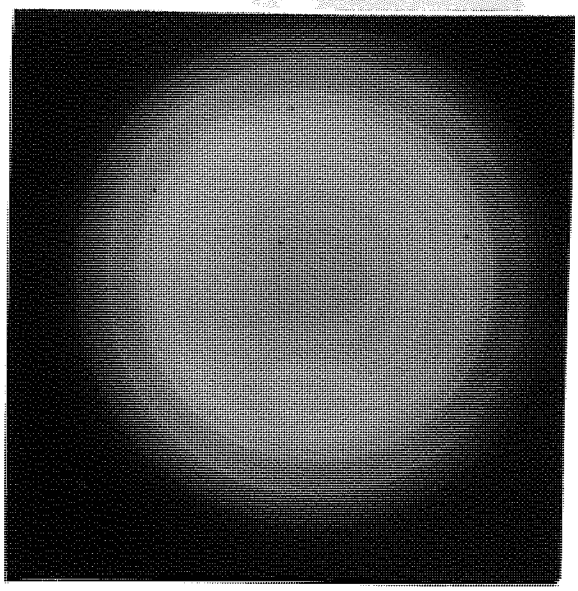

470°C

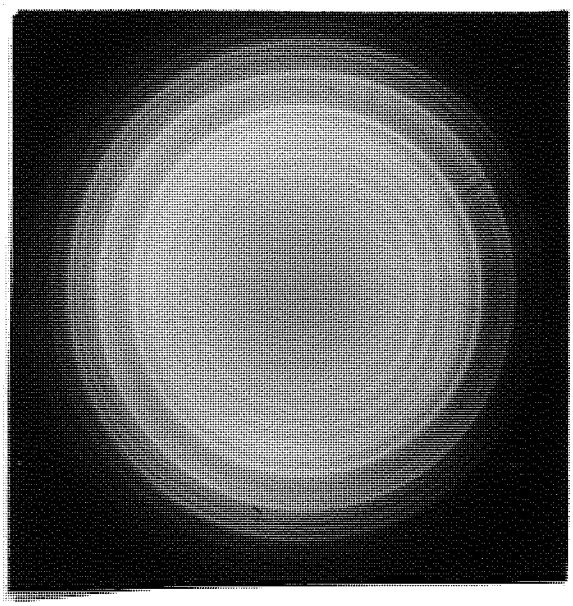

490°C

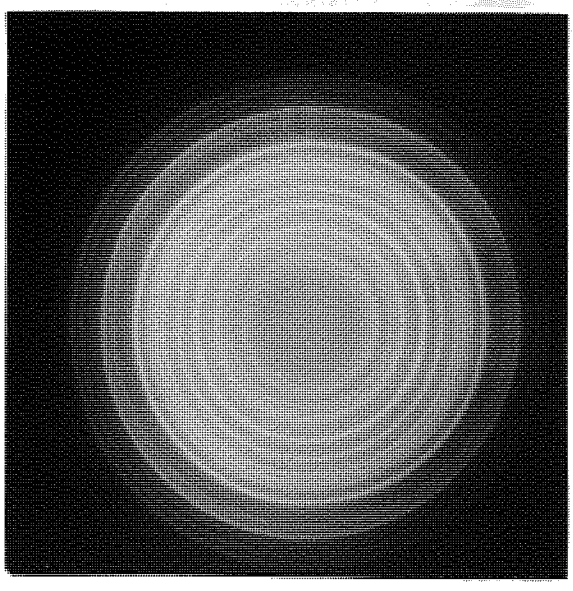

500°C

PLATE XX1. CHANGES OF STRUCTURE ON ANNEALING.

DIFFRACTION PATTERN

GENERAL REGION

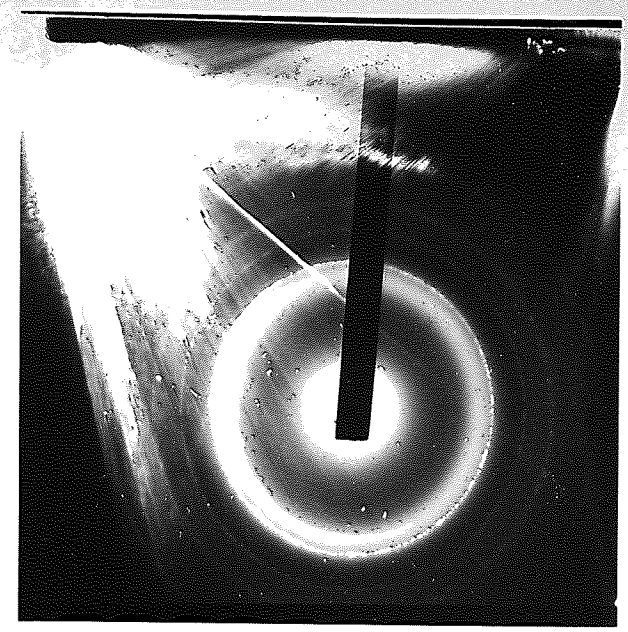

GENERAL REGION X51 K

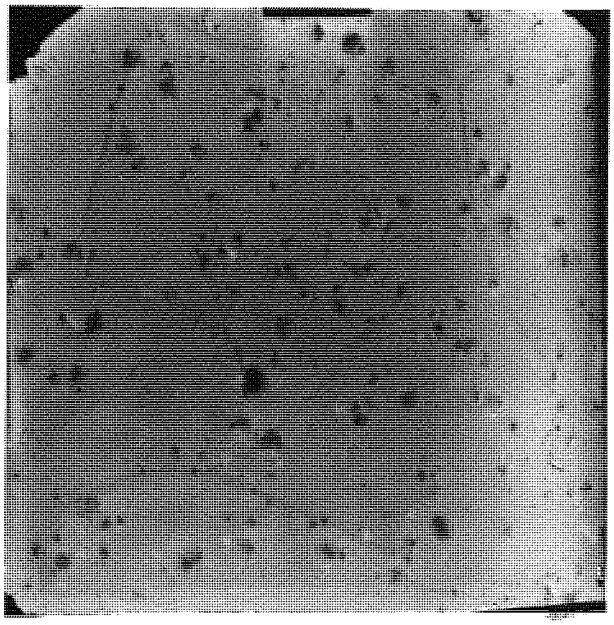

PLATE XX11. FILM 62. GENERAL REGION.

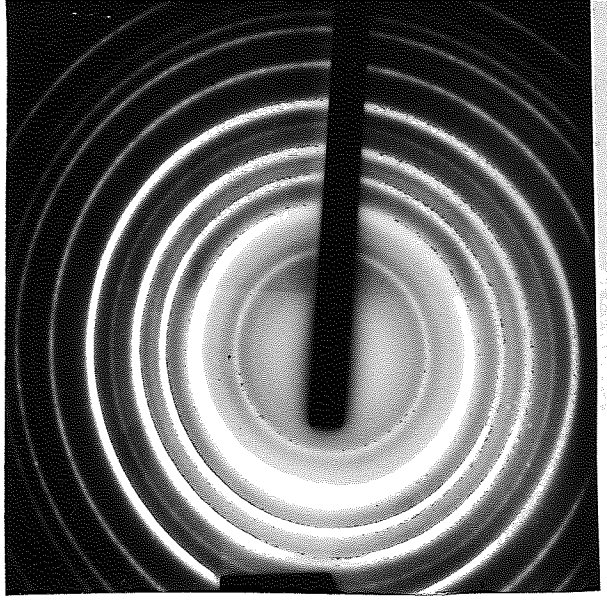

DIFFRACTION PATTERN

BEAM CRYSTALLISED REGION

BEAM CRYSTALLISED REGION

X 18 K

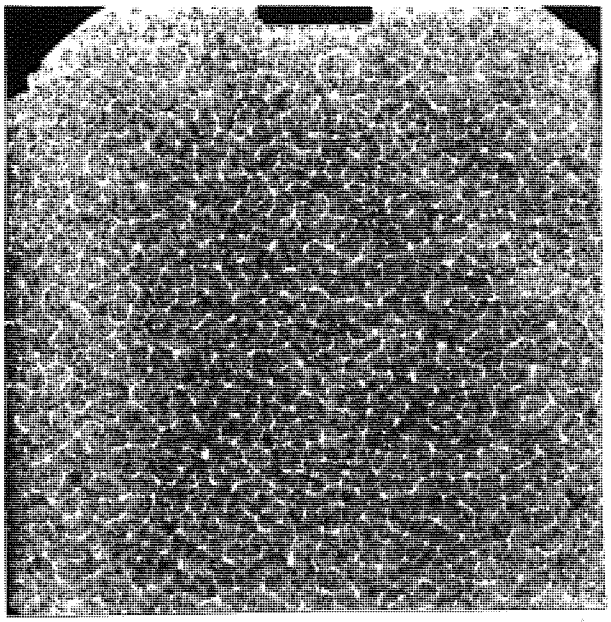

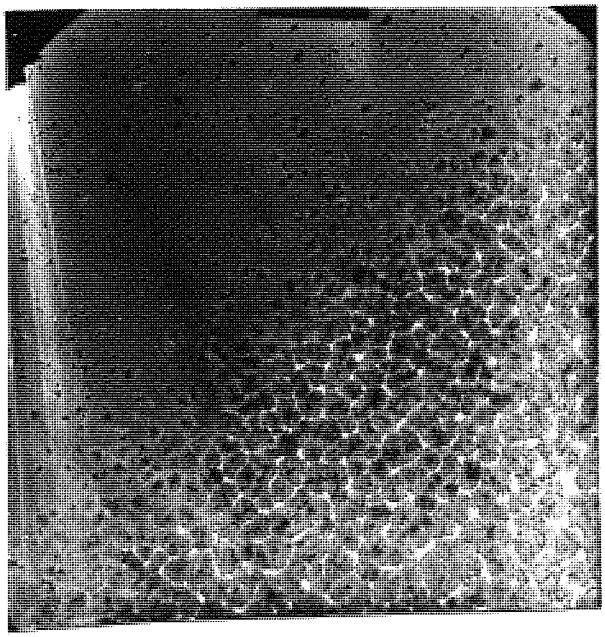

BOUNDARY OF BEAM

CRYSTALLISED REGION X 27 K

PLATE XX11. FILM 62. BEAM CRYSTALLISED REGION.

X 8 K

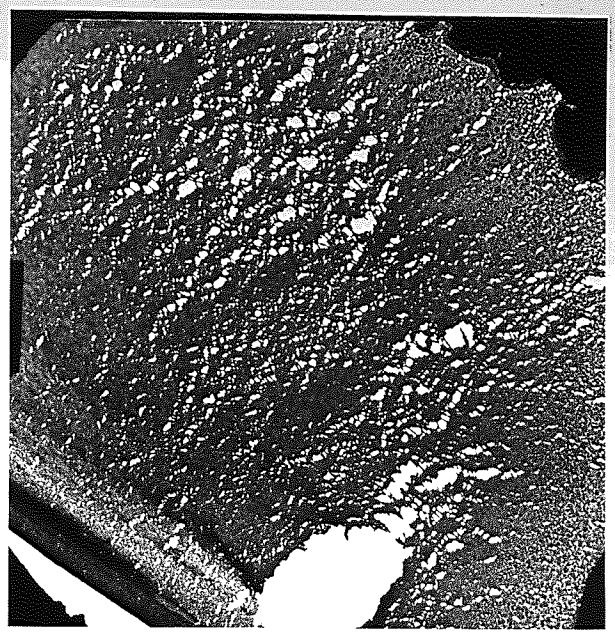

X 51 K

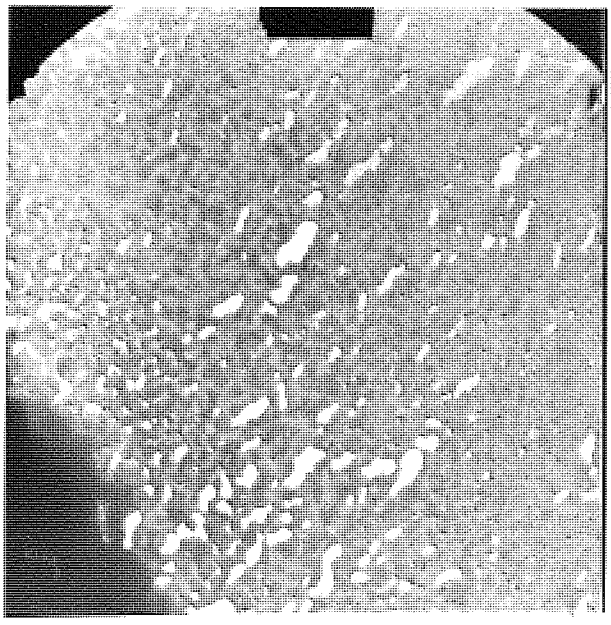

Plate XXIII FILM 59 TEARING OF CRYSTALLISED FILMS.

FILM 47. AMBIENT

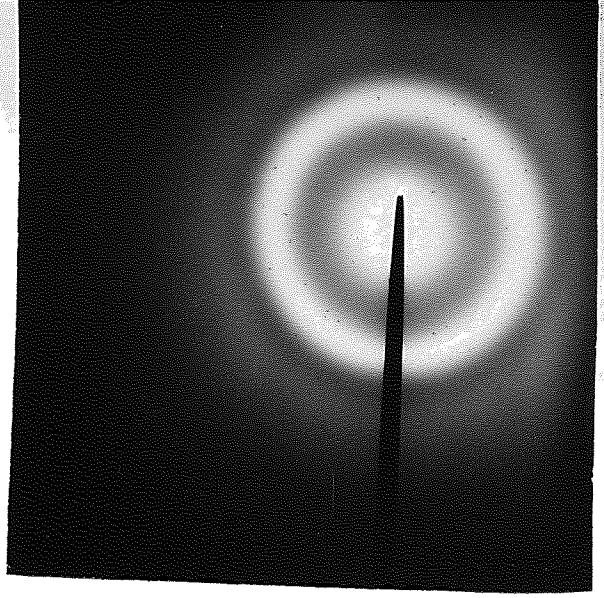

FILM 61 430°C

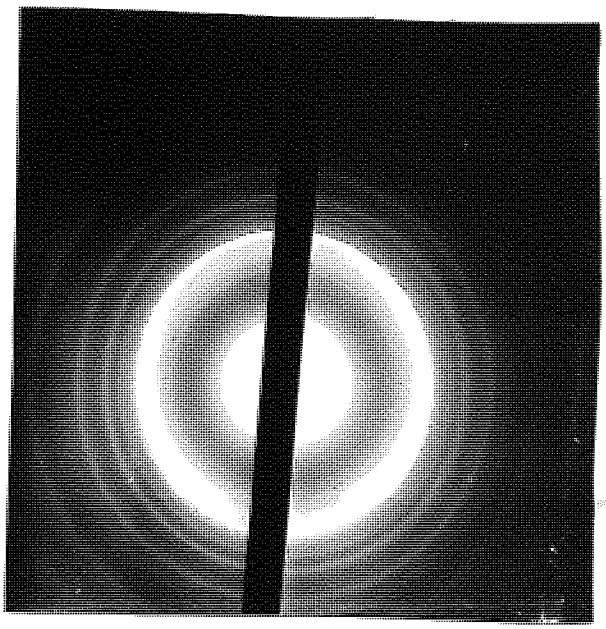

FILM 64 480°C

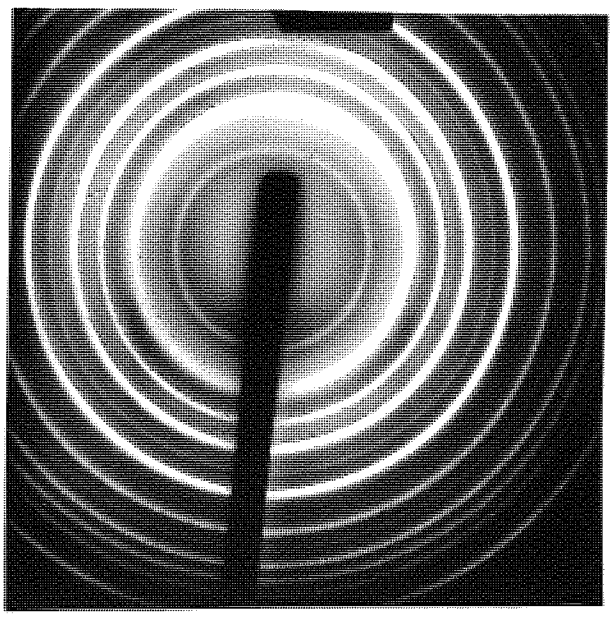

PLATE XXIV. DIFFRACTION PATTERNS AS A FUNCTION OF DEPOSITION TEMPERATURE

could be examined easily in the electron microscope. Some of the carbon films were first examined in the microscope to ensure that no structure was present. Titanate films deposited at ambient temperature were amorphous giving rise to four diffuse rings viewed on the high resolution diffraction stage (Plate XIX). The strongest band (Plate XX) corresponded to interplaner spacing ranging from 3.0 - 3.4. Å which is similar to that reported by Müller et al (47) and while including the strongest lines from barium oxide and titanium dioxide does not include the strongest barium titanate line (2.8 Å) and indeed includes no barium titanate reflections at all. A number of these films were then heated in the diffraction stage while simultaneously observing the diffraction pattern. The pattern showed no change up to a film temperature of 440°C but over a range of temperature above this the pattern became completely polycrystalline in structure. The exact temperature at which crystallisation began and finished varied slightly from film to film but the range was always 30-50°C and within the limit 460-530°C. Plates XXI show the crystallisation of a film in stages. It was possible to produce films with both the amorphous and polycrystalline phases present which Müller did not observe. Great care had to be taken to avoid crystallising the films by electron beam heating, and this necessitated the use of low beam current in all examinations. Beam crystallisation did not generally extend over more than a few grid spacings and could be detected easily by transmission microscopy. Plate XXII shows a film of mixed mainly amorphous - polycrystalline structure that had been beam crystallised. Films were deposited varying the partial pressure of oxygen from 0-10% of the sputtering gas, but this made no significant difference to the crystallisation temperature or the structure of the films. Transmission microscopy of annealed films showed considerable break up on crystallisation, with tears all over the surface and large sections of the films missing Plate XXIII. The next step was to heat the carbon coated grids during deposition and determine the crystallisation temperature under those conditions. As discussed in Section 5.A.1. the increased mobility of

titanate adatoms due to the sputtering process might be expected to contribute to the activation energies associated with nucleation and coalescence rearrangement processes so that a lower substrate crystallisation temperature would be required. A number of films were deposited varying substrate temperature from ambient to 500°C and the percentage of oxygen in the sputtering gas from 0-10% and all were examined in the electron microscope. Most of the films deposited, particularly those above 250°C, were very discontinuous, either due to failure of the carbon film with temperature or again due to cracking and tearing of the titanate film. All the depositions were at a rate of 12 Å.min$^{-1}$ and some crystalline growth was found to be present in films deposited above 420°C but was not complete in any films deposited at a substrate temperature below 450°C. Films which were amorphous still showed the same annealing characteristics as films deposited at ambient and the oxygen percentage was again found to make no difference to the crystallisation temperature or the proportion of each phase present at a given temperature. Plate XXIV shows the diffraction pattern for films deposited on carbon films over a range of temperature. Comparison of the line intensities with the Xray powder line data showed that the (200) lines were stronger and (111) lines weaker than anticipated. This could be due to the electron diffraction process but is more likely to be due to a slight single order texturing. Titanate (100) planes have a tendancy to be parallel to the substrate but are otherwise randomly orientated.

6B Single Crystal substrates.

All the available literature on barium titanate thin films reported that they only exhibit high permitivity in polycrystal or single crystal form. The crystallisation temperatures found necessary on the amorphous substrates however, were incompatible with microelectronic processes. Barium titanate was therefore R.F. sputtered onto single crystal substrates with the object of inducing epitaxial growth in single crystal or polycrystalline form at lower temperatures.

6.B.1. Potassium Bromide.

Barium titanate films were deposited onto air cleeved (100) planes of potassium bromide at temperatures ranging from ambient to 450°C, deposition rates of 5-25 Å/min$^{-1}$ and with 0-10% oxygen in the sputtering gas. The films were floated off the KBr, picked up on microscope grids, and their appearance and structure examined in the high resolution diffraction stage or by selected area diffraction. Mounting the films on the grids was a difficult operation and needed care. The KBr crystal was taken out of the deposition kit and lowered into a petri dish of distilled water at a low angle to the water surface. This operation was viewed through x 10 binocular microscope and illuminated with a lamp. Occasionally the films did not seem strong enough to withstand the surface tension forces of the water and broke up into many very small pieces spread over the water surface. Normally however the film broke only at faults in the KBr cleevage face and could be easily seen floating on the water. Using fine tweezers a carbon coated grid was then forced under the water, and viewed through the microscope, was lifted up under the film and out of the water. In this way some of the film was picked up on its surface. The grids were then covered with a petri dish and allowed to dry before being examined and filed in a specimen holder for reference.

6.B.1.1. Film Crystal structure.

The variation of film structure with substrate temperature and deposition rate did not appear to follow any of the patterns predicted. However all the films deposited on potassium bromide are plotted on a phase diagram as suggested by Krikorian in figure 6.1. All films deposited at substrate temperatures below 160°C were amorphous showing the same diffuse diffraction rings as the films deposited on carbon coated grids (Plate XXV). The films were again easily crystallised by the electron beam of the microscope to a polycrystalline structure (Plate XXVI) and also showed the same annealing properties. Above 160°C films started to grow with an epitaxial fibre texture of (100) planes parallel. The phase change was not sudden but

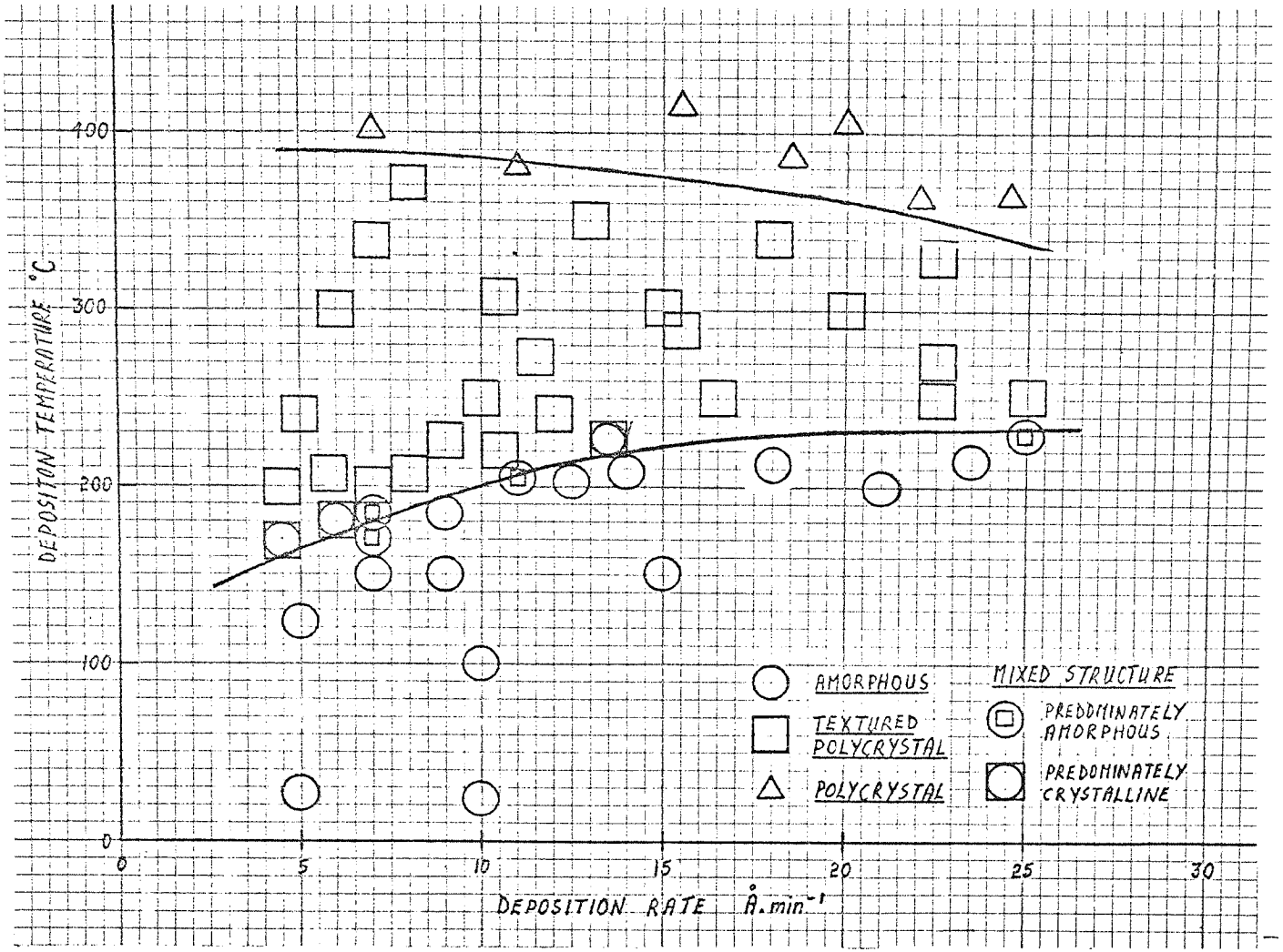
DEPOSITION TEMPERATURE °C
400
300
200
100
0
0
5
10
15
20
25
30
DEPOSITION RATE Å.min⁻¹
AMORPHOUS
TEXTURED POLYCRYSTAL
POLYCRYSTAL
MIXED STRUCTURE
PREDOMINATELY AMORPHOUS
PREDOMINATELY CRYSTALLINE

Figure 6.1.

occured over a range of temperature and films with mixed amorphous and textured polycrystalline structures were easily produced. Plate XXV11 is a diffraction pattern from film 89 deposited at 165°C with a rate of 7 Å.min$^{-1}$ and shows a mainly amorphous structure with some textured polycrystalline phase present. However Plate XXV111 of film 117 deposited with the same rate but at 200°C shows a mainly textured polycrystalline structure with a trace of the amorphous phase still present. Diffraction patterns were obtained from regions of these films as small as $6.10^{-6}$m diameter but both phases were still present. It is interesting to note that even in the very early stages of crystalline growth in films which are predominately amorphous the structure contained the epitaxial fibre texture and was not simply polycrystalline, as can be seen in Plate XXV11. The temperature at which crystalline growth initiated was lower with decreased deposition rate as shown in figure 6.2(a) and roughly followed an exponential law as discussed in Section 5.A.2. This is shown in figure 6.2(b) and from equation 5.3. yields an energy of surface diffusion of $3.6\ 10^{-1}$eV Joules. From discussion in Section 5.A.2. one would also expect the degree of fibre texture or epitaxy to be a function of substrate temperature and deposition rate. To obtain the variation with these two parameters each film examined was assigned a number from 0-5 roughly indicating the degree of texturing, ranging from zero for a purely polycrystalline structure to 5 for single crystal growth. This method was very subjective and was only capable of indicating trends; but it did enable the following conclusions to be reached.

(1) For a given temperature, a higher degree of epitaxy was obtained at a lower deposition rate. This is indicated by figure 6.3. and Plates XXV111 and is the behaviour predicted by theories of film growth

(2) Above the crystallisation temperature, at a given rate, the epitaxy initially showed a small improvement with increasing temperature but the texture generally became less marked with further increase in temperature. This is shown in figure 6.4. and Plates XX1X and is contrary

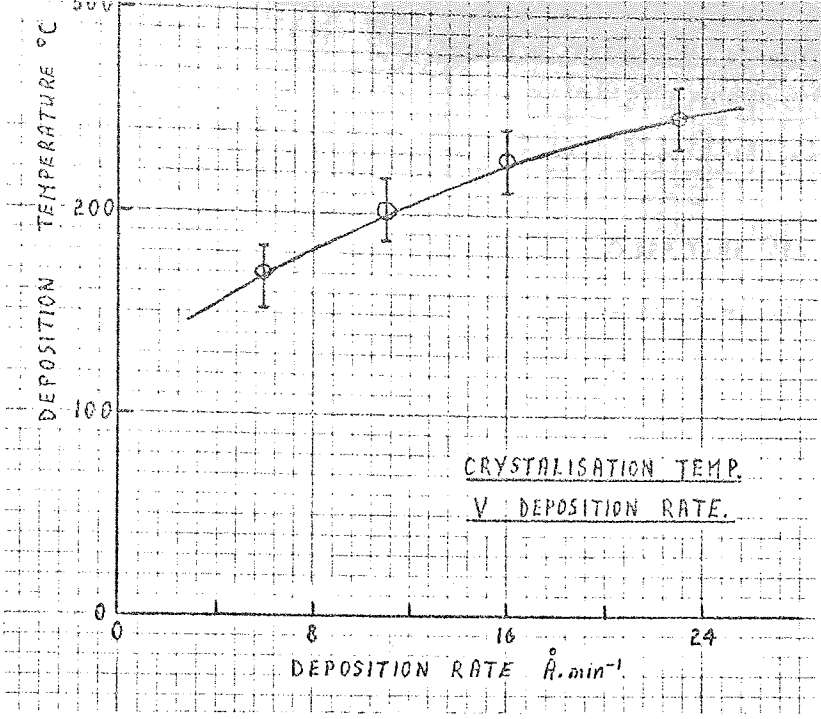


Figure 6.2.(a)

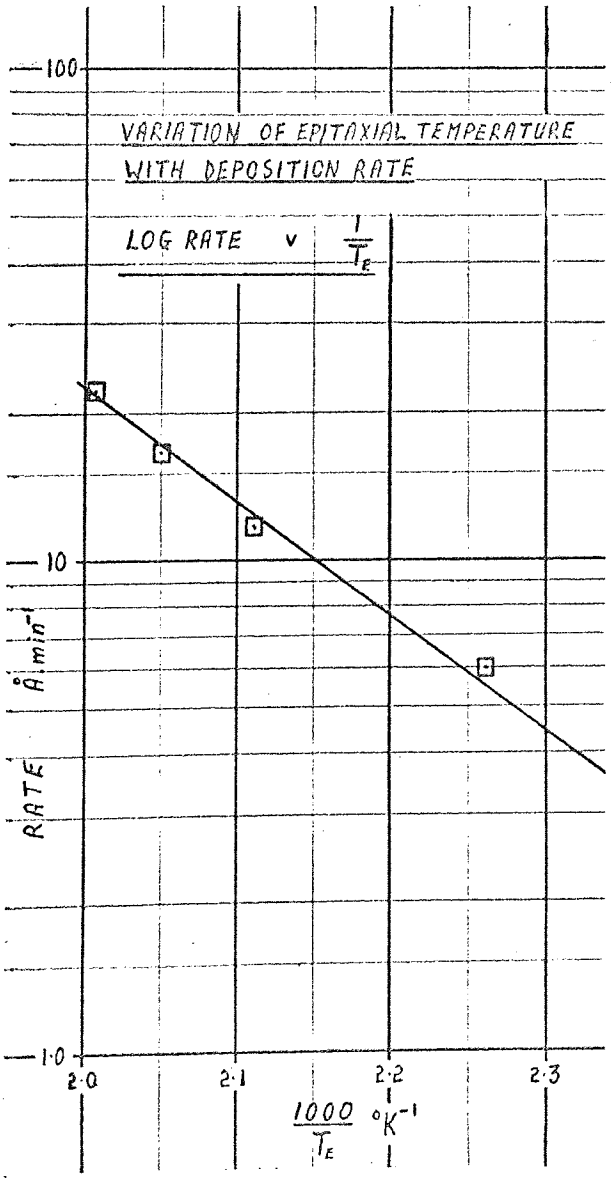


Figure 6.2.(b)

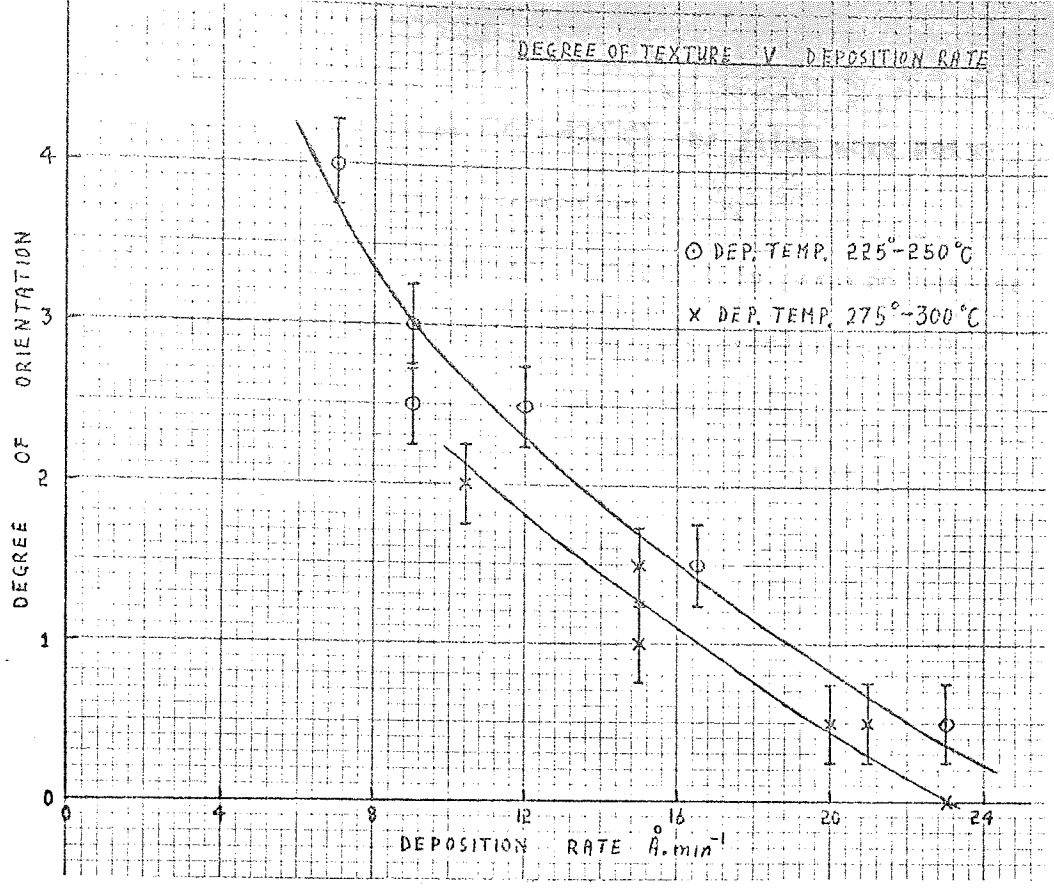


Figure 6.3.

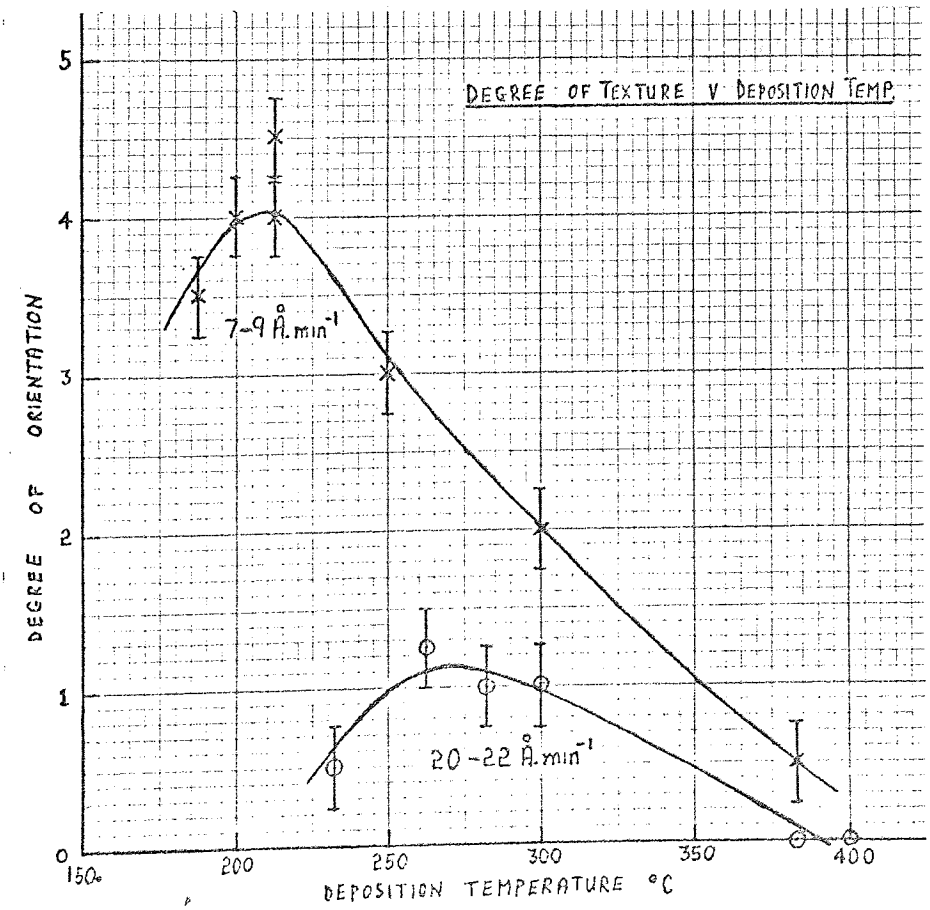


Figure 6.4.

to expected behaviour.

(3) Above a certain temperature (350-400°C) the films were polycrystalline with no particular fibre orientation.

A few films appeared to fall slightly outside this pattern but the structure of nearly all the fifty films examined was predictable. The diffraction pattern obtained from the films is shown schematically in figure 6.5. compared with the anticipated pattern for (100) epitaxy. It can be seen that there are additional spots present indicating that the (100) epitaxy was not perfect, but there is certainly a very pronounced second order texturing. Potassium bromide has a face centred cubic structure with a cell dimension of 6.6Å while barium titanate is tetragonal, but with an axial ratio of only 1.01 and a cell dimension of 4Å (Section 1.2.1.) This very large mismatch shows, as discussed in Section 5.A.2, that textured epitaxial growth is not directly related to cell dimensions, but must be a function of the potential surface presented by the crystal. The electron microscope lens constant was determined using a thin film polycrystalline aluminium standard and from the calibration the titanate film cell spacing was found to be 4Å. The accuracy of the system however was not sufficient to tell whether the films were of cubic or tetragonal crystal structure.

Electron micrographs of the films showed very small crystallite sizes, ~500 Å, in crystalline and amorphous films. The crystallite size did appear however to be larger with higher temperature and plates XXX show micrographs and corresponding diffraction patterns for a series of films together with their deposition conditions. The percentage of oxygen in the sputtering gas had no effect on film structure. This is not surprising, as a small loss of oxygen would not influence film structure. One might expect however to observe infra red anomolies due to the loss of oxygen and one would certainly expect some effect on electrical properties.

B.1.2. Infra Red Spectroscopy.

An extensive study of the infra red absorption of bulk barium titanate has been made by Last (187). He found slightly different spectra for the

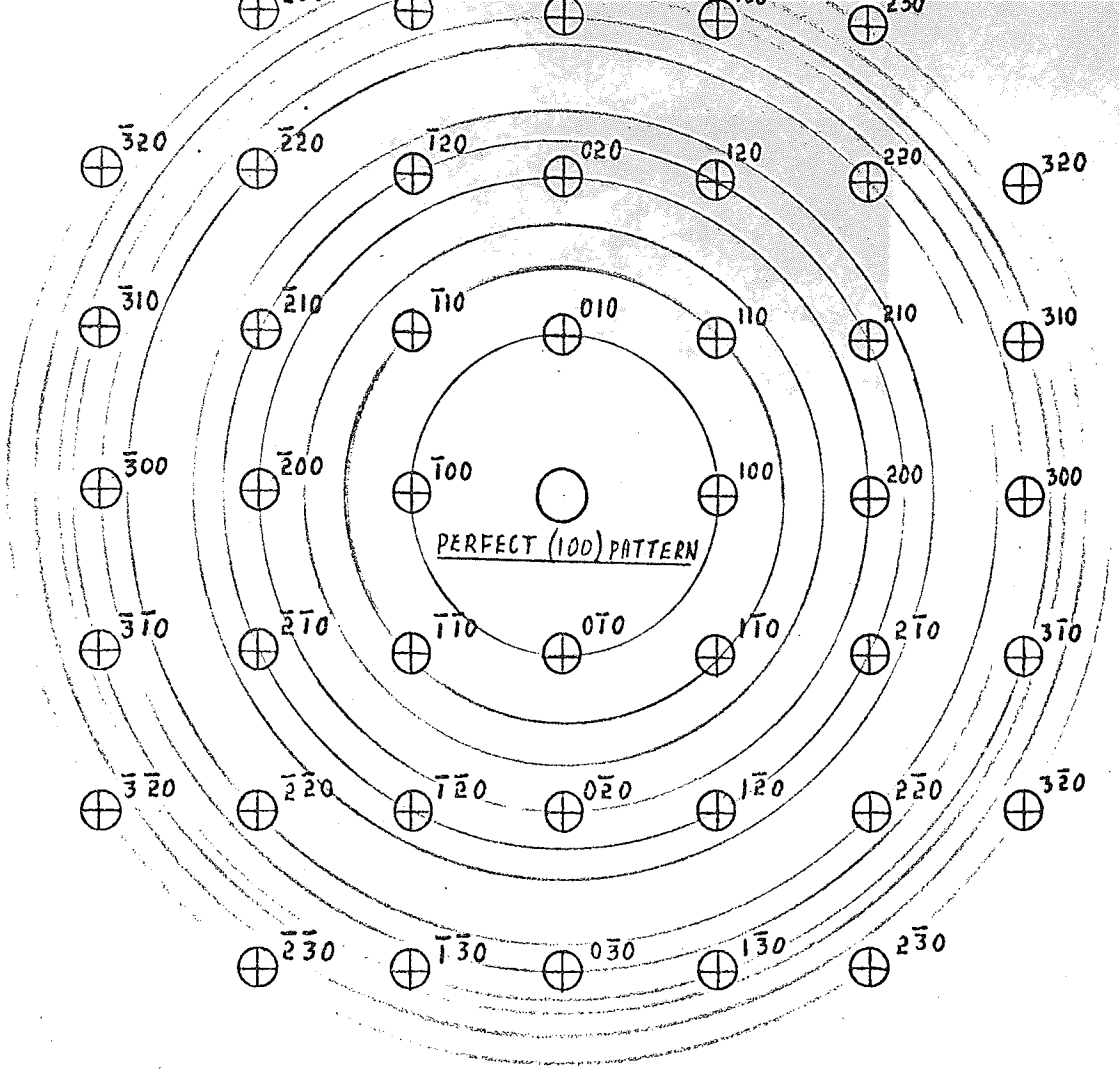
PERFECT (100) PATTERN

Figure 6.5.

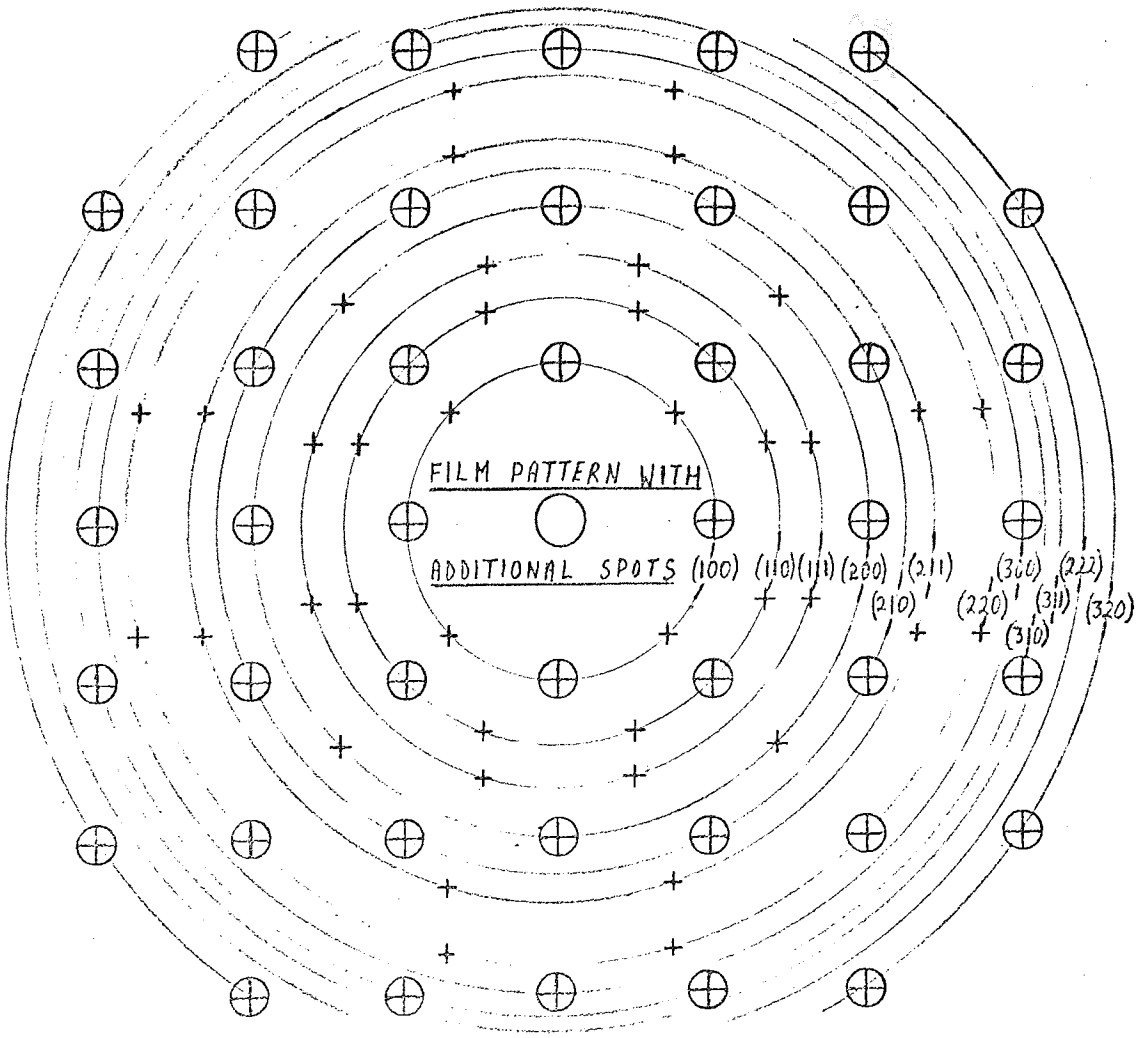
FILM PATTERN WITH
ADDITIONAL SPOTS (100) (110) (111) (200) (211) (300) (222)
(210) (220) (311) (320)
(310)

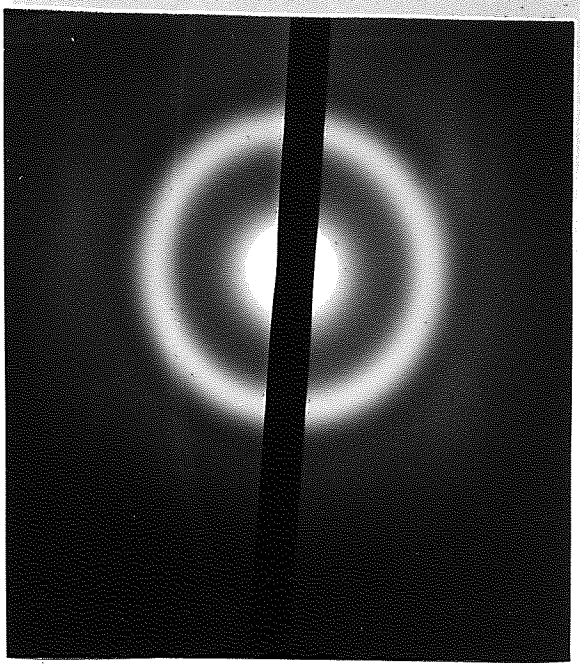

PLATE XXV

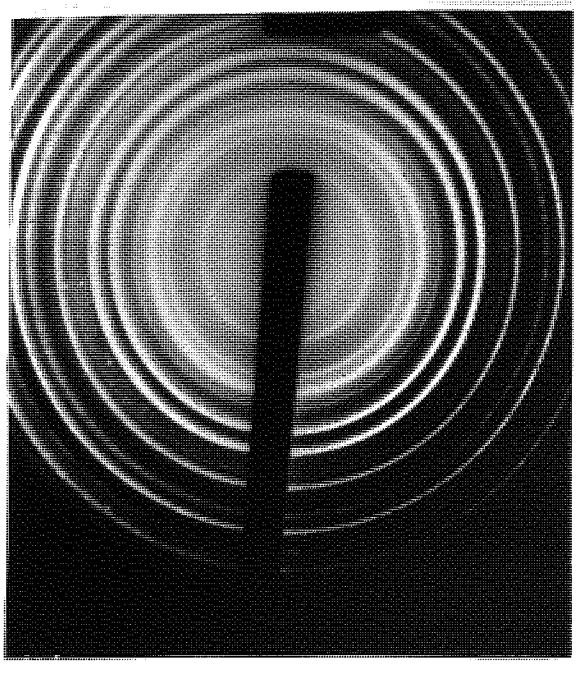

PLATE XXV1

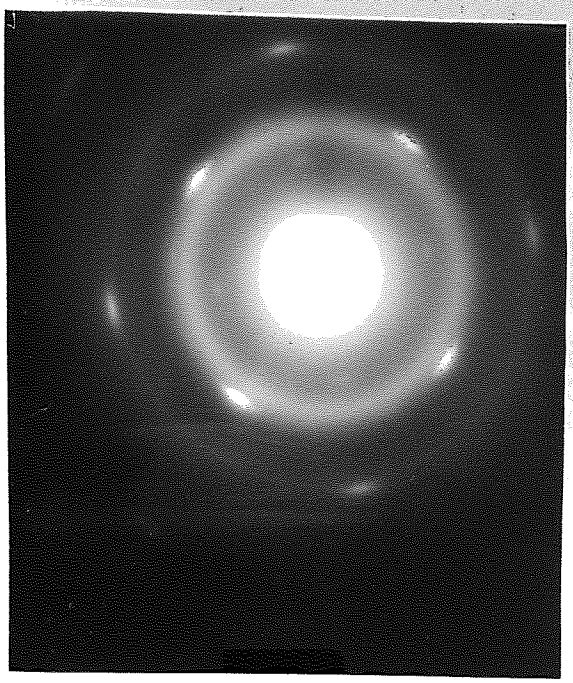

PLATE XXV11

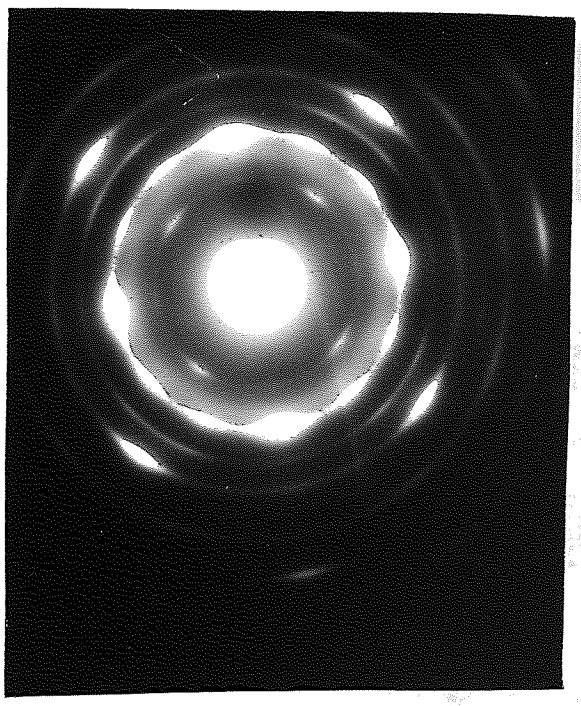

PLATE XXV111

FILM 109

DEP.TEMP.240°C

DEP.RATE 23 Å.min$^{-1}$

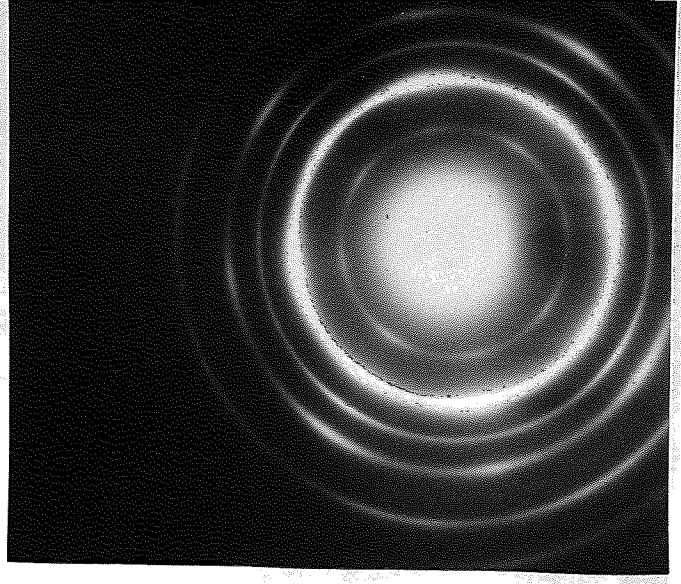

FILM 114

DEP.TEMP.240°C

DEP.RATE 13 Å.min$^{-1}$

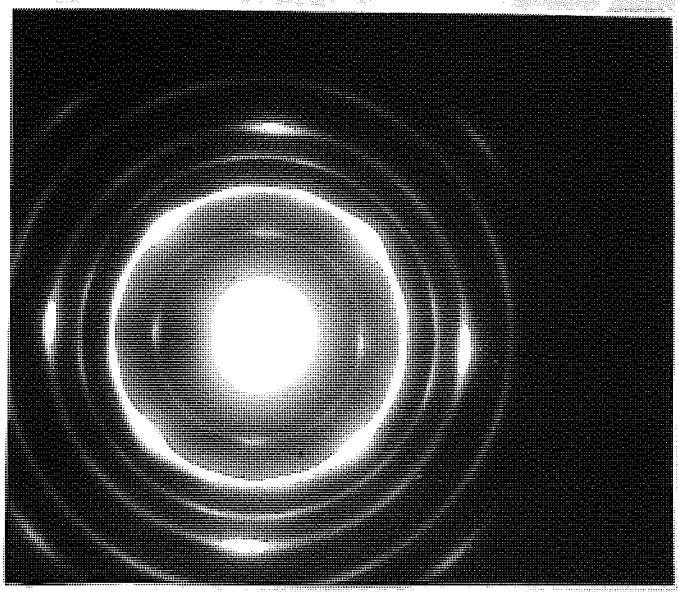

FILM 85

DEP.TEMP.225°C

DEP.RATE 7 Å.min$^{-1}$

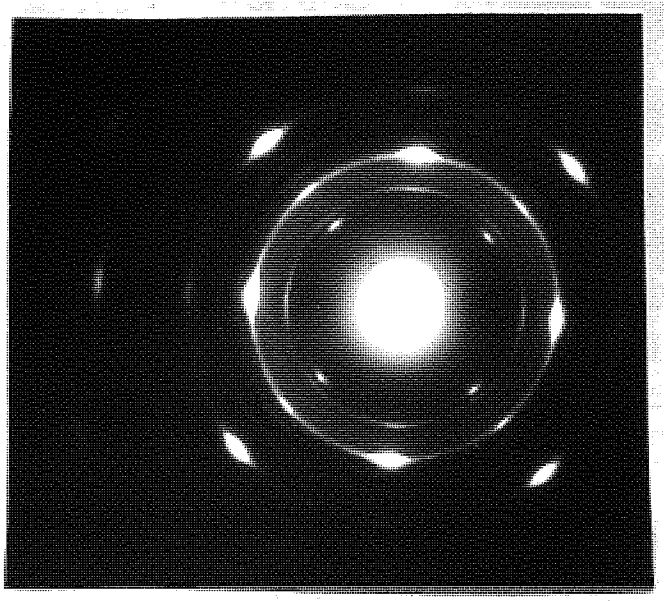

PLATE XXIX

DEP.TEMP. 200°C
DEP.RATE 6 Å.min$^{-1}$
X51K

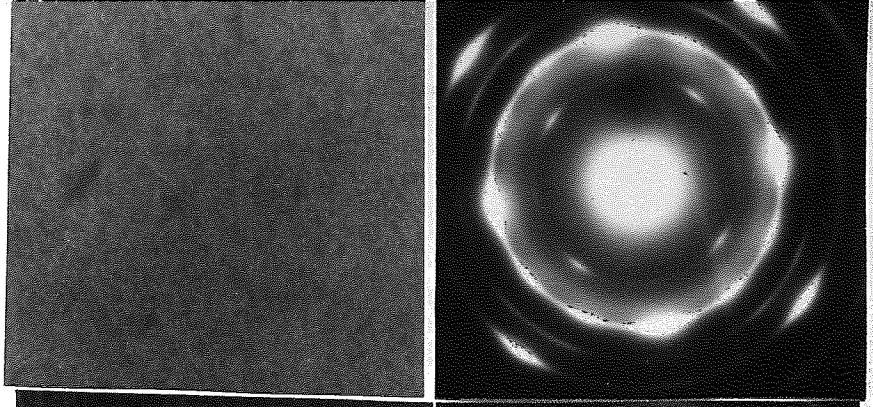

DEP.TEMP.270°C
DEP.RATE 11 Å.min$^{-1}$
X 51K

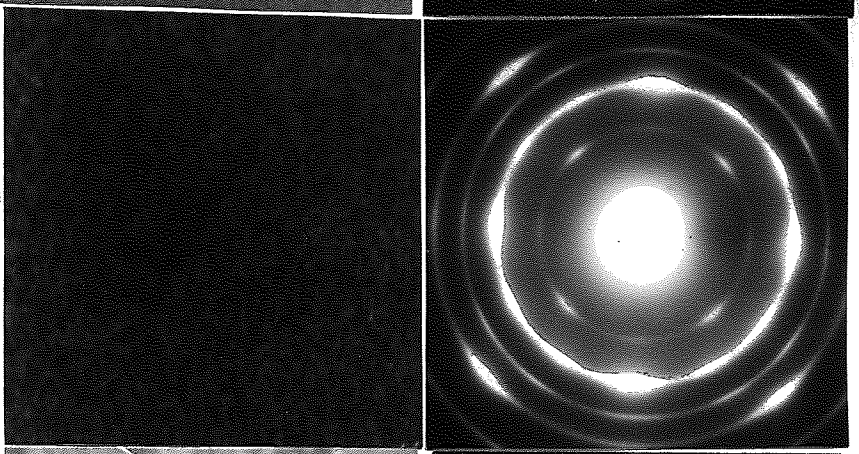

DEP.TEMP.290°C
DEP.RATE 14 Å.min$^{-1}$
X 98K

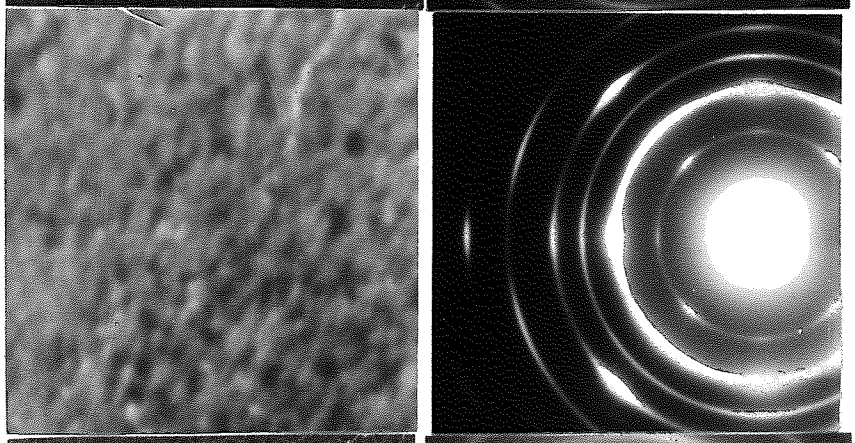

DEP.TEMP.300°C
DEP.RATE 22 Å.min$^{-1}$
X 36K

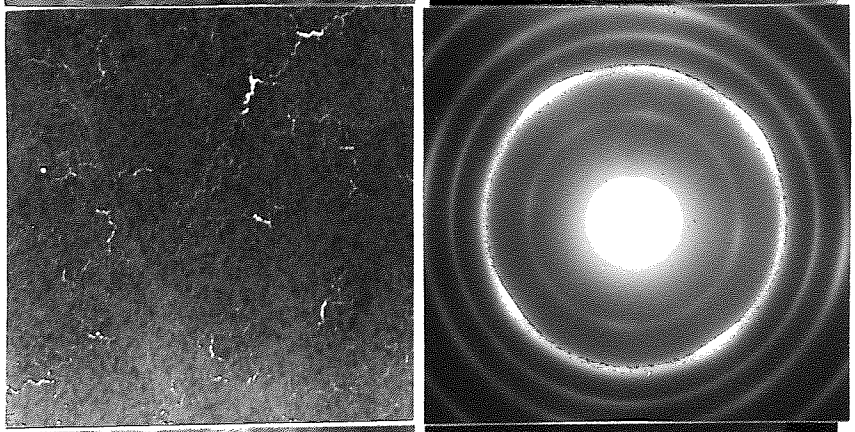

DEP.TEMP.370°C
DEP.RATE 9 Å.min$^{-1}$
X 120K

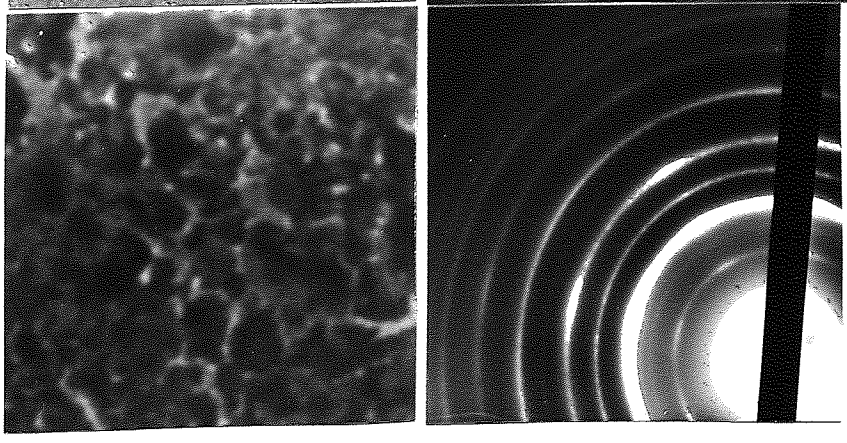

four normal crystal structures of barium titanate which were again all slightly different from the adsorption spectra for a powdered sample dispersed in potassium bromide. In all cases two absorption bands were observed both due to the normal vibration of the $TiO_6$ perovskite group. For the powdered sample the first band extended from 800 to 475 $cm^{-1}$ with a centre at 540 $cm^{-1}$ and the other from 475 to beyond 300 $cm^{-1}$ with a centre at 400 $cm^{-1}$. It was hoped, using infra red absorption, to detect any loss of oxygen from the normal stoichiometric ratio for barium titanate, in the same way as Pliskin (188) observed loss of oxygen from silica films, and to check for the presence of titanium octahedron short range order in all the films. Firstly the titanate target material was examined dispersed at a density of ~1 $mg.cm^{-2}$ in potassium bromide and gave the absorption spectra shown in figure 6.6. Even with the instrument set to maximum sensitivity and using the twin beam comparator method it was very difficult to obtain spectra from films deposited on potassium bromide. Those spectra which were obtained followed the same behaviour as the powdered target up to a wavelength of $13.10^{-6}$ m but did not show deep absorptions centred at 18-19 microns and 25 microns. A typical film spectra, shown in figure 6.7, revealed only shallow absorption bands, which were occasionally hardly noticeable, even for films later found to have the correct crystal structure by electron diffraction. The only explanation for the poor results is the very low sample densities used due to the thinness of the films. Even the thickest films examined had an effective dispersion, assuming bulk density, of only 0.05 $mgm.cm^{-2}$. With this sensitivity it was not surprising that no difference was detected between spectra for films deposited with and without oxygen in the sputtering gas. The absorption at 18 microns does however confirm the presence of $TiO_6$ octahedra in the films.

6.B.1.3. Electrical Measurements.

6.B.1.3.1. Mounting Techniques.

The main object of the project was to obtain useful electrical properties from the films so no further investigations into their structure

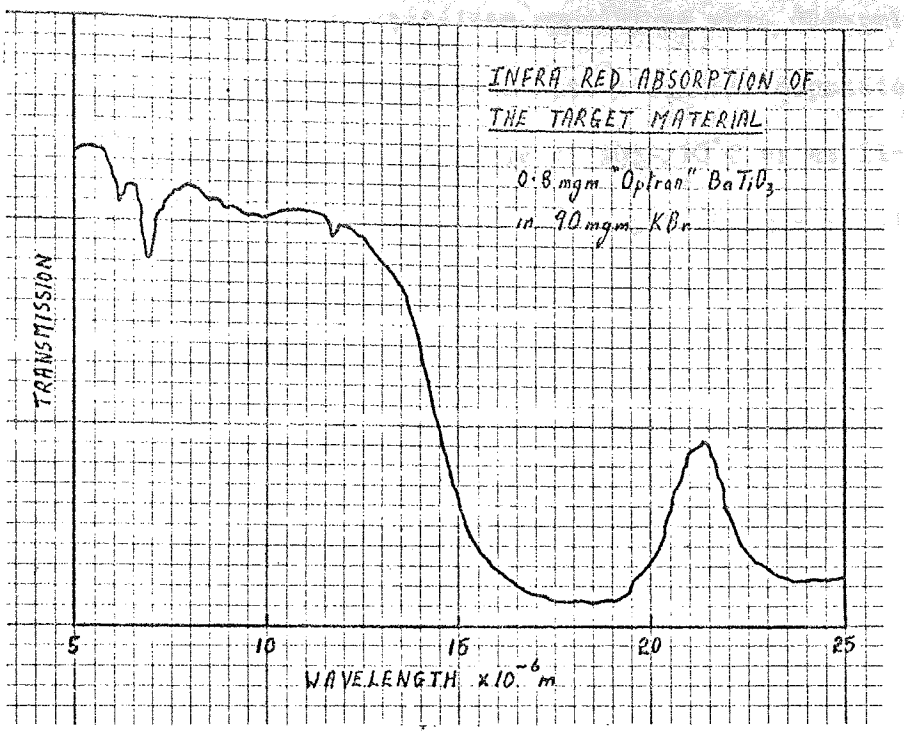


Figure 6.6.

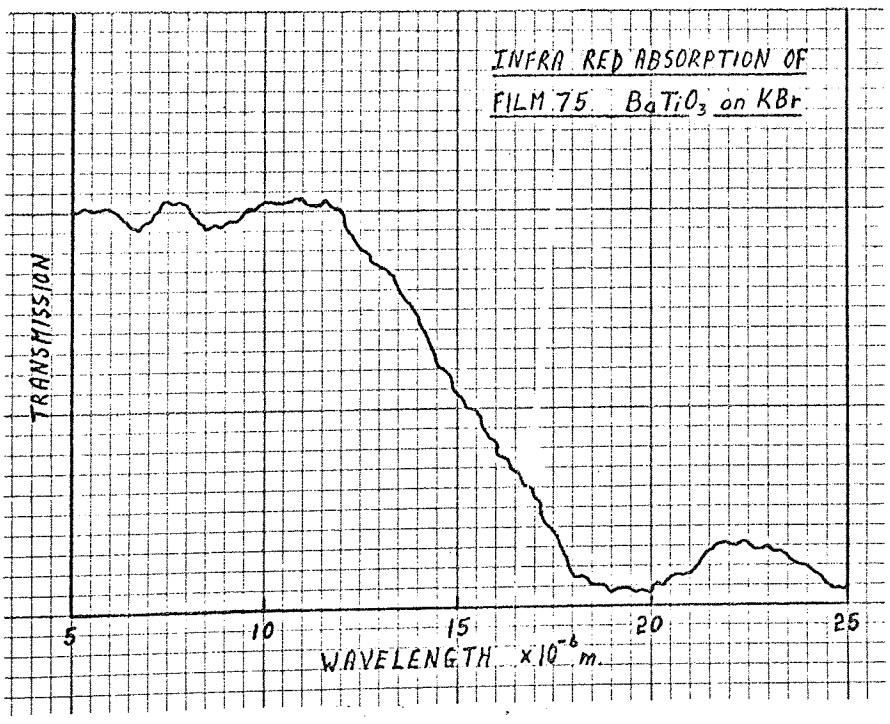


Figure 6.7.

or infra red absorption were made. However, from the results of the examination of film structure suitable deposition conditions were determined. All films on which electrical measurements were attempted were deposited either at a rate of 6-7 Å.min$^{-1}$ and a temperature of 205-210°C or at 11-12 Å min$^{-1}$ and 215-220°C. It was proposed to use a mounting technique similar to that described by Slack (38) for titanate films epitaxed on sodium fluoride. He deposited aluminium first and then a thick layer of gold on the films while they were still on the crystal. His titanate films were usually already peeling from the crystal on removal from the vacuum chamber and after the metal deposition quite large pieces (few $10^{-2}$ cm$^2$) could be picked off and fixed with silver paste, metal film down onto a tantalum sheet. Top contacts were then deposited through electron microscope grids. In our case, even thick films (7000 Å) showed no signs of peeling from the crystal so a number of mounting techniques were tried and are described below.

(1) Aluminium was deposited over the film while it was still on the crystal and then the combined films were floated off in water. The aluminium was found to be attacked by the water and the films disintegrated, spreading over the surface of the water; so that this method was unsucessful.

(2) Aluminium was again deposited over the film but the whole crystal was stuck, film down, onto a thin nickel sheet using silver paste. This arrangement was dried and immersed in water to dissolve away the crystal. The aluminium was still attacked and most of the two films had dissappeared before all the crystal had dissolved. The same happened when "aquadag" was used instead of silver paste and when a thick layer of gold was deposited over the aluminium to protect it. The probable explanation for these results lies in the fact that the aluminium at the interface with the titanate would be unoxidised evaporated material. This would have a much greater reaction rate with water than normal and water would penetrate the interface and dissolve the aluminium. Consequently a mounting was attempted using this technique but with only a layer of gold deposited on the film. This was much more sucessful and lead to the adoption of

the technique described in (3).

(3) A thick layer of gold ( 3000 Å) was deposited on the film and the double layer floated off as in (1); but the joint film was now stable. Pieces of the film were picked up with a special tool such that they overlapped a hole in the blade of the tool. After the film was allowed to dry a rod was gently pushed up the hole easing the film away from the tool blade so that it could be picked up with tweezers. The film was then stuck down with silver paste to thin nickel sheet and top contacts evaporated through a finegauze or an electron microscope grid.

6.8.1.3.2. Results.

Capacitance and conductance measurements were made on amorphous films giving a consistant value of permitivity between 15-20, independent of the partial pressure of oxygen during sputtering. The conductance was more variable but was generally in the range $0.001-0.030.10^{-6}$ mho. and again did not appear to be a function of the partial pressure of oxygen. However, all films expected to be crystalline on the above basis, gave shorted capacitors despite their good visual appearance and the small area of some top electrodes used ($\sim 2\ 10^{-4}$ cm$^2$). The shorted resistances were so small as to be indistinguishable from the resistance of the leads even at very small voltages ($\sim$ mV). The only explanation was the presence in the film of a very high density of structural faults which on evaporation of the top contact allowed a direct metallic link to be formed. To ensure this was not due to the deposition of gold, with its relatively high melting point (1063°C), indium with a melting point of only 156°C was used for some mountings. All the devices were still short circuits and this, together with the fact that a very thick film (8000 Å) which took nine hours to deposit, also yielded all shorted devices led to a reexamination of the films in the electron microscope. Cracks and tears had been noticed on some of the films during the determination of crystal structure Plates XXX1. In those cases film thickness was generally 400 Å and the faults had been thought to be due to the floating off and picking up of the films.

On the examination of thicker films many more cracks were found often in a regular rectangular pattern and the number of cracks increased with thickness up to the limit of electron penetration. Films were then examined using the optical microscope and the S.E.M. before the films were removed from the substrate to determine whether the problem was caused by the mounting technique or the deposition process.

It was found that all the films examined had a corrugated appearance which led to the electrical faults in the mounted films. The corrugations were generally rectangular and further film structure could be seen within each corrugation. They appeared to be formed by intersecting lines of well adhered film with those parts of the film between the lines raised away from the substrate. Films examined in the S.E.M. showed charging effects, as can be seen in Plate XXXII, confirming the insulating nature of the films. The corrugations for films deposited over a range of deposition conditions are shown viewed on the optical microscope in Plates XXXIII, and with the S.E.M. in Plates XXXIV. The corrugation dimensions on any one film varied by less than one order of magnitude and for all films fell in the range $1 10^{-4}$ - $3 10^{-3}$ cm. No relationship could be found between the average dimensions and the deposition conditions. This point is illustrated in figure 6.8 which shows the range of corrugation dimensions determined for a set of films plotted against deposition rate. Similar plots were obtained for substrate temperature and film thickness above 1000 Å. The series of plates XXXV show the same film viewed in the S.E.M. at increasing magnification and illustrate the ranges of structure within the films from mechanical effects to film growth. The corrugating effect is most likely a function of the difference in the thermal expansion coefficients of film and substrate. Potassium bromide has an expansion coefficient varying from $37.5.10^{-6}°C^{-1}$ at 0°C to $42.4.10^{-6}°C^{-1}$ at 200°C. Reported values for barium titanate depend on whether the material is in ceramic or single crystal form (189,190) and in the latter case on the crystallographic direction (191). The structure of the films in question was such that the figure applicable is probably

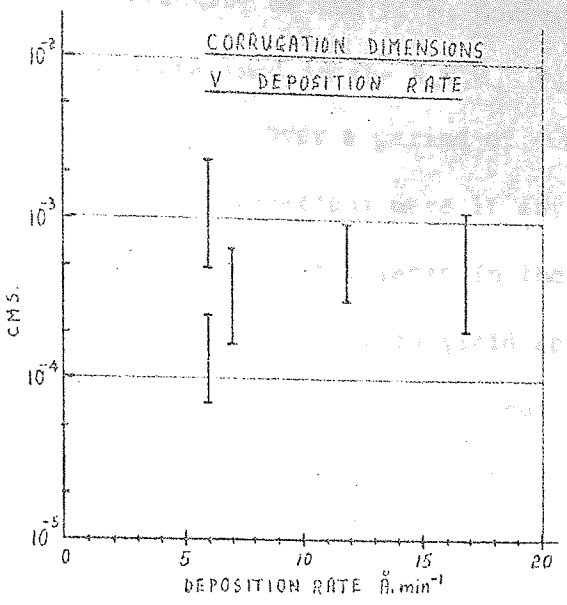


Figure 6.8.

between the two values, which are of the same order; and a value of $8.10^{-6}$ °C$^{-1}$ for the average expansion coefficient over the temperature range from room temperature to 200°C is reasonable. On cooling from 225-25°C the substrate will therefore suffer a linear contraction of 0.8% while the film with contract only 0.15%,so some accommodating process is inevitable. However, the accommodation might be a function of the cooling down process and under different conditions might take a form different from the

small scale buckling and cracking of the film. Consequently a number of films were cooled very slowly and examined in the S.E.M. Plate XXXVI shows the corrugations in a film cooled down over a period of 400 minutes and as in other films cooled slowly the corrugations were if anything slightly finer. All alkali halides have expansions coefficients in the range 30-40 $10^{-6}°C^{-1}$ so a change of substrate to another likely to yield epitaxial films was unlikely to overcome the problem. Slack (38) did not encounter this difficulty probably because the films were evaporated and would not adhere so well to the substrate. Consequently on cooling instead of small scale corrugating and cracking large scale peeling of the film away from the substrate occured. This explanation is supported by the fact that he reports being able to pick up relatively large pieces of film peeled away from the substrate surface. It is clear from the small dimensions of the buckling reported that for any useable size of top contact a direct short would always be formed, so it was not feasible to obtain electrical results from these crystalline films. The necessity of removing the films from their substrate in order to obtain useful electrical properties was in any case clearly not satisfactory for device application. What was required was a conducting substrate onto which barium titanate could be epitaxially deposited.

6.B.2. Epitaxial Gold Films on Potassium Chloride.

Gold has a Fm3m cubic structure with a unit cell of 4.08 Å which is very close to that of barium titanate and might be expected to promote epitaxial growth. As the expansion coefficient is 15.$10^{-6}°C^{-1}$ the problem of crazing is likely to be reduced and some sucess had been reported (192) in obtaining useful electrical measurements from a titanate film deposited on gold. Single crystals of gold in sufficient quantities to study the deposition of the titanate and to make electrical measurements on the films would have been a prohibitive price, but (100) epitaxial gold films could be relatively easily prepared in existing equipment. The production of gold films used was described in Section 5.D.1.3. Barium titanate was sputtered

FILM 83

X77K

DEP.TEMP.290°C

DEP.RATE 15 Å.min$^{-1}$

FILM 111

X36K

DEP.TEMP.300°C

DEP.RATE 20 Å.min$^{-1}$

PLATE XXX1

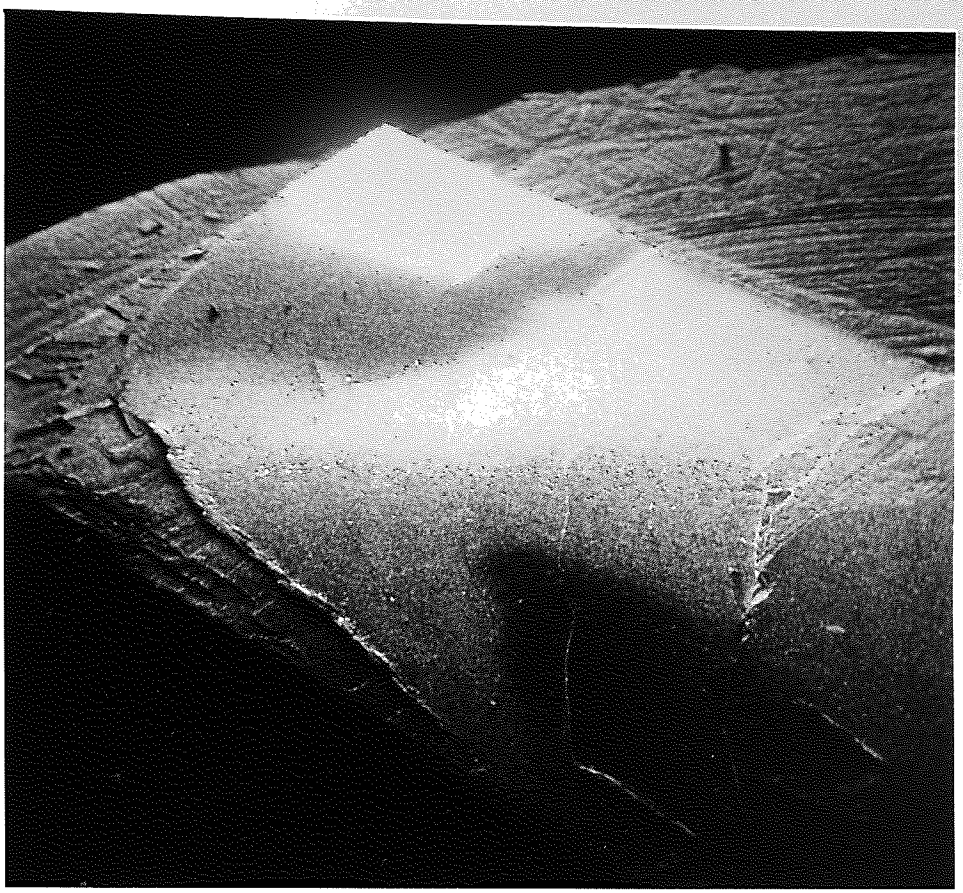

PLATE XXX11

FILM 107 X 1.92K
DEP. TEMP. 230 C
DEP.RATE 17 A.min

FILM 115 x 1.92 K
DEP.TEMP. 275 C
DEP.RATE 11½ A.min

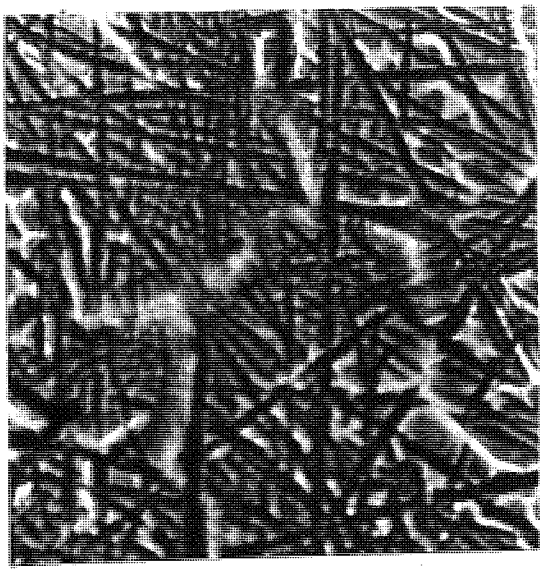

FILM 135 x 544
DEP.TEMP. 210 C
DEP.RATE 6½ A.min

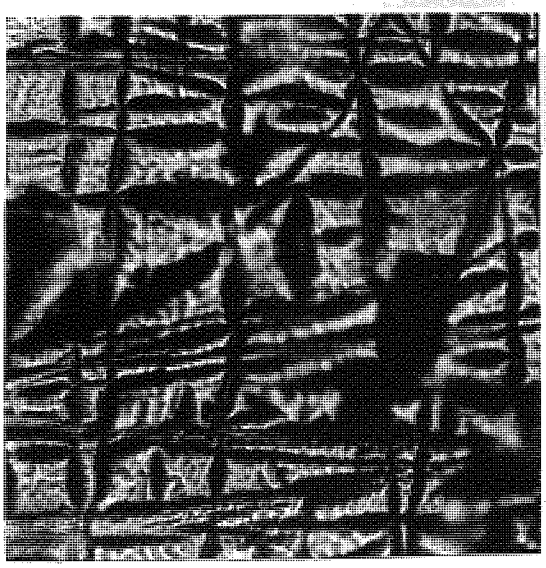

FILM 144 x 544
DEP.TEMP. 230 C
DEP.RATE 6½ A.min

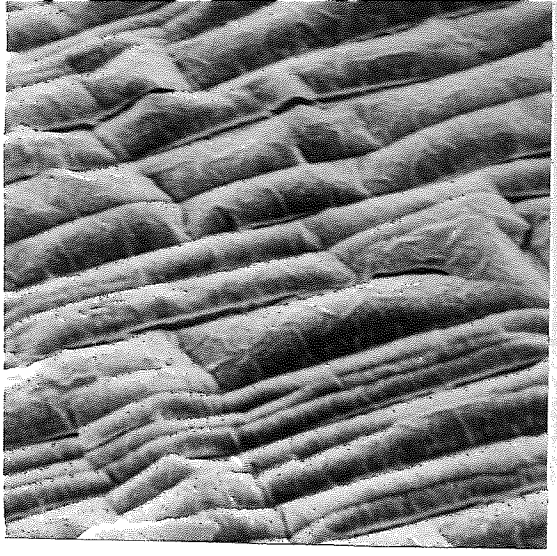

FILM 125 X 3.9K
DEP.TEMP.230°C
DEP.RATE 8 Å.min$^{-1}$

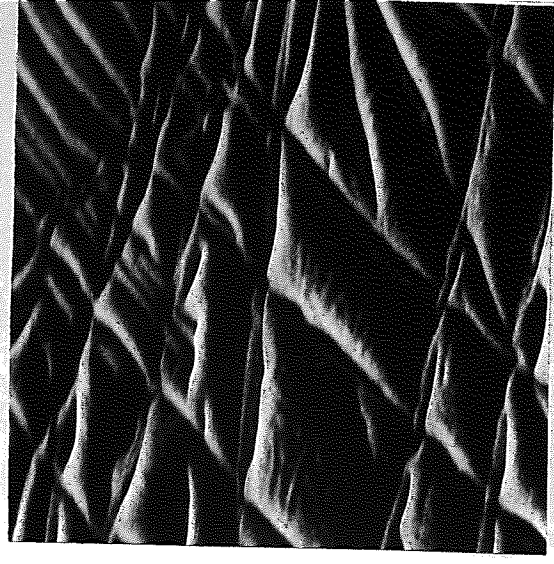

FILM 146 X 84K
DEP.TEMP. 210°C
DEP.RATE 7 Å.min$^{-1}$

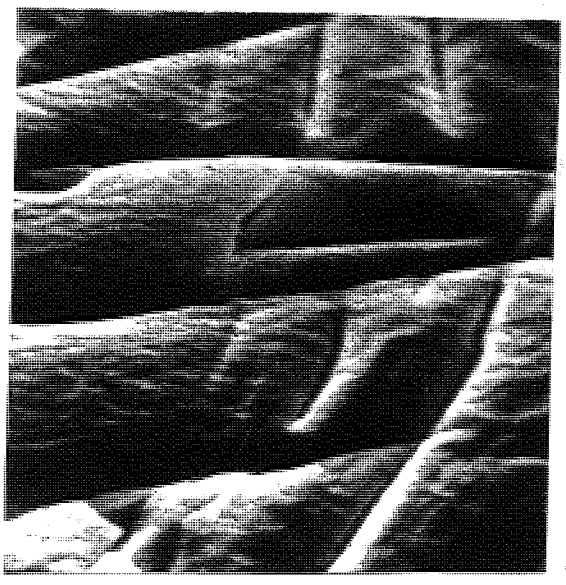

FILM 119 X 7.8K
DEP.TEMP. 240°C
DEP.RATE 11 Å.min$^{-1}$

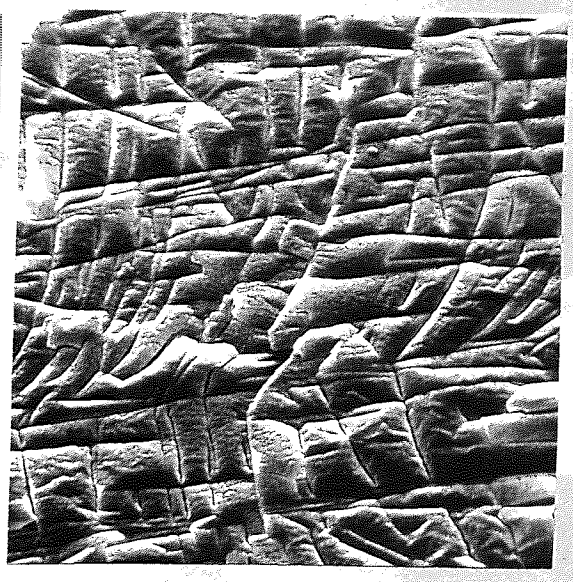

FILM 108 X 1.9k
DEP.TEMP. 300°C
DEP.RATE 16 Å.min$^{-1}$

PLATE XXXIV

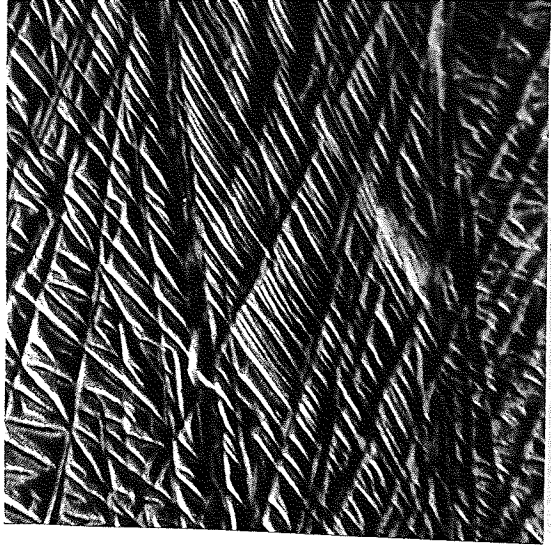

X 3.6K

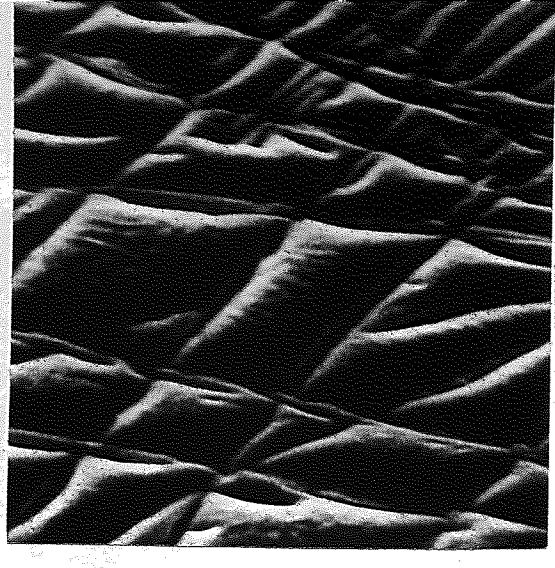

X 8.4K

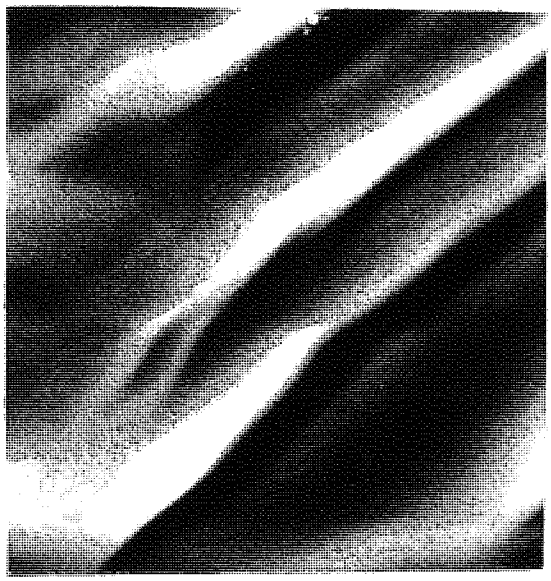

X 3.75K

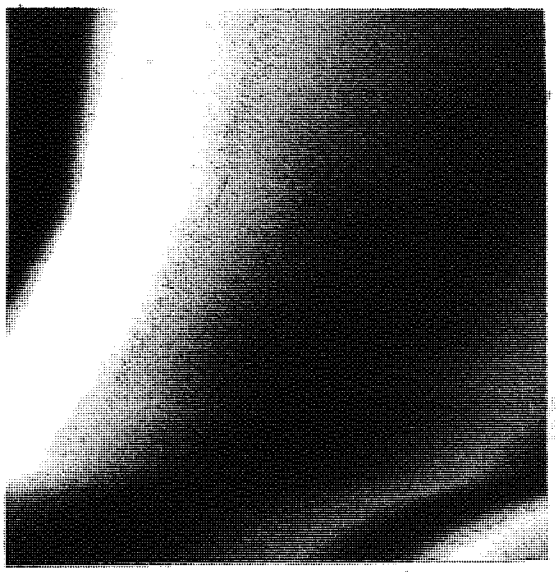

X 73.5K

PLATE XXXV

FILM 146

DEP.TEMP.210 C

DEP.RATE 7 A.min

FILM APPEARENCE AT

INCREASING MAGNIFICATION

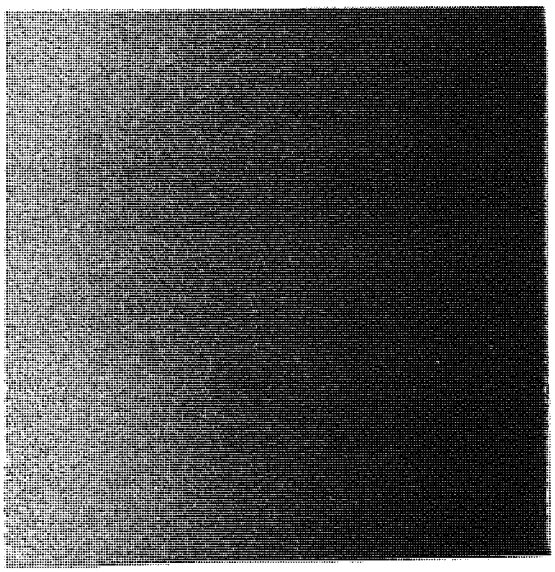

X 180K

APPEARENCE OF CORRUGATIONS IN

FILM COOLED OVER 400 MINUTES

X 3.6K

PLATE XXXVI

onto epitaxial gold film of thickness 1000-1500 Å over a wide range of deposition conditions. Substrate temperature was varied from ambient to 500°C, the deposition rate from 5 to 20 Å.min$^{-1}$ and the percentage of oxygen in the sputtering gas from 0 to 10%.

B.2.1. Growth and crystal structure.

At substrate temperatures above 480°C potassium chloride sublimation occured to such an extent that the gold layer was destroyed and no titanate film was formed. For films deposited below 450°C structure was determined using Xray and electron diffraction techniques. Films when studied by R.E.D. in the high resolution diffraction stage of the electron microscope were found to charge up distorting the image and making the determination of any structure very difficult. The use of the heating stage to provide a beam of neutralising electrons helped but was found to quickly damage the film. Consequently no crystal structure was determined with this technique. The Xray diffractometer patterns for all films deposited at temperatures up to the sublimation limit appeared little different from the pattern for gold films on KCl alone. This suggested that either the films were amorphous, or of such small crystallite size that no titanate lines were observable. It was attempted to verify which of these was true by examining one Au/$BaTiO_3$ layer by transmission electron diffraction. A (100) epitaxial gold film was deposited only 500 Å thick and about a further 500 Å of barium titanate was sputtered onto it at a substrate temperature of 360°C and a rate of 8 Å.min. The double layer was then floated off the KCl and examindd as described in Section 6.B.1.1. The thickness of the layer considerably reduced the intensity of the diffraction pattern but there appeared to be amorphous barium titanate rings present as well as some faint gold lines and a brighter spot pattern due to the gold. It was concluded that up to the temperature limit of 450°C sputtered barium titanate does not grow in any crystalline form on epitaxial gold films, a conclusion born out by the electrical measurements made on the films.

6.B.2.2. Structure and electrical measurements.

Aluminium was evaporated through a fine gauze onto the titanate film surface forming top capacitor contacts of area $2.56\ 10^{-4}\ cm^2$ which can be seen in Plate XXXVII. Capacitance measurements on films deposited over the whole substrate temperature range yielded values of permitivity consistent with amorphous barium titanate. The dielectric constant was in the range 10-25 anddissipation factor between 0.0005-0.1 for all films. At deposition temperatures above 220° C crazing appeared in the films which caused some devices to short circuit. The crazing was in a random pattern, which further supports the suggestion that these films were amorphous and occured at a much lower density than the regular effect found in films deposited on K Br. Most of the film normally adhered to the substrate with occasional ripples running through it. The reduced severity of the crazing is no doubt due to the fact that the gold withan expansion coefficient, $15.10^{-6}\ °C^{-1}$ between that of the KCl, $36-48.10^{-6}\ °C^{-1}$ (192) and the barium titanate, $8.10^{-6}\ °C^{-1}$ acted as a partial buffer and the ripples probably occured in it rather than in the titanate. Plate XXXVIII shows the relative sizes of the crazing and the top contacts for a film deposited at 280° C. The fact that most of the devices were not shorted despite the presence of a crazing ripple running through them showed that the titanate film was in general not severed. On films deposited at still higher temperatures (>400° C) pits occured along cleavage steps in the KCl as a first indication of the sublimation of the substrate already discussed. Plates XXXIX are a series of photographs at increasing magnification of film 134 deposited at 430° C and clearly show that the crazing did not break the film but there are deep pits along cleavage steps. This imposed an even lower temperature limit and to ensure that the limit was in no way connected with the deposition process a gold film on KCl was put in the vacuum chamber and heated up to 470° C. Plates XXXX are photographs of the substrate before and after being heated confirming that the effect was purely thermally initiated. Gold also forms epitaxial films on sodium chloride and to see if that material allowed

higher substrate temperatures a similar experiment was performed. A gold film was deposited on NaCl and heated in vacuum to 470°C but the same pitting effect was observed. KCl is reported to show considerable thermal etching above 400°C (193), and while the deposition temperature was well below this exposure times were much greater. The temperature restriction was not due to the gold, but due to the nature of the underlying substrate and a first alternative to try was glass. Nichrome/gold films on glass were available and while having only a polycrystalline structure they were capable of higher substrate temperatures and are also used in the microelectronics industry. Consequently they were chosen as the next substrate material.

6.C. Polycrystalline Substrates.

Polycrystalline films of either gold or aluminium deposited on glass as described in Sections 3.D.1.4 and 3.D.1.5. were used as substrates and the properties of the titanate films sputtered onto them will be discussed together. The aluminium films were always prepared just prior to titanate deposition, without letting the chamber up to atmosphere, in order to avoid aluminium oxide formation. This precaution was not necessary for the gold substrates, on which most of the measurements were made and unless otherwise specified all comments refer to films deposited on them. Barium titanate was sputtered over the normal range of deposition conditions; substrate temperature varying from ambient to 500°C, rate 5-20 Å. $min^{-1}$ and partial pressure of oxygen 0-10%.

6.C.1. Film Structure.

All films examined were transparent and well adhered to the substrate with no sign of any crazing even at deposition temperatures as high as 500°C. Borosilicate glass (Corning 7059) has an expansion coefficient of $4.5.10^{-6}\ °C^{-1}$ which is smaller than that of barium titanate, $7.6.10^{-6}\ °C^{-1}$. Therefore, in the device structure, the intermediate gold film, with an expansion coefficient of $15.10^{-6}$, after coolingfrom the depositon temperature was under compressional stress from both sides. Consequently any accommodation due to the differential expansion must take the form of a deformation of the

PLATE XXXV11

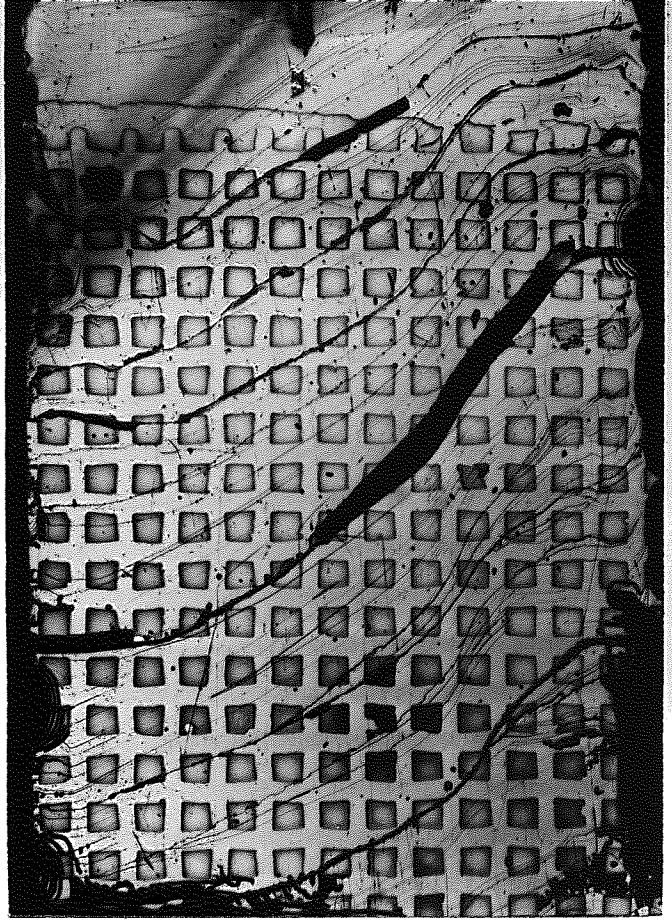

PLATE XXXV111

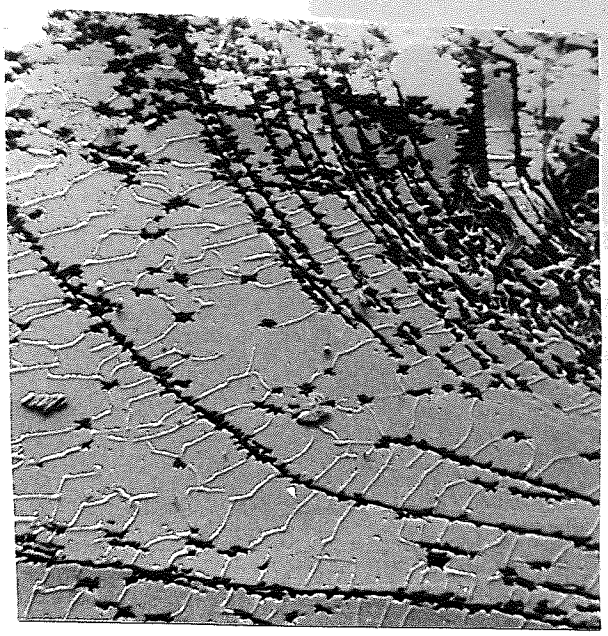

X 180

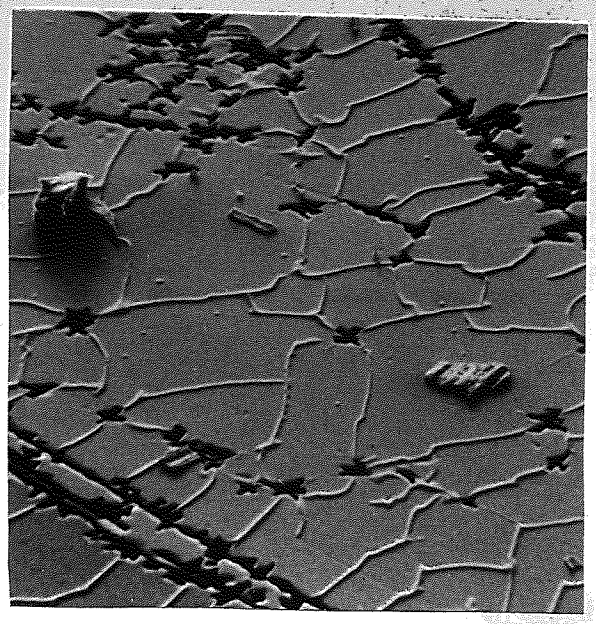

X 360

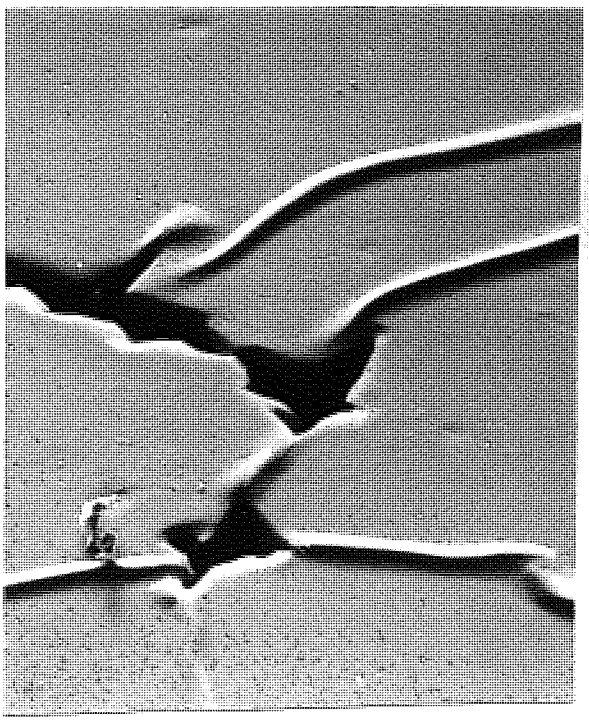

X 1.8 K

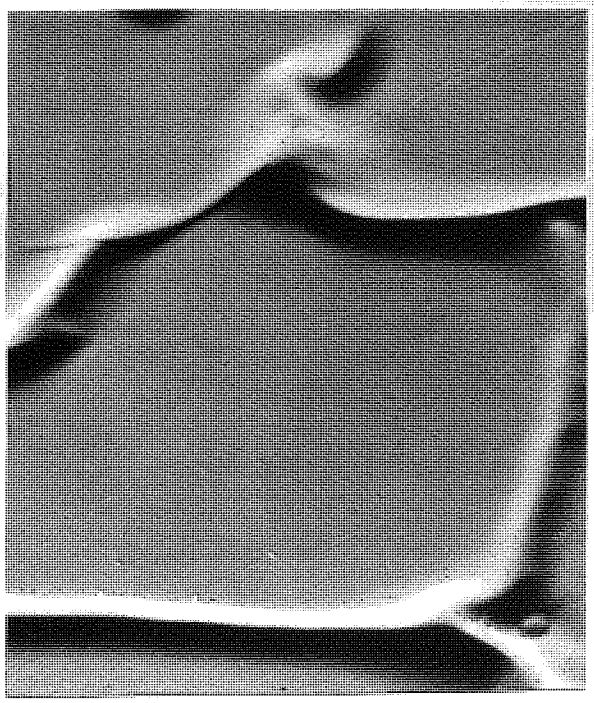

X 3.6K

FILM 134 AT INCREASING MAGNIFICATION.

PLATE XXX1X

FILM 148

BEFORE HEAT

TREATMENT

X23

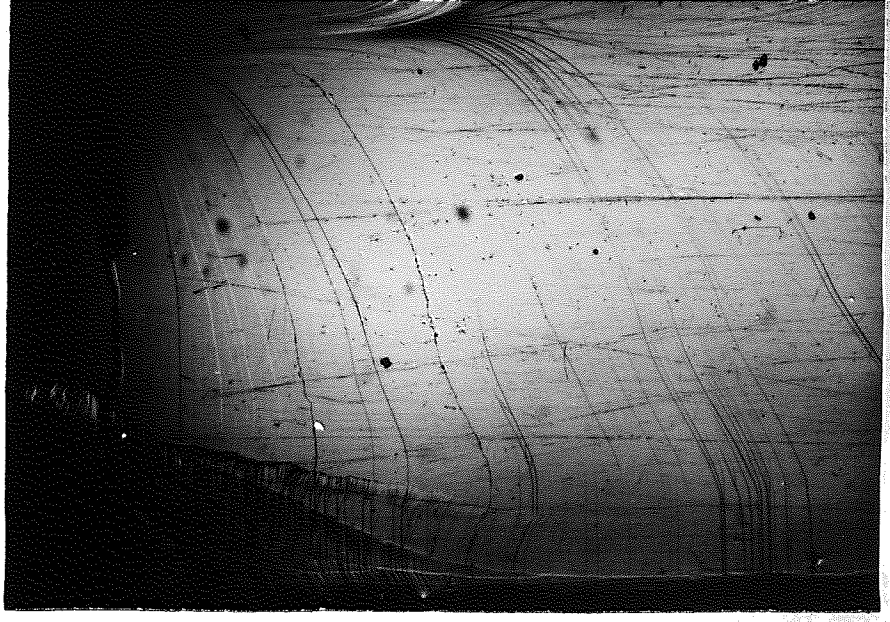

AFTER HEAT

TREATMENT

X23

AFTER HEAT

TREATMENT

X124

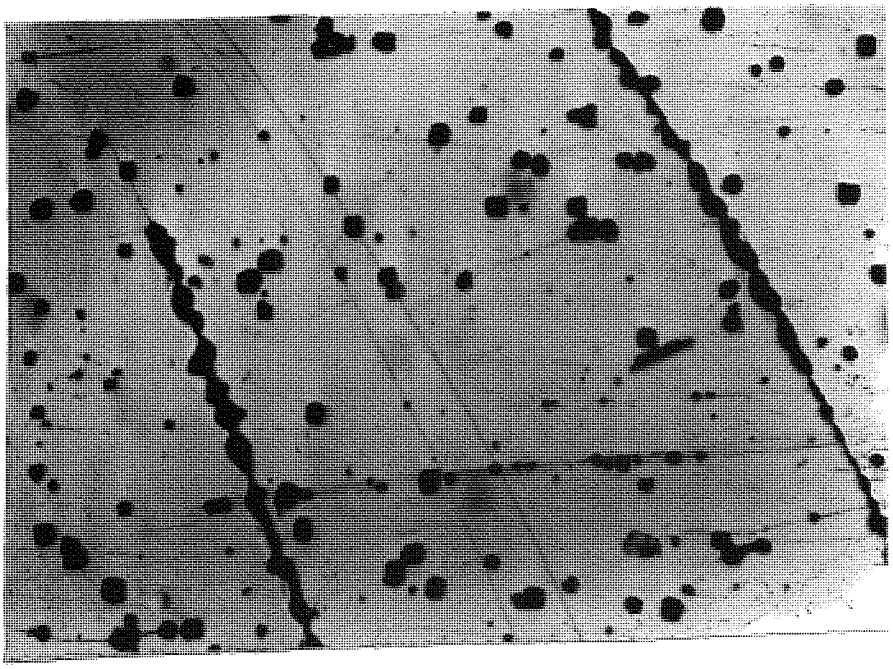

PLATE XXXX

metal film. Attempts to determine film crystal structure by R.E.D. again yielded no results so the only crystallographic technique available was Xray diffraction. The gold base films were found to be textured with (111) planes parallel to the glass surface as can be seen by the relative heights of the (111) and (200) peaks shown in figure 6.9. copied from a diffractometer chart output. For perfectly random polycrystalline films the two peaks should have amplitudes of (111)/(200) ; 100/52. For films deposited up to a substrate temperature of 450°C no significant difference could be detected between the diffractometer outputs from the film coated substrate and that obtained before the deposition. However films deposited at a substrate temperature above 450°C showed weak broad barium titanate diffraction lines as shown in figure 6.10. As the (111) $BaTiO_3$ line is masked by the corresponding gold line and the peaks were always very weak it was not possible to determine whether or not any fibre texture was present in the films. These observations pointed to the formation of amorphous films at temperatures below 450°C and polycrystalline films above that temperatue which is similar to the crystallisation and the transition temperatures found for films deposited on amorphous substrates. This account of film structure was not however completely supported by electrical measurements made on the films. Values of permitivity consistent with an amorphous film structure were observed only up to a deposition temperature of 200°C. At this temperature a sharp transition occured to values an order of magnitude higher. This anomolous value of permitivity persisted until a second steep rise was observed for films deposited above a substrate temperature of 450°C, corresponding to the observation of crystal growth. It can be concluded that films deposited at a temperature below 200°C are amorphous and those deposited above 450°C are polycrystalline. The values of dielectric constant measured for films deposited at temperatures in the range 200-450°C howeversuggest that some ordering must be present in the films. As the observation of crystallinity corresponds to a second permitivity transition and the value of dielectric constant is fairly constant over the whole intermediate range of deposition temperature, the most likely explanation is the existance of

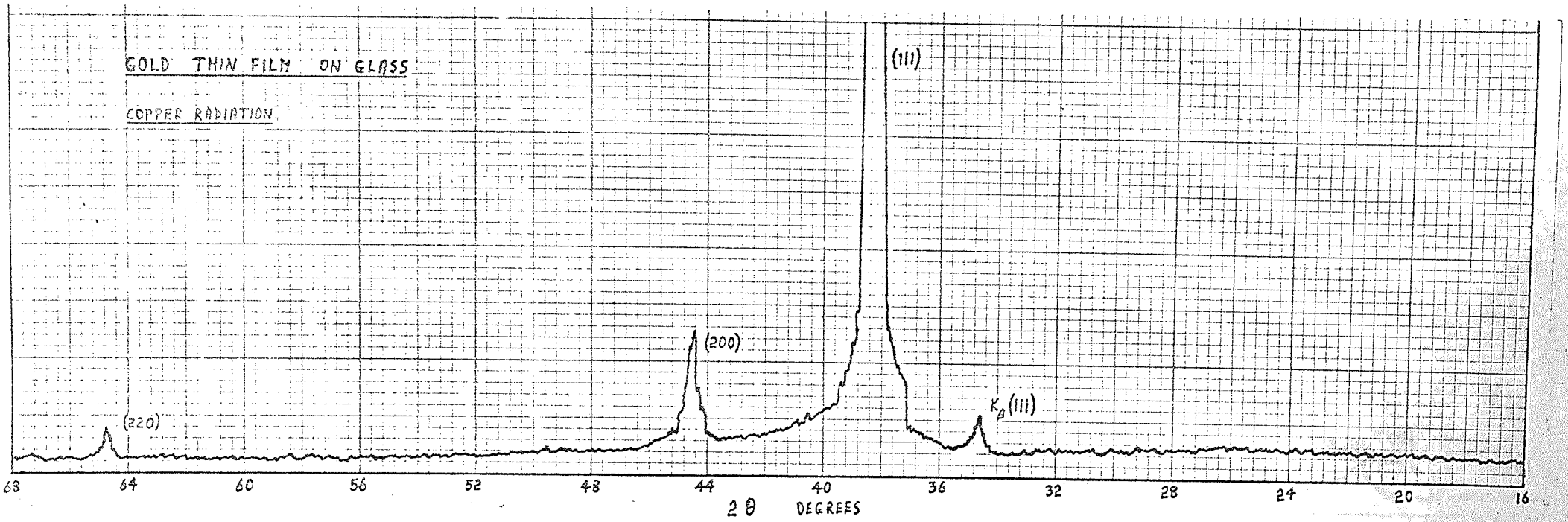
GOLD THIN FILM ON GLASS
COPPER RADIATION
(111)
(200)
(220)
$K_\beta$ (111)
68
64
60
56
52
48
44
40
36
32
28
24
20
16
2θ DEGREES

Figure 6.9

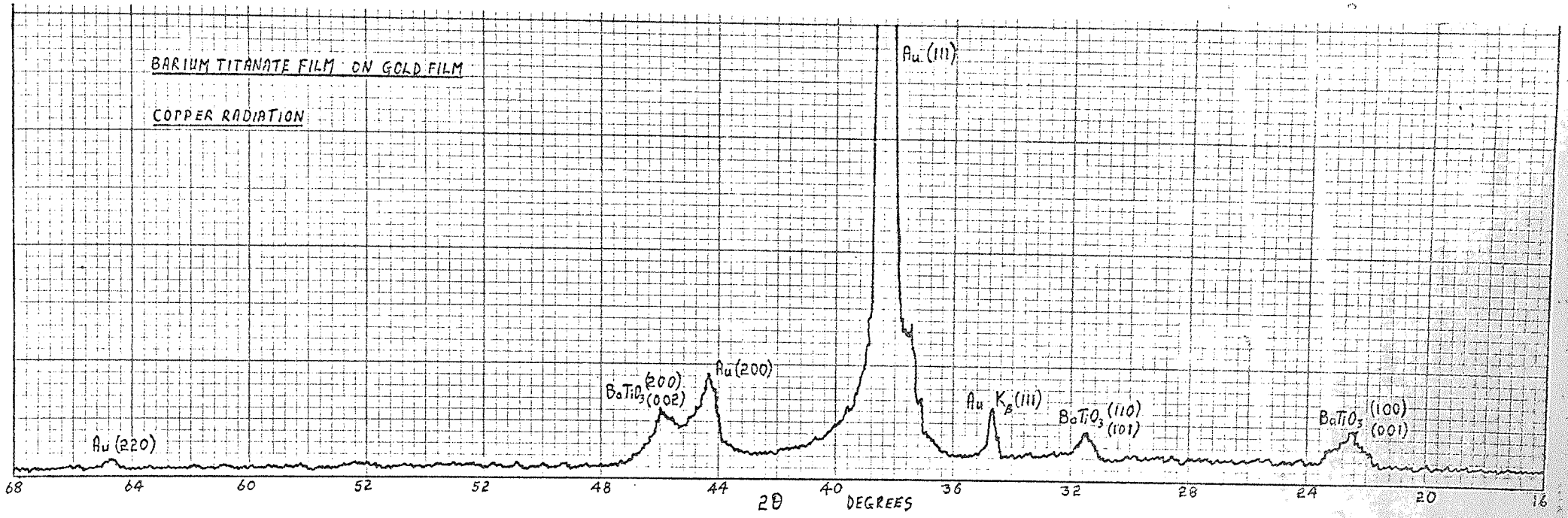
BARIUM TITANATE FILM ON GOLD FILM
COPPER RADIATION
Au (111)
Au (220)
BaTiO3 (200) (002)
Au (200)
Au Kβ (111)
BaTiO3 (110) (101)
BaTiO3 (100) (001)
68
64
60
52
52
48
44
40
36
32
28
24
20
16
2θ DEGREES

Figure 6.10

a metastable form of barium titanate. This state must only have some form of close range order, to explain the increase in permitivity without the observation of diffraction lines. The state must also have an ordering energy associated with it corresponding to the temperature of 200° C. The structure is therefore not strictly amorphous but neither is it polycrystalline.

6.C.2. Electrical Measurements.

6.C.2.1. Permitivity and loss.

Aluminium or gold was evaporated through a mask onto the films as top contacts so that Au/$BaTiO_3$/Al, Au/$BaTiO_3$/Al, and Al/$BaTiO_3$/Al thin film capacitive devices were formed. When conductivity and capacitive measurements were to be made between four and ten overlap electrodes were deposited of area in the range $4\ 10^{-3}$ - $110^{-2}$ $cm^2$ for gold base films and $6\ 10^{-2}$ $cm^2$ for aluminium base films as described in Sections 3.B.6.2.2. and 3.D.1.5. If only capacitive measurements were to be made a mask consisting of gauzes of a number of different grades was used to form a range of top contact areas varying from $\sim 2.5.10^{-2}$ to $2.5.10^{-4}$ $cm^2$ with a large number of devices on each film. Capacitance and dissipation factor or conductance were measured for devices using films prepared over the range of deposition conditions. From these measurements and the film thickness, the titanate film dielectric constant and resistivity were determined using equations 6.1 and 6.2. where C is the capacity in pico farads, $\mathcal{Y}$ is the conductance in micromhos,

$$K = \frac{dC}{A}\frac{10^{-6}}{8.85} \qquad 6.1.$$

$$\rho = \frac{A}{\mathcal{Y}d} \qquad 6.2.$$

A is the device area in $cm^2$ and d is the film thickness in angstrom units. The relationship between dissipation factor ($\tan\delta$), capacity and conductance using the same units is given by equation 6.3. The value of resistivity $\rho$ determined from equation 6.2. is the ac resistivity measured at a frequency of 1592 Hz and a voltage of a few mV. Consistent values of $\rho$ (ac) were obtained from these measurements whereas at dc voltages the resistivity was a function of field for a given film and varied enormously

$$\tan\delta = \frac{\mathcal{Y}}{C\,10^{-2}} \qquad 6.3$$

from one film to another. DC resistivities were found to vary from about the same value as the ac measurement to up to six orders of magnitude higher at a field of $10^4$ V.cm$^{-1}$ and four orders of magnitude higher at fields of $10^6$ V.cm$^{-1}$, depending on the type of conduction (Section 6.C.2.4.). All resistivities referred to in the rest of this Section (C.2.1.) are those derived from the ac conductance as described.

6.C.2.1.1. Variation with area of device.

The calculated values of K & $\rho$ for films with a number of devices were found, surprisingly, to be a function of device area. This variation occured for both gold and aluminium base films, gold and aluminium top contacts and over a wide range of deposition conditions and permitivities. The dielectric constant was found to rise and the resistivity fall as the device area tended to zero as can be seen in figures 6.11 and 6.12. It is significant that the area appears in the denominator of equation 6.1. and the numerator of equation 6.2., so that a consistant underestimate of the area could explain the effect. The errors in the measurement of area required to explain the effect, however, were in some cases higher than 50%; which was inconceivable and the phenomenum was too consistent to be due to any more random errors. A possible explanation lies in the fact that the area measured and used in the calculations was the area of the top contact. It is possible that more than just that area of the film plays a part in the determination of capacity between the contact and the effective infinite plane of the other electrode. If that part of the film contributing to the capacity was equivalent to a region bounded on each side by planes at angles to the top contact of more than 90°, the effective increase in the average length of each side of the contact would be indpendent of contact area. In that case the effective increase in the area of a square contact of side $\ell$ would be proportional to $\ell$ and not $\ell^2$. With increasing area the influence of the effect should therefore become negligeable as was observed for areas greater than $8.10^{-4}$ cm$^2$. These ovservations bring into doubt the determination of permitivities of thin films using very small contact areas ($<10^{-5}$ cm$^2$) without the use of a correction factor. For correlation

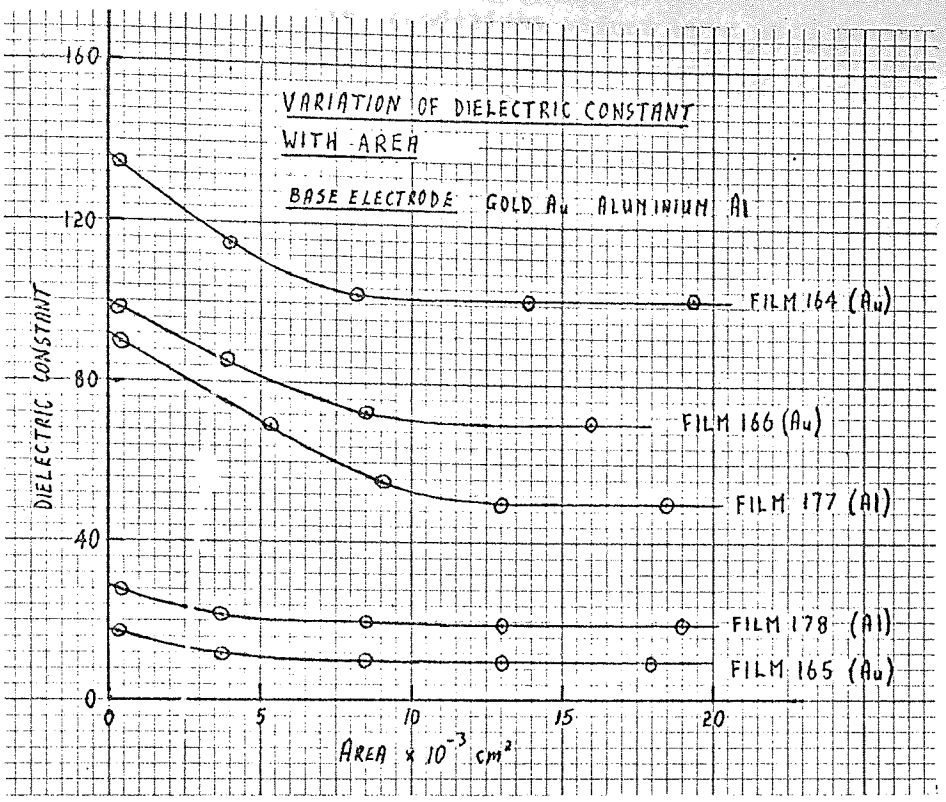


Figure 6.11.

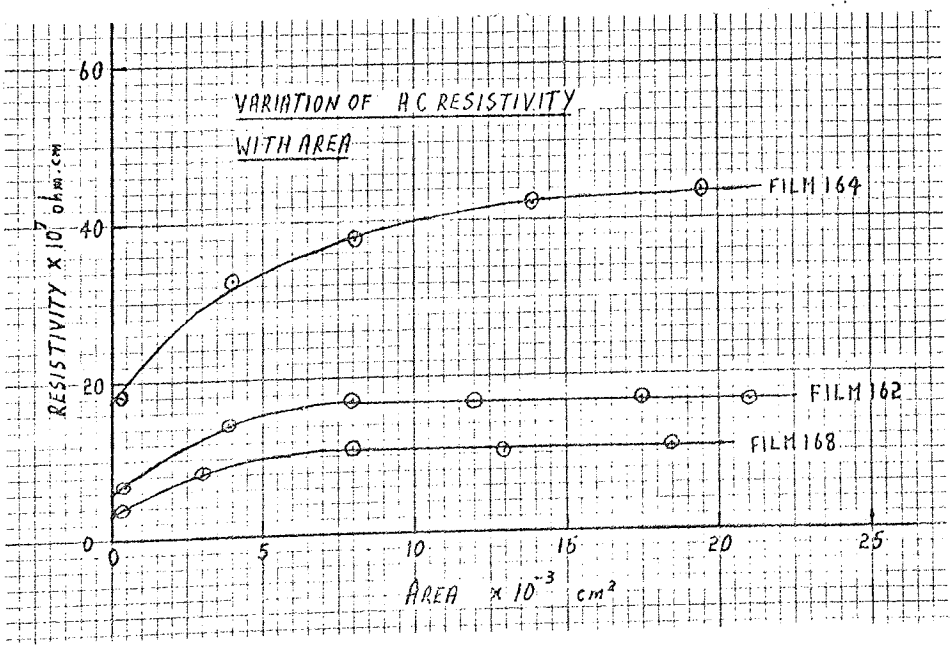


Figure 6.12

of K and $\rho$ with other deposition conditions values were used derived only from devices of area greater than $10^{-3}cm^2$.

6.C.2.1.2. Variation with film deposition conditions.

Film permitivity and resistivity were found to be functions of the deposition temperature but to be independant of deposition rate and oxygen percentage in the ranges given above. The variation of dielectric constant K withdeposition temperature is shown in figure 6.13. At ambient, and up to 200°C, K varied only slightly in the range 10-20, but above 200°C a sharp transition over a range of only 30°C occured and the value of K rose to above 100. Films deposited at temperatures between 230°C and 400°C gave values of K in the range 110-140 and for those films deposited above 400°C a second transition was observed such that the value of K was still increasing sharply at a deposition temperature of 500°C. This was the maximum temperature attainable by the substrate heater and considerable reconstruction of the substrate heater and chamber furniture would have been required to increase it by more than 100°C. Any application of the films deposited on existing microelectronic systems limits the substrate temperature to below 300°C and the properties of films within this limit were of more interest; so the variation of K with temperatures above 500°C was not pursued. The variation of film resistivity $\rho$ also showed a transition at 215°C as can be seen in figure 6.14. For amorphous, low K, films the resistivity was of the order of $10^{10}$ ohm.cm but for high K films it fell to as low as $\sim 5\ 10^{7}$ ohm.cm at a deposition temperature of 500°C. A clear second transition occured as for the variation of K with deposition temperature but the comparison of figures 6.13 and 6.14 indicated a relationship between K and $\rho$ which is demonstrated in figure 6.15. Clearly the improved ordering of the film, responsible for the increase in permitivity, causes a decrease in the resistance to charge movement as might be expected. The variation of dissipation factor $\tan\delta$ with deposition terperature was well behaved below 200°C but showed a large spread of values above the transition temperature. This is shown in figure 6.16 where it can be seen $\tan\delta$ was was of the order of

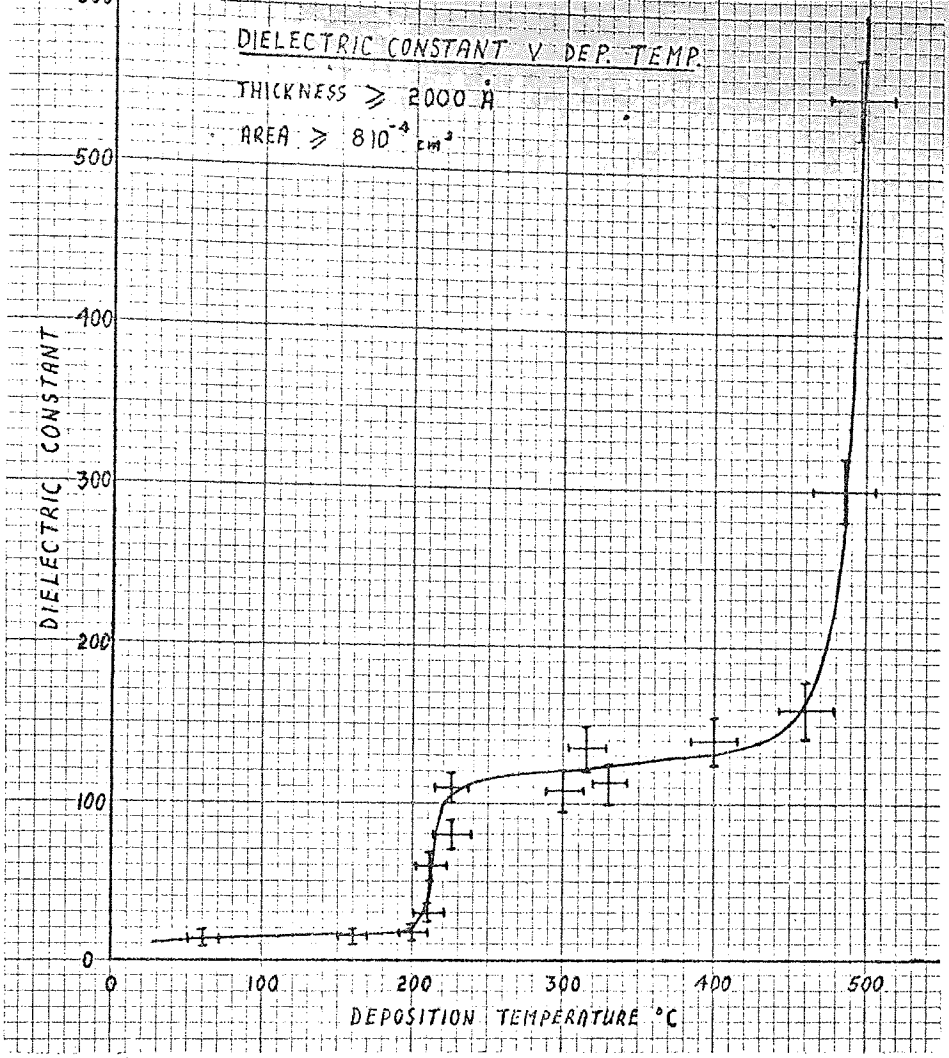


Figure 6.13

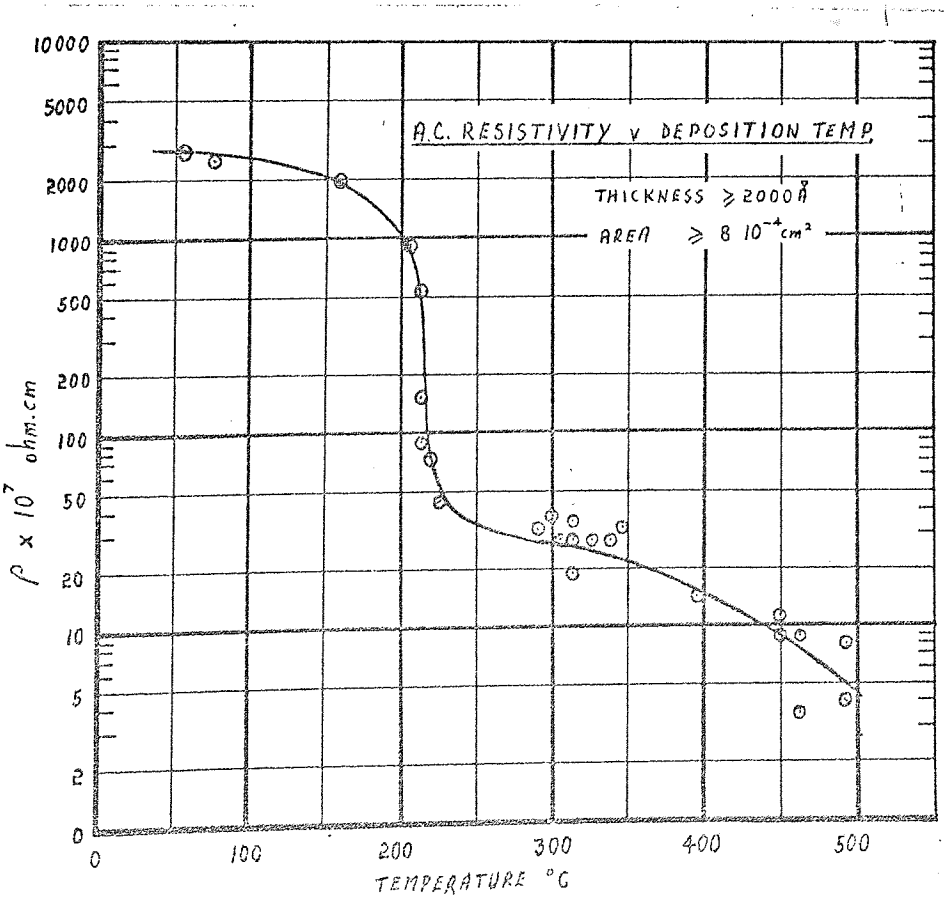


Figure 6.14

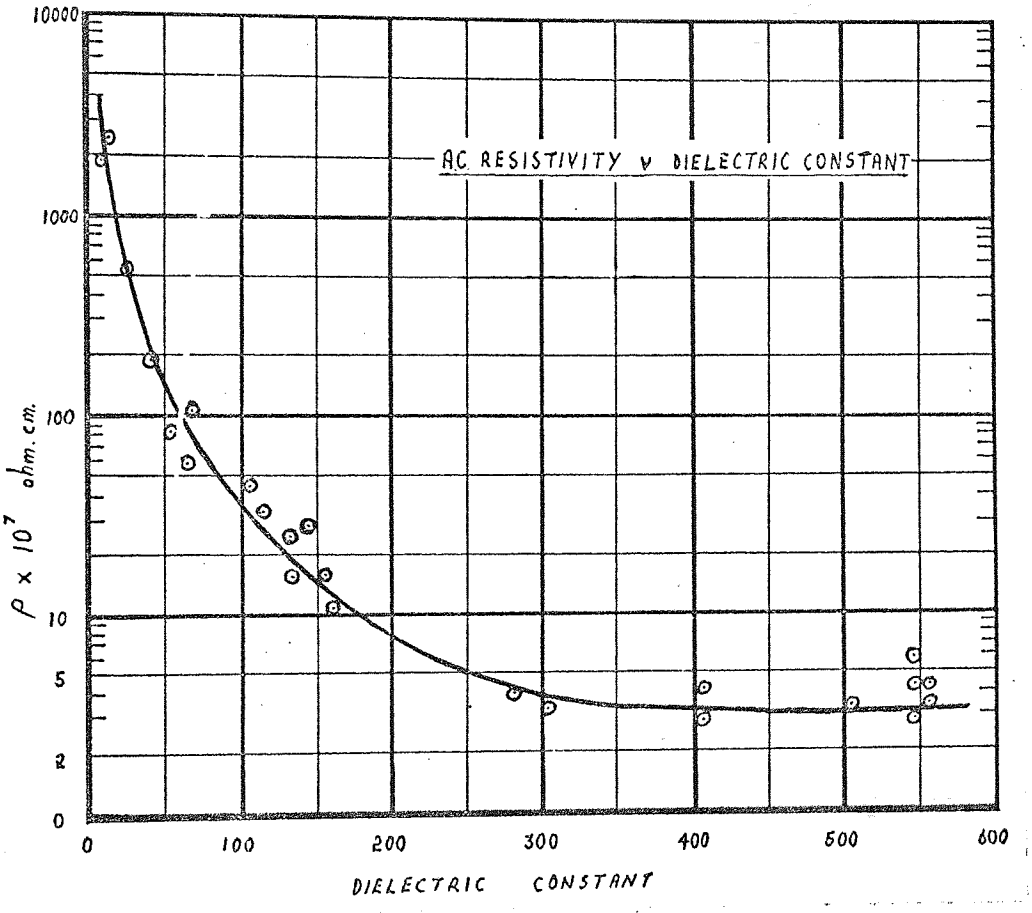
AC RESISTIVITY v DIELECTRIC CONSTANT
10000
1000
100
10
5
2
0
ρ x 10⁷ ohm. cm.
0
100
200
300
400
500
600
DIELECTRIC CONSTANT

Figure 6.15.

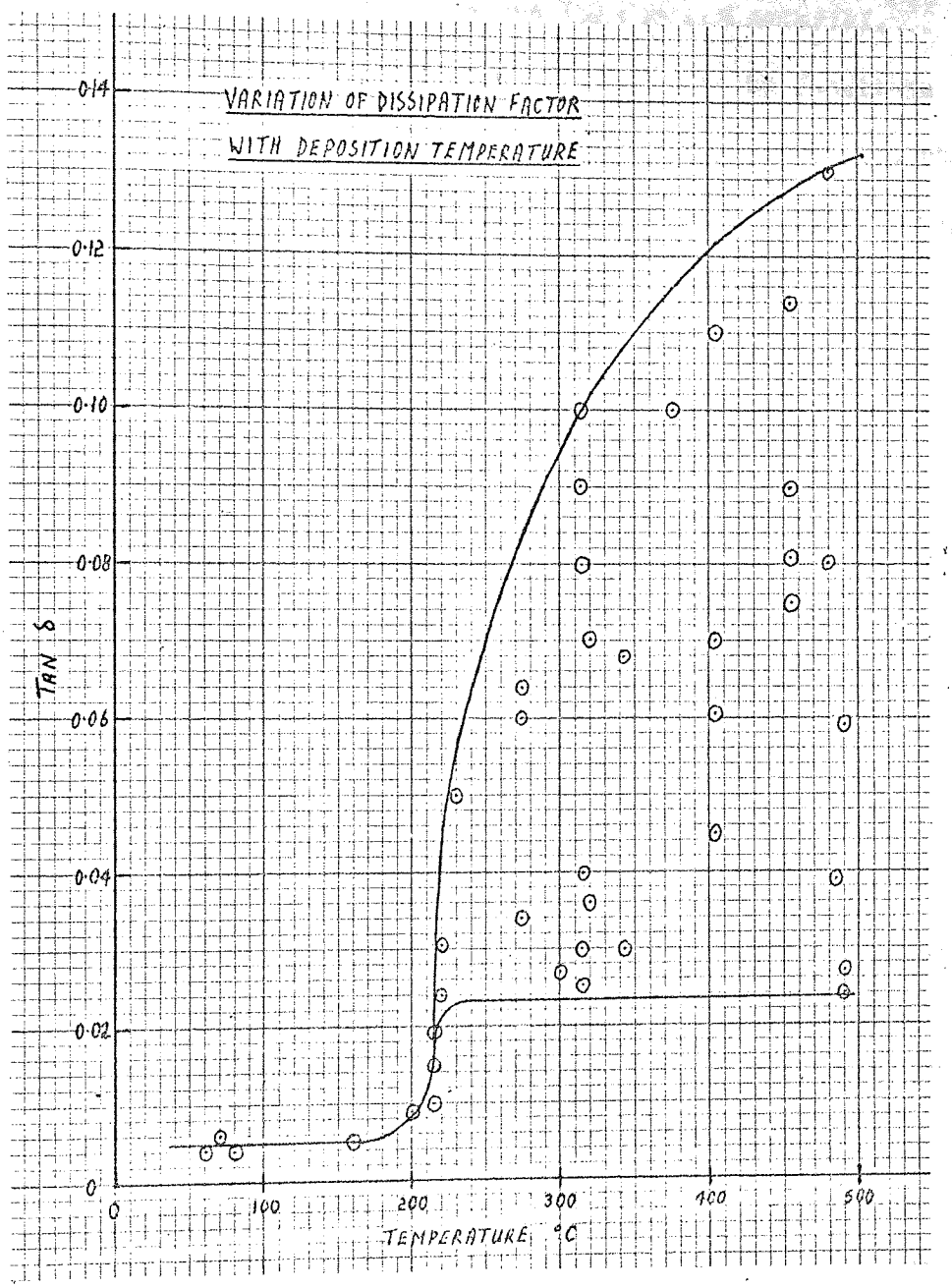
VARIATION OF DISSIPATION FACTOR
WITH DEPOSITION TEMPERATURE
TAN δ
0·14
0·12
0·10
0·08
0·06
0·04
0·02
0
0
100
200
300
400
500
TEMPERATURE °C

Figure 6.16

0.005 for low K films but ranged between 0.025 and 0.15 for high K films.

6.C.2.1.3. Variations with Film Thickness and Top Contact material.

The permitivity and resistivity were also found to be functions of film thickness and a consistant difference was also observed between the values for aluminium and gold top contacts. It had been reported in papers on thin single crystals (39), thin slip castings (43), and also thin films (38) of barium titanate that the electrical properties were a function of thickness. Consequently a series of films were prepared with the same deposition conditions; substrate temperature 300-310°C, deposition rate 14 Å.min$^{-1}$ and 3% oxygen in the sputtering gas, over a range of thickness up to 8000 Å. Figure 6.17 shows that K was found to be a function of thickness, particularly below 2000 Å, but the variation was much less than that reported by Slack for epitaxial titanate films. The figure also shows that devices on the same film with gold top contacts showed consistently lower values of K than devices with aluminium top contacts. A similar but less consistent variation was observed in the film resistivity $\rho$ plotted against thickness, figure 6.18. This shows a tendancy for $\rho$ to rise with the decrease in K towards thinner films and devices with gold top contacts were always found to have a higher resistivity than devices with aluminium top contacts. A thorough investigation was not made into the properties of films with aluminium base electrodes but from the few films examined a similar behaviour appeared to occur. Not enough films were examined to determine any variation with deposition rate but permitivities were independent of oxygen content in the sputtering gas and showed a transition in their dependence on deposition temperature. Films deposited at ambient and temperatures up to 300°C gave dielectric constants K in the range 10-20 while one film deposited at 320°C gave K = 70 and another deposited at 350°C, K = 145. As in the case of gold based films the resistivity $\rho$ fell and the dissipation factor, tan $\delta$, rose with increasing K.

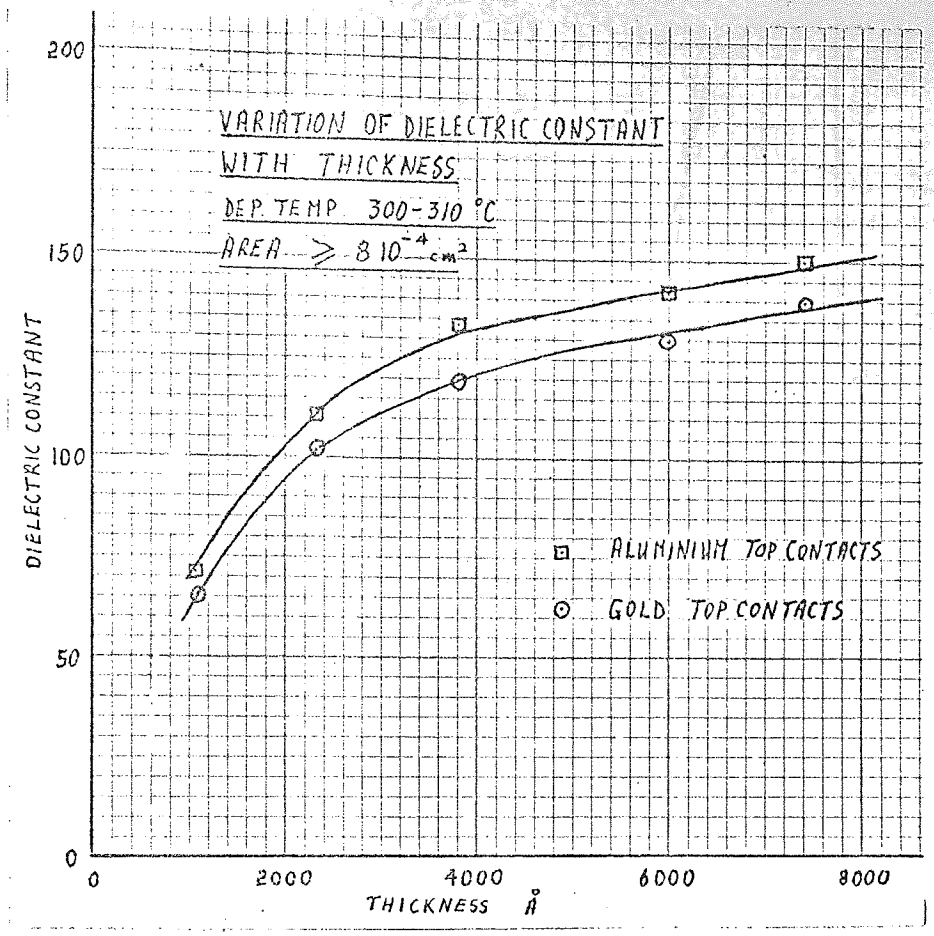


Figure 6.17

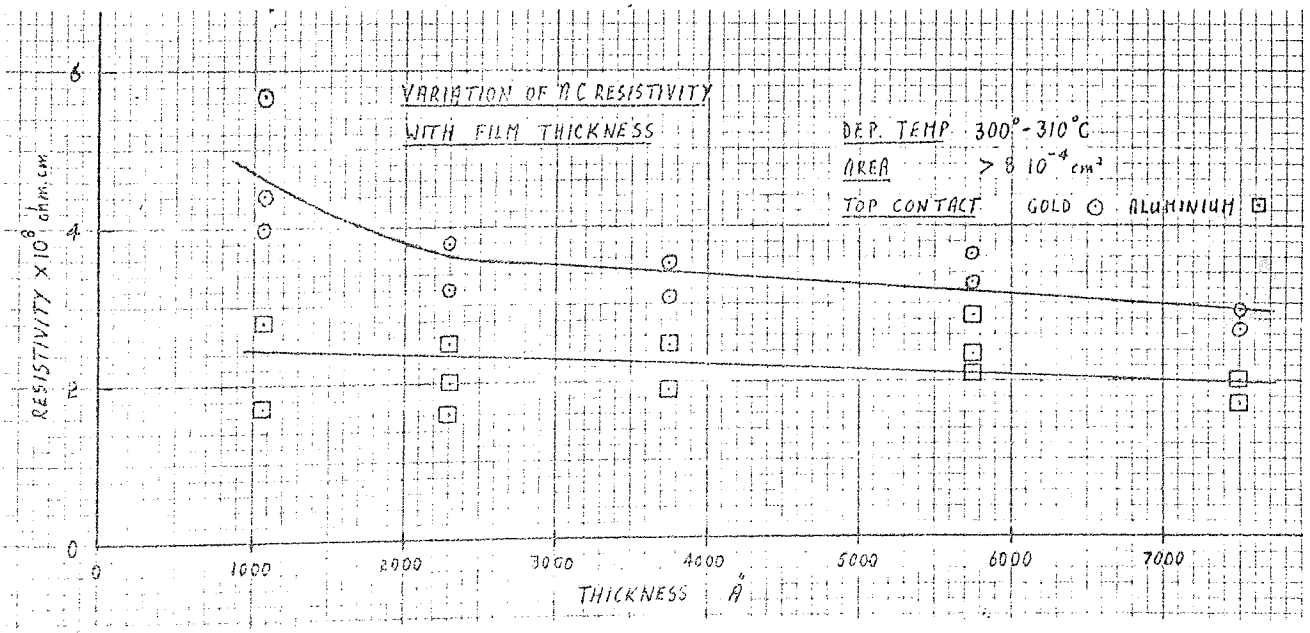


Figure 6.18

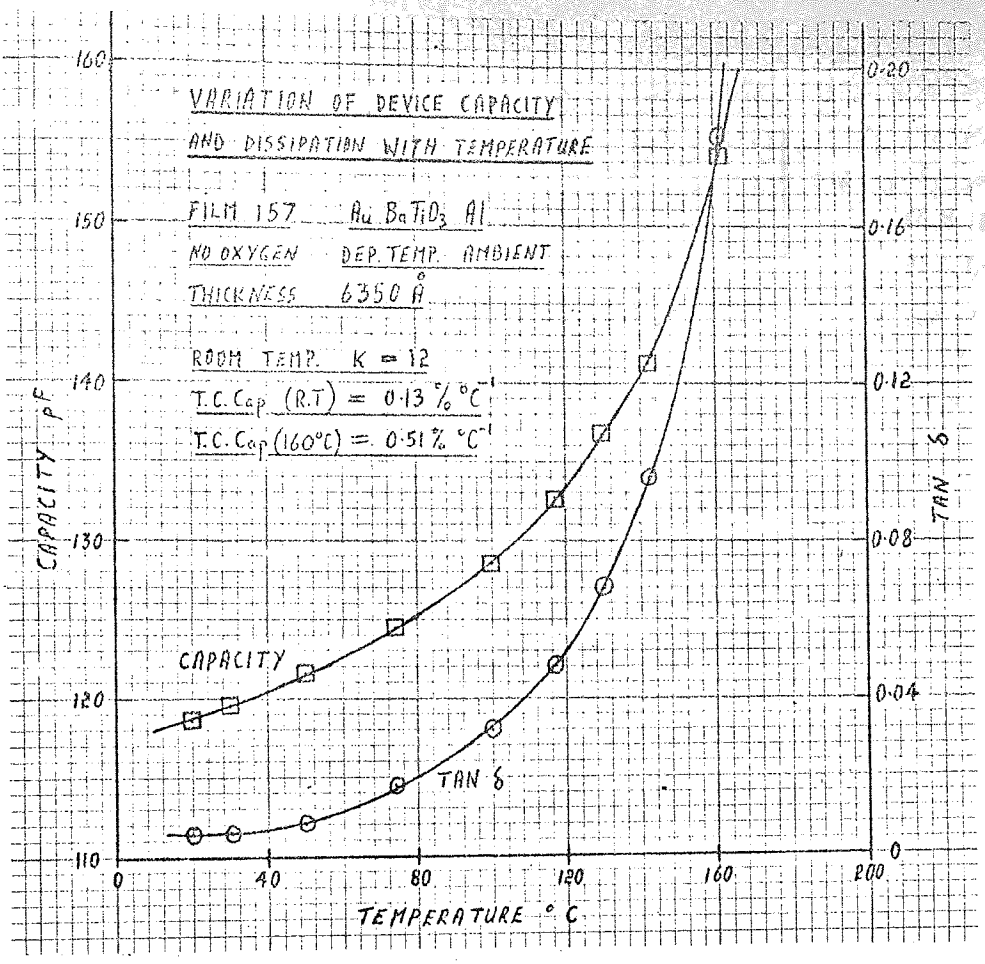


Figure 6.19

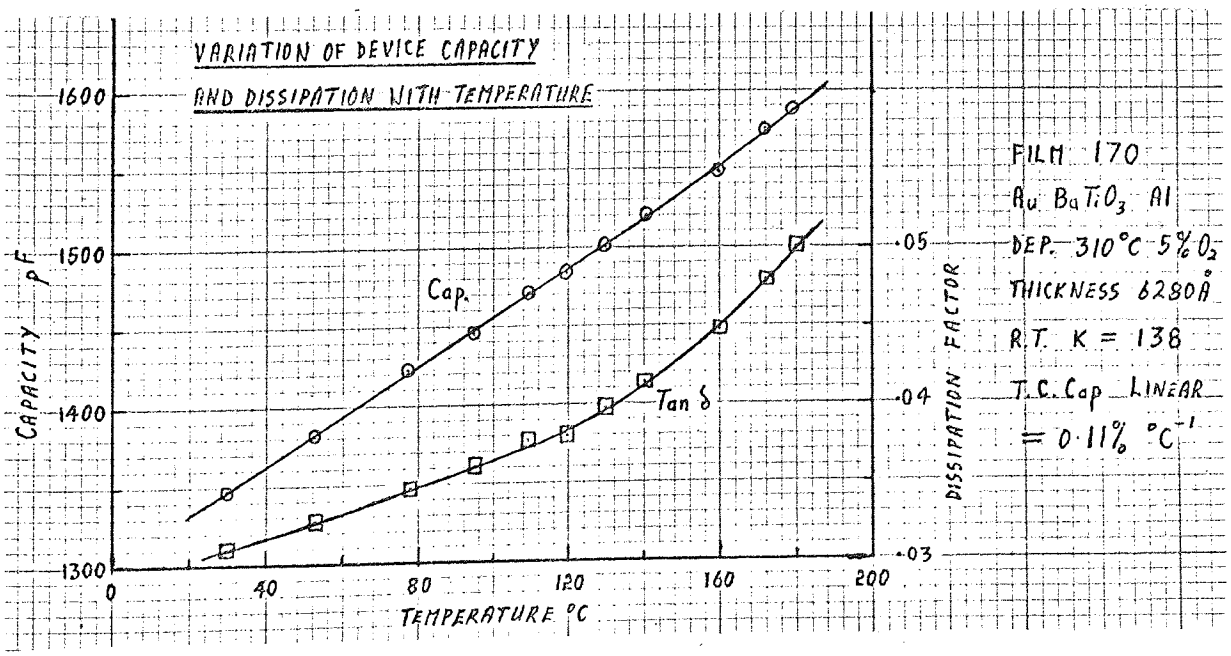


Figure 6.20

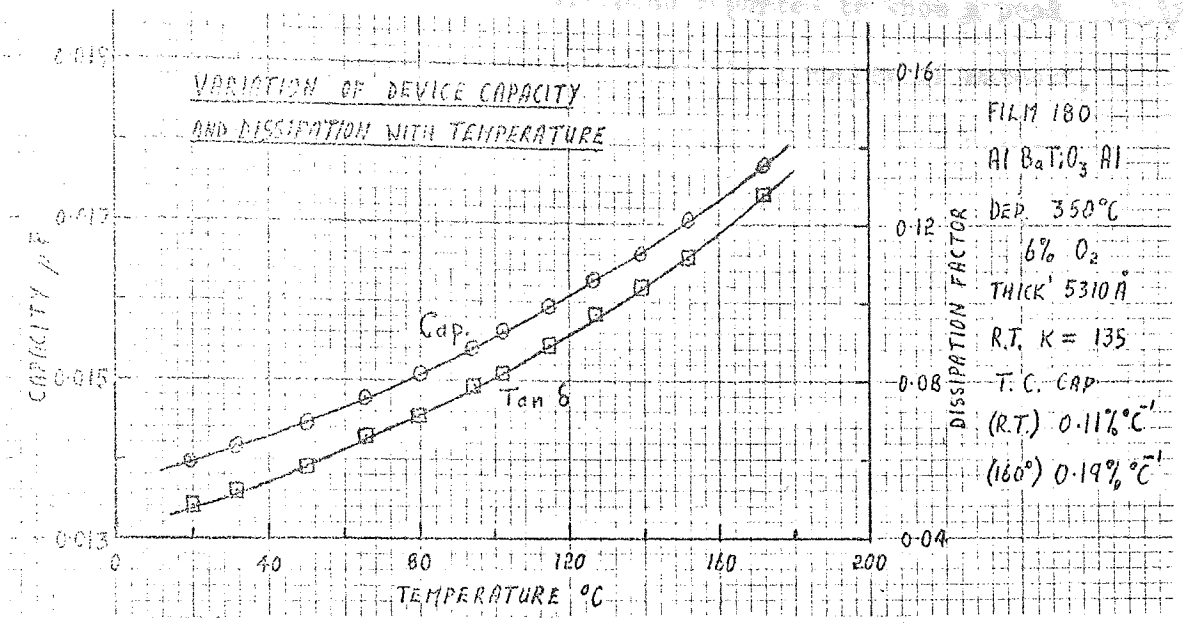


Figure 6.21

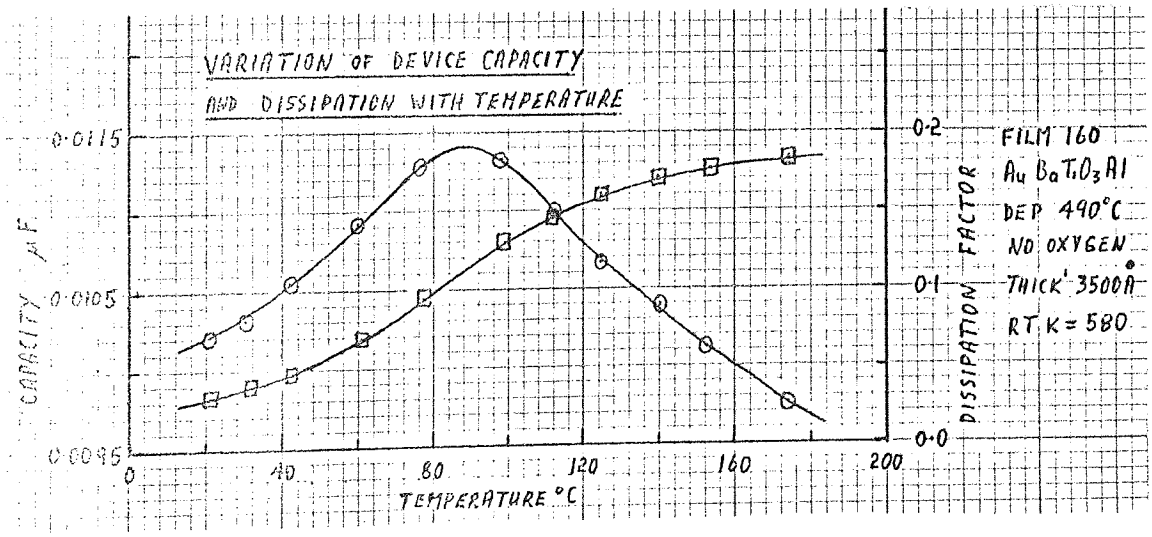


Figure 6.22

6.3.2.1.4. The variation of film permitivity with temperature.

Thin layers of barium titanate have been reported to show a peak in permitivity in the temperature range 80-150°C by a number of authors, (Section 1.3.) similar to the discontinuity in the variation of permittivity with temperature exhibited by the bulk material at the Curie point of 120°C (Section 1.2.5.). As permitivity is proportional to capacitance, the variation of capacitance and dissipation factor with temperature was measured in the range, R.T.-180°C, for a selection of films deposited under different conditions. All low K films, those deposited on both gold and aluminium base electrodes, were found to behave in the same manner. A typical example is given in figure 6.19 which shows that the permitivity and dissipation factor are non linear functions of temperature. The temperature coefficient of capacitance rises from a room temperature value of 0.05- 0.15%.°C$^{-1}$ by some four or five times to 0.3-0.6%°C$^{-1}$ at 160°C for all such films, and the dissipation rises at a rate exceeding a square law relationship. The permitivity of films exhibiting medium dielectric constant (100-200) was found to be a fairly linear function of temperature. For films deposited on gold base electrodes deviation from linearity only occured at the end of the temperature range, as can be seen in figure 6.20 and the temperature coefficients of capacity were in the range 0.1-0.2%°C$^{-1}$. Films deposited on aluminium base electrodes gave a gently curved temperature dependence over the whole temperature range as can be seen in figure 6.21, with the temperature coefficient of capacity rising from 0.1%°C$^{-1}$ at room temperature to 0.2%°C$^{-1}$ at 160°C. The variation of dissipation factor with temperature was again non-linear but showed no steep rise as for amorphous films. The permitivity of high K films deposited above 450°C were found to show a broad peak with temperature at a temperature that varied from film to film in the range 70-90°C. Typical results for the variation of capacity and dissipation factor with temperature for a film with a room temperature K=580 are shown in figure 6.22. The temperature coefficient of capacity $\gamma_c$ is related to the temperature coefficient of perm-

itivity $\gamma_p$ by equation 6.4, where $\alpha$ is the coefficient of linear thermal

$$\gamma_c = \gamma_p + \alpha \qquad 6.4.$$

expansion. All reported values of $\alpha$ for the bulk material are small compared to $\gamma_c$ so the approximation $\gamma_p = \gamma_c$ can be made.

6.C.2.2. Dielectric Strength.

No particular investigation was made into the dielectric strength or general breakdown phenomenae of the films but certain observations were made in the course of other measurements and are described below. At fields above 5 $10^5$ $V.cm^{-1}$ instabilities occured in the current passing through the capacitive devices. These consisted either of slow random variations over about one third of a decade of current or of sudden very large increases in current followed by a slow decay to a level about the same or lower than the initial current. The latter behaviour is consistent with healing breakdowns, which are reported to occur in similar films, where weak paths in the film are prefferentially burnt out thus increasing the resistivity and dielectric strength of the film. These instabilities continued with increasing voltage until destructive breakdown occured generally at 1-2 $10^6$ $V.cm^{-1}$, when a permanent decrease in resistivity of about one million times occured. The dielectric strength was the same for both low and high K films and between one and two orders of magnitude higher than values reported for bulk barium titanate (194).

6.2.3. Ferroelectricity.

A number of films were examined for ferroelectricity using a Sawyer Tower circuit (Section 1.2.2.) which was built into an earthed case as shown in plate XXXXI. A Marconi T.F. 1382 low frequency signal generator capable of sine, square, or ramp output with a frequency range of 0.01-1000 Hz. and a Solartron oscilloscope were used. A hysterisis like loop could be obtained for all films at about 50 Hz which might be confused with ferroelectric behaviour but which was due to the slight phase change associated with the relatively low resistance of the film and was easily reproduced by a capacitor of similar value and a $10^9\Omega$ resistor connected in parallel.

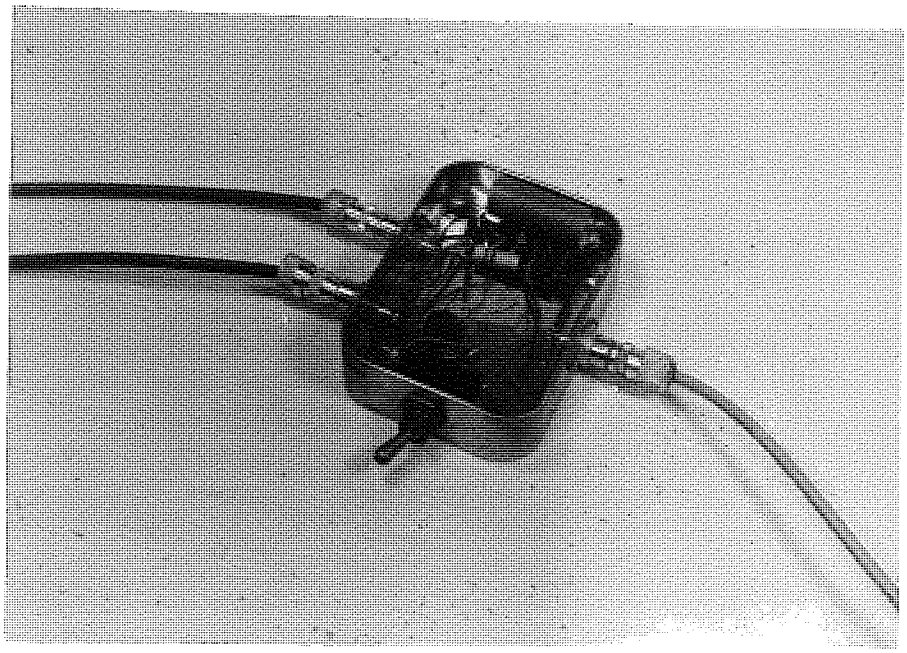

PLATE XXXX1

The switching transients of the films were also examined, as described in Section 1.2.2., but both measurements failed to find any ferroelectric behaviour even in the crystalline films of high dielectric constant for which a peak of permitivity with temperature had been observed.

6.C.2.4. Electrical conduction.

The I.V. characteristics of a number of capacitive devices were measured over a range of temperature from 4°K to 370°K using the apparatus and techniques described in Section 4.8. As most of the measurements were made on films deposited on gold base electrodes the results referred to apply to those films unless otherwise specified. The main interest was conduction through the metastable films, giving medium values of dielectric constant; but some low K, amorphous films were also examined. The latter films exhibited the unusual phenomenum of the current at a given constant voltage increasing with time and these results will be considered seperately.

6.C.2.4.1. Conduction in the amorphous films.

The electrical conduction through films exhibiting low permitivity was found to be a function of the contact materials and the presence of oxygen in the sputtering gas during deposition. At room temperature, the current density for a given field was also a function of the bias, forward or reverse applied to both Au-BaTiO -Au and Au-BaTiO -Al devices (figure 6.23). At low fields, currents were slow to reach consistent values for a given voltage, persisted for several minutes after the removal of the voltage, and standing voltages of the order of $10^{-8}$V could be measured. The sudden application or reversal of the applied voltage caused sharp increases in displacement current followed by a decay as shown in figure 6.24 copied from a chart recorder output. The decays were equivalent to a forward bias (base gold contact positive) relaxation time of the order of 10 minutes and a reverse relaxation time of about 20 minutes. These obervations are consistent with the occurence of some sort of ionic process. Above a certain applied field the current flowing through a device maintained at a given voltage was found to increase with time.

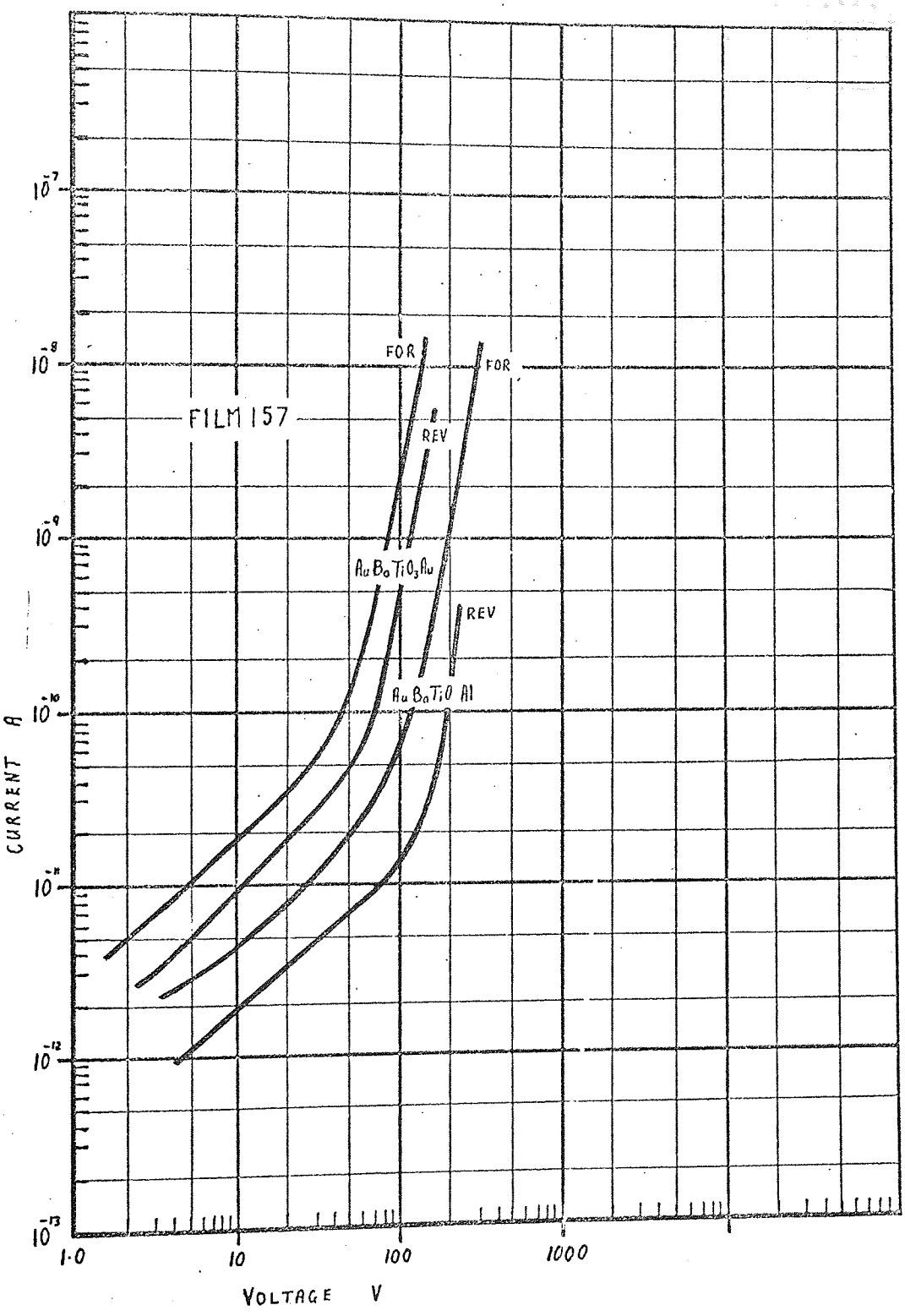


Figure 6.23

Characteristics Amorphous Films

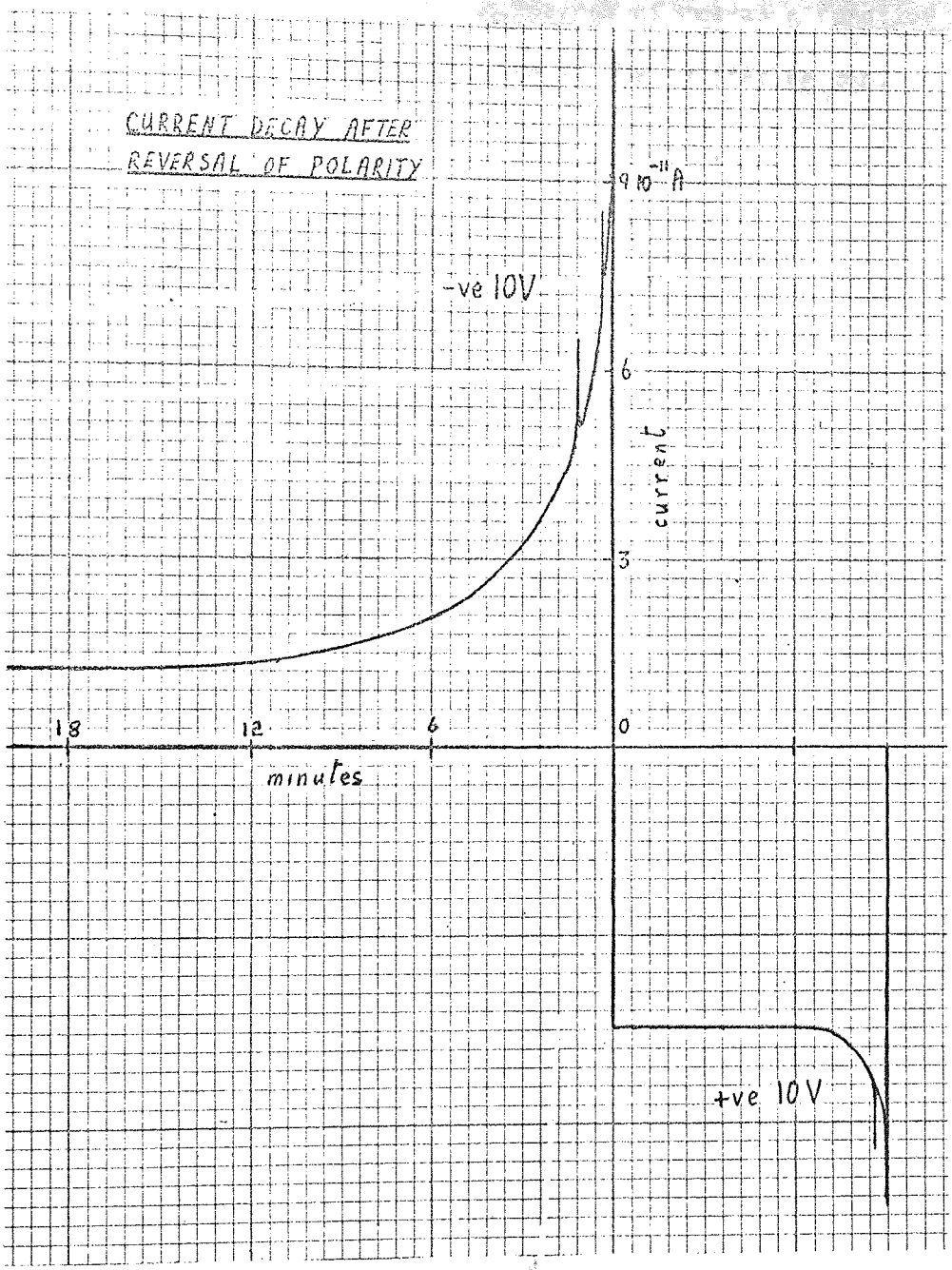
CURRENT DECAY AFTER
REVERSAL OF POLARITY
-ve 10V
9 10⁻¹¹A
6
3
0
current
18
12
6
minutes
+ve 10V

Figure 6.24.

TABLE 6.1.

Critical field for onset of time dependent current effect as a function of anode material and the percentage of oxygen in the sputtering gas.

| Oxygen Percentage | Fields $V.cm^{-1}$ for various anodes | | |
|---|---|---|---|
| | base Au | top Au | top Al |
| 0 | $6.15\ 10^5$ | $8.5\ 10^5$ | |
| 5 | $5.7\ 10^4$ | | $2.85\ 10^5$ |

TABLE 6.2.

Variation in the rate of current increase with time for a device maintained at 10 Vdc

| Time Mins | 0 | 50 | 220 | 460 | 1440 |
|---|---|---|---|---|---|
| Rate of Increase x $10^{-15}$ $A.sec^{-1}$ | 14.5 | 5.55 | 5.40 | 5.45 | 5.35 |

The field above which this effect occured was much lower for films deposited in a partial oxygen atmosphere and also lower when the gold contact of a Au-BaTiO -Al device was made positive while onset fields for Au-BaTiO -Au devices were almost independent of bias. The actual onset field varied slightly from device to device but typical values for each case are given in table 6.1. The increase of current with time persisted in some cases for minutes and in other cases for days. For films deposited in an oxygen atmosphere the rate of increase of current showed very little decline over a period of many hours. This is shown in table 6.2. which gives the variation of the rate of increase with time for a film maintained at 10 V over a period of 24 hours, after which the measurement was discontinued. A long term increase in current occured with both gold and aluminium contacts positive. However, for films deposited with no oxygen partial pressure, while a similar long term increase was observed with the top contact positive,

when the base gold was made positive the increase persisted only for a matter of minutes. These observations and the fact that no increase of current with time was found in devices with an Al $BaTiO_3$ Al structure deposited on aluminium base films led to a number of conclusions concerning the process responsible for the behaviour. The phenomenum would seem to be connected with gold contacts and the exposure of the contact or film to oxygen during preparation. This is not contradicted by the non-oxygen films showing the long term effect for top contacts because while no oxygen absorption is possible at the base film interface resulting in only a short term effect, oxygen absorption could occur in the top layers of the titanate film after removal from the chamber and before top contact deposition. The rate of increase of current was found to be higher at higher voltages and after the application of a high voltage for any length of time, if the voltage was then reduced to a low value the current was considerably higher than first observed and was found to slowly decay until the rate of increase at the lower voltage became dominant. The variation of $\frac{dI}{dt}$ with voltage was measured returning to no field and waiting for the current to decay to zero between each reading. Plots of $\log\frac{dI}{dt}$ against $V^{\frac{1}{2}}$ were found to be straight lines within the accuracy of measurement as shown in figure 6.25. This suggested that the increased rate of rise was due to excitation over a field lowered barrier with a barrier lowering factor of $53.10^{-19}$ in MKS units. This was supported by the fact that at liquid nitrogen temperature the current was constant for a given voltage and forward and reverse bias leakage currents were approximately the same in every device. I.V. characteristics were obtained for these films by extrapolating back the increasing currents to the point of application of the voltage and using that value of current. For fields below $5\ 10^4 - 10^5\ V.cm^{-1}$ the current was a linear function of voltage and above $10^5 - 10^6\ V.cm^{-1}$ obeyed a power law of order in the range 3-6. Between these two limits a transition region existed which tended to be longer and more curved for thinner films but for some thick films con-

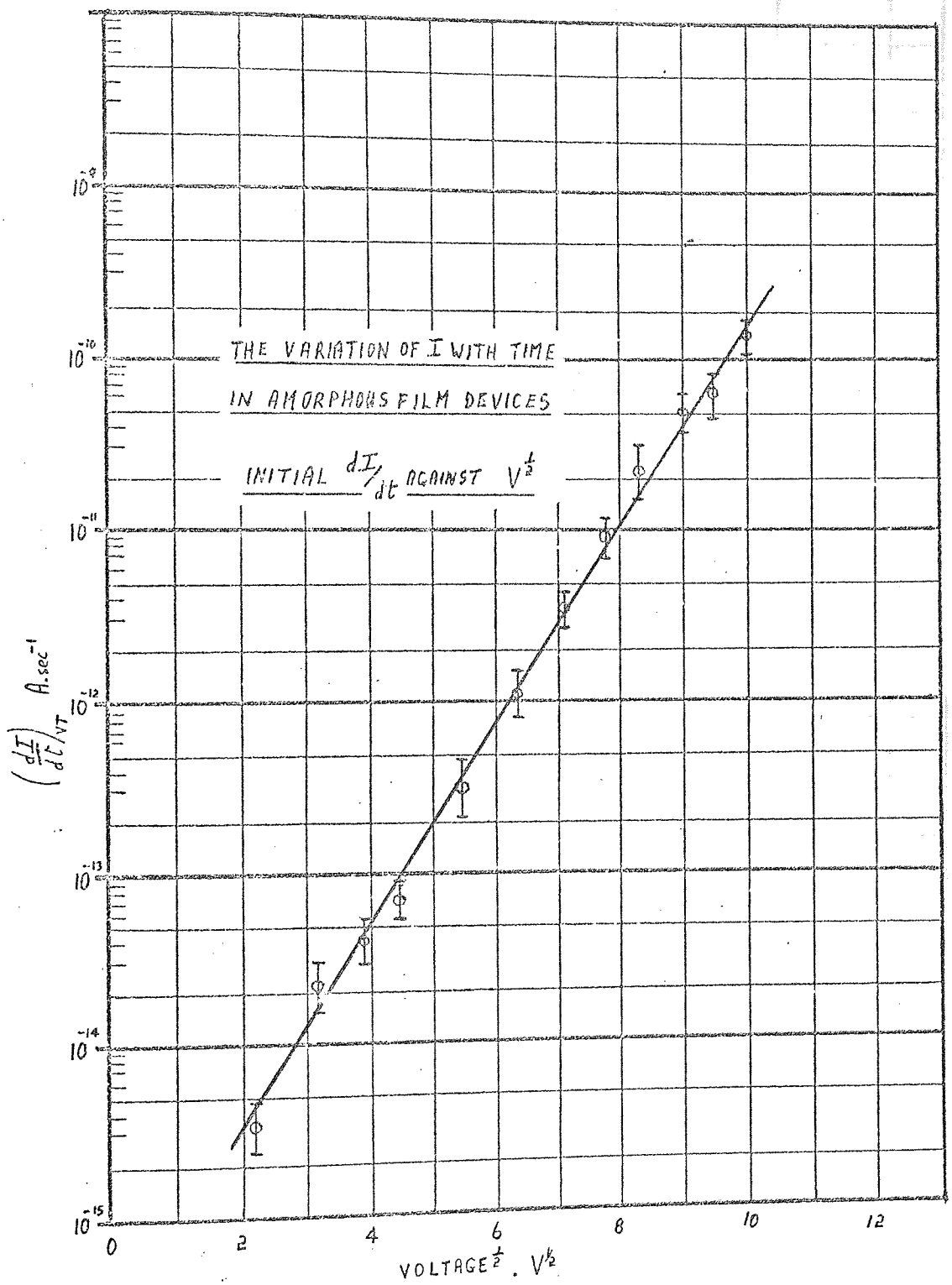
THE VARIATION OF I WITH TIME
IN AMORPHOUS FILM DEVICES
INITIAL dI/dt AGAINST V^½
(dI/dt)_VT A.sec^-1
10^-9
10^-10
10^-11
10^-12
10^-13
10^-14
10^-15
0
2
4
6
8
10
12
VOLTAGE^½ . V^½

Figure 6.25

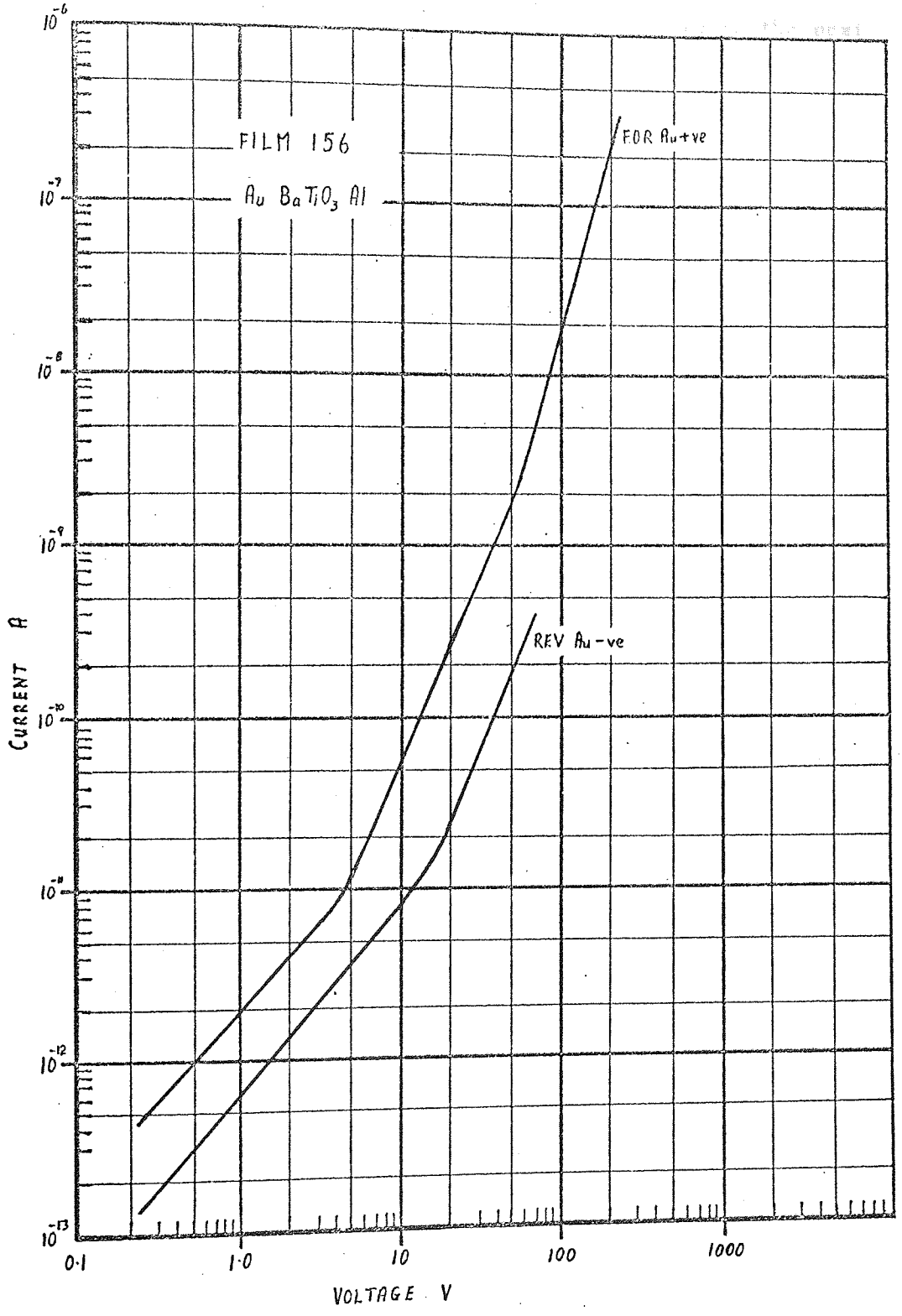


Figure 6.26

Characteristics Amorphous Films.

stated of a well defined $V^{\frac{1}{2}}$ or $V^2$ relationship as can be seen in figure 6.26. This behaviour is similar to that observed in some cases for the medium permitivity films and will be discussed more fully in the next section.

6.C.2.4.2. Conduction in films exhibiting medium permitivity.

As described in Section C.2.1., films deposited at substrate temperatures above 220°C were found to have dielectricconstants above 100. These films were the most interesting because they could be used to form thin film capacitors at temperatures compatible with other microelectronic components, (<300°C), with capacitance per unit area at the same film thickness an order of magnitude above that obtained from the materials usually used. The leakage currents in these films were therefore examined more closely in an attempt to define a conduction process. The ac resistivity of these films was found to be a consistent function of the deposition conditions but the dc resistivity varied considerably and the form of the VI characteristics behaved in a similar manner. The characteristics were in general non ohmic, but an ohmic region or tendancy towards ohmic behaviour was observed in all films under conditions of high temperature and low field. The dc conductivity calculated at a field of $1.10^4$ V.cm$^{-1}$ varied from film to film by up to six orders of magnitude and between devices on one film by more than an order of magnitude, with a minimum observed value of $10^{-14}$ ohm$^{-1}$. cm$^{-1}$. This high sensitivity of dc conductivity to deposition conditions has been found in other dielectric films (195) where variations over nine orders of magnitude are reported. The precise form of the characteristics were found to be a function of the film conductivity. For films with conductivity of less than $10^{-12}$ ohm$^{-1}$.cm$^{-1}$. the logarithmic current voltage characteristics were typically as shown in figure 6.27, which will be termed type 1 conduction. Figure 6.28 shows the same plot for a film typical of those with conductivities greater than $10^{-11}$ ohm$^{-1}$. cm$^{-1}$ which is termed type 3 behaviour. Type 2 conduction, intermediate between 1 and 3 is shown in figure 6.29 and was observed for films with conductivities in the range $10^{-12}$ to $10^{-11}$ ohm$^{-1}$. cm$^{-1}$. No long term variation of

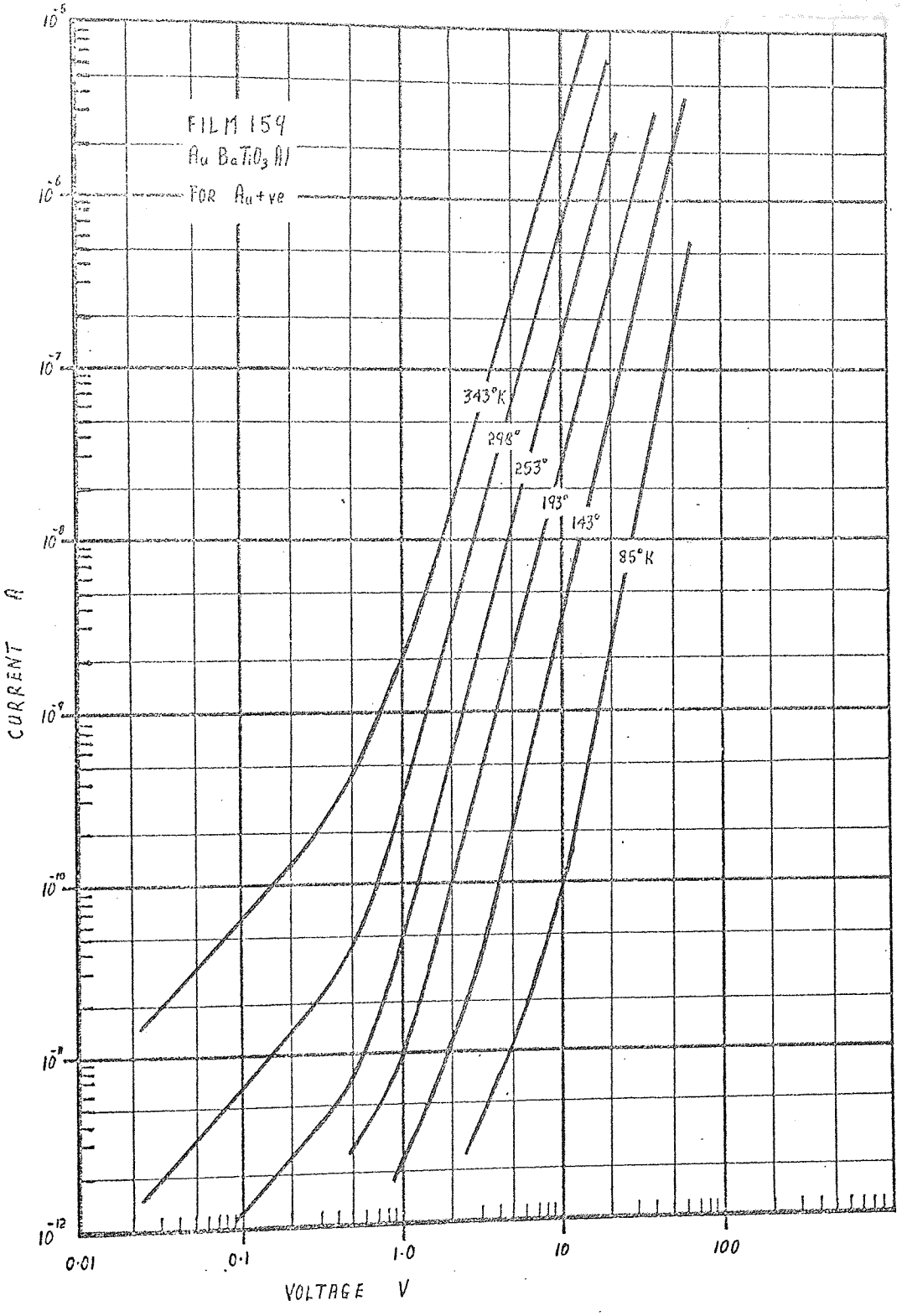


Figure 6.27

Type 1 Conduction.

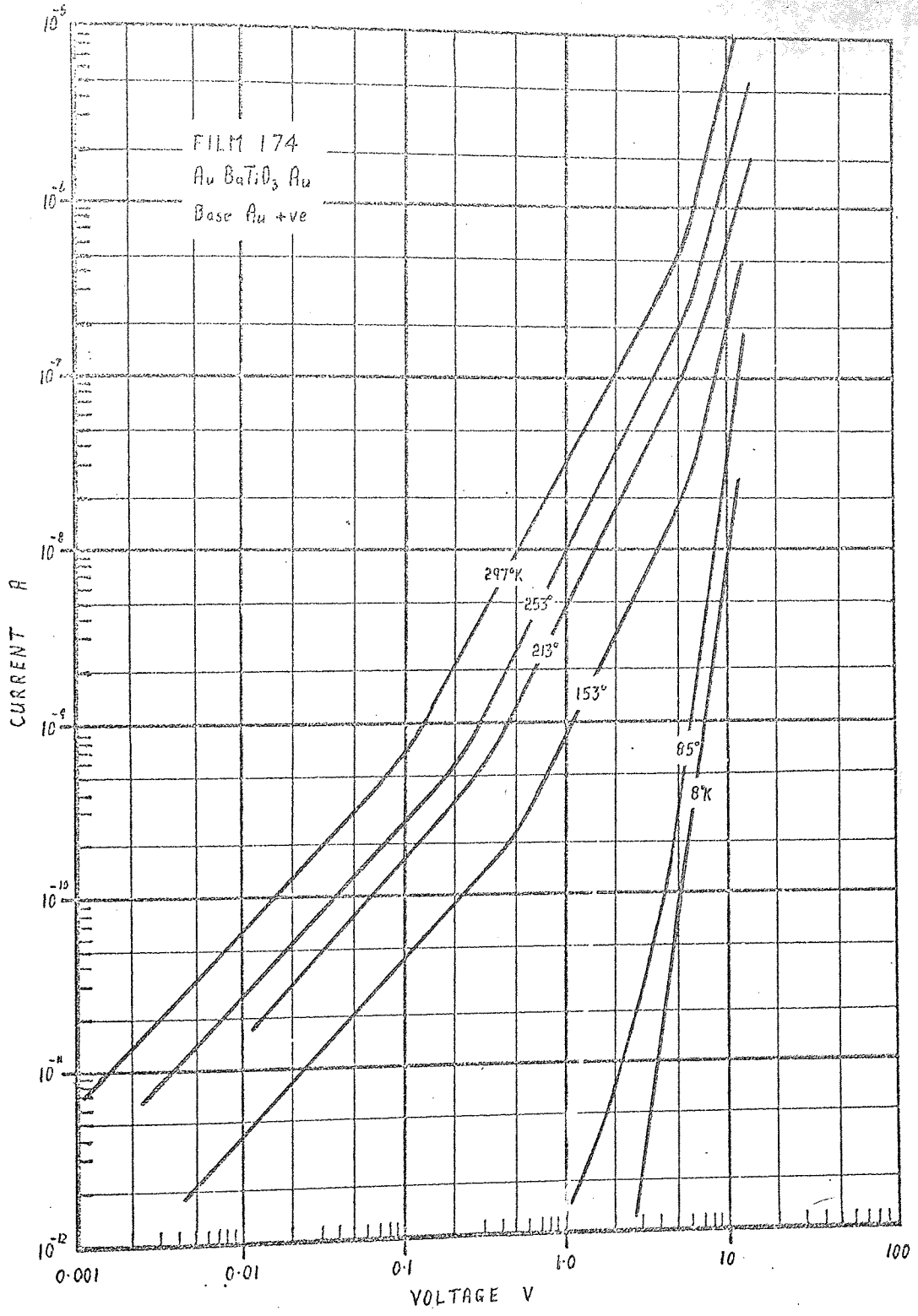


Figure 6.28

Type 3 Conduction.

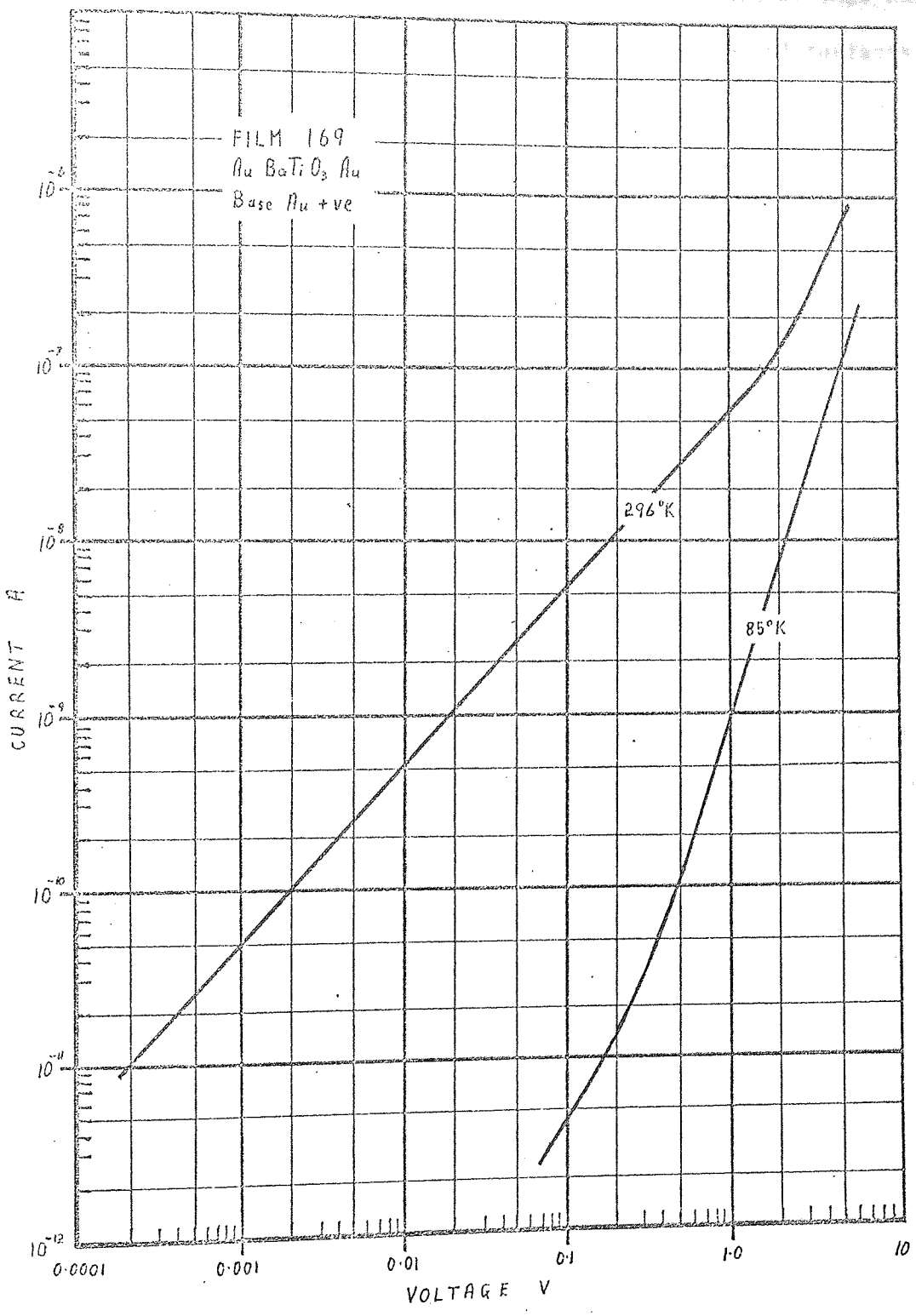


Figure 6.29

Type 2 Conduction.

current with time was observed at constant voltage and approximately the same current was observed under forward and reverse bias for Au/BaTiO /Au, Au/BaTiO /Al and Al/BaTiO /Al devices. The slight differences that were observed were such that the current for some films with mixed contacts was higher with the base gold film positive and for others with the aluminium contact positive. This suggests that the exact nature of the interface, dependent on the local conditions at the time of formation was of more importance to the current passed by the device than the metal of the contact. Type 1 conduction was characterised by an ohmic region at low fields; followed by a power law extending to the limit of the voltage scale. At room temperature the current voltage power law characteristics approximated to a cube law while at lower temperatures less of the ohmic region was observed and the power law became steeper. This was such that at liquid helium temperature the relationship was linear over the entire range with an exponent falling between five and eight. In the intermediate, type 2, behaviour the ohmic region stretched to much higher fields before transition to a smilar power law but was still absent at very low temperatures. In type 3 conduction a third region was observed between the ohmic region and the power law relationships represented by a variation of current with $V^{3/2}$ or $V^2$. The transition from one region to another moved to higher fields and lower currents as the temperature was reduced such that both the ohmic and $V^{3/2}$, $V^2$ regions were not observed at very low temperatures. Some curvature of the characteristics could still be detected at liquid nitrogen temperature but at liquid helium temperature the plot was completely straight. The current drawn through a device was strongly dependent on temperature for all three types of conduction. This can be seen in figure 6.30 which plots log I against log T at constant voltage for two films typical of type 1 and type 3 conduction and shows a sharp rise in current with temperature above about 100°K comparable to a power law with an exponent of the order of six. The characteristics of figures 6.27, 6.28 and 6.29 were also replotted in the form $\log \frac{I}{T^2}$ or $\log \frac{I}{T^{3/2}}$ against $\frac{1}{T}$ at constant voltages in order to determine

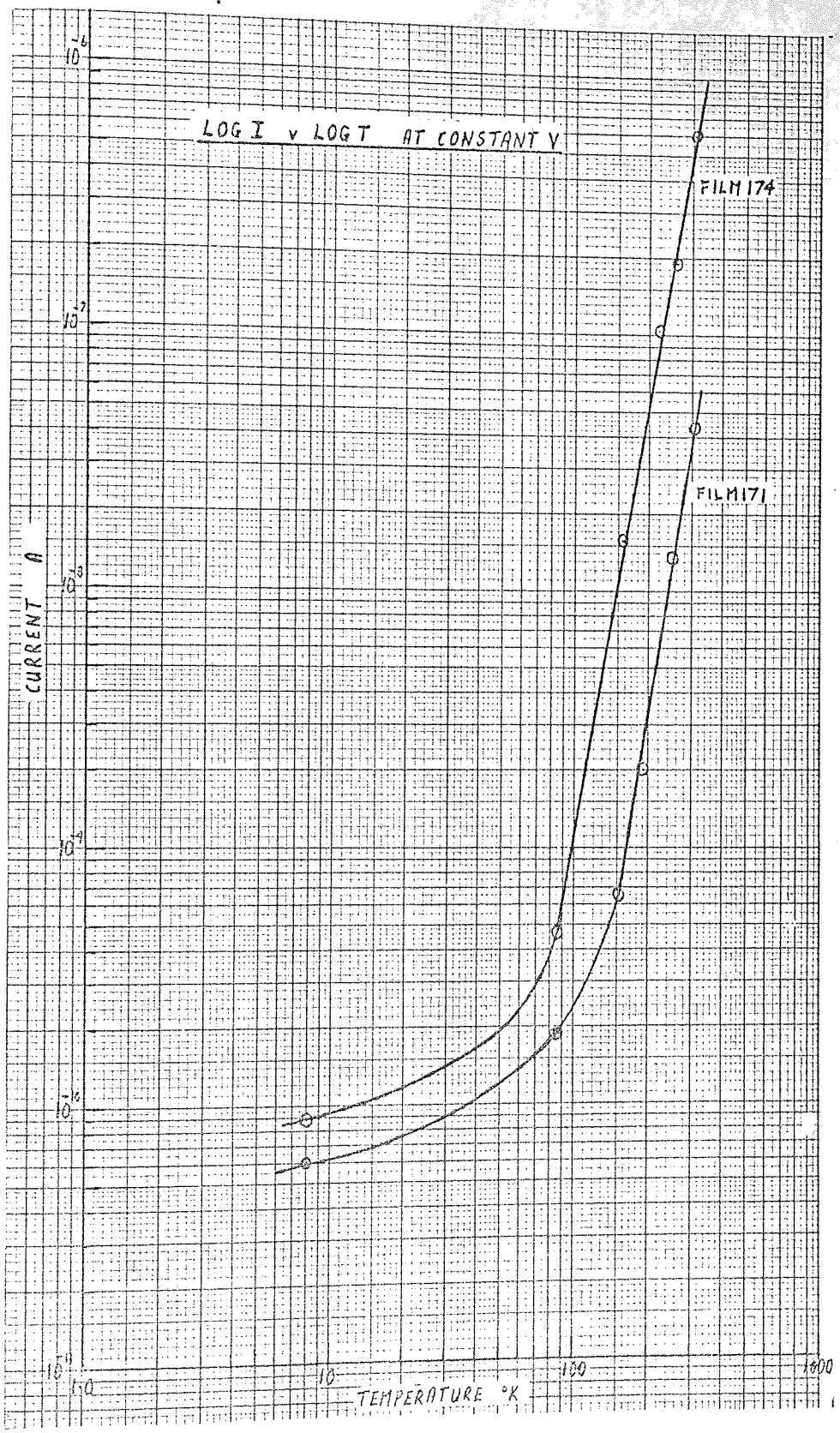
LOG I v LOG T AT CONSTANT V
FILM 174
FILM 171
CURRENT A
TEMPERATURE °K
10
100
1000

Figure 6.30

activation energies according to the relationship $J = J_o T^n \exp \frac{\phi}{kT}$ A typical graph is given in figure 6.31 which shows the continuous curvature common to all the results. This does not necessarily mean that an activation process is not occuring, as such results are often observed in thin films, due to the absence of sharply defined electronic levels. It is clear from the curves however that if a thermal excitation process is occuring at low temperatures it is associated with a very small activation energy. Also, by drawing a tangent to the curve at the high temperature end the maximum activation energies obtainable were typically of the order of 0.2 eV and varied only slightly over the whole range of field. In all cases relaxation times were much shorter than those observed for the amorphous films with gold contacts but were still long, particularly at low fields. This can be partly explained by the relatively high dielectric constant of the material but ionic conduction cannot be ruled out in the ohmic regions. Conduction in bulk barium titanate is almost entirely electronic (178) and one would expect thin films of the material to behave similarly, certainly at high fields. Furthermore as the highest activation energy observed was 0.3eV it is most likely that conduction at all fields is electronic. The conduction was unlikely to be electrode limited because that would have required the almost unimpeded propagation of injected carriers through the bulk of the film. However the film must contain a high density of trapping centres and even in bulk barium titanate the negative carrier mobility is reported to be less than 1 $cm^2 V^{-1} sec^{-1}$ (196). The absence of electrode limited conduction was supported by the fact that Au/BaTiO /Al devices showed no consistent variation in the magnitude of leakage current under forward and reverse bias, whereas electrode limited mechanisms would show an exponential dependence on the work function of the metal-insulator interface. Results typical of all three types of conduction were plotted as log I against $V^{\frac{1}{2}}$ but the characteristics were always continuously curved as can be seen in the example given in figure 6.32. Normalisation according to $\frac{J}{T^n} = JT^{-n} \exp \frac{E}{kT}$ against $V^{\frac{1}{2}}T^{-1}$ or $VT^{-1}$ for Poole Frenkel and Pooles Law

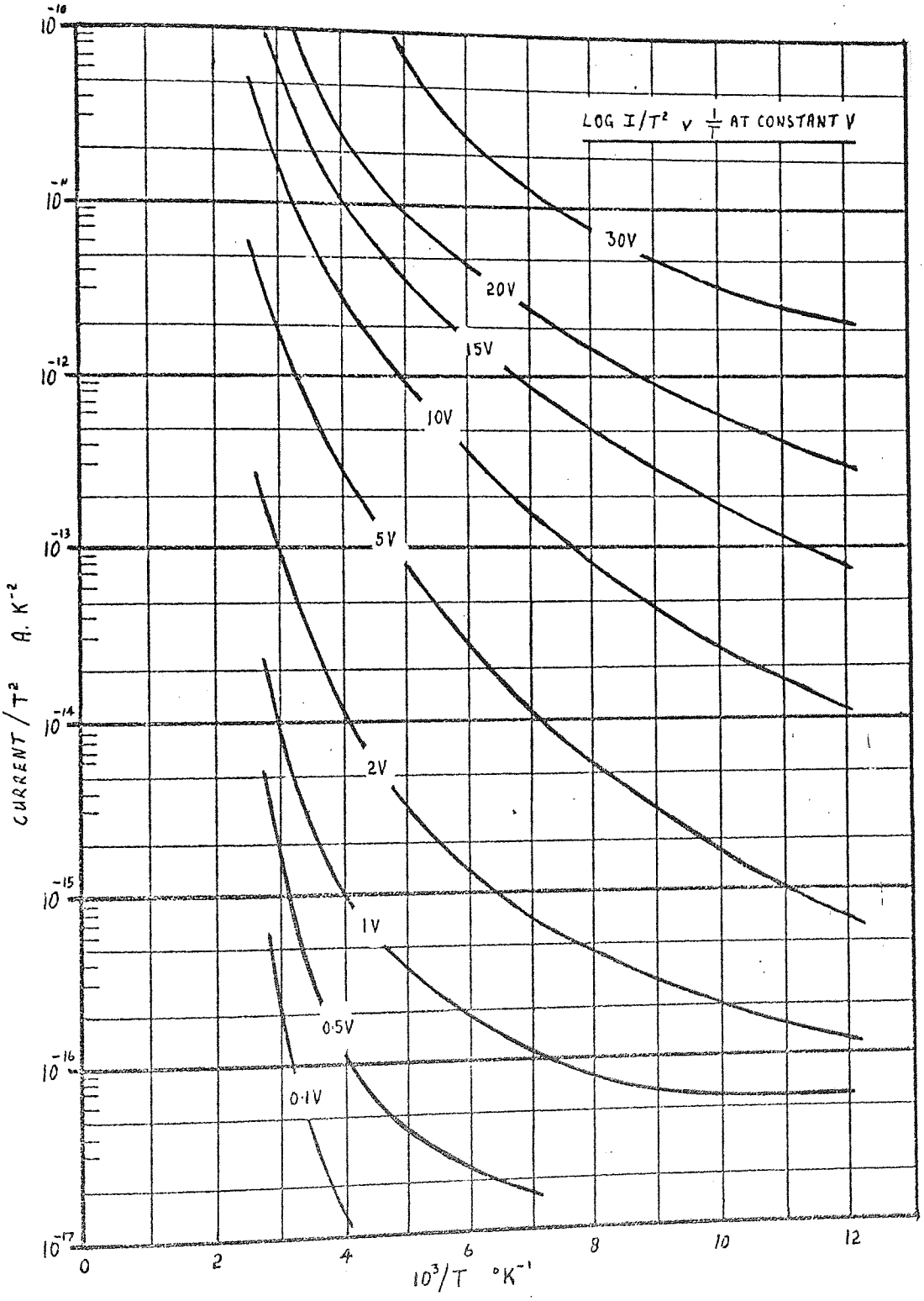
LOG I/T² v 1/T AT CONSTANT V
30V
20V
15V
10V
5V
2V
1V
0·5V
0·1V
CURRENT / T² A. K⁻²
10³/T °K⁻¹
10⁻¹⁰
10⁻¹¹
10⁻¹²
10⁻¹³
10⁻¹⁴
10⁻¹⁵
10⁻¹⁶
10⁻¹⁷
0
2
4
6
8
10
12

Figure 6.31..

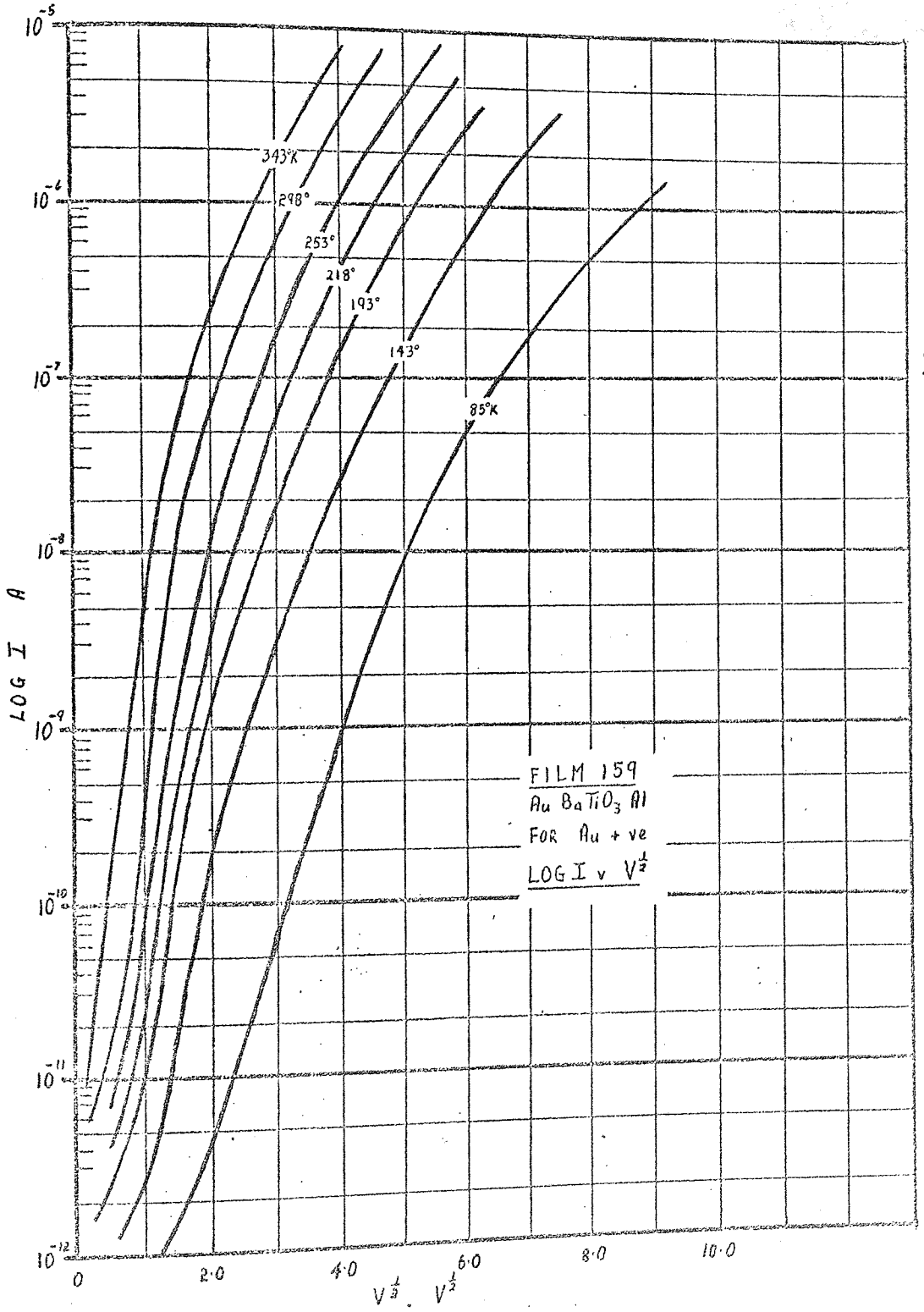
343°K
298°
253°
218°
193°
143°
85°K
FILM 159
Au BaTiO3 Al
FOR Au + ve
LOG I v V½
LOG I A
V⅓ V½
0
2·0
4·0
6·0
8·0
10·0

Figure 6.32

conduction respectively as suggested by Hill (186) was not found to be possible. An activation energy of 0.2 eV, as determined by the temperature dependence, was used but the curves were consistently displaced to lower values of $\phi$ at lower temperatures. It would seem therefore that any process initiating from impurity centres with excitation over a field lowered barrier was not the dominant conduction mechanism. The observation of power law characteristics at high temperatures and fields, with regions giving a current relationship according to $V^{\frac{1}{2}}$ or $V^2$ was suggestive of space charge effects. All modifications of space charge limited conduction (S.C.L.C) also show ohmic regions at very low fields. Conduction in bulk barium titanate is attributed to S.C.L.C. and all metal contacts normally act as electron injectors showing only very slight dependence on the work function of the contact. Gold and aluminium have similar work functions, 4.7eV and 4.2eV respectively, and could explain why no consistent difference was observed between forward and reverse bias currents. S.C.L.C. is very trap dependent, Section 5.B.3.2.3, and is probably the only one mechanism capable of explaining the change in form of the characteristics observed between films deposited under similar conditions. In order to test the conduction against the criterian for S.C.L.C. suggested by Murgatroyd a series of films of thickness varying from 1000 Å to 8000 Å were deposited under the same conditions. As can be seen from the plot shown in figure 6.33 on which the characteristics should superimpose S.C.L.C. was not confirmed. However no consistent trend could be seen in the plot and the same results plotted as the logarithm of current density log J against applied field F showed that J at a constant field was a random function of thickness. The only explanation for this behaviour is that as suggested by the spread in conductivity, the deposition conditions could not be closely enough controlled to produce consistent trap densities and distributions. The trap sensitivity of S.C.L.C. could then explain the large variation of conductivity and the changes in the form of the characteristics. As the temperature of a material, with a high trap density, which exhibits S.C.L.C., is reduced a higher proportion of injected

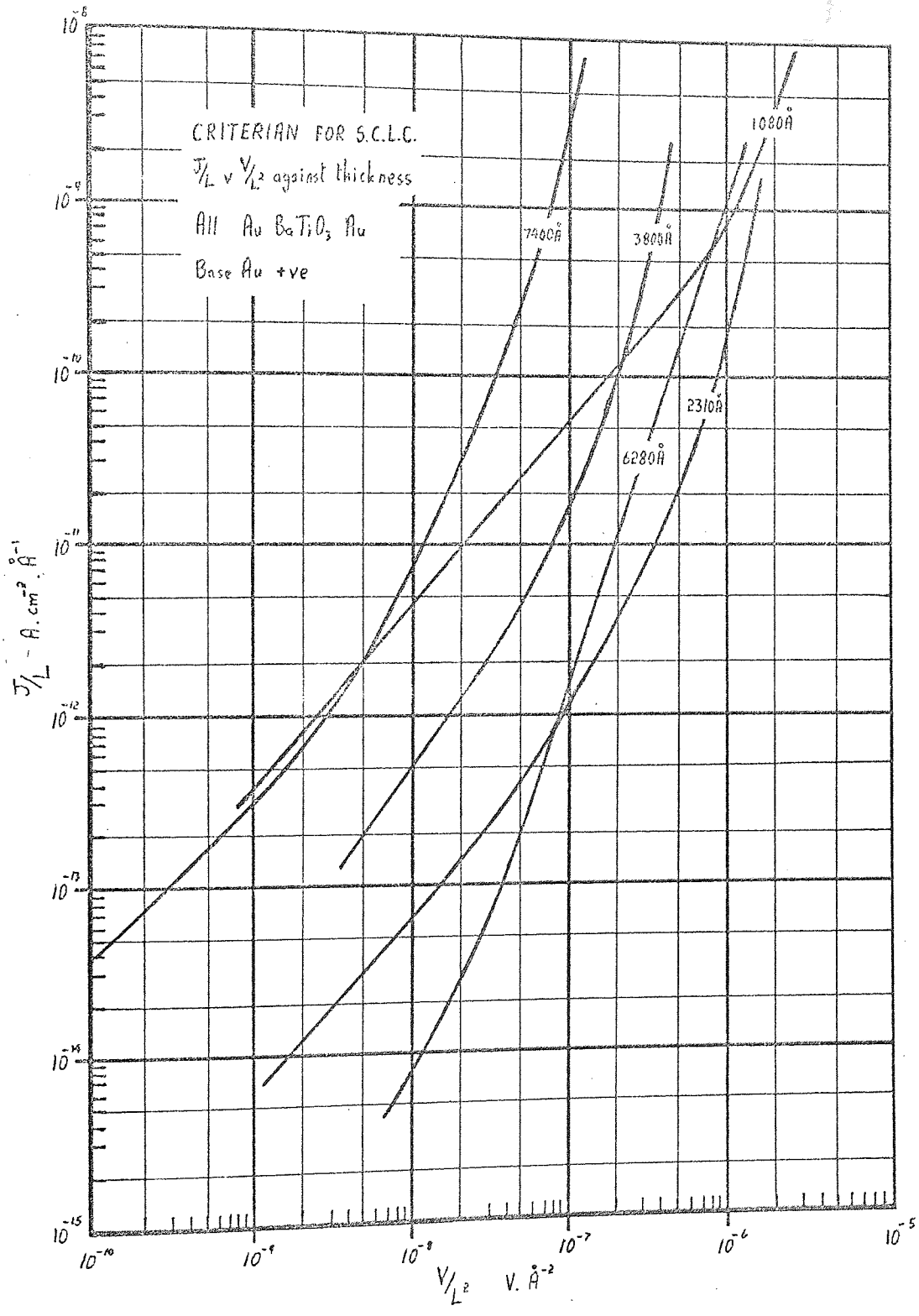


Figure 6.33

Criterian for Space Charge Limited Conduction.

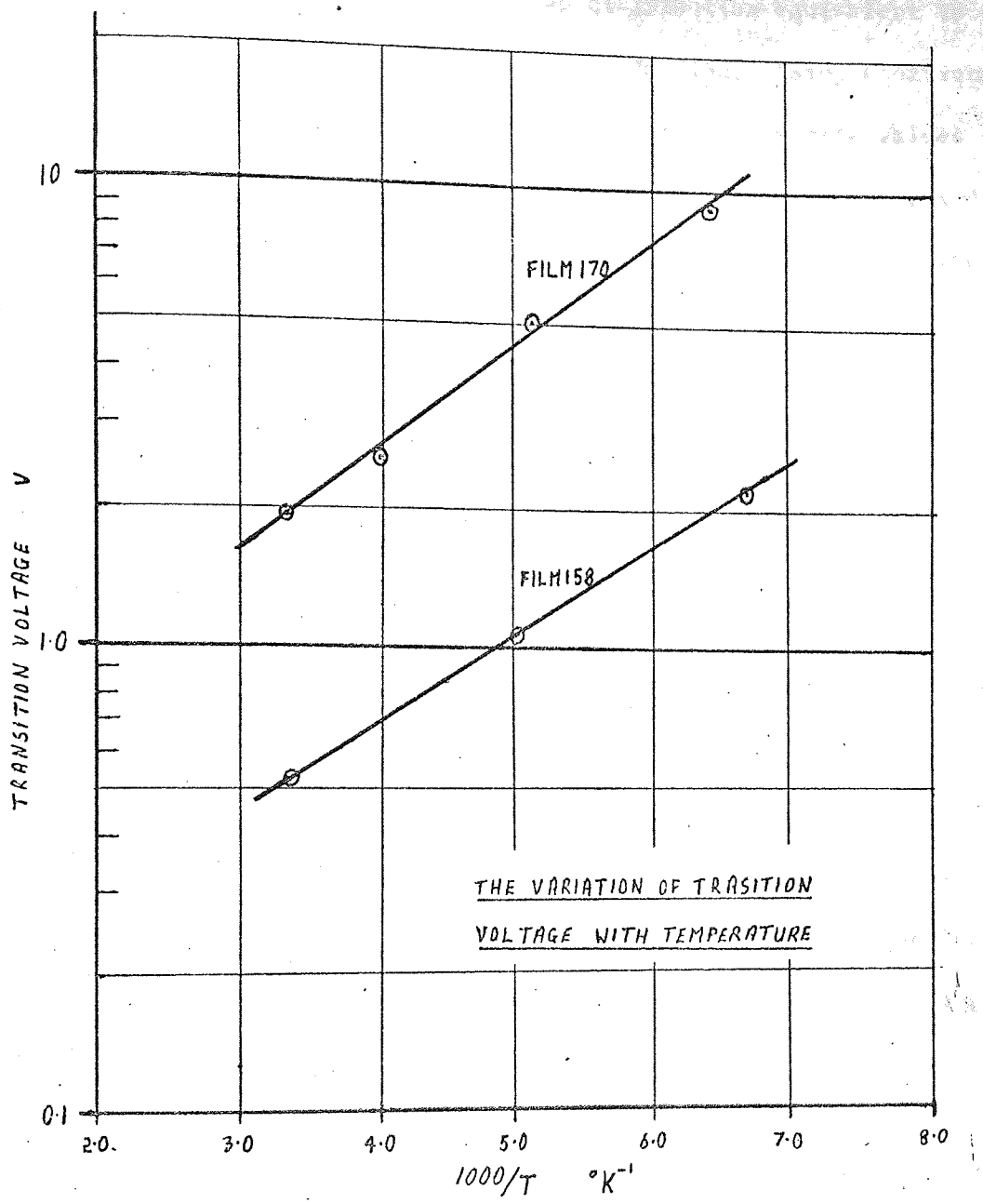
10
1·0
0·1
TRANSITION VOLTAGE V
FILM 170
FILM 158
THE VARIATION OF TRASITION
VOLTAGE WITH TEMPERATURE
2·0
3·0
4·0
5·0
6·0
7·0
8·0
1000/T °K⁻¹

Figure 6.34

carriers will be trapped and the current will fall. A model using only a single level of shallow traps or a trap distribution equivalent to shallow traps appears to be applicable to type 3 conduction. Using equations 5.17 and 5.24, derived from such a simplified model, approximate values of the ratios of the mobility $\mu$ to the thermal free electron density $n_o$ and to the ratio of the free to trapped charge $\theta$ can be calculated. Using the data of figure 6.28 and the measured value of the film permitivity reported in Section C.6.2.1. the values obtained are given below. Absolute values of

$$n_o\mu \sim 10^{9}\ cm^{2}.V^{-1}.sec^{-1} \qquad \frac{n_o}{\theta} \sim 10^{19}\ cm^{-3} \qquad \theta\mu \sim 10^{-10}\ cm^{2}.V^{-1}.sec^{-1}$$

each parameter can not be obtained but table 6.3. gives the values of $n_o$ and $\theta$ consistent with mobility values of 0.001, 0.01, 0.1 and 1.0 $cm^2.V^{-1}.sec^{-1}$. The curvature of the activation energy plot, figure 6.31, suggests that the space charge is not affected by one level of traps but by a distribution of traps. If it is further assumed that the departure from the $V^{\frac{3}{2}}$-$V^2$ law at high fields is equivalent to the onset of a trap filled limit, made less steep by the trap distribution, then a value for the density of traps can be calculated. Using equations 5.23 and thedata of figure 6.28 the trap density is found to be of the order of $10^{20}cm^{-3}$. The voltage $V_{TR}$ at which the transition from the ohmic to the space charge regions occurs should be an exponential function of the reciprical of temperature due to the dependence of $\theta$ on the Fermi distribution. Plots of log $V_{TR}$ against $\frac{1}{T}$ for films exhibiting type 3 conduction were found to show general agreement with this behaviour above about 150°K as shown in figure 6.34. The extension of the ohmic region to higher fields in type 2 conduction could be explained by a higher density of traps. Again using equations 5.17 and 5.24 on the data for film 169 values of the ratio $\frac{n_o}{\theta}$ of the thermally free electron density $n_o$ and the ratio of the free to trapped charge $\theta$ and the product $n_o\mu$ of the film mobility $\mu$ and the free electron density were calculated. These quantities were then used to compute table 6.4. which is equivalent to that given for type 3 conduction and shows that for similar values of $n_o$ and $\mu$ the ratio of free to trapped charge is lower. The characteristics observed for type 1 conduction can be explained in terms of a further increase in

the density of the traps accompanied by their distribution through the energy gap in the manner suggested by Jonscher. At room temperature and above, the ohmic region was equivalent to a value $\mu n_0$ equal to $10^7$ $cm.V^{-1}.sec^{-1}$ and $\frac{n_0}{\theta}$ of $10^{20}$ $cm^{-3}$. These values lead to table 6.5. which gives consistent values of the three parameters over the likely range of values of the mobility. Due to the energy distribution of the traps $\theta$ is not a constant and hardly any temperature variation of $V_{TR}$, the transition voltage at which the characteristics became space charge limited, was observed. The power law region can be explained by an exponential distribution of traps, equation 5.30; where the characteristic temperature is approximately 600°K. The slope of the power law increased with decreasing temperature as one would expect but at a slower rate than the simplified theory predicts. At very low temperatures all three types of conduction gave linear, fairly temperature independent log-log characteristics similar to results found in a number of dielectric films but with somewhat lower exponents. At these low temperatures however the density of thermal free carriers will be negligeable and the trapping efficiency of all centres will be very high such that current flow through the conduction band must be very small. In other films the power law has been explained in terms of a tunnelling process between close packed centres in the band gap, but the theory of such a mechanism is not advanced. In our case it could also be associated with the injection of a small number of carriers into a situation with the distribution of traps equivalent to a trap filled limit.

Relative Values of mobility $\mu$, the thermally free electron density $n_o$ and the ratio of free to trapped charge $\theta$ for the three types of conduction at room temperature.

TABLE 6.3.

Typical of Type 3 Conduction.

| Film 174 Dielectric const. 140 Thickness 7500 Å | | | | |
|---|---|---|---|---|
| $\mu$ $cm^2.V^{-1}.sec^{-1}$ | 0.001 | 0.01 | 0.1 | 1.0 |
| $n_o$ $cm^{-3}$ | $10^{12}$ | $10^{11}$ | $10^{10}$ | $10^{9}$ |
| $\theta$ | $10^{-7}$ | $10^{-8}$ | $10^{-9}$ | $10^{-10}$ |

TABLE 6.4.

Typical of Type 2 Conduction.

| Film 169 Dielectric Const. 70 Thickness 3780 Å | | | | |
|---|---|---|---|---|
| $\mu$ $cm^2.V^{-1}.sec^{-1}$ | 0.001 | 0.01 | 0.1 | 1.0 |
| $n_o$ $cm^{-3}$ | $2\ 10^{12}$ | $2\ 10^{11}$ | $2.10^{10}$ | $2\ 10^{9}$ |
| $\theta$ | $5\ 10^{-9}$ | $5\ 10^{-10}$ | $5\ 10^{-11}$ | $5\ 10^{-12}$ |

TABLE 6.5.

Typical of type 1 Conduction.

| Film 159 Dielectric Const. 55 Thickness 3750 Å | | | | |
|---|---|---|---|---|
| $\mu$ $cm^2.V^{-1}.sec^{-1}$ | 0.001 | 0.01 | 0.1 | 1.0 |
| $n_o$ $cm^{-3}$ | $10^{10}$ | $10^{9}$ | $10^{8}$ | $10^{7}$ |
| $\theta$ | $10^{-10}$ | $10^{-11}$ | $10^{-12}$ | $10^{-13}$ |

6.C.3 Optical Measurements.

The optical constants of barium titanate films exhibiting low and medium permitivity were determined using an ellipsometer as described in Section 4.9. Values of the parameters $\Psi$ and $\Delta$ for a nichrome/gold film substrate were determined after being cleaned by the process used prior to deposition. Using equations 4.9 and 4.10 these results gave a refractive index n of 0.33 and an extinction coefficient k of 2.04 for the gold film compared to reported values of n=0.35 and k=1.62. With these initial conditions, values of $\Psi$ and $\Delta$ were then computed as a function of the thickness of a barium titanate film deposited on the substrate assuming a range of values of the optical constants of the titanate. The titanate films appeared transparent and bulk crystals were translucent so that the absorption of the films is likely to be very small or zero at the wavelength used, 5478 Å. As can be seen from figure 6.35 the initial computation was found to be consistent with values of $\Psi$ and $\Delta$ obtained from amorphous titanate films deposited at room temperature. As film thickness was determined to no better than ± 100 Å one can only say that the amorphous form of the titanate has a refractive index falling between 2.1 and 2.2. The same computation, however, did not fit results obtained from films exhibiting medium permitivity. The results appeared to have a fairly consistent shift of about 4° to lower values of $\Psi$ than those predicted, as though the initial value of $\Psi$ was in error. The optical constants of the substrate were therefore re-examined and found to be a function of the hea treatment to which the nichrome/gold film was subjected. Values of $\Psi$ and $\Delta$ were determined for a gold film before and after being heated in the vacuum chamber to a typical deposition temperature (300°C) for two hours. This resulted in a shift in the values of $\Psi$ and $\Delta$ which were then similar to values obtained from an uncoated area of a substrate which had been masked during deposition. The results are given in table 6.6. and resulted in values for the optical constants of the gold film of n=0.47 and k=1.71. This is a considerable increase in the refractive index which might be explained by diffusion of

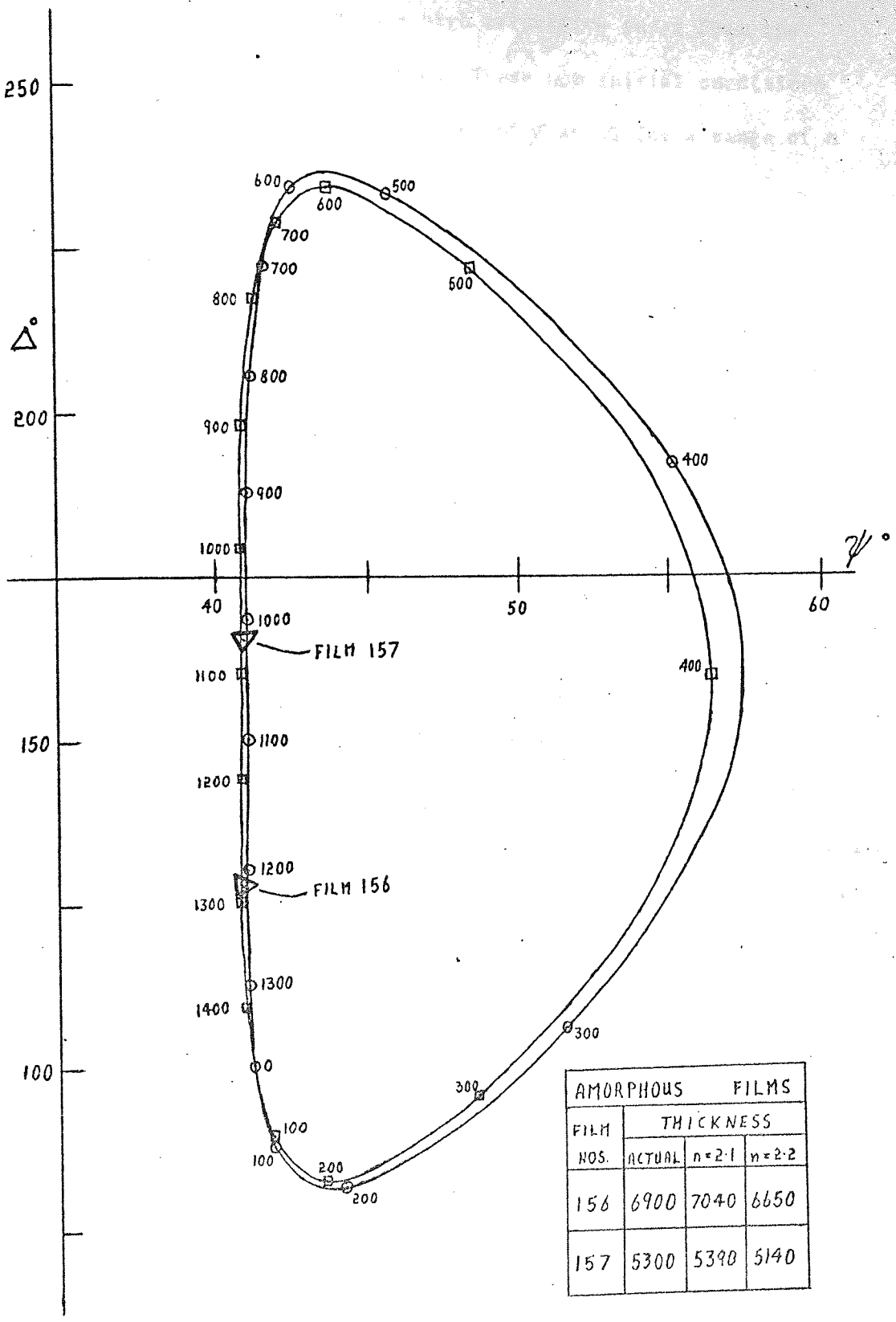


| AMORPHOUS FILMS | | | |
|---|---|---|---|
| FILM NOS. | THICKNESS | | |
| | ACTUAL | n = 2·1 | n = 2·2 |
| 156 | 6900 | 7040 | 6650 |
| 157 | 5300 | 5390 | 5140 |

Figure 6.35.

some active chromium ions with a high refractive index from the nichrome to the surface layers of gold. These new initial conditions were used in a second computation. Values of $\Psi$ and $\Delta$ for a range of n

TABLE 6.6.

Values of the ellipsometric parameters for gold substrates

| Parameter | Cleaned Unheated | Cleaned heated to 300 in vac' for 2 hours | Uncoated Region of used substrate |
|---|---|---|---|
| $\Psi$ | 41.01 | 39.05 | 38.82 |
| $\Delta$ | 102.07 | 95.38 | 94.05 |

with zero absorptionare shown in figure 6.36. As shown in table 6.7 the variation of $\Psi$ and $\Delta$ with extinction coefficient k for values of k below 0.01 was small, except for very thick films. This relative insensitivity of a normally highly sensitive instrument can be attributed to the high value of k exhibited by the substrate film. With extinction coefficients above 0.01 more pronounced effects were observed as plotted in figure 6.37 which shows the locus of $\Psi$ and $\Delta$ with increasing thickness for values of n of 2.2 and k equal to zero and 0.05 respectively. From figure 6.38 it can be seen

TABLE 6.7.

The variation of $\Psi$ and $\Delta$ for non zero absorption.

| | | Extinction coefficient k | | | | |
|---|---|---|---|---|---|---|
| | Film thickness | 0 | 0.001 | 0.015 | 0.01 | 0.05 |
| $\Psi$ | 300 Å | 60.70 | 60.79 | 61.16 | 61.63 | 65.02 |
| | 1000 | 38.30 | 38.24 | 38.04 | 37.77 | 35.80 |
| | 2000 | 39.62 | 39.50 | 39.24 | 38.85 | 35.47 |
| | 4000 | 38.35 | 38.19 | 37.42 | 36.46 | 29.03 |
| $\Delta$ | 300 Å | 115.40 | 115.26 | 114.66 | 113.89 | 106.33 |
| | 1000 | 162.15 | 162.14 | 162.12 | 162.08 | 161.79 |
| | 2000 | 225.7 | 225.74 | 225.87 | 226.05 | 228.10 |
| | 4000 | 110.07 | 110.04 | 109.97 | 109.88 | 108.73 |

that the $\Psi\Delta$ values measured for the films were consistent with a value of refractive index again between 2.1 and 2.2 but there was still a scatter

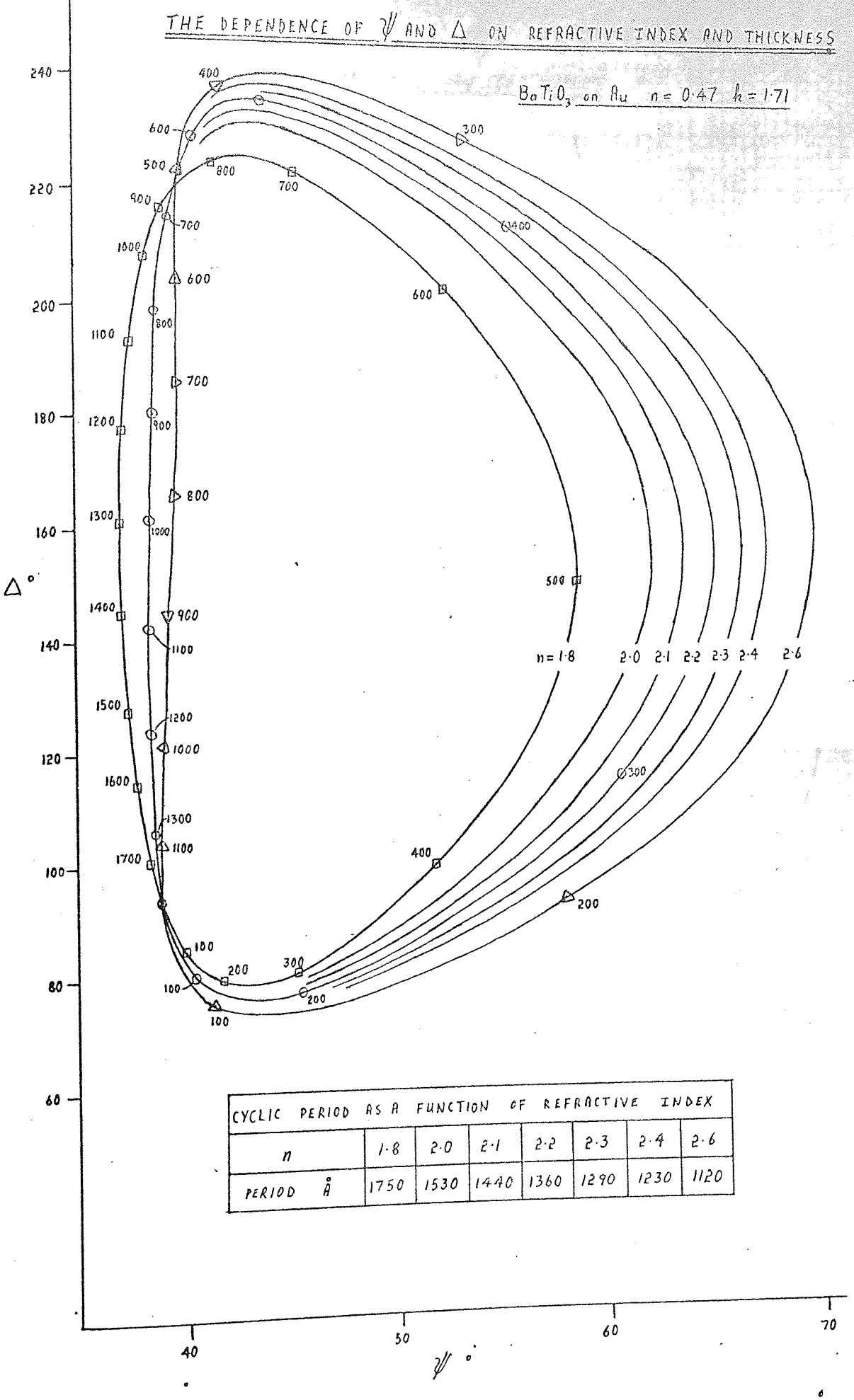


| CYCLIC PERIOD AS A FUNCTION OF REFRACTIVE INDEX | | | | | | | |
|---|---|---|---|---|---|---|---|
| n | 1·8 | 2·0 | 2·1 | 2·2 | 2·3 | 2·4 | 2·6 |
| PERIOD Å | 1750 | 1530 | 1440 | 1360 | 1290 | 1230 | 1120 |

Figure 6.36.

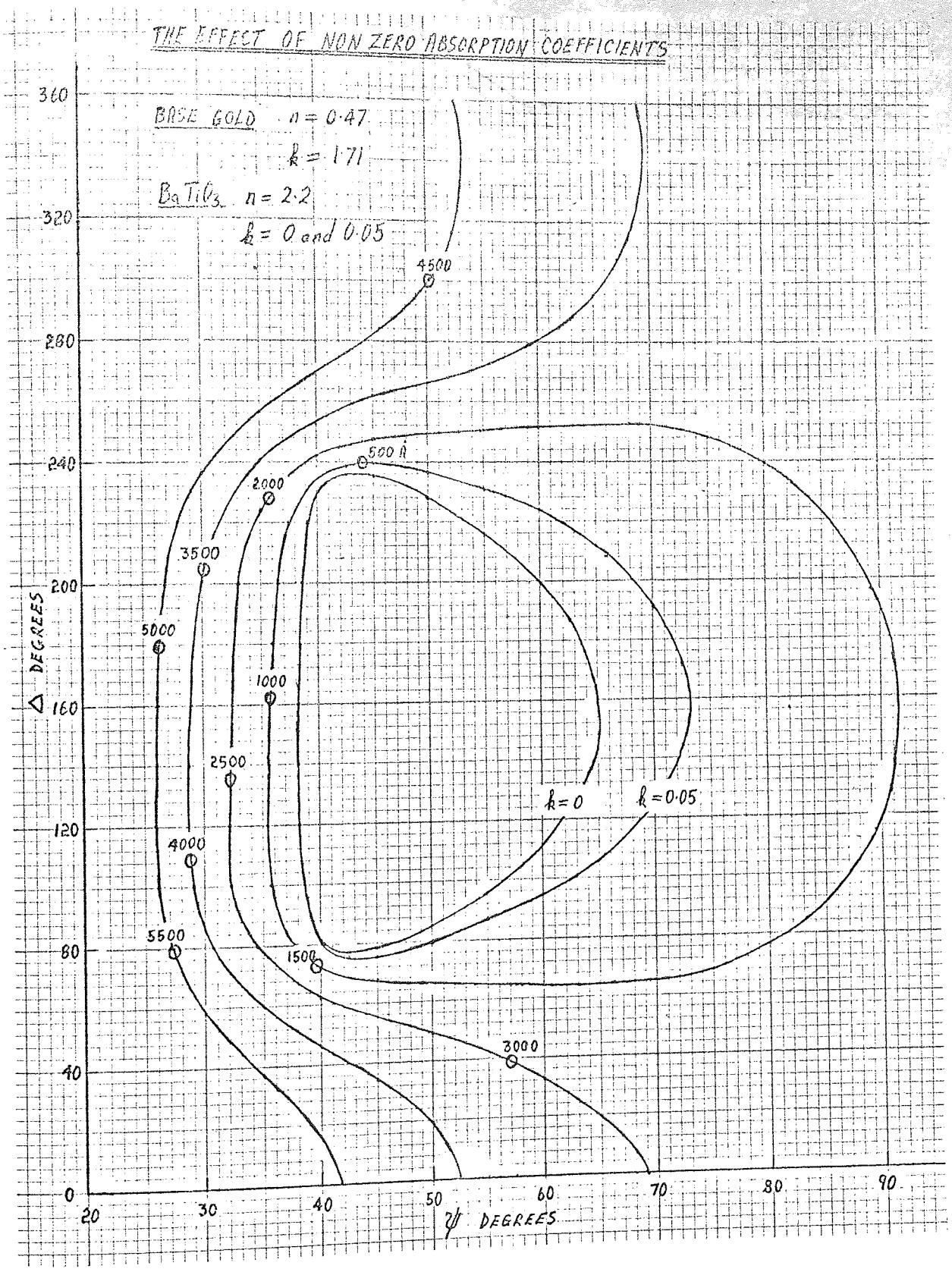
THE EFFECT OF NON ZERO ABSORPTION COEFFICIENTS
BASE GOLD n = 0·47
k = 1·71
BaTiO3 n = 2·2
k = 0 and 0·05
4500
3500
2000
500 Å
5000
1000
2500
4000
5500
1500
3000
k = 0
k = 0·05
Δ DEGREES
ψ DEGREES
0
40
80
120
160
200
240
280
320
360
20
30
40
50
60
70
80
90

Figure 6.37

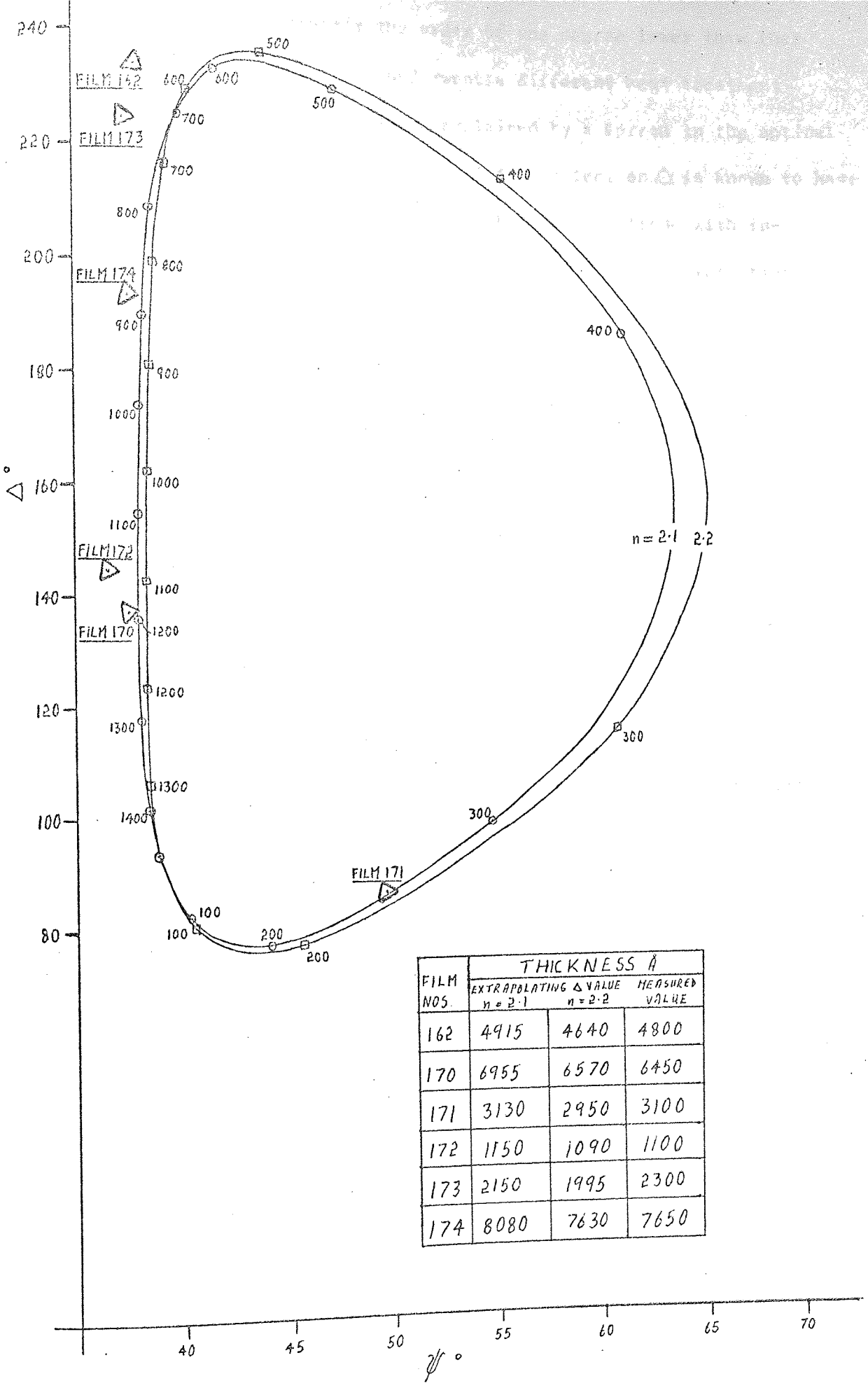


| FILM NOS. | THICKNESS Å | | |
|---|---|---|---|
| | EXTRAPOLATING Δ VALUE n = 2·1 | n = 2·2 | MEASURED VALUE |
| 162 | 4915 | 4640 | 4800 |
| 170 | 6955 | 6570 | 6450 |
| 171 | 3130 | 2950 | 3100 |
| 172 | 1150 | 1090 | 1100 |
| 173 | 2150 | 1995 | 2300 |
| 174 | 8080 | 7630 | 7650 |

Figure 6.38

in the value of $\Psi$, predominantly the order of one degree lower than that predicted. As each substrate film underwent a different heat treatment during deposition some scatter could be explained by a spread in the optical constants of the gold, which while having little effect on $\Delta$ is known to have more affect on $\Psi$ (148). Consequently one might expect a trend with increasing deposition time or deposition temperature but no such variation was observed. A non-zero extinction coefficient also has more affect on on the $\Psi$ parameter and moves the value in the required direction but if $k(\text{Film}) \neq 0$ it is below 0.01 as the results were certainly not approaching th se of figure 6.37. However the insensitivity of the instrument under the conditions used at values of the extinction coefficient below 0.01 defies any determination of a non-zero factor. Changes in structure or orientation are also known to influence the $\Psi$ parameter so a number of measurements were made on one film turning the substrate through an angle of 90° 45° and 30° with respect to normal incidence between each reading. The maximum change in the values of $\Psi$ and $\Delta$ that was observed was 0.1° so orientation effects were negligibly small. A spread of $\Psi$ values has been observed in other ellipsometric measurements made investigating chemisorption on clean silicon surfaces (197). The anomolous values of $\Psi$ obtained were explained by assuming a very thin optically absorbing surface layer (10 Å) which was made less absorbing by the chemisorption process. A similar process could be occuring in the present case particularly as a chemisorption process is also used to explain some film conduction phenomena expecially in films exhibiting medium permitivity (Section 7.3.).

# CHAPTER SEVEN

# COMMENTS AND CONCLUSIONS.

## 7.1. The Sputtering Apparatus.

A vacuum deposition system has been designed and built capable of sputtering in a grounded diode, balanced diode or triode configuration. In the diode configurations the apparatus could be used to deposit sandwich thin film capacitors with evaporated electrodes and had an ultimate vacuum of $2.10^{-7}$ torr. A full R.F. matching network was not employed but the sputtering rate was found to be a function of coil voltage fed to the oscillator and was 30 $Å.min^{-1}$ for barium titanate and 70 $Å.min^{-1}$ for quartz. The deposition rate of barium titanate was not a function of the percentage of oxygen in the sputtering gas, as reported for the deposition of other oxide materials in a similar apparatus (93), but due to the reduction in sticking coefficient at higher temperatures showed a small dependence on the inverse of the substrate temperature.

## 7.2. The Growth and Structure of Sputtered Barium Titanate Films.

All sputtered titanate films were transparent and well adhered to their substrates, although in some cases film crazing was observed. Crazing was particularly severe in films deposited on heated potassium bromide crystals and on carbon films supported by a copper grid. The effect was reduced for films deposited on gold epitaxed on potassium chloride crystals, and completely absent with plain glass or metal coated glass substrates. These variations were explained in terms of the differential thermal expansion between the titanate and the various substrate materials. Crazing of R.F. sputtered barium titanate films has also been reported by Pratt et al (51) and Toombs (52) and in the present investigation was the fundamental reason for the inability to obtain electrical measurements from the crystalline films grown on potassium bromide.

After the completion of the present experimental work a number of papers of interest to the project were published (207-211) and the results will be

titanate films deposited on substrates at ambient temperature were amorphous. Films deposited on a carbon film supported on an electron microscope specimen grid were post annealed and found to crystallise slowly as the temperature was raised over a 40°C interval starting at about 470°C. Due to the energy associated with the sputtering process, the crystallisation temperature observed during deposition on heated substrates was lower, about 450°C, although some crystallinity was present above 420°C. This crystallisation temperature was the same for the apparatus for all amorphous and polycrystalline substrates investigated. This temperature is confirmed by Pratt (207) and is lower than the values reported for evaporated films (500°C)(54). It is clear however that the high atomic energies associated with sputtering compared to evaporation result in no large reduction in crystallisation temperature. Films deposited on single crystal materials behaved differently. Titanate films grown on single crystal potassium bromide at a temperature of 200°C, had an epitaxial fibre texture. This temperature is far below that at which barium titanate crystalline growth has been observed before. The epitaxy was by no means perfect, some polycrystalline phase always being present but the structure showed a strong second order texturing. The crystallinity showed a dependence on rate and deposition temperature consistent with existing theories of epitaxy. However, due to thermal etching and consequent surface roughening of the alkali halide, the structure of films deposited at temperatures above 350°C became progressively less textured. The same effect explained why no crystalline films could be deposited on crystalline gold films epitaxed on potassium chloride. This etching process therefore limited the quality of the titanate films that could be grown on alkali halides.

Crystallographic techniques showed that films grown on gold and aluminium films evaporated on glass were amorphous at deposition temperatures below 450°C, although electrical results indicated that some fundamental change also occurred at 220°C. It is suggested that this is connected with a metastable close range ordered phase of the titanate.

The use of infra red absorption to examine the structure of the films was not

BARIUM TITANATE ON VARIOUS SUBSTRATES.

| SUBSTRATE | VARIATION WITH RATE | VARIATION WITH TEMPERATURE. | | |
|---|---|---|---|---|
| | | BELOW 200°C | 200°- 400°C | ABOVE 400°C |
| GLASS | Rate not varied | Amorphous | Amorphous | Polycrystalline above 450°C |
| AMORPHOUS CARBON FILM | Rate not varied | Amorphous Crystallisation induced by post annealing | Amorphous to 500°C | Polycrystalline above 450°C Film tearing. |
| POTASSIUM BROMIDE SINGLE CRYSTAL | Generally better texture and crystallinity with lower rate | Amorphous | Textured Polycrystalline above 200°C Film crazing | Polycrystal due to deterioration of substrate surface above 350°- 400°C |
| CRYSTALLINE GOLD FILM ON KCl | No Variation Determined | Amorphous | Amorphous Limited film crazing | Substrate surface destruction above 400°C |
| POLYCRYSTALLINE GOLD FILM ON GLASS | No Variation Determined | Amorphous | Undefined Metastable structure above 200°C | Polycrystalline above 450°C |

very sucessful due to the low effective sample densities involved. However, the observation of adsorption bands at 18 and 25.$10^{-6}$m. for the textured films confirmed the presence of $TiO_6$ octahedra.

7.3. The electrical and optical properties of sputtered barium titanate films.

The main object of the project was to obtain electrical measurements on barium titanate films. No measurements were possible on the films deposited on carbon and used for electron microscope investigation or on the films deposited on plain glass, due to the substrate materials. The electrical properties of the films were a function of the film structure which, as discussed above, was strongly dependent upon the nature and temperature of the substrate. Both the permittivity and ferroelectric behaviour of barium titanate are known to be a function of crystallite size (39,212); both effects deteriorating with decreasing grain size. The dielectric constant of hot pressed ultra fine grained barium titanate gives a maximum value at a grain size of 1.$10^{-6}$m and decreases rapidly as the grain size is reduced below 0.05.$10^{-6}$m (213). Some suggestion has been made that ferroelectricity is not possible below a certain very small grain size (56), for example, in a glass/barium titanate system, crystallites of greater than 0.2 $10^{-6}$m were required before ferroelectric behaviour was observed. However, there is no fundamental reason why an array of small crystallites, as one would expect in a thin film, should not behave cooperatively and ferroelectric properties have been observed recently in polycrystalline bismuth titanate (210). In this case the effects varied widely and were a marked function of the type and degree of fibre texture present in the films. It does seem however that a higher dielectric constant will result and ferroelectric behaviour will be more likely the nearer a film approaches perfect crystallinity.

This conclusion immediately suggests the epitaxial deposition of the material and after the initial experiments on glass and carbon film substrates films were deposited with the object of epitaxially growing barium titanate.

Unfortunately while electrical measurements were obtained from amorphous films floated off potassium bromide, none were possible from the crystalline fibre

textured films due to the crazing present in these films as discussed in Section 6B 1.3.2. This led to the deposition of barium titanate on epitaxially grown single crystal gold films. Crystal growth did not occur below a temperature of 400°C and thermal etching of the potassium chloride on which the gold was prepared restricted the use of any higher temperature. As a result of these difficulties and the fact that single crystal substrates are not in general suitable for use in devices, films were deposited on metal films on glass, which allowed detailed electrical measurements to be made.

All amorphous films exhibited a dielectric constant between 10 and 20 and an ac resistivity between $6.10^{9}$ and $3.10^{10}$ ohm.cm. Barium titanate deposited on gold and aluminium films at a temperature below 200°C gave values of permittivity and conductance consistent with these, and the polycrystalline films deposited above 450°C gave permittivity values rising sharply with deposition temperature to dielectric constants of several hundred. This temperature was approaching the temperature rating of the apparatus and the highest dielectric constant measured was 615 for a film deposited at 500°C. However films deposited at temperatures above 220°C and below 450°C exhibited a dielectric constant in the range 100-150, with a sharp transition from the amorphous value covering the temperature range 200-220°C. This suggests that the intermediate values of dielectric constant must be due to some ordering of the films at deposition temperatures above 200°C but no barium titanate, constituent oxide, or any crystal structure could be identified. Similar results have been reported recently by Pratt (207) for barium titanate sputtered onto platinum, although dielectric constants of only 350 were obtained at a deposition temperature of 900°C and no step in permittivity at a deposition temperature of 200°C was reported. This could mean that the gold substrates are of particular significance or could be due to the few results Pratt reported for films deposited below 400°C. Pratt did observe higher dielectric constants but only after post annealing the films to temperatures as high as 1400°C.

As permittivity is a tensor property (Section 1.2.5.), it is a function of crystal direction and arises from the polarizability of the material. In most

materials permitivity shows little dependence on loss and can be said to be a function of four components as in equation 7.1. (198); $\varepsilon_{ex}$ is the entrinsic contribution, $\varepsilon_e$ and $\varepsilon_n$ the electronic and ionic polarizability contributions respectively and $\varepsilon_d$ a contribution due to the deformation of an ion. In polarizable materials $\varepsilon_{ex}$ can be neglected and $\varepsilon_n$ and $\varepsilon_d$ are only applicable beyond

$$\varepsilon = f(\varepsilon_{ex}\, \varepsilon_e\, \varepsilon_n\, \varepsilon_d) \qquad 7.1.$$

infra red wavelengths so that at optical frequencies equation 7.2. holds, where

$$\varepsilon = \varepsilon_e = n^2 \qquad 7.2.$$

$n$ is the refractive index. In oxides in general and in perovskites in particular the crystal structure is such that the contribution to the polarizability due to the deformation of the oxygen ion dominates. It is also the structure of perovskites which gives rise to their ability to possess a resident polarisation, but the high permittivity is not dependent on the ferroelectric behaviour although will be affected by it. As measurements of the refractive index of the films gave values of $n^2$ much less than the determined values of $\varepsilon$ it could be seen using equation 7.2. that the main contribution to the polarizability was ionic in all cases, but particularly in films deposited above 200°C. As $\varepsilon_n$ is a function of the density and type of ions but not their arrangement it is unlikely to vary greatly in any of the films, from the amorphous to crystalline phases, so the large changes in K observed must be due to $\varepsilon_d$. The deformability of the oxygen ion and hence the permittivity of the film deposited will be a function of the degree of crystal structure present in the films, and, due to the tensorial nature of the property, it will also be a function of the type and degree of any fibre orientation. In this way one would expect a considerable increase in the permitivity to accompany the crystallisation and increased crystallite size caused by increasing the preparation temperature above the crystallisation temperature of 450°C. The step in permitivity at 200°C however must also be due to an ordering of the close range structure of the films to a metastable state such that the environment of the oxygen ion causes an increase in its deformation compared to a completely random amorphous structure. The polycrystalline films deposited above 450°C showed a weak peak in permittivity at a temperature some 20-40°C below the

bulk Curie temperature. A blurring of the phase change from tetragonal to cubic structure over the temperature range has been observed with decreasing crystallite size in small barium titanate crystals (214) and in ceramic barium titanate (215). This could explain the generally weak peaks common to this work and most vacuum deposited barium titanate thin films (38,45,207). No ferroelectric behaviour was found even in these polycrystalline films, exhibiting a peak in permittivity. This is in general agreement with the findings of Pratt(51,207),Toombes (52)and Shintani et al (50) for sputtered barium titanate and with results for most evaporated films(45,46,47). Evaporated epitaxial films deposited on sodium fluoride reported by Slack (38) are a notable exception. Pratt (207) did observe hysterisis but only on films of very high permittivity induced by post annealing to 1400°C, while Shintani reported ferroelectric behaviour only for films deposited above 1000°C. Barium titanate is not ferroelectric in its cubic form and the present films were produced at temperatures at which this phase should be formed. As the crystallographic techniques used did not distinguish between the cubic and tetragonal form, it is possible that the cubic structure was in some way frozen into the films thereby inhibiting any ferroelectric behaviour. The observation of a peak in the permittivity/temperature curve however does suggest the presence of some tetragonality in the films. Another possible explanation for the lack of ferroelectric behaviour in titanate films is the existence of surface effects. Variations between a surface layer and the interior of barium titanate crystals have been used to explain some anomolous results in the bulk material (216,217,218). The surface layers are said to be of thickness between $10^{-4}$ and $10^{-6}$ cm (219) and are therefore of the same order of size as the films examined. This could lead to a minimum thickness for the observation of ferroelectricity. In cases where ferroelectric behaviour has been observed in titanate thin films thicknesses have tended to be several times thicker than those used in this present research. It has also been suggested that films are generally more easily affected by grain size, and the associated large surface to volume ratio (207).

The films with dielectric constant in the range 100-150 had poorer electrical properties than the amorphous films of low permittivity. The dc resistivity of

both types of film varied over many orders of magnitude but the amorphous films gave generally lower leakage. This might be expected as more conduction processes, associated with grain boundaries, should be available in structured materials and the higher trap density in the completely amorphous films would reduce the current levels. A.c resistivity was a better behaved function of permittivity giving values of loss ranging from 0.3% for amorphous low K films to 5% for some films with K ~ 150. Even this latter figure is much lower than values reported by Feuersanger et al (48) and Muller et al (54) for evaporated films. The values are comparable to loss determined by Slack (38) only for niobium doped evaporated barium titanate but are similar to the results of Pratt (51) for other sputtered barium titanate films. The temperature variation of the permittivity of the medium K films was fairly linear over the range 20 - 180°C and gave an average temperature coefficient of capacity of 0.1% $C^{-1}$. The dielectric strength appeared only slightly dependent on structure and was found to fall between one and two $10^6$ $V.cm^{-1}$ for all films. This is in the range reported for most dielectric films (198), higher than values determined for evaporated titanate films (48, 54) and, as is often found, an order of magnitude above typical values reported for bulk barium titanate viz 0.02 - 0.12 $10^6$ $V.cm^{-1}$ (194). Pratt (207) reported a value of dielectric strength of $0.9.10^6$ $V.cm^{-1}$ for films deposited at 400-500°C which reduced to $0.5.10^6$ for deposition temperatures of 900°C.

The production of very high dielectric constants or ferroelectric barium titanate films appear to require excessive deposition or post deposition temperatures which would render their use in most applications impossible and denied their production in this research. However the dielectric constants of 100-150 produced at the low temperature of 200°C could be of use in thin film circuitry particularly as the dielectric strength is little reduced at this deposition temperature. Consequently investigations were made into the electrical conduction of the films.

Leakage currents in devices formed from amorphous barium titanate including at least one gold contact were found to increase with time over a long time scale.

The effect was more marked if the gold contact was positive and if oxygen absorption occured at the anode during deposition. The same effect has been observed in bulk barium titanate crystals with gold or silver contacts, when leakage currents have increased for up to ten days (199). Ohmic contacts can be formed more easily on barium titanate than on other capacitor materials because of its relatively small band gap 4.2 eV, much less than that of most insulators (typically 8eV), and resulting in a valence band edge 5eV below vacuum level. The potential step formed at the interface of a metal film and barium titanate is consequently likely to be small and injecting or ohmic contacts would result. Hughes(200) has pointed out that while aluminium and most other metals would form electron injecting contacts, gold, with a work function of 4.8 eV, should form hole injecting contacts on a clean barium titanate surface. However the exposure of the titanate surface to oxygen increases the electron affinity of the insulator(200) and if the effect is large enough the condition for electron injection holds. Double injection is then possible; hole injection from relatively clean areas of the interface and electron injection from patches where the chemisorption of oxygen is considerable(180). The increase of current with time is then explained by an electrochemical process which induces the gold contact to become a more efficient hole injector. From the present observations of the variation in the rate of current rise with field and the slow relaxation times, the electro chemical process must involve the escape of some ionic species over a potential barrier. The conduction was predominantly space charge limited due to hole injection from gold contacts and this explains why the current was lower when the gold electrode of a Au/BaTiO/Al capacitor was made the anode. The current densities observed were lower than found in films where electron injection occured due to the very low hole mobility, the order of $10^{-14}$ $cm^2.V^{-1}.sec^{-1}$, in barium titanate(201). If one applies the shallow trap model to the hole injection and assumes the value of mobility quoted, the trap density is of the order of $5.10^{20}$ $cm^{-3}$. This is high but not unfeasible in an amorphous material. Capacitive devices formed from medium-K films showed no variation of leakage current with time. The explanation for this lies in the fact that the chemisorption of oxygen on the titanate sur-

face is enhanced at higher temperatures (200). The higher temperature used in the preparation of medium K films could therefore increase the electron affinity of the insulator so as to make the contact totally electron injecting. The increased substrate temperature is also known to affect the nature of the gold film as indicated by ellipsometric measurements. The lack of hole injection would then explain the absence of the effect. The form of the I.V. characteristics of these films was a function of the dc conductivity which varied over six orders of magnitude for films deposited under similar conditions. The characteristics were again explained in terms of space charge limited conduction but due to electron injection and under the influence of traps. Changes in the density and distribution of the traps then explained the variation in the form of the characteristics and the spread in dc conductivities of the films. Trap densities assuming the equation derived from the simple model of Lampert were typically $5.10^{19} cm^{-3}$. Space charge limited conduction (179) and other space charge effects (219) are well known in bulk barium titanate with trap densities somewhat less but of the same order as observed in the films and space charge effects have also been reported in other barium titanate thin films (38). The refractive indeces of amorphous low K and medium K films were the same; falling between 2.1 and 2.2. The absorption coefficient was measured as less than $2.10^{3} cm^{-1}$, but the extinction coefficient was indeterminate below 0.01. Single crystal barium titanate has a refractive index (Section 1.2.6.) that is a function of temperature but at room temperature is 2.4 (202). The lower value observed for films is probably due to the very small crystallite sizes reported.

## 7.4. Suggestions for Further Work.

Refinements could be made to the deposition system to facilitate a higher rate and more controlable power input. This could include a matching network, following the work of Healey et al (203) and others (204,205,206) and the use of a standing wave meter. The discovery that barium titanate grows in an epitaxially textured manner on single crystal potassium bromide at a temperature of only 200°C is of interest and worthy of further investigation. It seems clear that barium titanate films, especially of thicknesses normally associated with

thin film circuits, cannot be produced with very high dielectric constants and ferroelectric properties without the use of temperatures over 1000°C. However applications except for discrete chip capacitors as suggested by Pratt (207) would limit the deposition temperature greatly below this. The observation of a short range ordered form of barium titanate with dielectric constant in the range 100-150 at temperatures below 250°C offers some application in thin film circuits. The loss and temperature coefficient of capacity of the films are relatively high limiting its use to instances where higher capacity per unit area is required but with less critical leakage requirements. Further work would be required to control film properties, yield and breakdown strength more closely. The dc conductivity and dissipation could be reduced by the introduction of niobium or antimony into the films. This could be done easily by making a target with the required level of impurity dispersed in the powder before firing.

# APPENDIX 1

## CONDUCTANCES OF THE COMPONENTS USED IN THE CONSTRUCTION OF THE VACUUM SYSTEM

### High Vacuum Components.

The following list of pumping column conductances were obtained from manufacturers literature or estimated from tables given by Dushman (122). Taking the diffusion pump speed $S_v$ as 600 lt. $sec^{-1}$ and using equations (1) and (2)

| Components | Conductance lt.$sec^{-1}$ |
|---|---|
| Diffusion pump guard ring | 700 |
| DCB6 thermoelectric baffle | 690 |
| 6" Spacer | 1670 |
| QSB6 Butterfly valve | 1670 |
| NTM6A nitrogen trap | 550 |

relating conductancies $C_1$-$C_n$ in series and their effect on pumping speeds the effective pump speed at the chamber outlet would be 125 lt.$sec^{-1}$. This

$$\frac{1}{C} = \frac{1}{C_1} + \frac{1}{C_2} + \frac{1}{C_3} \cdots\cdots \frac{1}{C_n} \quad (1)$$

$$\frac{1}{S_e} = \frac{1}{S_v} + \frac{1}{C} \quad (2)$$

pumping speed should produce, using equation (3), an ultimate pressure $P_o$ of

$$P_o = Q_L S_e \quad (3)$$

$10^{-7}$ torr with a total leak and outgassing rate $Q_L$ as high as $1.10^5$ torr.lt. $sec^{-1}$. This ultimate pressure was within the specifications required for the pumping system.

### Fore-line components.

The relevant conductances of components in the fore line are given below

| | |
|---|---|
| Fore line trap | 80 lt. $sec^{-1}$ |
| Complete backing line pipework | 1.6 " |
| Complete roughing line pipework | 1.5 " |

again estimated from tables given by Dushman (122). Using equations 1 and 2 and taking the roughing pump speed as 290 lt.$sec^{-1}$ the effective pump speed at the chamber outlet would be 1.4 lt.$sec^{-1}$ and at the diffusion pump backing outlet 1.5 lt.$sec^{-1}$. With a total chamber volume of 33 lt and using the

pumping time relationship given in equation 4 where $P_1$ and $P_2$ are initial

$$t = \frac{V}{S_e} \log_e \frac{P_1}{P_2} \qquad 4$$

and final pressures respectively the system should reduce the chamber pressure to $10^{-1}$ torr in approximately $3\frac{1}{2}$ minutes. The time might well be up to one third longer due to outgassing and the variation of the pump speed over the five decades covered by the pump down. During sputtering the chamber pressure has to be maintained at a pressure up to $4\ 10^{-3}$ torr of argon which would represent a throughput of 0.6 torr lt.sec$^{-1}$ that the pump is required to pump away. With the effective pump speed of only 1.5 lt.sec$^{-1}$ the backing pressure will rise, using equation (3), to 0.3 torr which is within the limit recommended for the diffusion pump to operate satisfactorily.

APPENDIX 2

DESIGN OF THE CRYOSTAT SUBSTRATE HEATER

Figure 1 shows a schematic diagram of the proposed heater arrangement for maintaining intermediate temperatures. The dimensions finally used were obtained in the following manner. Firstly a number of assumptions

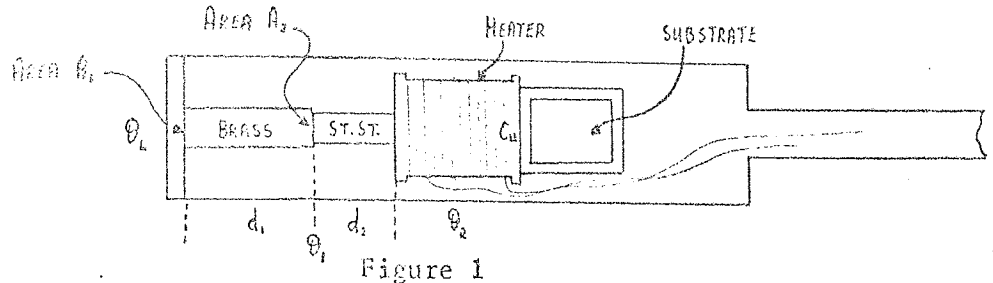

Figure 1

were made to enable an approximate calculation, as described under.

1) It was assumed that all of the substrate and heater section made of copper was at the same temperature.

2) With the heater on the temperatures $\theta_1$ and $\theta_2$ rise until $\frac{dQ}{dt}$ the loss of heat down the brass/stainless steel support rod to the liquid nitrogen at temperature $\theta_L$ is exactly balanced by the power input IV to the heater.

3) Convection losses are neglected.

4) Radiation losses are also neglected.

The last approximation introduces an error of about 10% into the calculation when maintaining a temperature of 300°K and the error would be correspondingly less at lower temperatures. Despite this error the calculation enabled approximate working values of the heater voltage to be determined. The assumptions contained in 1 to 4 mean that equation (1) holds

$$\frac{dQ}{dt} = IV \qquad (1)$$

Now the heat flow down the brass and stainless steel sections of the support rod, given by equations (2) and (3) respectively must be the same and can be

$$\text{BRASS} \quad \frac{dQ}{dt} = K_B \frac{A_1(\theta_1 - \theta_L)}{d_1} \qquad (2)$$

$$\text{ST.ST.} \quad \frac{dQ}{dt} = K_{St} \frac{A_2(\theta_2 - \theta_1)}{d_2} \qquad (3)$$

solved simultaneously, eliminating $\theta_1$ and thereby deriving the relationship between IV and $\theta_2$ given in equation (4). Using values of the thermal conduct-

$$IV\left(1 + \frac{K_{ST} A_2 d_1}{K_B A_1 d_2}\right) = \frac{K_{ST} A_2}{d_2}(\theta_2 - \theta_L) \qquad (4)$$

invities of brass and stainless steel of 0.9 and 0.15 joule.$cm^{-1}$ $sec^{-1}$ $°C^{-1}$ respectively the heater power required for various dimensions could be determined.

REFERENCES.


1. Weiner P.K. Proc. I.R.E. 50 1462 (1962)

2. Weiner P.K. The Physics of Thin Films. Ed. Haas Thun. Academic Press (1964)

3. Zuleeg R. Solid State Electronics 6. 193 (1963)

4. Shallcross F.V. Proc I.E.E.E. 51. 851.

5. Barkan H and Weiner P.K. R.C.A. Review 24 153 (1963)

6. Abraham D and Poehler T.O. Int J. Electronics 19. 165 (1965).

7. Kunig H.E. Solid State Electronics 11 335 (1968)

8. Blois M.S.Jr. J.App Phys 26 975 (1955).

9. Smith D.O. J.App Phys 29 264 (1958)

10. Rosenberger G.M. Solid State Electronics 1 4 388 (1960)

11. Foster N.F. Coquin G.A. Rozgonyi G.A. Vornatta F.A. I.E.E.E. Trans. on Sonics and Ultrasonics. Vol SU-15 No 1 p 28 (1968)

12. Weber R. Rev. Sci. Inst. 37 955 1966.

13. Mallion R.M. Walsh D.J. Winslow D.K. App. Phys. Lett. 10 9 (1967)

14. Harrop P.J. Campbell D.S. Thin Solid Films 2 273 (1968)

15. Anderson J.R. Electl. Engr. 71 916 (1952).

16. Peacock R.V. Crystalline Barium Titanate as a digital store medium. Thesis Univ. London 1959.

17. Burfoot J.C. Proc. Inst. Elect. Eng. 109 B Suppl 22 362 (1962)

18. Kaufman A.B. Electronics p47 25th Aug. (1961).

19. Burfoot J.C. Ferroelectrics p 13 pub. Van Nostrand (1967).

20. McQuarrie M. Bull Am Ceramic Soc. 34. (195 ).

21. De la Perelle. I.P.Meeting on R.F.sputtering September 1968

22. Johnson K.M. J. App. Phys. 33 2826 (1962).

23. DiDomenico M. Johnson D.A. Pambell R.H. J. App. Phys. 33. 1697 (1962).

24. Billeter T.R. Giarola A.J. Bjorkstam J.L. J.App.Phys. 35 2159 (1964);

25. Wohlers M.R. Leib K.G. J.App.Phys. 35.2311 (1964).

26. S.E.Cummins Proc I.E.E.E. 55 1536, 1537 (1967).

27. Smolenskii G.A. Krainik N.N. Soviet Physics Uspekhi 12 2 271 (1969)

28. Nye J.F. Physical Properties of Crystals. Clarendon Press Oxford (1957)

29. Sawyer C.B. Tower C.H. Phys. Rev. 35. 269 (1930).

30. Chynoweth A.G. J. App. Phys. 27. 78. (1956).

31. Burfoot J.C. Latham R.V. Br.J.App. Phys. 14. 933 (1963).

32. Burfoot J.C. Ferroelectrics. Van Nostrand p. 7

33. Merz W. Phys. Rev. 76. 1221 (1949).

34. Triebwasser S. I.B.M. J.Res.Dev. 2. 212 (1958).

35. Busch G. Plurey H. Merz W. Helv. Phys. Acta 21 212 (1948).

36. Meyerhofer D. Phys. Rev. 112 413 (1958).

37. Kay H.F. Vousden P. Phil. Mag. Ser. 7. 40 1019 (1949).

38. Slack J.R. Deposition and Properties of Barium Titanate. Thin Films Thesis Univ. of London (1970).

39. Bursian E.V. Zaikovskii O.I. Smirnova N.P. Shapkin V.V. Proc.Int. Meeting on Ferroelectrics Prague 1 387 (1966).

40. Luré M.S. Dokl 128. 73 1959.

41. DeVries R.C. J.Am. Ceramic Soc. 45. 225 (1962)

42. Hultquist A.E. Sibert M.E. Nasa C.R. 364 (1966).

43. Bursian E.V. Smirnova N.P. Fiz Tverdogo Tela 4 1675 (1962).

44. Feldman C. Rev Sci. Inst. 26, 5, 463 (1955).

45. Sekine E. Toyoda H. Rev. Elec. Comm. Lab. Japan 10 9-10 457 (1962)

46. Masson S. Minn S. Comptes Rendus Acad. Sci. Paris 268 Ser.B. 1668

47. Müller E.K. Nicholson B.J. Francombe M.H. Electrochem. Tech. 1. 5-6 158 (1963).

48. Feuersanger A.E. Hägenlocher A.K. Solomon A.L. J.Electrochem. Soc. 111 12 1387 (1964).

49. Vu Huy Dat R. Baumberger C. Phys. Stat. Sol. 22. K67 (1967)

50. Shintani Y. Tada O. J. App. Phys. 41 2376 (1970).

51. Pratt. I.H. Firestone S. J. Vac. Sci. Tech. 8.1. 256 (1971).

52. Toombs P.A.B. Proc. Brit. Ceram. Soc. 10 237.(1968).

53. Brown V. The Electrical Optical and Infra Red Properties of BaTiO Thin Films Thesis Univ of Michigan (1966).

54. Müller E.K. Nicholson B.J. Turner G.L'E. J.Electrochem Soc. 110 9 969 (1963).

55. Shibata H. Toyoda H. J.Phys. Soc. Jap. 17 404 (1962).

56. Ivanchik I.I. Sov. Phys. Sol. St. 3 2705 (1962).

57. Thun R. Ramsey J.B. Trans. 6th Nat.Vac.Symp. A.V.S. 192 (1959)

58. Varian "c" Gun Varian Associates Ltd Vacuum Products Division

59. Heavens O.S. J. Sci. Inst. 36. 95.

60. Holland L. Brit. Pat. Nos 754 102.

61. Barry R.W. Hall P.M. Harris M.T. Thin Film Technology. Van Nostrand.

62. Grove,W.R. Phil. Trans. Roy. Soc. (London) 142 87 (1842).

63. Wright A.W. Am.J.Sci. Arts 13 49 (1877)

64. Crookes W. Proc. Roy. Soc. (London) 50 88 (1891)

65. Von Hippel A. Ann. Physik, 81 1043 (1926).

66. Wehner G.K. Phys. Rev. 102 690 (1955).

67. Wehner G.K. J. App. Phys. 31 177 (1960)

68. Stark F. Z. Electrochem. 15 509 (1909).

69. Silsbee R.H. J. App. Phys. 28 1246 (1957).

70. Penning F.M. Electrical Discharges in Gases Macmillan (1957)

71. Ivanov R.D. Spivak. G.V. Kislova G.K. Izv. Akad. Nauk. S.S.S.R. Ser Fiz 25 1524 (1961).

72. Huss W.N. S.C.P. and Solid State Tech. 12 50 (1966).

73. Nickerson J.W. Moseson R. S.C.P. and Solid State Tech. 12 (1964)

74. Seeman J.M. Pro. 6th AM. Structures and Mat. conf. (1965).

75. Brodie I. J.Vac. Sci. Tech. 6. 5. 795 (1969).

76. Muly E.C. Aronson A.J. Proc. 4th Int. Vac. Cong. (1968).

77. Holland L. Vacuum Deposition of Thin Films. Chapman and Hall. Ionic Bombardment Cleaning.

78. Frerichs R., J.App. Phys. 33 1898. (1962).

79. Maissel L.I. Schaible P.S. J. App. Phys. 36 237 (1965).

80. Layton C.K. Ph.D. Thesis Univ. of London (1968).

81. Theurer H. Hauser J. J. App. Phys. 35. 3 (1964).

82. Kay E. Advances in Electronics and Electron Physics 17 245 (1962)

83. Schwartz N. Trans. 10th Nat.Vac. Symp. A.V.S. 325 (1963).

84. Puls F.N. Hensler D.H. Ross A.R. App. Phys. Lett. 10 7 199 (1967)

85. Hollands E. Campbell D.S. J. Mat. Sci. 3. 544 (1968).

86. Bickby P. Campbell D.S. Le Vide 99 214 (1962).

87. Lakshmanan T.K. Mitchell J.M. Trans. 10th Nat.Vac.Symp. A.V.S. 335 (1963)

88. Noreika A.J. Francombe M.H. Zeitman S.A. J.Vac.Sci. Tech. 6 194 (1969)

89. Wehner G.K. Advances in Electronics and Electron Physics 7 239 (1955)

90. Anderson G.S, Mayer W.N. Wehner G.K. J.App. Phys. 33 2991 (1962)

91. Davidse P.D. Maissel L.I. Trans 3rd Int.Vac.Cong.(Stuttgart)(1965).

92. Butler H.S. Kino G.S. Phys. Fluids 6 1346 (1963).

93. Davidse P.D. Maissel L.I. J. App. Phys. 37 2 574 (1966).

94. Holland L. Putner T. Jackson G.N. J.Sci.Inst.(J.Phys.E.) Ser. 2 1 32 (1968).

95. Toombs P.A.B. Brit.J.App. Phys. (J.Phys.D) Ser 2 Vol 1 662 1968

96. Kay E. Trans. Conf. and School Elements Techniques and Applications of Sputtering (1969).

97. Aanak J.J. Trans. Conf. Sch. Elements Tech' Appl' Sputtering (1969)

98. Moulton C. Nature 195 793 (1962).

99. Kay E,Sawatzkye E. J. App. Phys. 39 4700 (1968).

100. Chapman B.N. Thesis Univ. of London (1968).

101. Neugebauer C.A. Physics of Thin Films. Vol.2 Ed.G.Hass and R.E.Thun (1964) Academic Press.

102. Anderson J.C. Ed.Uses of Thin Films in Physical Investigations. Chapman and Hall (1966).

103. Single Crystal Thin Films. Ed.M.H. Francombe and H.Sato. Pergamon Press (1964).

104. Krikorian E. Sneed R.J. Trans. 10th Nat, Vac. Symp. A.V.S. 368 (1963).

105. Layton C.K. Cross K.B. Thin Solid Films. 1 (1967).

106. Wolsky S.P. Piwkowski T.R. J. Vac. Sci. Tech. 2 97 (1965).

107. Pliskin W.A. Davidse P.D. Lehman H.S. Maissel L.I. I.B.M. J.Res. Dev 461 (1967).

108. Putner T. Thin Solid Films. 1 165 (1967).

109. Probyn B.A. Vacuum 18 5 253 (1968).

110. Farkass I. Barry E.J. Vac. Symp. Trans. A.V.S. (1960)

111. Carpenter L.G. Vacuum Technology Hilger (1970).

112. Laegreid N. Wehner G.K. J. App. Phys. 32 365 (1961).

113. Batzer T. H. Ryan J.F. 10th Nat.Vac. Symp. A.V.S. 166 (1963).

114. A.H.Beck Ed. Hand Book Vacuum Physics Vol 3 Pergamon Press.

115. Ceramic Development Company Limited

116. Dayton B. B. Proc 6th Nat. Vac. Symp. A.V.S. 101 (1959).

117. Pirani Yarwood Principles of Vacuum Engineering Chapman and Hall

118. Edwards High Vacuum Information Sheet 09C171/2 Edwards High Vacuum Ltd. Crawley Sussex.

119. Yarwood J. High Vacuum Technique Chapman and Hall.

120. Speedivac Data Sheet 05626/1 Edwards High Vacuum Ltd. Manor Royal Crawley Sussex.

121. Cruickshank R.J. Pvt. Comm.

122. Dushman S. Scientific Foundation of Vacuum Technique Wiley (1949)

123. Baker M. Laurenson L. Vacuum 16 633 (1966).

124. Holland L. Laurenson L. Baker M.A. 13th Nat.Vac.Symp. A.V.S. (1966).

125. Olejniczak J.S. 4th Int. Vac Cong. Inst.Phys. Phys. Soc. (1968).

126. Baker M.A. Holland L. Laurenson L. 3rd Int.Conf.on Fluid Sealing (Cambridge) (1967).

127. Hockley D.A. Bull C.S. Vacuum 4 40 (1954).

128. Laurendon L. Holland L. Baker M.A. Symp. on Lubrication in Hostile Environment (1969).

129. Baker M.A. Staniforth G.H. Vacuum 18 17 (1968).

130. Fulker M.J. Vacuum 18 445 (1968),

131. Bailey J.R. Handbook of Vacuum Phys. Vol 3 Ed. A.H. Beck. Pergamon Press (1964).

132. Barton R.S. Govier R.P. J. Vac. Sci. Tech. 2. 113 (1965).

133. Roth A. Vacuum Sealing Techniques Pergamon Press (1966).

134. Smith C.J. Electricity and Magnetism p 313 Edward Arnold.

135. Dayal M. Mullard Tech. Comm. Vol 7 No 68 (1964).

136. Hughes C. Pvt. Comm. Lucas Group Research Centre Solihull.

137. Radio Amateurs Handbook(1965).

138. Tsui R.T.C. 4th Int. Vac. Cong. Manchester (1968).

139. Healey D.J. Lariente M. 13th Nat. Vac. Symp. A.V.S. (1966).

140. Eccleshall J. J. Sci. Inst. (J.Phys.E.) Ser 2 1 (1968).

141. Chopra K.L. Thin Film Phenomena McGraw Hill (1969).

142. Matthews J.W. Phil Mag. 12 1143 (1965).

143. Love R.C. Attributed by Holland L. Vapour Deposition of Thin Films. Chapman and Hall.

144. Servini A. DC Conduction in Insulating Thin Films. Thesis Univ. of London (1968).

Ebden A.J. Pvt. Comm. Lucas Group Research Centre Shirley.

145. Cruickshank R.J. Thesis Univ. of Aston(1970)

146. Tolansky S. Multiple Beam Interferometry of Surfaces and Films. Oxford Univ. Press (1948).

147. O'Shea K. Thesis Univ. of Aston (1971).

148. Archer R.J. Manual on Elipsometry. Gaertner Scientific Corporation

149. Heavens O.S. Optical Properties of Thin Films. Butterworth (1955).

150. Jones R.E. Zuegal M.A. Schwartz G.G. 4th Int.Vac.Cong.(1968). (Manchester)

151. Chopra K.L. Phys. Stat. Sol. 32. 489 (1969).

152. Rhodin T.N. Walton D. Single Crystal Films.Ed.Francombe M.H. Sato H Pergamon Press p31 (1964).

153. Walton D. J. Chem. Phys. 37 2182 (1962).

154. Sloope B.W. Tiller C.O. J.App. Phys. 32. 1331 (1961).

155. Chopra K.L. Thin Film.Phenomena McGraw Hill (1969) p 288.

156. Krikorian E. Single Crystal Films. Ed.Francombe M.H. Sato H. Pergamon Press p. 113 (1964).

157. Chopra K.L. Randlett M.R. J.App. Phys. 39 1874 (1968).

158. Moll A. Z.Angew Phys. 10 410 (1958).

159. Roder O. IBID 12 323 (1960).

160. Chopra K.L. App. Phys Lett. 7 140 (1965).

161. Joffe A.F. Phys. Semiconductors Izd. Akad. Nank SSSR M-L (1957).

162. Cohen M.H. J. Non Cryst. Sol. 4 391 (1970)

163. Johnscher A.K. Thin Solid Films. 1 213 (1967).

164. Murphy E.L. Good R.H. Phys. Rev 102 1464 (1956).

165. Tantraporn W. Solid State Electronics 7 81 (1964).

166. Simmonds J.G. Phys. Rev Lett. 15 (967) (1965).

167. Hill R.M. Thin Solid Films. 1 39 (1967).

168. Simmonds J.G. Phys. Rev. 155 657 (1967).

169. Hartle J.L. J. App. Phys. 39 4871 (1968).

170. Hill R.M. Thin Solid Films. 8 R 21 (1971).

171. Boon M.R. Thin Solid Films. 8 R 5 (1971).

172. Hall E.B. Thin Solid Films.8 263 (1971).

173. Simmonds J.G. Phys. Rev. 166 912 (1968).

174. Lampert. M.A. Phys. Rev. 103 1648 (1956).

175. Rose A. Phys. Rev. 97 1538 (1955).

176. Murgatroyd P.N. J. Phys. D. 3 151 (1970).

177. Lampert. M.A. Rept. Prog. Phys. 27 329 (1964).

178. Murgatroyd P.N. J.Phys. D. (App. Phys.) 3 1488 (1970).

179. Tredgold R.H. Space Charge Conduction in Solids Elsevier (1966).

179. Lampert M.A. Phys. Rev. 125 1 (1962).

180. Thomas R.T. J. Phys. D. App. Phys. 3 1434 (1970).

181. Lampert M.A. Many A. Mark E. Phys. Rev. 135 A 1444 (1964).

182. O'Dwyer J.J. J. App. Phys. 37 599 (1966).

183. Miller A. Abrahams E. Phys. Rev 120 745 (1960).

184. Mycielski J. Phys. Rev. 125 1 (1962).

185. Hill R.M. Phil Mag. 23 59 (1971).

186. Hill R.M. Thin Solid Films 7. R 57 (1971)

187. Last. J.T. Phys. Rev. 105 6 1740 (1957).

188. Pliskin W.S. Thin Solid Films 2. 1. (1968)

189. ShirakeG. Takeda A Phys Soc Jap. 6 128 (1951).

190. Rhodes R.G. Acta. Cryst. 4 105 (1951).

191. Bunting E.N. Shelton G.R. Creamer A.S. J.Am Ceram.Soc. 30 114 (1947).

192. Kirby R.K. AM Inst. Phys. Handbook McGraw Hill.

193. Sella C. Trillat J.J. Single Crystal Films. Ed.M.H.Francombe. H.Sato (1964)

194. Hodgman C.D. Handbook Chem. Phys. Ohio Rubber (1968).

195. Johansen I.T. J. App. Phys. 37 (1966) 499.

196. Kawabe K. Inuishi Y Jap. J. App. Phys. (1963) 2 590.

197. Meyer F. Bootsma G.A. Surface Sci. 16(1969) 221.

198. Harrop P.J. Campbell D.S. Handbook Thin Film Technology. Eds.Glang.R. Maissel L.I.(1968) McGraw Hill

199. Brandwood A. Tredgold R.H. Proc. Phys.Soc. 76 93 (1960).

200. Hughes O.H. Tredgold R.H. Williams R.H. J. Phys.Chem Sol. 27 79 (1966).

201. Cox G.A. Tredgold R.H. Phys. Lett. 11 22 (1964).

202. Busch G. Flury H. Merz W. Helv.Phys.Acta. 21 (1948)212.

203. Healey D.J. Lauriente M. 13th Nat.Vac.Symp. Am.Vac.Soc.(1966).

204. Tsui R.T.C. 4th Int.Vac.Cong. (Manchester) 1968.

205. Logan J.S. Mazza N.M. Davidse P.D. J.Vac.Sci.Tech. 6 (1969).

206. Eccleshall J. J.Sci Inst. (J.Phys.E.) 2 Vol 1 (1968).

207. Pratt I.H. Proc I.E.E.E. Vol 59 No 10 1440 (1971)

208. Schartz H. Tourtellotte H.A. J. Vac. Sci. Tech. 6 373 (1969).

209. Takei W.J. N.P. Francombe M.H. App. Phys. Lett. 15 256 (1969).

210. Wu S.V. Takei W.J. Francombe M.H. Cummins S.E. Ferroelectrics 3 2,3 and 4 217 (1972).

211. Francombe M.H. Ferroelectrics 3. 2,3 and 4 199 (1972).

212. Kniepkamp H. Heywang W, Z. Angew Math Phys Vol 6 385 (1954).

213. Brandmayr R.J. Brown A.E. Dunlop A.H. U.S.A.F. Command FT. Monmouth Tech. Rept Com-2614 (1965).

214. Anliker M. Brugger H.R. Kanzig W. Helv.Phys. Acta 27 99 (1954).

215. Harkulich T.H. Magder J. Vukasovich M.S. Lockhart R.J. J.Am.Ceram. Soc. 49 295 (1966).

216. Goswani A.K. J. App. Phys. 40 619 (1969).

217. Bhide V.G. Gondhalekar R.T. Shringi S.N. J. App. Phys. 36 3825 (1965).

218. Masuno K. Murakahi T. Waku S. Ferroelectrics 3 315 (1972)

219. Kanzig W. Phys. Rev. 98 549 (1955).

ACKNOWLEDGEMENTS.

The research programme reported in this thesis was carried out at the University of Aston during the tenure of an industrial studentship. I am indebted to the Science Research Council and to Joseph Lucas Gas Turbine Equipment Ltd for the joint award.

I would like to thank Dr. R.W. Fane for his advice during the research programme and for critically reading the manuscript.

Finally I must thank my wife for her support while the thesis was written and for typing it.